MECHANISTIC INVESTIGATIONS AND OPTIMIZATIONS OF THERMAL STABILITY IN POLYETHYLENE AND POLYVINYL CHLORIDE BLENDS

A Thesis
Presented to
The Academic Faculty

by

Mark L. Conley

In Partial Fulfillment
of the Requirements for the Degree
Doctor of Philosophy in the
School of Chemical & Biomolecular Engineering

Georgia Institute of Technology

August 2015

MECHANISTIC INVESTIGATIONS AND OPTIMIZATIONS OF THERMAL STABILITY IN POLYETHYLENE AND POLYVINYL CHLORIDE BLENDS

Approved by:

Dr. Charles Liotta, Advisor
School of Chemistry & Biochemistry
Georgia Institute of Technology

Dr. Francis Schork
School of Chemical & Bimolecular Engineering
Georgia Institute of Technology

Dr. Sven Behrens
School of Chemical & Biomolecular Engineering
Georgia Institute of Technology

Dr. Stefan France
School of Chemistry & Biochemistry
Georgia Institute of Technology

Dr. William Koros
School of Chemical & Biomolecular Engineering
Georgia Institute of Technology

Date Approved: June 18, 2015

This thesis is dedicated to my family and friends whose support and encouragement were critical in furthering my educational pursuits.

ACKNOWLEDGEMENTS

The entirety of my graduate work was made possible with the help of my graduate advisors, Dr. Charles Eckert (now retired) and Dr. Charles Liotta. Both of these outstanding scholars have guided my education, taught me how to be an effective scientist and engineer, and taught me to always ask the right questions. Dr. Eckert had a remarkable way of putting our research into a practical perspective. He always encouraged us to consider how the results of our work could be applied to actual engineering problems of practical benefit. Dr. Liotta's unparalleled knowledge of physical organic chemistry helped broaden the skills I obtained studying undergraduate chemical engineering. He challenged me to approach chemical engineering problems from a mechanistic perspective, instilling in me a stronger knowledge of organic chemistry. Additionally, Dr. Liotta provided me extensive coaching on thoughtful and effective presentation.

I also owe a debt of gratitude to Dr. Pamela Pollet. As a critical part of the Eckert-Liotta research group, she has provided vital assistance and advice to help design my experiments throughout my graduate studies. Her extensive knowledge of organic chemistry was invaluable multiple occasions.

Finally, I wish to formally thank my family and friends to whom this thesis is dedicated. Since I was young, my family has always encouraged and supported my education and learning. Their constant encouragement undoubtedly contributed to the success of my graduate studies. The friends I have made out of colleagues here at Georgia Tech have made my graduate studies truly enjoyable. In particular, Chris Butch

and Wesley Woodham have both provided helpful input and entertaining discussion during my graduate studies. Addtionally, I am extraordinarily grateful to Christa Lee, whose daily encouragement and company maintained my sanity through the process of writing this thesis.

Table of Contents

Acknowledgements iv

List of Tables xiii

List of Figures xv

List of Abbreviations xxx

Summary xxxii

Chapter 1 – Introduction 1

1.1 Polymers on the Global Scale 1

1.2 Electrical Cable Insulation 3

1.3 Crosslinked Polyethylene 4

1.3.1 Mechanistic Function of a Thiosynergist Antioxidant Additive 6

1.3.2 Acid-Catalyzed Decomposition of DCP 7

1.4 Polyvinyl Chloride 7

1.4.1 Model Compound Studies and Polymer Blend Studies 9

1.4.2 Epoxidized Linolenic Acid Salts as Sacrificial Epoxide Stabilizers 10

1.4.3 Salts of Maleimidoundecanoic Acid as Novel PVC Stabilizers 11

1.5 References 12

Chapter 2 – Mechanistic Investigation of a Polyethylene crosslinking system 14

2.1 Introduction 14

2.1.1 Crosslinked Polyethylene Processing 15

2.2 Methodology 23

2.2.1 Materials 23

2.2.2 Reaction techniques 24

2.2.3 High-Pressure Liquid Chromatography 25

2.2.4 Gas Chromatography and Mass Spectroscopy 25

2.2.5 ^{1}H Nuclear Magnetic Resonance 25

2.3 Thermal Decomposition of DCP 26

2.3.1 HPLC Rate Determination 26

2.3.2 Identification of Products By NMR 31

2.3.3 Quantification of DCP Thermal Decomposition Products 34

2.4 Thermal Decomposition of DCP Under Argon 37

2.4.1 Determination of DCP Thermal Decomposition Products Via NMR 37

2.4.2 Rate Determination of DCP Thermal Decomposition Using HPLC 39

2.5 Experiments With DSTDP 41

2.5.1 Purification of Stock DSTDP Material 41

2.5.2 Thermal Treatment of DSTDP 44

2.5.3 Reactions of DCP with DSTDP in Dodecane in Air 45

2.5.4 Reactions of DCP with DSTDP in Dodecane Under Argon 56

2.5.5 Additional Experiments Regarding Experimental Atmosphere 63

2.6 Hypothesized Mechanism for the Interaction of DCP with DSTDP 67

2.6.1 Thermal Treatment of Sulfoxide Derivative of DSTDP 73

2.6.2 Verification of Step 5: Reactions of DSTDP with CHP 80

2.6.3 Reactions of DCP With the Sulfoxide Derivative of DSTDP 82

2.7 Explanation of Beneficial Reduction in Premature Crosslinking 84

2.7.1 Results With Other Peroxide Crosslinkers 89

2.8 Conclusions 90

2.9 References 92

Chapter 3 – Formation of Cumene Hydroperoxide Via the Acid-Catalyzed Decomposition of Dicumyl Peroxide 94

3.1 Introduction 94

3.1.1 Reported Decomposition of Dicumyl Peroxide 94

3.1.2 Phenol-Acetone Process 97

3.2 Methodology 98

3.2.1 Materials 99

3.2.2 Reactions of DCP and Additives in Dodecane 99

3.2.3 Determination of the Critical Micelle Concentration of DBSA in Dodecane 100

3.2.4 ^{1}H Nuclear Magnetic Resonance (NMR) 102

3.2.5 High Pressure Liquid Chromatography (HPLC) 102

3.2.6 Gas Chromatography (GC) 103

3.3 Decompositions Reactions of DCP 103

3.3.1 Thermal Decomposition of DCP 103

3.3.2 Observation of CHP via the Acid-Catalyzed Decomposition of DCP 104

3.3.3 Kinetics Analysis of the Reaction of DCP with DBSA 112

3.4 Mechanism of Reaction of DCP with DBSA in Dodecane 120

3.5 Quantification of Acid-Catalyzed DCP Decomposition Products 121

3.6 Conclusions 129

3.7 References 130

Chapter 4 – Mechanistic Investigation of Polyvinyl Chloride DEgradation and Stabilization 132
4.1 Introduction 132
4.1.1 Thermal Decomposition of Polyvinyl Chloride 132
4.1.2 Use of PVC Model Compounds 133
4.1.3 Thermal Stabilization of PVC 134
4.1.4 Overall Experimental Approach 135
4.2 Methodology and Materials 137
4.2.1 Materials 137
4.2.2 Experimental 138
4.3 Kinetics Studies with Acetates 144
4.4 Mechanistic Investigations with Stearates 164
4.4.1 Investigation of Color Change in Reactions with 2,4-dichloropentane 171
4.4.2 Analysis of Headspace Over Reactions of 2,4-dichloropentane with Stearate 178
4.4.3 Mechanism of Zn/Ca Stearates Interaction with PVC 182
4.5 Comparison to Studies of PVC Polymer 184
4.6 Conclusions 188
4.7 References 191
Chapter 5 – Use of Epoxidized Linolenic Acid Salts as Multifunctional Stabilizers in Plasticized PVC Blends 194
5.1 Introduction 194
5.1.1 Plasticizer Selection Considerations 195
5.1.2 PVC Stabilization 197

5.2 Methodology 199

5.2.1 Materials 200

5.2.2 Synthesis of 9,12,15-Triepoxylinolenic Acid 201

5.2.3 Synthesis of Zinc or Calcium Salt of Triepoxylinolenic Acid 201

5.2.4 Fabrication of Blends of PVC, Plasticizers, and Additives 202

5.2.5 Thermogravimetry of PVC Blends 203

5.2.6 Epoxide Ring-Opening Studies 203

5.2.7 UV-Visible Spectroscopy of PVC 203

5.2.8 Color Examination of Heated PVC Blends 204

5.3 Reactions of ESO with Hydrogen Chloride 204

5.4 TGA of Untreated PVC and Plasticized PVC 208

5.5 Measurement of Activation Energies for Dehydrochlorination of PVC Blends 211

5.6 Effects of ZnEp and CaEp as Stabilizers in Blends of PVC Plasticized with DIDP 216

5.7 Effects of ZnEp and CaEp as Stabilizers in Blends of PVC Plasticized with ESO 222

5.8 Studies of Epoxide Ring-Opening 225

5.9 Conclusions 232

5.10 References 234

Chapter 6 – Use of Zinc and Calcium Salts of 11-Maleimidoundecanoic acid As Thermal Stabilizers for PVC 236

6.1 Introduction 236

6.2 Methodology 239

6.2.1 Materials 240

6.2.2 Synthesis of 11-Maleimidoundecanoic acid 240
6.2.3 Preparation of Blends of PVC, Plasticizers, and Novel Additives 241
6.2.4 Thermogravimetric Analysis of PVC Blends 242
6.2.5 UV-Visible Spectroscopy of PVC 244
6.2.6 Color Change Examination of PVC Blends..... 244
6.3 UV-Visible Absorption of PVC (With No Additives) Heated at 180 °C 244
6.4 Zn11M and Ca11M as Stabilizers in Blends of PVC and DIDP 247
6.5 . UV-Visible Absorption..... 250
6.6 Zn11M and Ca11M as Stabilizers in Blends of PVC and ESO..... 252
6.7 Preliminary Studies with Beta-Carotene..... 256
6.8 Conclusions..... 259
6.9 References..... 261
Chapter 7 – Conclusions 262
7.1 Mechanism of the Interactions of DCP with DSTDP..... 264
7.1.1 Future Work and Recommendations 265
7.1.2 Improvement of Blend Performance..... 268
7.2 Acid-Catalyzed Degradation of DCP to Produce Cumene Hydroperoxide..... 271
7.2.1 Future Work and Recommendations 272
7.3 Degradation and Stabilization of PVC..... 274
7.3.1 Future Work and Recommendations 275
7.4 Epoxidized Salts of Linolenic Acid as Dual-Function PVC Stabilizers..... 276
7.4.1 Future Work and Recommendations 277

7.5 Salts of Maleimidoundecanoic Acid as PVC Stabilizers 278

7.5.1 Future Work and Recommendations 278

7.6 References 280

Vita 281

LIST OF TABLES

Table 2.1. Reduction in premature crosslinking induced by the special blending technique employed by Dow Chemical. 21

Table 3.1. Reaction temperatures and first-order rate constants of the thermal decomposition of DCP. 103

Table 3.2. Select species concentrations and selectivities and DCP conversion after sealed reactions of 0.0589 M DCP with 0.03 equivalents of DBSA in dodecane at 70 °C for 2 hours and 110 °C for 1 hour. 126

Table 3.3. Final species concentrations and selectivities for the sealed reactions of 0.0589 M CHP with 0.03 equivalents of DBSA at 70 °C for 45 minutes and 110 °C for 25 minutes (complete conversion). 127

Table 3.4. Relative kinetic parameters from Figure 3.19 as determined from acid-catalyzed reactions of DCP and CHP. 127

Table 4.1. Effective first-order reaction rate constants from reactions with 1,3-dichlorobutane at 100 °C. 150

Table 4.2. Summary of effective reaction rate constants of model compounds reacted with 0.5 eq NaOAc and 0.05 eq tetra-n-butylammonium chloride at 100 °C. 156

Table 4.3. Times required to reach the defined colors for the reactions of 2,4-dichloropentane with various compositions of carboxylates at 140 °C. 165

Table 4.4. Stereoisomer ratios and conversion of 2,4-dichloropentane for reactions of 2,4-dichloropentane with various compositions of stearates at 140 °C for 3 hours. 168

Table 6.1. Ratio of the magnitude of the maximum absorptions for the reactions of beta-carotene in o-DCB at 145 °C (Figure 6.17) as a function of time. 259

Table 7.1. Viscosities of some polyethylene model solvents. 266

LIST OF FIGURES

Figure 1.1. Data for the global demand and growth rate of the most common thermoplastics. 2

Figure 1.2. Simple mechanism for the radical-initiated crosslinking of polyethylene. 5

Figure 1.3. Chemical structures of the radical crosslink initiator (DCP) and antioxidant additive (DSTDP). 6

Figure 1.4. Structure of defect-free PVC along with the three common defects in the polymer backbone: allylic, tertiary, and vicinal defects. 8

Figure 1.5. Initiation of PVC thermal degradation and subsequent “chain-unzipping” process..... 8

Figure 1.6. Structure of epoxidized soybean oil (ESO). 10

Figure 1.7. Conjugated polyene chain undergoing a (a) Diels-Alder reaction and a (b) Ene reaction..... 11

Figure 2.1. Representative high-voltage power transmission cable featuring an XLPE sheath. 15

Figure 2.2. Peroxide-induced crosslinking of polyethylene using DCP (top-left structure). 16

Figure 2.3. Structure of distearyl thiodipropionate (DSTDP)..... 17

Figure 2.4. Mechanism of antioxidant scorch prevention..... 18

Figure 2.5. Hypothesized mechanism for interaction of DSTDP with organic peroxide. 18

Figure 2.6. Moving die rheometer results for a polyethylene sample. 20

Figure 2.7. Representative HPLC chromatogram of the reaction of 0.0589 M DCP at 120 °C for 30 minutes. 27
Figure 2.8. HPLC calibration curve for DCP in solutions of dodecane. 27
Figure 2.9. DCP concentrations as a function of time at various temperatures. 28
Figure 2.10. Linearized form of the first-order decomposition rate expression. 28
Figure 2.11. First-order plot for the thermal decomposition of DCP in dodecane. 29
Figure 2.12. Arrhenius plot for the thermal decomposition of DCP in dodecane. 30
Figure 2.13. Linearization of the Arrhenius equation. 30
Figure 2.14. Proton NMR of 0.1178 M DCP in dodecane. 31
Figure 2.15. Proton NMR of 0.1178 M DCP in dodecane after 3.5 hours at 120 °C. 32
Figure 2.16. Proton NMR spectrum of a standard of acetophenone in dodecane. 33
Figure 2.17. Concentration of acetophenone as a function of time for the reaction of 0.0589 M DCP in dodecane at various temperatures. 35
Figure 2.18. Concentration of cumyl alcohol as a function of time for the reaction of 0.0589 M DCP in dodecane at various temperatures. 36
Figure 2.19. Concentration ratios of acetophenone:cumyl alcohol at various temperatures. 36
Figure 2.20. Proton NMR spectrum of 0.0589 M DCP in dodecane after 3.5 hours at 120 °C. 38
Figure 2.21. The concentration of DCP as a function of time for a sample of 0.0589 M DCP reacted at 120 °C under argon. 40
Figure 2.22. Proton NMR of stock DSTDP obtained from City Chemical. 42
Figure 2.23. Proton NMR of purified DSTDP. 43

Figure 2.24. Proton NMR spectra of 0.321 M DSTDP in dodecane both before and after 7 hours of thermal treatment at 110 °C. 45
Figure 2.25. Proton NMR of the mixture of 0.0589 M DCP with 1 equivalent of DSTDP. 47
Figure 2.26. Proton NMR spectrum of the reaction of 0.0589 M DCP with 1 equivalent of DSTDP after 3.5 hours at 120 °C. 48
Figure 2.27. Mechanism for the retro-Michael addition to form an acrylate. 49
Figure 2.28. TOP: proton NMR spectrum of the acrylate species that could be formed via the mechanism in Figure 2.27. BOTTOM: zoomed view of the NMR spectrum in Figure 2.26 for comparison purposes. 50
Figure 2.29. DCP concentrations as a function of time for the reactions of 0.0589 M DCP with varying amounts of DSTDP at 120 °C. 52
Figure 2.30. Photograph of 0.0589 M DCP + DSTDP reactions after reaction. 53
Figure 2.31. Proton NMR spectrum of the reaction of 0.0589 M DCP with 0.25 and 1 equivalent of DSTDP at 120 °C for 3.5 hours. 54
Figure 2.32. DCP concentrations as a function of time for the reactions of 0.0589 M DCP with varying amounts of DSTDP at 120 °C. 55
Figure 2.33. Proton NMR spectrum of 0.0589 M DCP with 1 equivalent DSTDP reacted at 120 °C for 3.5 hours. 57
Figure 2.34. Proton NMR spectrum of 0.0589 M DCP with 1 equivalent DSTDP reacted at 120 °C for 3.5 hours, zoomed in to show the formation of cumyl alcohol. 58
Figure 2.35. Photograph of reaction solutions of 0.0589 M DCP with 0.5 equivalents of DSTDP after 3.5 hours at 120 °C. 59

Figure 2.36. HPLC concentration data for the reactions of 0.0589 M DCP with 1 equivalent DSTDP at 120 °C as a function of time. 60
Figure 2.37. HPLC concentration data for the reactions of 0.0589 M DCP with 0.25 equivalent DSTDP at 120 °C as a function of time. 61
Figure 2.38. Proton NMR spectrum of the reaction of 0.0589 M DCP with 1 equivalent of DSTDP under humidified argon. 64
Figure 2.39. Zoomed proton NMR spectrum of the reaction of 0.0589 M DCP with 1 equivalent of DSTDP under humidified argon. Cumyl alcohol is observed, as shown with peak ‘i’. 65
Figure 2.40. Proton NMR spectrum of the reaction of 0.0589 M DCP with 1 equivalent of DSTDP under dry air. 66
Figure 2.41. Proton NMR spectrum of the reaction of 0.0589 M DCP with 1 equivalent of DSTDP under dry air, zoomed to show the region where cumyl alcohol would be visible. 67
Figure 2.42. Hypothesized mechanism for the reaction of DCP with DSTDP in the presence of air. 69
Figure 2.43. Possible mechanism of oxidation of DSTDP by a general hydroperoxide species. 70
Figure 2.44. Possible mechanism of the oxidation of sulfenic acid to sulfinic acid by a hydroperoxide. 71
Figure 2.45. A possible mechanism for an acid-catalyzed decomposition of DCP. Acid is regenerated at the end of reaction. 72

Figure 2.46. Literature proton NMR spectra highlighting the relative proton shifts of sulfides, sulfoxides, and sulfones..... 74
Figure 2.47. Proton NMR spectrum of our synthesized sulfoxide derivative of DSTDP. The sulfoxide exhibits the peak splitting observed in Figure 2.46. 75
Figure 2.48. Proton NMR spectrum of synthesized sulfone derivative of DSTDP..... 76
Figure 2.49. Proton NMR spectra of the thermal decomposition of 0.0589 M sulfoxide in dodecane at 102 °C. 78
Figure 2.50. Conversion data for the thermal decomposition of 0.0589 M sulfoxide in dodecane over the course of 2 hours..... 79
Figure 2.51. Conversion data for the thermal decomposition reactions of 0.0589 M sulfone in dodecane at various temperatures. 80
Figure 2.52. Proton NMR of the reaction of 0.1178 M DSTDP in dodecane with 1 equivalent of CHP..... 81
Figure 2.53. HPLC concentration data for the reactions of 0.0589 M DCP with the sulfoxide derivative of DSTDP in varying amounts at 120 °C for up to 5.5 hours..... 83
Figure 2.54. Proposed mechanism of radical stabilization by α-methyl styrene and stearyl acrylate, both of which are produced during reactions of DCP with DSTDP in air..... 85
Figure 2.55. Possible mechanism of radical polymerization of α-methyl styrene..... 86
Figure 2.56. Proton NMR of the reaction of 0.0589 M DCP with 0.25 equivalents of α-methyl styrene after 15 minutes..... 87
Figure 2.57. Proton NMR of the reaction of 0.0589 M DCP with 0.25 equivalents of α-methyl styrene after 3 hours..... 88

Figure 2.58. Structures and names of other peroxide crosslinkers examined in combination with DSTDP. 89
Figure 3.1. Mechanism of the thermal decomposition of DCP through homolytic cleavage 95
Figure 3.2. Literature mechanism for the acid-catalyzed decomposition of DCP.[1,8] 96
Figure 3.3. Aqueous acid-catalyzed decomposition of cumene hydroperoxide to form phenol and acetone.[12] 97
Figure 3.4. UV-visible absorption and structure of DBSA. 101
Figure 3.5. Maximum absorption of DBSA in dodecane plotted as a function of concentration. 102
Figure 3.6. Proton NMR of the reaction of 0.0589 M DCP with 0.25 equivalents of DSTDP and 0.05 equivalents of DBSA in dodecane at 120 °C after 15 mintues. 106
Figure 3.7. Proton NMR spectra of THTP and its oxidized derivatives in $CDCl_3$. 107
Figure 3.8. Reactions of THTP with peroxide species and acid. 109
Figure 3.9. Proton NMR spectrum of 0.0589 M DCP in dodecane, zoomed to show the methyl peaks of DCP and the methyl peaks of dodecane. 111
Figure 3.10. Representative chromatogram from the HPLC analysis of reactions of DCP with DBSA. 113
Figure 3.11. Concentrations of DCP as a function of time for the reactions of 0.0589 M DCP with 0.03 equivalents of DBSA in dodecane.. 113
Figure 3.12. First-order plot of the concentration profiles from the reactions of 0.0589 M DCP with 0.03 equivalents DBSA in dodecane 114

Figure 3.13. Arrhenius plot for the reactions of 0.0589 M DCP with 0.03 equivalents of DBSA in dodecane. 115
Figure 3.14. Proposed mechanism involving a hydrogen-bonded complex during the reaction of DCP with DBSA. 116
Figure 3.15. Derivation of an analytical expression for the rate of consumption of DCP when reacted with DBSA 117
Figure 3.16. Proposed form of the rate expression for the reaction of DCP with DBSA in dodecane at low temperatures. 118
Figure 3.17. Proposed form of the rate expression for the reaction of DCP with DBSA in dodecane at high temperatures. 118
Figure 3.18. Proton NMR spectra of the reaction of 0.0589 M DCP with 0.03 equivalents of DBSA at 120 °C. 120
Figure 3.19. Proposed mechanism of the acid-catalyzed decomposition of DCP. 120
Figure 3.20. Expression for the selectivity of phenol during the acid-catalyzed decomposition of DCP. 122
Figure 3.21. Full derivation of Figure 3.20. 123
Figure 3.22. GC chromatogram for the reaction of 0.0589 M DCP with 0.00177 M DBSA at 90 °C for 60 minutes. 125
Figure 3.23. Reported structures of AMS dimers when AMS was reacted with pTSA. 129
Figure 4.1. Tacticities and defects that affect the thermal degradation and stabilization of PVC. 133

Figure 4.2. Mechanism of initial thermal degradation, “chain-unzipping,” autocatalysis, and stearate substitution of PVC. 135
Figure 4.3. Structures of model compounds used for determination of relative kinetics of PVC defects. 137
Figure 4.4. Overview of the synthesis of 2,4-dichloropentane. 139
Figure 4.5. Overview of the synthesis of 3-chloro-3-ethylepentane. 140
Figure 4.6. Overview of the synthesis of 3,4-dichlorohexane. 140
Figure 4.7. Overview of the synthesis of (E)-6-chloronon-4-ene. 142
Figure 4.8. Expected reaction pathways of model compounds reacted with metal carboxylates. 146
Figure 4.9. GC chromatograph of the reaction of 1,3-dichlorobutane (0.006 mol) with NaOAc, $Ca(OAc)_2$, and $Zn(OAc)_2$ (0.003 mol $^-$OAc) in the presence of PTC (0.0003 mol) at 100 °C with added tetradecane (0.001 mol) as internal standard. 147
Figure 4.10. Reaction mechanism of 1,3-dichlorobutane with acetate salts. 148
Figure 4.11. Conversion as a function of time for the reaction of 1,3-dichlorobutane with NaOAc at 100 °C with PTC. 149
Figure 4.12. Rate expression for the consumption of model compound when reacted with metal acetate salts in the presence of PTC. 149
Figure 4.13. Expression for conversion of model compounds when reacted with metal acetates in the presence of PTC. 149
Figure 4.14. First-order plot for the reaction of 1,3-dichlorobutane with NaOAc in the presence of PTC at 100 °C. 150

Figure 4.15. Conversion data for the reaction of 2,4-dichloropentane with NaOAc at 100 °C in the presence of PTC. 151

Figure 4.16. First-order plot for the reaction of 2,4-dichloropentane with NaOAc at 100 °C with PTC. 152

Figure 4.17. Conversion data for the reaction of 3-chloro-3-ethylpentane with NaOAc at 100 °C in the presence of PTC. 152

Figure 4.18. First-order plot for the reaction of 3-chloro-3-ethylpentane with NaOAc at 100 °C with PTC. 153

Figure 4.19. Conversion data for the reaction of 3-chloro-1-butene with NaOAc at 100 °C in the presence of PTC. 153

Figure 4.20. First-order plot for the reaction of 3-chloro-1-butene with NaOAc at 100 °C with PTC. 154

Figure 4.21. Conversion data for the reaction of 3,4-dichlorohexane with NaOAc at 100 °C in the presence of PTC. 154

Figure 4.22. First-order plot for the reaction of 3,4-dichlorohexane with NaOAc at 100 °C with PTC. 155

Figure 4.23. Conversion data for the reaction of 6-chloro-4-nonene with NaOAc at 100 °C in the presence of PTC. 155

Figure 4.24. First-order plot for the reaction of 6-chloro-4-nonene with NaOAc at 100 °C with PTC. 156

Figure 4.25. GC chromatogram of 2,4-dichloropentane in THF. 158

Figure 4.26. Mass spectrum of the peak at 4.9 minutes in Figure 4.25. 158

Figure 4.27. Gas chromatogram of the reaction of 2,4-dichloropentane after reaction at 100 °C with NaOAc in the presence of PTC.. 159
Figure 4.28. Mass spectra of the products seen in Figure 4.27..... 160
Figure 4.29. Bimolecular basic elimination to form the substituted alkene pent-3-en-2-yl acetate from the reaction of 2,4-dichloropentane with NaOAc at 100 °C with added PTC. 162
Figure 4.30. Color appearance of a representative reaction of 2,4-dichloropentane with 2.5 phr $ZnSt_2$ and 2.5 phr $CaSt_2$ at 140 °C..... 165
Figure 4.31. Proton NMR spectra of reactants measured at 100 °C. 167
Figure 4.32. Proton NMR spectra of the reaction of 2,4-dichloropentane with $ZnSt_2$ at 140 °C. 169
Figure 4.33. ^{13}C NMR confirming the presence of stearic acid in reaction solutions of 2,4-dichloropentane with stearates after 3 hours at 140 °C. 170
Figure 4.34. Color change of the reaction of 1.2 M 2,4-pentadiene with 10 phr $ZnCl_2$ in o-DCB at 140 °C. 172
Figure 4.35. Reaction of 1.2 M 2,4-pentadiene in o-DCB at 140 °C.. 173
Figure 4.36. Hypothesized mechanisms for the formation of colored conjugated double bond systems via reaction of 2,4-penadiene with $ZnCl_2$..... 173
Figure 4.37. Proton NMR spectra for the reaction of 1.2 M 2,4-pentadiene with 10 phr ZnCl2 in o-DCB at 140 °C. 175
Figure 4.38. ^{1}H NMR spectra for the reaction of 1.2 M 2,4-pentadiene in o-DCB at 140 °C. 178

Figure 4.39. Gas chromatograph and associated species of the vapor phase above the reaction of 2,4-dichloropentane with $ZnSt_2$ at 140 °C for 3 hours. 179
Figure 4.40. Mass spectra used in identification of the GC peaks in Figure 4.39. 180
Figure 4.41. Proposed mechanisms for the formation of species with retention times of 2.2 minutes and 4.6 minutes in Figure 4.39. 182
Figure 4.42. Proposed mechanism of interaction of metal stearates with PVC. 183
Figure 4.43. Mass loss of PVC blends during thermogravimetric analysis at 170 °C. . 185
Figure 4.44. Photographs of PVC blends after thermal treatment at 170 °C for 2 hours. 186
Figure 5.1. Chemical structure of epoxidized soybean oil (ESO). 195
Figure 5.2. Mechanism of the attack of ESO by HCl to open oxirane rings and to form a chlorohydrin. 196
Figure 5.3. Structure of ideal, defect-free PVC. Structures of several of the most common defects are also shown. 197
Figure 5.4. Initiation of PVC thermal degradation (at an allylic site), “chain-unzipping,” and autocatalysis of degradation. 198
Figure 5.5. Method of synthesis of the zinc and calcium salts of 9,12,15-triepoxylinolenic acid. 200
Figure 5.6. Example of a ring-opening reaction caused by attack of HCl. 204
Figure 5.7. Proton NMR spectrum of ESO used in this study. 205
Figure 5.8. Proton NMR spectrum of the products of the reaction of ESO wth HCl at a 1:1 molar ratio. 206

Figure 5.9. Proton NMR spectrum of the products of the reaction of ESO with HCl at a 20:1 molar ratio. 207
Figure 5.10. Weight profiles as a function of time for PVC and PVC plasticizer blends at 170 °C. 209
Figure 5.11. Isothermal weight loss of PVC additives as a function of time at 180 °C. 210
Figure 5.12. Color formation in PVC and PVC blends heated at 170 °C for 2 hours. ... 211
Figure 5.13. Isothermal TGA weight profiles for isothermal treatments of ESO..... 212
Figure 5.14. Isothermal weight loss profiles of untreated PVC over the course of 3 hours. 213
Figure 5.15. Isothermal weight loss profiles of PVC plasticized with DIDP over the course of 2 hours. 214
Figure 5.16. Isothermal weight loss profiles of PVC plasticized with ESO over the course of 2 hours. 214
Figure 5.17. Arrhenius plots for the isothermal dehydrochlorination of PVC unplasticized, plasticized with DIDP, and plasticized with ESO. 215
Figure 5.18. Weight loss profiles of DIDP-plasticized PVC blends incorporating novel epoxide salt stabilizers and stearate salts for comparison. 217
Figure 5.19. Weight loss profiles for blends of DIDP-plasticized PVC with stearate stabilizers and zinc chloride at 170 °C. 219
Figure 5.20. Color retention photographs of DIDP-plasticized PVC blends incorporating novel epoxide salt stabilizers compared directly with stearates. 220
Figure 5.21. Color retention photographs of blends of PVC, DIDP, and stearates after heating at 170 °C for 2 hours. 221

Figure 5.22. Color retention photographs of blends of PVC, DIDP, and novel epoxide salts after 2 hours at 170 °C. 221
Figure 5.23. Weight loss profiles of ESO-plasticized PVC blends incorporating novel epoxide salt stabilizers and stearate salts for comparison. 222
Figure 5.24. Color retention photographs of ESO-plasticized PVC blends incorporating novel epoxide salt stabilizers. 224
Figure 5.25. Color retention photographs of blends of PVC, ESO, and stearates after 2 hours at 170 °C. 225
Figure 5.26. Proton NMR spectrum of 1,2-epoxyhexane. 226
Figure 5.27. Carbon NMR spectrum of 1,2-epoxyhexane. 226
Figure 5.28. Mechanism of epoxide ring opening of 1,2-epoxyhexane by dry HCl in the gas phase. 227
Figure 5.29. Proton NMR spectrum of the reaction of 1,2-epoxyhexane with HCl at a 1:1 molar ratio at room temperature for 90 minutes. 228
Figure 5.30. Carbon NMR spectrum of the reaction of 1,2-epoxyhexane with HCl at a 1:1 molar ratio at room temperature for 90 minutes. 229
Figure 5.31. Proton NMR spectrum of cyclohexene oxide. 229
Figure 5.32. Carbon NMR spectrum of cyclohexene oxide. 230
Figure 5.33. Mechanism of the epoxide ring opening reaction of cyclohexene oxide with HCl in the gas phase. 230
Figure 5.34. Proton NMR spectrum of the reaction of cyclohexene oxide with HCl at a 1:1 molar ratio at room temperature for 90 minutes. 231

Figure 5.35. Carbon NMR spectrum of the reaction of cyclohexene oxide with HCl at a 1:1 molar ratio at room temperature for 90 minutes. 231
Figure 5.36. Proton NMR spectrum of the competitive reaction of 0.5 equivalents 1,2-epoxyhexane and 0.5 equivalents cyclohexene oxide with 1 equivalent of HCl at room temperature for 90 minutes. 232
Figure 6.1. The reaction of a conjugated polyene with a dienophile via (a) Diels-Alder Reaction, and (b) the Ene Reaction..... 237
Figure 6.2. Structures of the novel maleimide stabilizers Zn11M and Ca11M. 239
Figure 6.3. Synthesis pathway of the zinc or calcium salt of 11-maleimidoundecanoic acid. "M" represents a metal cation, either Zn or Ca. 240
Figure 6.4. Isothermal weight losses of several additives after 2 hours at 180 °C. 243
Figure 6.5. Isothermal weight losses of maliemide salts and zinc stearate after treatment at 170 °C. 243
Figure 6.6. UV-Visible absorption spectra of unblended PVC heated at 180 °C for various time increments. 245
Figure 6.7. Integrated UV-Absorption areas (obtained from Figure 6.6) plotted as a function of time. 246
Figure 6.8. Cyclization processes by polyene sequences that can limit conjugation of polyenes. 247
Figure 6.9. Weight loss of PVC plasticized by DIDP with added zinc and calcium stearates and zinc and calcium maleimide salts as thermal stabilizers. 248
Figure 6.10. Color comparison photographs of blends of PVC plasticized with DIDP with added stearate and maleimide salts for thermal stabilization..... 250

Figure 6.11. Integrated areas of UV-Visible absorption peaks of PVC plasticized with DIDP as a function of time. 251

Figure 6.12. Weight loss of PVC plasticized by ESO with added zinc and calcium stearates and zinc and calcium maleimide salts as thermal stabilizers. 253

Figure 6.13. Mechanism of the scavenging of HCl by ESO, producing chlorohydrins. 254

Figure 6.14. Color comparison photographs of blends of PVC plasticized with DIDP with added stearate and maleimide salts for thermal stabilization..... 255

Figure 6.15. Structure of beta-carotene..... 256

Figure 6.16. UV-Visible absorption spectra of beta-carotene and Zn11M in o-DCB, measured at room temperature..... 257

Figure 6.17. UV-Visible spectra for the reactions of (i) beta-carotene in o-DCB at 145 °C (blue lines) and (ii) beta-carotene with equimolar Zn11M in o-DCB at 145 °C (red lines). 259

Figure 7.1. Commercially available, potential sulfur additives. 269

Figure 7.2. Possible novel compounds for use in preventing premature crosslinking of polyethylene by DCP. 270

LIST OF ABBREVIATIONS

ACP	acetophenone
AMS	α-methyl styrene
CA	cumyl alcohol
$CaCl_2$	calcium chloride
CaEp	calcium salt of epoxidized linolenic acid
$CaSt_2$	calcium stearate
Ca11M	calcium salt of maleimidoundecanoic acid
CDCl3	deuterated chloroform
CHO	1,2-cyclohexene oxide
CHP	cumene hydroperoxide
DBSA	dodecylbenzenesulfonic acid
DCM	dichloromethane
DCP	dicumyl peroxide
DIDP	diisodecyl phthalate
DMSO	dimethyl sulfoxide
DMSO-D6	deuterated dimethyl sulfoxide
DSTDP	distearly thiodipropionate
EH	1,2-epoxyhexane
ESO	epoxidized soybean oil
GCMS	gas chromatography / mass spectroscopy
HCl	hydrogen chloride

HPLC	high-pressure liquid chromatography
mCPBA	meta-chloroperbenzoic acid
min	minutes
NMR	nuclear magnetic resonance
o-DCB	ortho-dichlorobenzene
PE	polyethylene
phr	parts per hundred resin
PTC	phase transfer catalyst
PVC	polyvinyl chloride
THF	tetrahydrofuran
UV-Visible	ultraviolet-visible spectroscopy
XLPE	crosslinked polyethylene
$ZnCl_2$	zinc chloride
ZnEp	zinc salt of epoxidized linolenic acid
$ZnSt_2$	zinc stearate
Zn11M	zinc salt of maleimidoundecanoic acid

SUMMARY

The thermal stability of two distinct blended polymer systems was examined. A model for polyethylene was used to investigate the vulnerability of polyethylene to premature crosslinking in industrial crosslinking conditions. Careful experiments were conducted to gather evidence of the interaction between a peroxide crosslinking agent and a specific antioxidant additive. Multiple lines of evidence were combined to propose a complete mechanism of interaction between the two species. The mechanism was further tested and a hypothesis was proposed for the reduction in premature crosslinking exhibited when the two species are present in polyethylene blends. A specific aspect of the proposed mechanism warranted further investigation on its own. The acid-catalyzed degradation of the peroxide initiator was thoroughly investigated.

The thermal degradation of polyvinyl chloride was also studied. Model compounds were reacted with carboxylates to determine the relative rates of stabilization at various polymer defect sites. These model studies were combined with weight loss and color change investigations of bulk polymer systems. The knowledge gained from the model and polymer studies allowed for the proposal and examination of two novel stabilizing salt systems. The efficacy of the new stabilizers is presented.

CHAPTER 1 – INTRODUCTION

1.1 Polymers on the Global Scale

Since the invention of the first thermosetting rubber in 1851, plastics and thermopolymers have gained importance in virtually all of modern life and product areas.[1] In the 1860s in the United States, research began to produce billiard balls using cellulose nitrate with camphor as a plasticizer. Today's major thermoplastics (polyvinyl chloride, low density polyethylene, polystyrene, and polymethyl methacrylate) were developed between 1930 – 1940. The advent of World War II brought with it a greatly increased demand for plastics both in the United States and abroad. The plastics industry has grown rapidly ever since.[1]

The two polymers addressed in this thesis (polyvinyl chloride and polyethylene) are among the most widely produced globally. In 2013, polyethylene had the highest demand of all thermopolymers; polyvinyl chloride had the third highest demand.[2] The demand growth rate of both polymers is only expected to increase, as shown below in Figure 1.1.

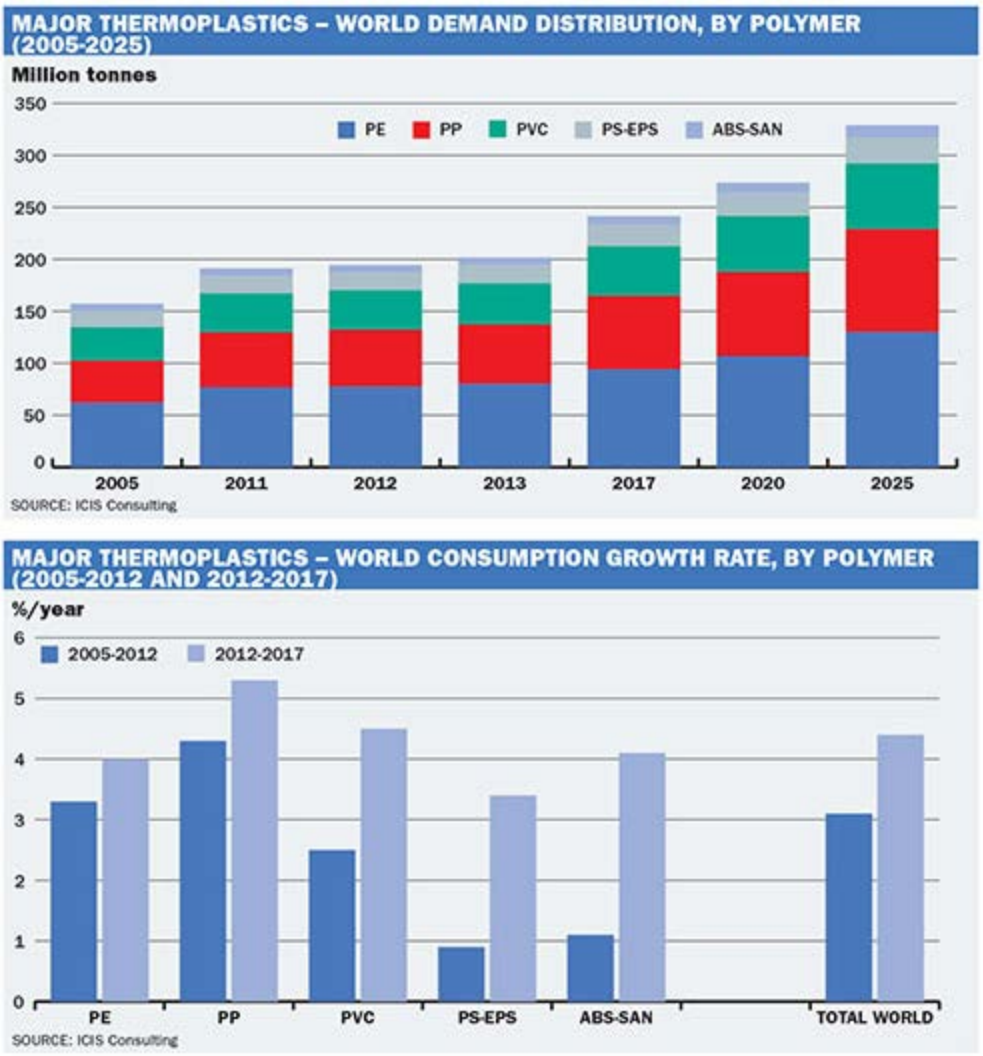

Figure 1.1. Data for the global demand and growth rate of the most common thermoplastics. Data were gathered in 2013.[2]

The high demand for both polyethylene (PE) and polyvinyl chloride (PVC) obviates the importance of characterizing and optimizing the processing techniques of each polymer. The work contained herein is applicable to these polymers in a variety of applications. Specifically, this thesis focuses on the use of PE and PVC as insulation sheathing for electrical cables.

1.2 Electrical Cable Insulation

As early as 1900, insulated electrical cables were commonplace. High-voltage cables at the time were insulated with oil-impregnated paper. A major drawback of this early insulation method was the necessary exclusion of moisture. A metallic sheath was required as a barrier to humidity. Vulcanized rubber was the earliest alternative to the paper-based insulators and eliminated the drawbacks of its competitors.[3]

With the flourishing of polymer processing around the time of the second World War, synthetic polymers (such as PVC) saw use as electrical insulators.[3] Modern power cables are made with a variety of compositions and insulating materials. Insulation is selected based on the cable's voltage, structural, and color requirements.[4] This thesis focuses on specific applications of PE and PVC as electrical insulation materials. Specifically, PE is discussed in the framework of high voltage power transmission cables. PVC is discussed in the framework of smaller, lower voltage conductors.

Each of these polymer insulator systems comes with its own set of processing concerns and challenges. PE must undergo crosslinking for suitability as an insulator.[5,6] Crosslinking can be facilitated via several methods, including irradiation, reaction with peroxides, and reaction with silanes.[6] Variables that must be considered during the crosslinking process include ultimate crosslink level, survivability of crosslinking agents during other processing steps, and the rate at which crosslink will occur. This thesis focuses on the challenges inherent in the crosslinking of PE.

PVC presents a more significant problem with maintaining polymer performance after processing.[7] Specifically, PVC can undergo a thermal degradation process known as dehydrochlorination. Thermal degradation changes the electrical resistance, physical

flexibility, and color properties of the final PVC product. All of the results of degradation are highly undesirable. PVC wire sheaths are often color-coded to indicate the gauge of the wire. Color degradation reduces the clarity of this color coding technique. Reduction in flexibility hinders the use of small, flexible wiring in residential or electronics applications. This thesis focuses on understanding and improving the thermal degradation of PVC products.

1.3 Crosslinked Polyethylene

As mentioned above, PE is unsuitable for use as an electrical insulator for high voltage power transmission. The polymer must first be crosslinked to form crosslinked polyethylene (XLPE). When compared to the untreated polymer, XLPE has high tensile strength and high resistance to thermal and chemical stresses.[6] Additionally, the crosslinked polymer exhibits better retention of physical integrity when subjected to high electrical stress,[8] making it far superior for electrical insulator applications.

This thesis will focus on XLPE generated via a radical initiator. The specific organic peroxide and its mechanistic details are discussed in Chapter 2. The mechanism of radical crosslinking is well understood. A simple illustration of the crosslinking mechanism is shown below in Figure 1.2.

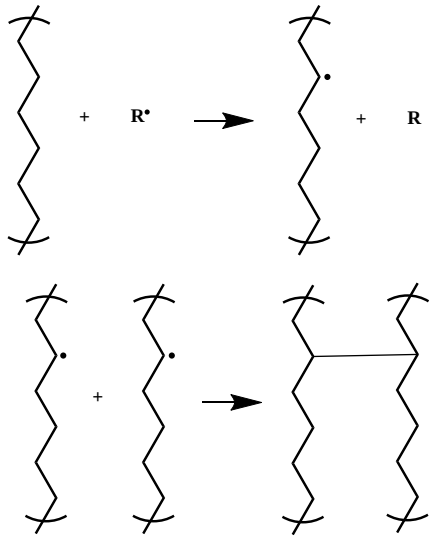

Figure 1.2. Simple mechanism for the radical-initiated crosslinking of polyethylene.

The studies in this thesis are relevant to XLPE used for low voltage (0.6-5 KV) to high voltage (>69 kV) power transmission cables.[9] Fabrication of XLPE-insulated cables generally consists of three basic steps:

1. Blending of PE, crosslink initiator, and any required additives at a low temperature;
2. Melt-extrusion of blended PE onto the conductor at an intermediate temperature;
3. High-temperature vulcanization of the resulting sheathed cable.

With the PE processing as described, the general design goal for crosslinking of PE is to minimize the level of crosslink during the first two steps while maximizing the ultimate level of crosslink achieved in the third step. This goal is usually achieved through the use of antioxidant additives.

1.3.1 Mechanistic Function of a Thiosynergist Antioxidant Additive

Chapter 2 of this thesis examines the behavior of a specific PE composition during the blending step. This composition was proposed to the Eckert-Liotta research group by collaborators at Dow Chemical and features the same compounds used in industry. Specifically, the compositions examined include a model for PE, dicumyl peroxide (DCP) as a crosslink initiator, and distearyl thiodipropionate (DSTDP) as an antioxidant stabilizer. The structures of DCP and DSTDP are shown below in Figure 1.3.

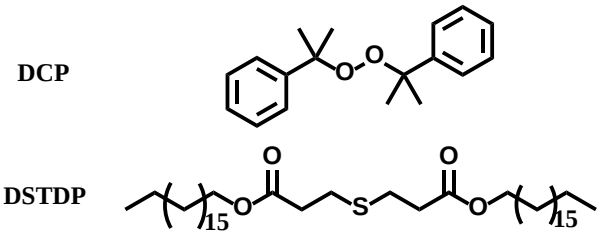

Figure 1.3. Chemical structures of the radical crosslink initiator (DCP) and antioxidant additive (DSTDP).

The performance of a PE blend can be measured using rheology. PE can be melted and a viscosity measured. As a sample undergoes crosslinking, the viscosity dramatically increases. The rate of this increase can be compared between different compositions and processing conditions. Researchers at Dow Chemical experimented with their PE compositions and discovered that when DCP and DSTDP were combined under a specific set of blending conditions (described in Chapter 2), a beneficial decrease in the rate of crosslinking was observed.[10] The exact cause of the beneficial results was unknown. Chapter 2 discusses in detail the efforts to understand the interaction between DCP and DSTDP in a nonpolar medium. An in-depth discussion of experiments, observations, and conclusions will be presented and combined into an overall reaction mechanism for the reactions of DCP with DSTDP.

1.3.2 Acid-Catalyzed Decomposition of DCP

As will be discussed in Chapter 2, the presence of DSTDP gives rise to acidic species that can react with DCP. A secondary portion of the work with PE focuses on this acid-catalyzed decomposition of DCP which is covered in detail in Chapter 3. The acid-catalyzed decomposition of DCP is mentioned in literature,[11,12] but has never before been thoroughly investigated. The work with DCP and DSTDP led to an accidental discovery regarding the mechanism of this acid-catalyzed reaction.

To simplify reactions and analysis, the interaction of DCP with DSTDP was monitored in dodecane as a model for polyethylene. Dodecane, as a nonpolar solvent, is an acceptable substitute as the liquid phase enables us to use traditional spectroscopic and analysis techniques. It was discovered that in such a highly nonpolar medium, the acid-catalyzed decomposition of DCP does not likely follow a simple protonation step. Rather, a complexation step gives rise to a more complex reaction system. The investigation into this reaction system is covered in detail in Chapter 3 of this thesis.

1.4 Polyvinyl Chloride

Concerns with PVC focus mainly on maintaining polymer performance after processing. The shelf-life and thermal resistance of PVC insulation sheaths are difficult to ensure because of the polymer's structure and degradation pathways. PVC is largely comprised of multiple vinyl chloride units. However, the polymer also invariably contains defect sites that are highly susceptible to thermal degradation.[13-15] These defects include allylic, tertiary, and vicinal chlorides as depicted below in Figure 1.4.

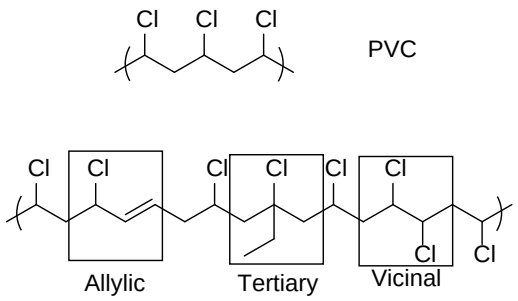

Figure 1.4. Structure of defect-free PVC along with the three common defects in the polymer backbone: allylic, tertiary, and vicinal defects.

The presence of defects in PVC means that polymer end products are necessarily vulnerable to thermal degradation. The problem of thermal degradation is exacerbated by the production of autocatalytic hydrogen chloride (HCl) gas. The liberated HCl can attack the PVC backbone and induce further degradation in a process known as "chain-unzipping." The autocatalysis is illustrated below in Figure 1.5.

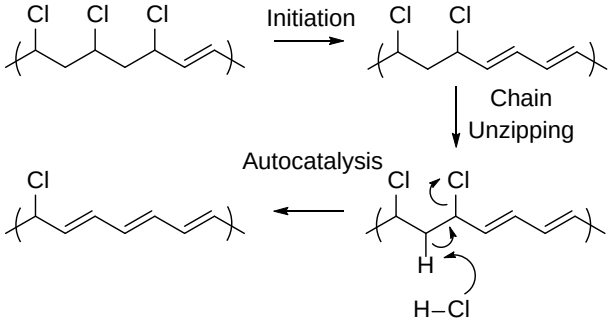

Figure 1.5. Initiation of PVC thermal degradation and subsequent "chain-unzipping" process.

To counteract the thermal vulnerability of PVC, stabilizers are often included in PVC products to mitigate degradation and maintain color and mechanical properties. Common commercial products employ metal stearate salts. In particular, this thesis focuses on calcium and zinc stearates as a synergistic stabilizer system.[16-18] A more detailed presentation of the function of these stabilizers is discussed in Chapter 4.

The primary goal of the PVC portion of this thesis is to investigate and understand the thermal degradation of PVC and its defects with the aim to improve thermal resistance. In particular, the interactions of thermal stabilizers with defect sites in PVC were investigated through the use of small model compounds that mimic the chemical properties of defects. The model studies were combined with weight loss data from blends of actual PVC polymer with various additives. The combined knowledge from model and polymer studies was used to synthesize and examine two novel stabilizer systems.

1.4.1 Model Compound Studies and Polymer Blend Studies

The investigation of structural and mechanistic details in the thermal degradation of PVC is inherently challenging. The structural changes of interest are small relative to the number of monomer units in the polymer. As such, literature contains numerous studies of small organic compounds that act as models for specific PVC structural elements.[19,20] However, many such studies examine the model compounds diluted in a solvent. Other studies do not pay attention to the particular stabilizer system of zinc and calcium stearates.[21,22] The studies contained in Chapter 4 therefore contain a suite of studies examining neat model compounds. First, a kinetic study allowed for the determination of the relative importance of various defects in the PVC system. Second, a qualitative color study allowed for the examination of the synergistic behavior of calcium and zinc stearates. Finally, thermogravimetric analysis of actual PVC blends gave more qualitative information regarding the effects of specific additives in PVC. Evidence from

these multiple lines of experimentation were combined to propose a modified mechanism of PVC stabilization.

1.4.2 Epoxidized Linolenic Acid Salts as Sacrificial Epoxide Stabilizers

Final PVC products almost always include a plasticizer to improve mechanical properties.[23] Plasticizers increase flexibility and workability of the polymer system and are therefore vital for the final end product. Dow Chemical employs epoxidized soybean oil (ESO) as a bio-based, sustainable plasticizer. As a bio-based compound, ESO avoids the negative environmental and health effects exhibited by traditional petroleum-derived plasticizers. The structure of ESO is shown below in Figure 1.6.

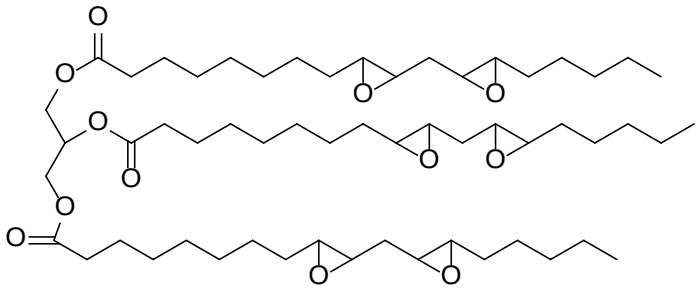

Figure 1.6. Structure of epoxidized soybean oil (ESO).

The oxirane rings in the structure of ESO are vulnerable to attack by HCl liberated via PVC degradation. The resulting structure is less compatible in the PVC matrix and therefore less effective as a plasticizer.[24] The focus of Chapter 5 of this thesis is the development and testing of a stabilizer that can protect the oxirane rings of ESO. Therein will be described the synthesis of our novel stabilizer and the experimentation showing its effectiveness.

1.4.3 Salts of Maleimidoundecanoic Acid as Novel PVC Stabilizers

The "chain-unzipping" process depicted in Figure 1.5 leads to long chains of conjugated polyenes in the PVC matrix. The polyene chains lead to color change (darkening to brown and black) and change the mechanical properties of the polymer. Additionally, chlorine atoms adjacent to the conjugated polyene chain are more labile and more likely to dehydrochlorinate. A possible strategy to combat the color change and increased lability that accompany polyene chains is to reduce the length of the polyene chains themselves. Two possible reactions are known that can readily reduce the extent of conjugation in polyene chains: the Ene reaction and the Diels-Alder reaction. Both reactions are illustrated below in Figure 1.7.

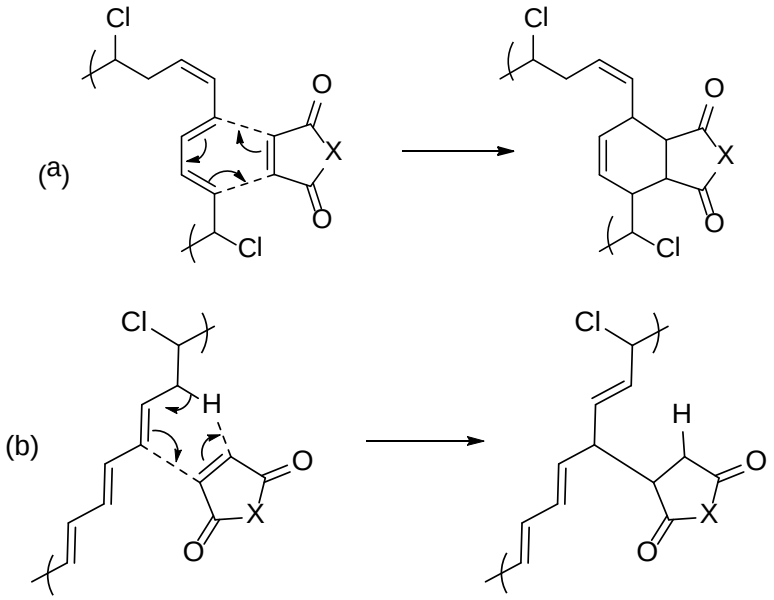

Figure 1.7. Conjugated polyene chain undergoing a (a) Diels-Alder reaction and a (b) Ene reaction.

Chapter 6 of this thesis discusses the synthesis and testing of a novel salt stabilizer system based on maleimidoundecanoic acid. Similar to Chapter 5, results will be presented to highlight the efficacy of our new stabilizers.

1.5 References

(1) History of Plastics www.plasticsindustry.org, 2015; Vol. 2015.

(2) Richardson, J.; Market outlook: Polymers world turned on its head; ICIS: 2013; Vol. 2015.

(3) Black, R. M. *The history of electric wires and cables*; IET, 1983.

(4) Terrell, C.; Wilford, S.; Frederic, H. American Electricians' Handbook**2008**.

(5) Piringer, O. G.; Baner, A. L. *Plastic packaging: interactions with food and pharmaceuticals*; John Wiley & Sons, 2008.

(6) Khonakdar, H.; Morshedian, J.; Wagenknecht, U.; Jafari, S. An investigation of chemical crosslinking effect on properties of high-density polyethylene. *Polymer* **2003**, *44*, 4301.

(7) Wypych, G. *PVC degradation & stabilization*; ChemTec Publishing, 2008.

(8) Han, S. J.; Gross, L. In *Electrical Insulation Conference and Electrical Manufacturing Expo, 2007*; Crosslinking and electrical characterization of metallocene linear low density polyethylene; IEEE: 2007, p 80.

(9) Mackevich, J. P.; Hoffman, J. Insulation enhancement with heat-shrinkable components. III. Shielded power cable. *Electrical Insulation Magazine, IEEE* **1991**, *7*, 31.

(10) Chaudhary, B. I.; Cogen, J. M.; Sun, Y. Dow Elastomers, Electrical and Telecommunications: Chemistry Options for Advanced Power Transmission Applications **2013**.

(11) Ogunniyi, D. S. Peroxide vulcanisation of rubber. *Progress in rubber and plastics technology* **1999**, *15*, 95.

(12) Leffler, J. E. Cleavages and Rearrangements Involving Oxygen Radicals and Cations. *Chemical Reviews* **1949**, *45*, 385.

(13) Frye, A. H.; Horst, R. W. The mechanism of poly (vinyl chloride) stabilization by barium, cadmium, and zinc carboxylates. I. Infrared studies. *Journal of Polymer Science* **1959**, *40*, 419.

(14) Frye, A. H.; Horst, R. W. The mechanism of polyvinyl chloride stabilization by barium, cadmium, and zinc carboxylates. II. Radioactive tracer studies. *Journal of Polymer Science* **1960**, *45*, 1.

(15) Frye, A. H.; Horst, R. W.; Paliobagis, M. A. The chemistry of poly (vinyl chloride) stabilization. III. Organotin stabilizers having radioactively tagged alkyl groups. *Journal of Polymer Science Part A: General Papers* **1964**, *2*, 1765.

(16) Atakul, S.; Balköse, D.; Ülkü, S. Synergistic effect of metal soaps and natural zeolite on poly (vinyl chloride) thermal stability. *Journal of Vinyl and Additive Technology* **2005**, *11*, 47.

(17) Bensemra, N.; Van, H. T.; Guyot, A.; Gay, M.; Carette, L. Thermal dehydrochlorination and stabilization of poly (vinylchloride) in solution: Part IV—

Synergistic effects of β-diketone compounds and metal soap stabilizers. *Polymer degradation and stability* **1989**, *24*, 89.

(18) Ureta, E.; Cantu, M. E. Zinc maleate and zinc anthranilate as thermal stabilizers for PVC. *Journal of applied polymer science* **2000**, *77*, 2603.

(19) Varma, I.; Grover, S. Thermal degradation of some model compounds of PVC. *Die Makromolekulare Chemie* **1974**, *175*, 2515.

(20) Asahina, M.; Onozuka, M. Thermal decomposition of model compounds of polyvinyl chloride. I. Gaseous thermal decomposition of model compounds having secondary and tertiary chlorine. *Journal of Polymer Science Part A: General Papers* **1964**, *2*, 3505.

(21) Boughdady, N.; Chynoweth, K.; Hewitt, D. Thermal Dehydrochlorination of Poly (vinyl chloride) Model Compounds. I. *Australian Journal of Chemistry* **1991**, *44*, 567.

(22) Blazso, M.; Jakab, E. Effect of metals, metal oxides, and carboxylates on the thermal decomposition processes of poly (vinyl chloride). *Journal of Analytical and Applied Pyrolysis* **1999**, *49*, 125.

(23) Amos, S.; Zweifel, H.; Maier, R. D.; Schiller, M. *Plastics Additives Handbook*; Hanser Verlag, 2009.

(24) Karmalm, P.; Hjertberg, T.; Jansson, A.; Dahl, R.; Ankner, K. Network formation by epoxidised soybean oil in plastisol poly (vinyl chloride). *Polymer degradation and stability* **2009**, *94*, 1986.

CHAPTER 2 – MECHANISTIC INVESTIGATION OF A POLYETHYLENE CROSSLINKING SYSTEM

2.1 Introduction

Polyethylene (PE) is one of the most widely used polymers globally. It is used in a wide variety of everyday products, such as plastic bags and bottles.[1] As ubiquitous and useful as PE is for everyday use, its mechanical and chemical properties leave it with low resistance to environmental effects and high stresses.[1-3] By comparison, crosslinked polyethylene (XLPE) has high tensile strength and higher resistance to thermal and chemical stresses.[3]

As such, XLPE is used in applications requiring a mechanically robust material including piping and power cable insulation.[4] As an additional benefit, XLPE retains its physical integrity when exposed to high electrical stress,[5] making it even more ideal for use as an electrical insulator. This chapter focuses on XLPE specifically as it's used as electrical insulation for high voltage power transmission cables. The chemistry involved is potentially valuable for a wider range of applications as well.

Power transmission cables can be manufactured under a variety of conditions. For the purposes of this chapter, I examine a process wherein a blend of polyethylene (including crosslinking agent and costabilizers) is melt-extruded onto a conductive cable at 140 °C. The polyethylene sheath is later vulcanized at temperatures up to 200 °C. Thus, PE blends may be subjected to a range of processing temperatures and, depending upon additives, a range of chemical environments.[5] The exact crosslinking mechanism and coadditives must be carefully selected for use in the intended temperature ranges.

The interaction of a crosslinking agent with coadditives at a specific set of conditions is the subject of this study.

An illustration of a representative power cable insulated by XLPE is shown below in Figure 2.1.

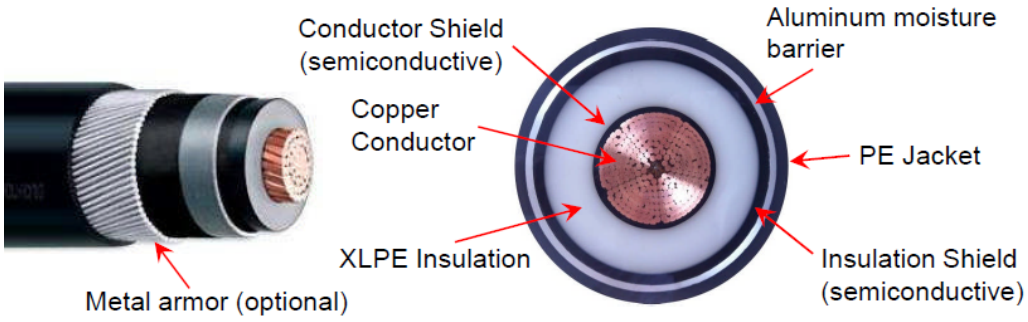

Figure 2.1. Representative high-voltage power transmission cable featuring an XLPE sheath. The layer of XLPE provides both mechanical strength and electrical insulation to the cable structure.[6]

The XLPE to be discussed in this chapter is suitable for low voltage (0.6-5 kV) to high voltage (>69 kV) power transmission applications.[4,6] The specific processing details of interest are discussed here.

2.1.1 Crosslinked Polyethylene Processing

There are several methods commonly used to produce XLPE from PE, including irradiation, reaction with peroxides, and reaction with silanes.[3] Peroxides reactions are common because the peroxide crosslinker can be selected based on cure rate and target degradation temperature.

2.1.1.1 Peroxide-Induced Crosslinking

This chapter focuses on the use of dicumyl peroxide (DCP) as the crosslink initiator for PE blends. DCP is a commonly used initiator in industrial PE processing.[5,7,8] The chemical structure of DCP is given below in Figure 2.2.

When heated, DCP homolytically cleaves at the oxygen-oxygen bond to give two cumyloxy radicals. The radicals are then free to propagate via abstraction of hydrogen atoms from surrounding species (for example, polyethylene chains). These radicals are capable of forming bonds, giving rise to crosslinked species. The general reaction scheme for radical crosslinking is shown below in Figure 2.2.

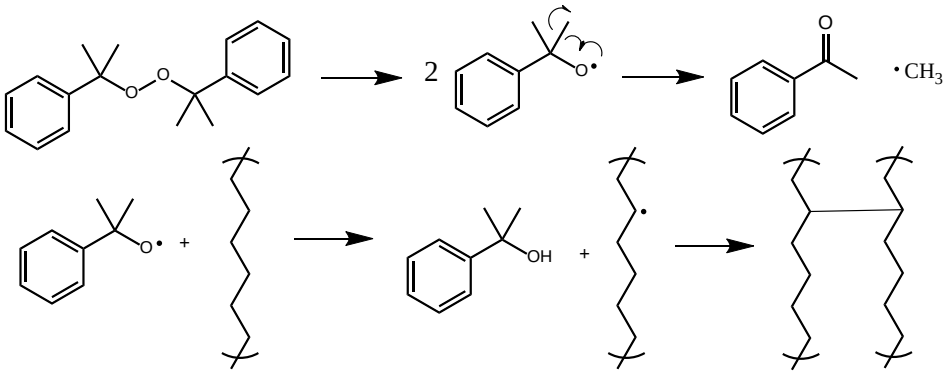

Figure 2.2. Peroxide-induced crosslinking of polyethylene using DCP (top-left structure). Two of the main products from this process include acetophenone (top-right) and cumyl alcohol (bottom-middle).[9]

Since DCP is commonly used in industry, its thermal decomposition kinetics are well-measured. The homolytic cleavage reaction is first order with an activation energy of 144 kJ/mol, with a half-life of 19 hours at 110 °C.[10] The half-life decreases dramatically with increasing temperature, lowering to approximately 1 minute at 180 °C. As will be discussed, the crosslinking step in the process of interest occurs between 140 – 180 °C.[5]

The thermal decomposition of DCP can lead to several end products through varying pathways. A detailed examination of possible products is available in literature.[9] By far the most common products from the thermal decomposition reaction are acetophenone and cumyl alcohol, both of which form from the cumyloxy radical as shown in Figure 2.2. The presence of DCP, cumyl alcohol, and acetophenone in reaction mixtures will be examined moving forward.

2.1.1.2 Radical Scavenging Antioxidants

Thermal stability in polyethylene crosslink blends entails the prevention of crosslinking before the melt is extruded onto a conductive cable. Crosslinking dramatically increases the viscosity of the melt and makes melt-extrusion impossible. As such, the level of crosslinking must be minimized through selection of an appropriate crosslink agent and through addition of costabilizers.

The antioxidant investigated in this chapter is distearyl thiodipropionate (DSTDP), which is commonly used in industry and known by a variety of trade names. DSTDP is a greasy, symmetric sulfide with the structure given below in Figure 2.3.

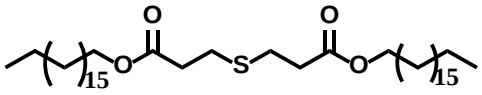

Figure 2.3. Structure of distearyl thiodipropionate (DSTDP).

There are two types of antioxidants used in crosslinking blends: chain-breaking antioxidants, and preventive antioxidants.[11] The two types of antioxidants typically work synergistically to prevent premature radical proliferation in polyethylene compositions. Chain-breaking antioxidants are intended to interrupt the chain of radical propagation,

usually by donating a labile hydrogen to form a more stable radical. Such a reaction slows the formation of additional radicals, thereby stabilizing the blend. Preventive antioxidants, on the other hand, are intended to convert hydroperoxides (formed via radical propagation[9]) into nonradical (less reactive) products.[11] A general scheme of the intended processes is shown below in Figure 2.4.

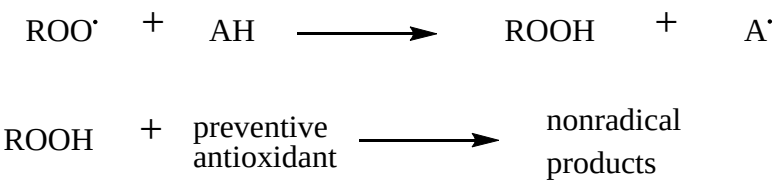

Figure 2.4. Mechanism of antioxidant scorch prevention. In this case, "AH" represents a chain-breaking antioxidant.[11]

More specifically, there are literature hypotheses for the mechanism of interaction of sulfide antioxidants with peroxides.[12] One hypothesis suggests that DSTDP interacts with peroxides to form a sulfoxide. The sulfoxide is then thought to undergo a retro-Michael addition reaction to form a sulfenic acid, which can then interact with any hydroperoxides to remove them from the system. A scheme detailing this proposed process is below in Figure 2.5.

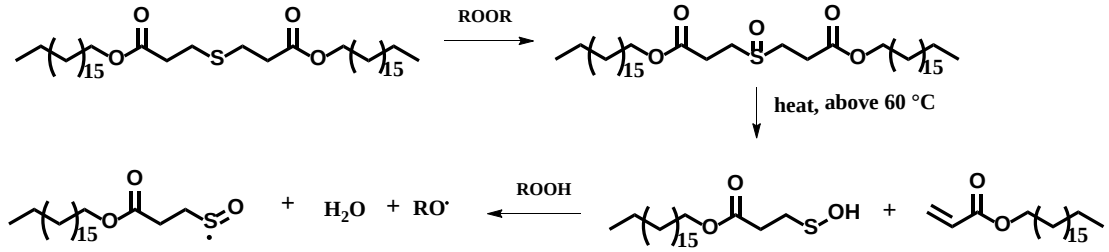

Figure 2.5. Hypothesized mechanism for interaction of DSTDP with organic peroxide.[12] The end radical products can combine with themselves or other radical species in the system to give nonradical products.

It should be noted that the hypothesized scheme in Figure 2.5 is not intended to be comprehensive. The interaction of DSTDP with DCP is likely complex, with many

possible products and intermediates. This chapter discusses the detailed investigation of the complete interaction of the two species DCP and DSTDP.

2.1.1.3 Polyethylene Compounding and Processing Conditions

The three steps in PE crosslinking are compounding, melt extrusion, and crosslinking (vulcanization). Compounding is the physical incorporation of necessary additives into PE pellets. Ordinarily, a sample of pellets is placed into a mechanical mixer above the melting point of polyethylene. The melting point of PE ranges depending on density and molecular weight, but most PE used for cable insulation melts between 104 °C – 110 °C.[13] Once the PE pellets are fully melted, the peroxide, antioxidants, and coagents are added. Components are mixed for 5 minutes, cooled, and prepared for extrusion.

The extrusion process generally takes place at approximately 140 °C. During this stage, blended PE pellets are physically extruded onto a conductor. The temperature is kept near this temperature to prevent rapid and complete decomposition of the peroxide.[6,14,15] The extrusion process lasts for 5 – 10 minutes.

The crosslinking stage occurs after extrusion. The conductor (and accompanying PE sheath) is passed through a tube furnace with pressurized nitrogen at 180 °C – 200 °C for approximately 5 minutes.[5] During crosslinking, almost all peroxide is decomposed and the PE sheath becomes maximally crosslinked. The half-life of the thermal decomposition reaction of DCP at 180 °C is approximately 1 minute[16], so the decomposition proceeds rapidly.

2.1.1.4 Research Problem: Reduction in Premature Crosslinking

The extent of crosslink in polyethylene is measured using rheometry. A moving die rheometer measures the torque required to spin a pair of parallel disks containing a liquid sample. The torque required to shear the sample increases as the level of crosslinking increases. As such, the required torque increases as a function of time for a sample subjected to high temperatures.[6,15] Figure 2.6 below shows a typical plot generated by a moving die rheometer for a heated sample of PE.

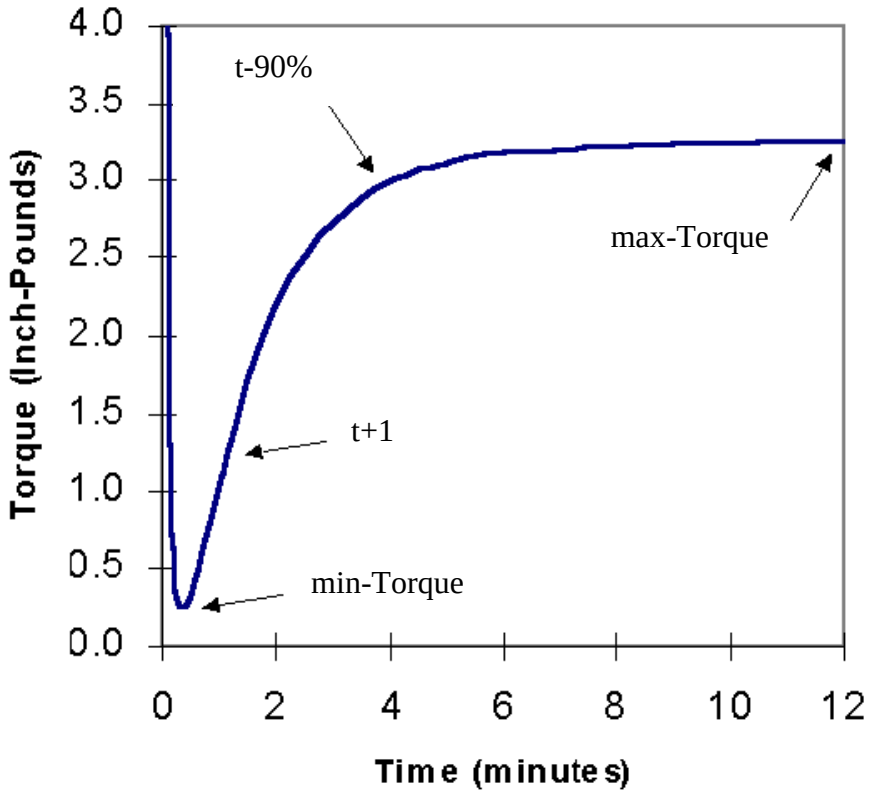

Figure 2.6. Moving die rheometer results for a polyethylene sample. Torque required increases as a function of crosslinking.
min-Torque = minimum torque; max-Torque = maximum torque; t-90% = time to reach 90% of max-Torque; t+1 = time to reach (min-Torque + 1 inch-pound)[6]

Shown in Figure 2.6 are several numerical criteria used to evaluate the crosslinking performance of a PE blend, all of which are related to the minimum and maximum torque values reported for a particular sample. The characteristic "t+1" is

particularly powerful for evaluating the performance of a PE-additive blend. It measures the initial rate of crosslinking in a sample which reveals its viability for a melt-extrusion process. "t+1" is typically obtained at extrusion temperatures (approximately 140 °C), while "max-Torque" is obtained at curing temperature (180 °C – 200 °C). Results for a blend using DCP and DSTDP are tabulated below.

Table 2.1. Reduction in premature crosslinking induced by the special blending technique employed by Dow Chemical. The examined blend includes 98 wt% polyethylene, 1.70 wt% DCP, and 0.30 wt% DSTDP.[6]

	Compounding Procedure (melt blend, 120 °C)	**Blending Procedure (proprietary)**
ΔTorque† (dN-m), 180 °C	3.9	3.0
t+1 at 140 °C (minutes)	36	180
Normalized scorch improvement* (minutes)	1	132

†ΔTorque = max-Torque – min-Torque
*Normalized versus formulation that contains ONLY peroxide and PE

Table 2.1 contains crosslinking performance data from PE compositions created using two different mixing techniques: a traditional compounding method highlighted above, and the proprietary method developed by Dow Chemical researchers. A PE blend with DCP and DSTDP was produced using each technique. Samples from each blend were then examined via rheology at multiple temperatures to gather the performance data in the table above.

The data in Table 2.1 show a profound reduction in premature crosslinking when the special blending procedure is used in place of the typical compounding procedure. The "t+1" is dramatically increased by a factor of 5, representing a large decrease in the rate of crosslinking at the extrusion temperature. This is accompanied by only a minor decrease in the total crosslink level, reported by ΔTorque. It is clear that the special

blending procedure, used with DCP and DSTDP, provides an excellent reduction in premature crosslinking.

There are several other observations relating to the beneficial combination of DCP and DSTDP for preventing early crosslinking. The beneficial effects are only observed if the blending procedure is completed under an air atmosphere. Attempts to use the blending procedure under nitrogen could not produce the beneficial effects shown in Table 2.1. Additionally, the beneficial effects are not observed if DCP and DSTDP are heated separately and then mixed. There is a required interaction between the two compounds that begets the observed benefits. Finally, Dow researchers examined several peroxides with DSTDP using the blending technique. The other peroxides include di-(tert-butylperoxyisopropyl)benzene (BIBP), 2,5-bis(tert-butylperoxy)-2,5-dimethylhexane (BTBPDMH), and di-tert-amyl peroxide (DTAP) (all shown in Figure 2.58). The largest beneficial effect was observed with DCP.[6] In order of ability to prevent premature crosslinking, the performance of the 4 peroxides was DCP>BIBP>BTBPDMH>DTAP. In other words, DCP exhibited the least premature crosslinking, while DTAP exhibited the most. The observations listed here were used in designing our investigation and influenced our conclusions.

The goal of this work was to determine the exact nature of the interaction between DCP and DSTDP and to thereby explain the reduction in premature crosslinking. Our approach incorporated all the observations reported to us by Dow Chemical. The detailed approach we took and the results we obtained are included below.

2.2 Methodology

In a broad sense, a set of overarching research goals was developed to organize the investigation into the interaction of DCP and DSTDP. The four goals were formulated as follows:

1. Examine the kinetics of DCP thermal decomposition under relevant conditions.
2. Determine the effects of DSTDP on the DCP decomposition under both air and inert atmospheres.
3. Screen various sulfur functionalities and radical scavengers and determine their impact on the reaction system.
4. Screen any possible impurities in the reaction components and identify their effects on the system, if any.

Initial investigations sought to answer the questions posed by the four research goals. The interaction between DCP and DSTDP represents a powerful method of radical inhibition which was initially very poorly understood. The experimental techniques employed in addressing the four research goals are summarized below.

2.2.1 Materials

Dicumyl peroxide, dodecane, and meta-chloroperbenzoic acid (used as discussed later) were obtained from Sigma-Aldrich. Argon and helium were obtained in high-pressure cylinders from Airgas. Distearyl thiodipropionate was obtained from City Chemical, LLC.

2.2.2 Reaction techniques

The observations made by Dow Chemical (Table 2.1) were gathered from a system involving solid PE pellets. A multiphase system is inherently much more difficult to analyze than a homogeneous solution. As such, dodecane was employed as a model solvent to emulate the chemical environment of polyethylene. As an unbranched, saturated hydrocarbon, dodecane allows a way to produce homogeneous solutions and a good imitation of polyethylene.

By far the most common reaction technique used in this chapter was the heating of solutions via hot oil baths. Reaction solutions were typically reacted in small (10-30 mL) glass roundbottom flasks for cylindrical vials. The reactor vessels were then placed into well-stirred baths of silicone oil heated to the desired temperature and monitored with a mercury thermometer.

Reaction solutions were generally prepared from stock solutions. Usually, a stock solution was prepared at a large volume (~100 mL) and at double the required concentration for reaction. For example, if a reaction called for 0.0589 M DCP, the stock solution was prepared at 0.1178 M DCP. The stock solution could be combined with other stock solutions (or diluted with dodecane) to reach the target reaction concentration.

The compositions of reaction mixtures were identified and measured using a combination of nuclear magnetic resonance (NMR), gas chromatography and mass spectroscopy (GC-MS), and high-pressure liquid chromatography (HPLC).

2.2.3 High-Pressure Liquid Chromatography

Samples prepared for HPLC were diluted at either 1 part sample to 3 parts isopropanol or 1 part sample to 4 parts isopropanol, measured using a 1000 µL micropipette. HPLC spectra were gathered using a Shimadzu LC-20AD Liquid Chromatograph with SPD-20A UV-Visible detector. The column was a Shimadzu C18 4.6 mm x 50 mm column with a 5 µm particle size. The mobile phase was 85% methanol / 15% water at a flow rate of 1 mL / minute. LC was used primarily for tracking the concentration of DCP and some of the reaction products in the reaction mixture.

2.2.4 Gas Chromatography and Mass Spectroscopy

Samples prepared for GC were diluted at exactly 1 part sample to 3 or 4 parts isopropanol. GC spectra were gathered using a Shimadzu GCMS-QP2010S with a Supelco PTA-5 column. The inlet temperature was 250 °C and a constant velocity method was used with a velocity of 40 cm / second. The oven used a variable temperature method starting at 150 °C for 5 minutes and ramping at 25 °C per minute to 250 °C for 6 minutes. The mass spectrometer ion source and interface were set at 225 °C. GC spectra aided in product identification and quantification.

2.2.5 ^{1}H Nuclear Magnetic Resonance

Some reactions were sampled and prepared for NMR analysis. Small aliquots were taken and diluted at approximately a 1:3 ratio with $CDCl_3$. Proton NMR spectra were gathered using a Brüker 400 MHz NMR instrument and Topspin processing software. Spectra were taken using 16 scans with 2-second relaxation time. NMR was used mainly for product identification.

2.3 Thermal Decomposition of DCP

The first step in examining the interaction of DCP with DSTDP was to characterize the thermal behavior of DCP alone. This allowed for the deconvolution of the reaction products formed from the systems of DCP and of DCP and DSTDP. As such, initial experiments were run to gather kinetic parameters for DCP thermal decomposition.

2.3.1 HPLC Rate Determination

A solution of DCP in dodecane was prepared at 2 wt% (0.0589 M) to be representative of the systems studied by Dow Chemical. Solutions with this initial concentration were heated at temperatures between 110 °C – 150 °C for times of up to 8 hours. The concentration of DCP remaining as a function of time was determined for each reaction by HPLC peak integration. A representative HPLC chromatogram is shown below in Figure 2.7.

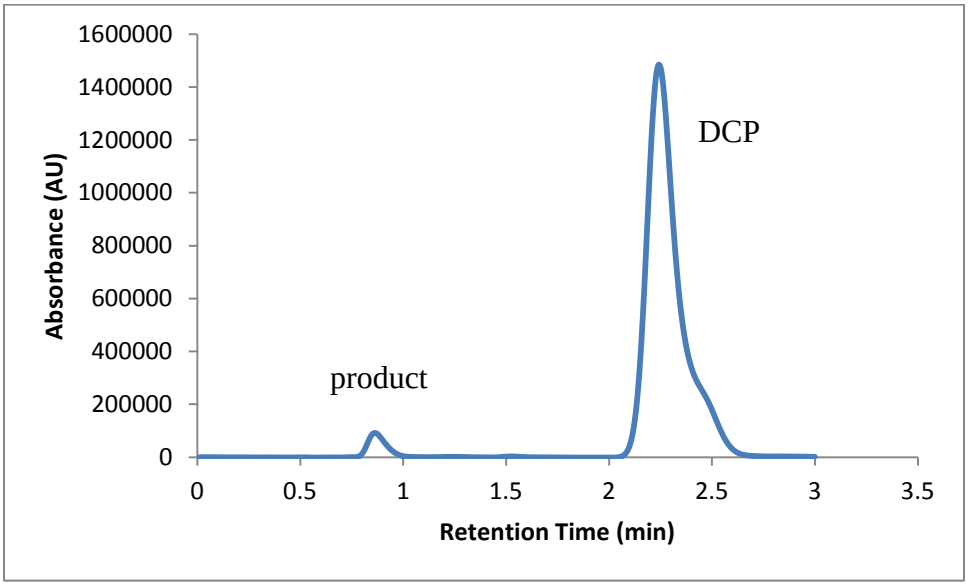

Figure 2.7. Representative HPLC chromatogram of the reaction of 0.0589 M DCP at 120 °C for 30 minutes.

The DCP peak in Figure 2.7 was identified using both UV absorption and a standard solution of DCP run through the same LC method. The other visible peak is a product formed via thermal decomposition of DCP. The area under the DCP peak was correlated to the concentration of DCP using a calibration curve. The calibration curve is provided below for examination as Figure 2.8.

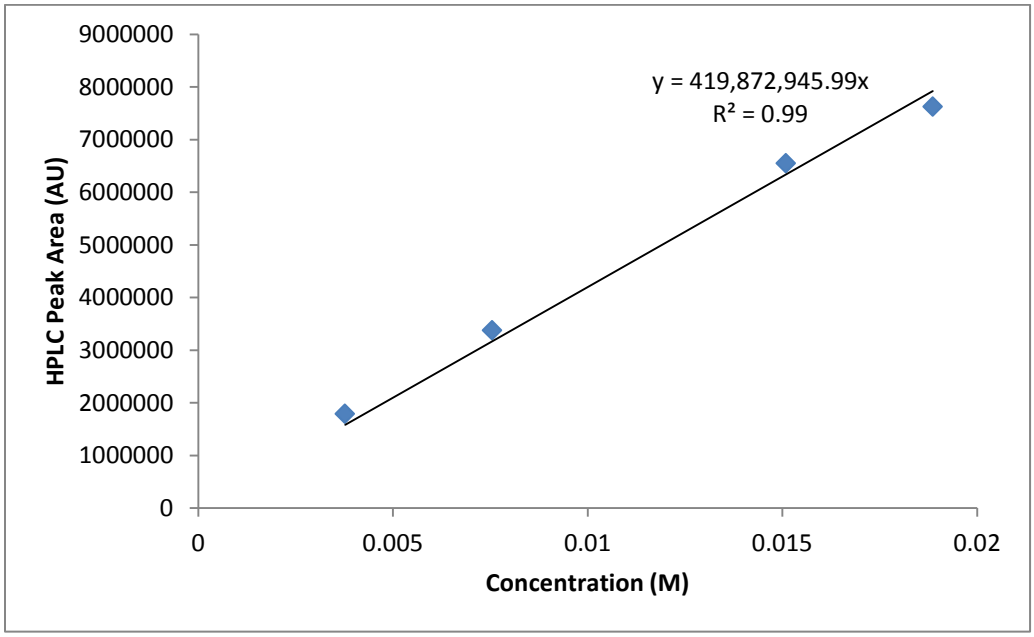

Figure 2.8. HPLC calibration curve for DCP in solutions of dodecane. The concentrations are reported after the dilution of each sample by a factor of 3.

With a reliable HPLC technique for measuring DCP and a calibration curve to obtain concentrations, a kinetics analysis was conducted. Solutions of DCP were placed into cylindrical glass vials and stir bars. The reactors were then placed into a heated oil bath for the duration of reaction. Samples were removed from the reactors via syringe

periodically for analysis. A plot of DCP concentration as a function of time at various temperatures is shown below as Figure 2.9.

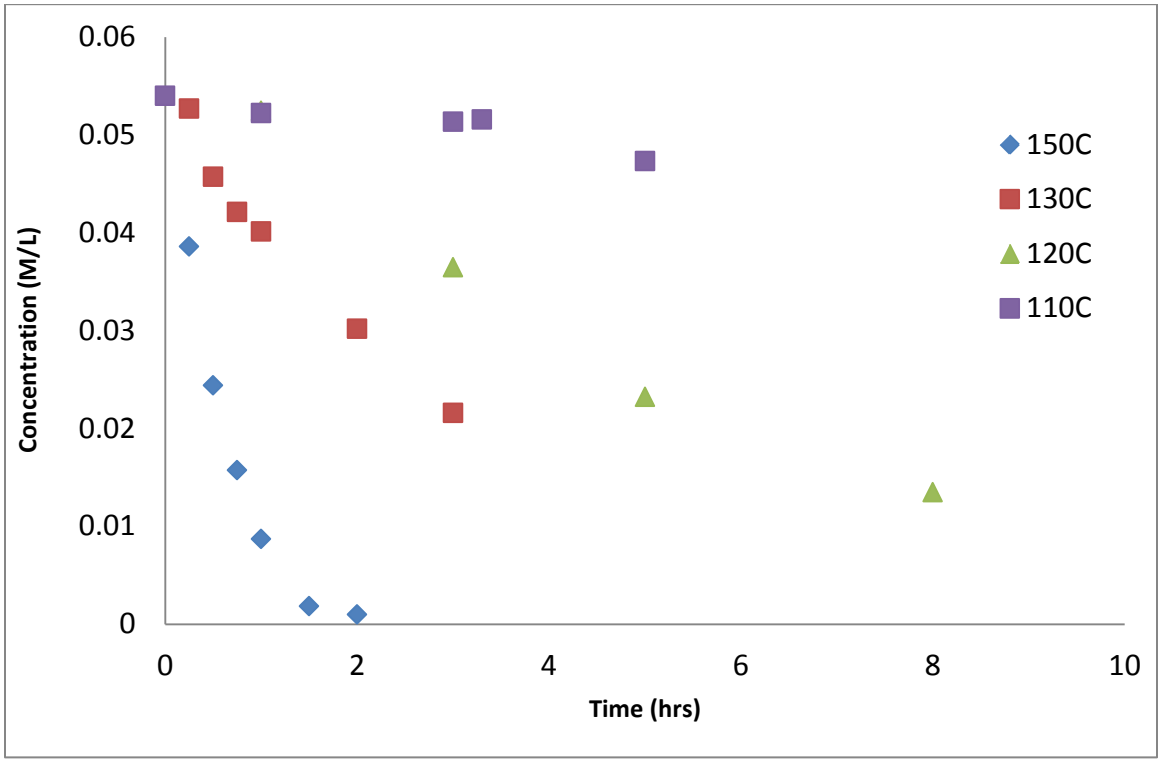

Figure 2.9. DCP concentrations as a function of time at various temperatures.

As expected, the rate of DCP decomposition increases dramatically as the reaction temperature increases. The decomposition of DCP is due to a homolytic cleavage to form 2 cumyloxy radicals. As such, the reaction is expected to follow a first-order rate law. Following simple kinetics derivations for a first-order reaction, the linearized form is shown in Figure 2.10.

$$ln\left(\frac{C_0}{C}\right) = kt$$

Figure 2.10. Linearized form of the first-order decomposition rate expression.

With the linearized form of the first-order decomposition, the DCP decomposition data was plotted on a first-order plot as below in Figure 2.11.

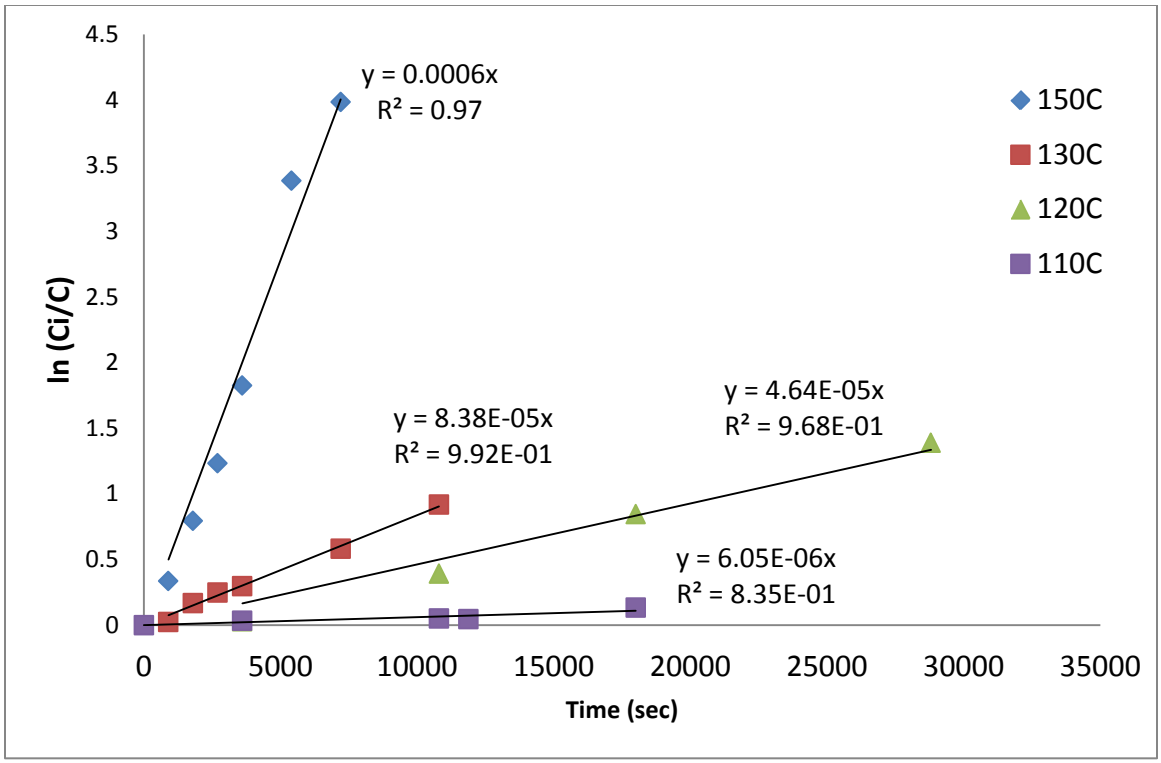

Figure 2.11. First-order plot for the thermal decomposition of DCP in dodecane.

The linearized data in Figure 2.11 confirm the first-order behavior of DCP thermal decomposition. If the reaction were not first order, the lines in the first-order plot would not appear linear. The R^2 values are, for the most part, very close to 1 and confirm the first-order hypothesis. The slopes of the fit lines in Figure 2.11 were taken to be the first-order rate constants at each temperature in accordance with Figure 2.10. The natural log of the rate constants was plotted against inverse temperature to form an Arrhenius plot as shown below in Figure 2.12.

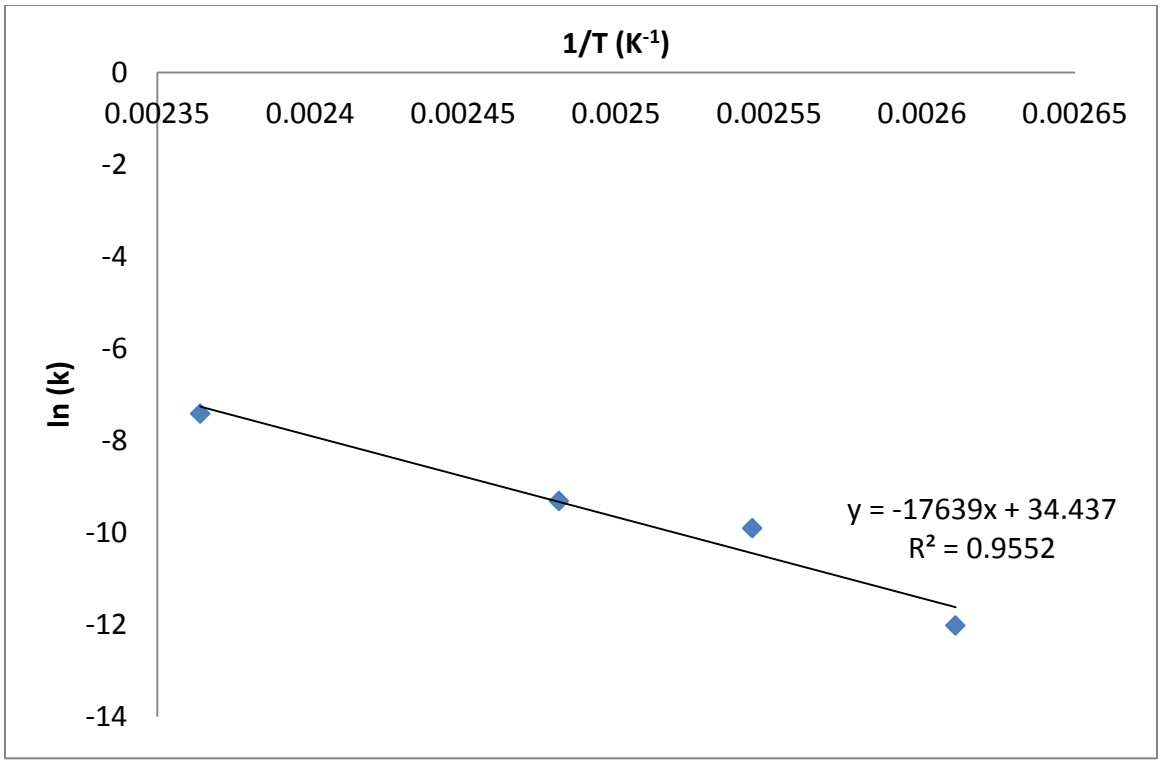

Figure 2.12. Arrhenius plot for the thermal decomposition of DCP in dodecane.

The slope of the fit line in the Arrhenius plot allows for the calculation of activation energy. A simple derivation using Arrhenius kinetics is shown below in Figure 2.13.

$$k = Ae^{\frac{-E_a}{RT}}$$

$$\ln k = \ln A - \frac{E_a}{RT}$$

Figure 2.13. Linearization of the Arrhenius equation. The linearized form reveals that the slope of the fit line on the Arrhenius plot is equal to $-E_a/R$.

The activation energy was determined from the Arrhenius plot to be 147 kJ / mole. Literature records the activation energy to be 144 kJ / mole.[9,16] At this stage, the agreement of this measured activation energy with literature values was taken as

validation of the experimental technique. It appears the methodology is valid for at least the thermal decomposition of DCP.

2.3.2 Identification of Products By NMR

As shown in Figure 2.2, the expected products from the thermal decomposition of DCP are acetophenone and cumyl alcohol. To confirm that the model system in dodecane accurately represents polyethylene systems, thermal reaction systems were examined with NMR. To begin, a sample was examined of 4 wt% DCP in dodecane (0.1178 M) with a capillary of DMSO-D6. The proton NMR spectrum is shown below in Figure 2.14.

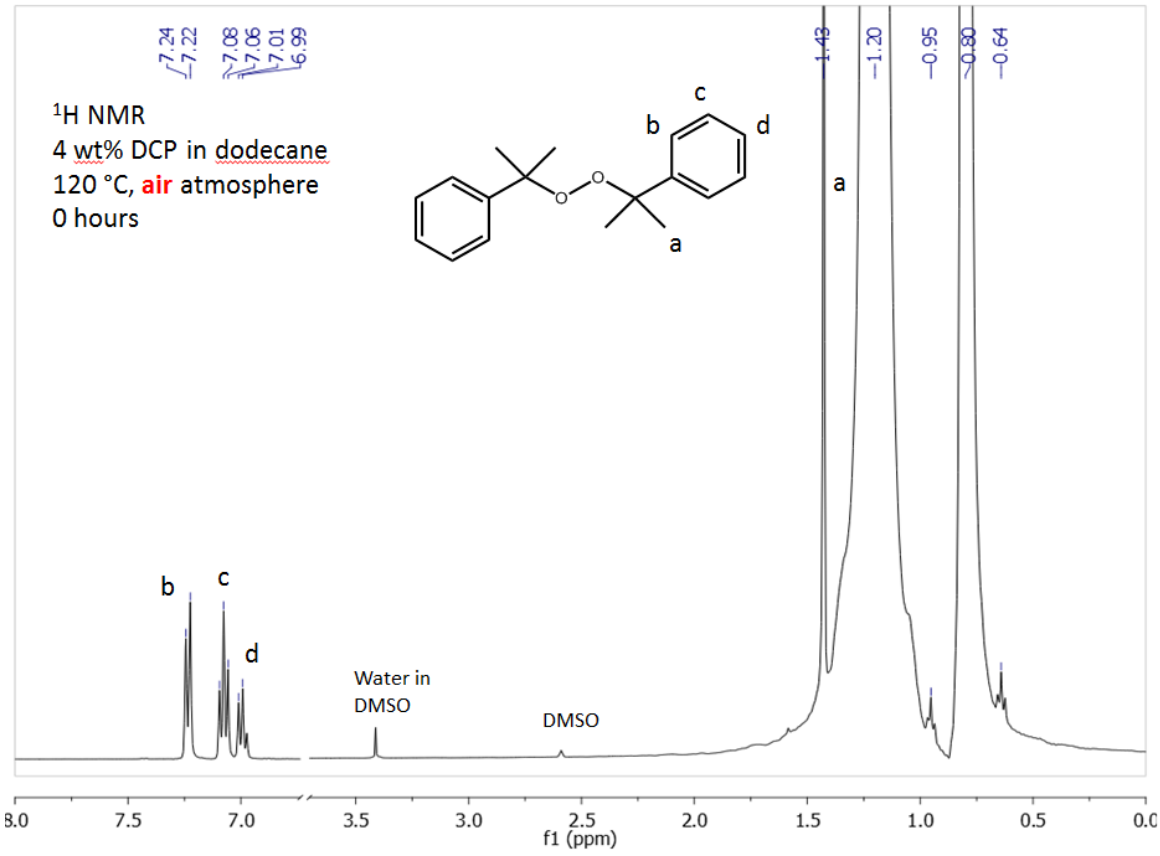

Figure 2.14. Proton NMR of 0.1178 M DCP in dodecane. A capillary of DMSO-D6 was used as a lock solvent.

The peaks in the unreacted NMR spectrum are easy to identify as the only species present are DCP and dodecane. The peaks corresponding to DCP are labeled ‘a’, ‘b’, ‘c’, and ‘d’. The two large peaks at 0.80 ppm and 1.20 ppm correspond to dodecane. We also examined a sample of DCP at the same concentration (0.1178 M) after a thermal treatment at 120 °c for 3.5 hours. The resulting NMR spectrum is shown below in Figure 2.15.

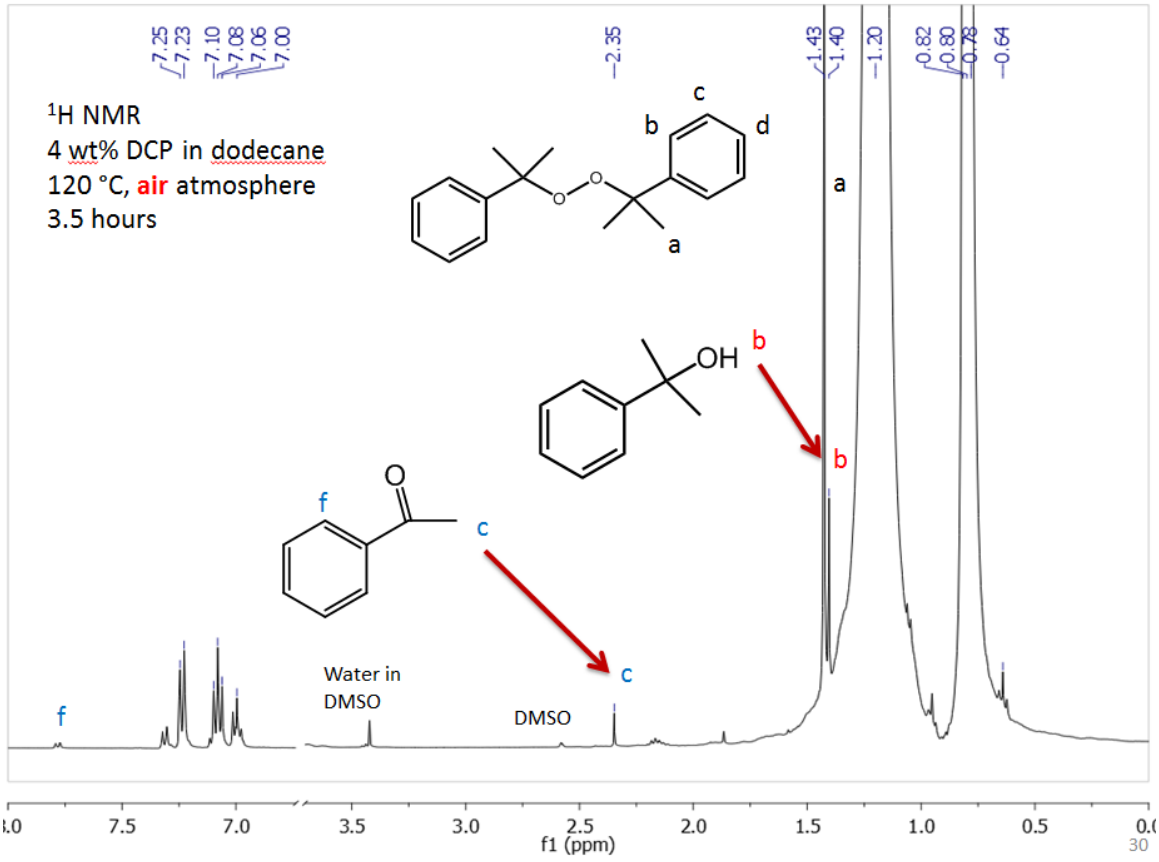

Figure 2.15. Proton NMR of 0.1178 M DCP in dodecane after 3.5 hours at 120 °C. The two expected products, cumyl alcohol and acetophenone, are identified by their methyl protons.

The proton NMR of the post-heating DCP sample reveals what is reported in literature: the only two products worth noting are cumyl alcohol, labeled with the red ‘b’, and acetophenone, labeled with the blue ‘c’. There are some other minuscule peaks that appear in the spectrum, but they are not in high enough concentrations to be significant.

The presence of acetophenone in solution was confirmed by spiking a sample of 0.1178 M DCP heated at 120 °C for 3.5 hours with acetophenone. The proton NMR of this spiked sample is shown below in Figure 2.16.

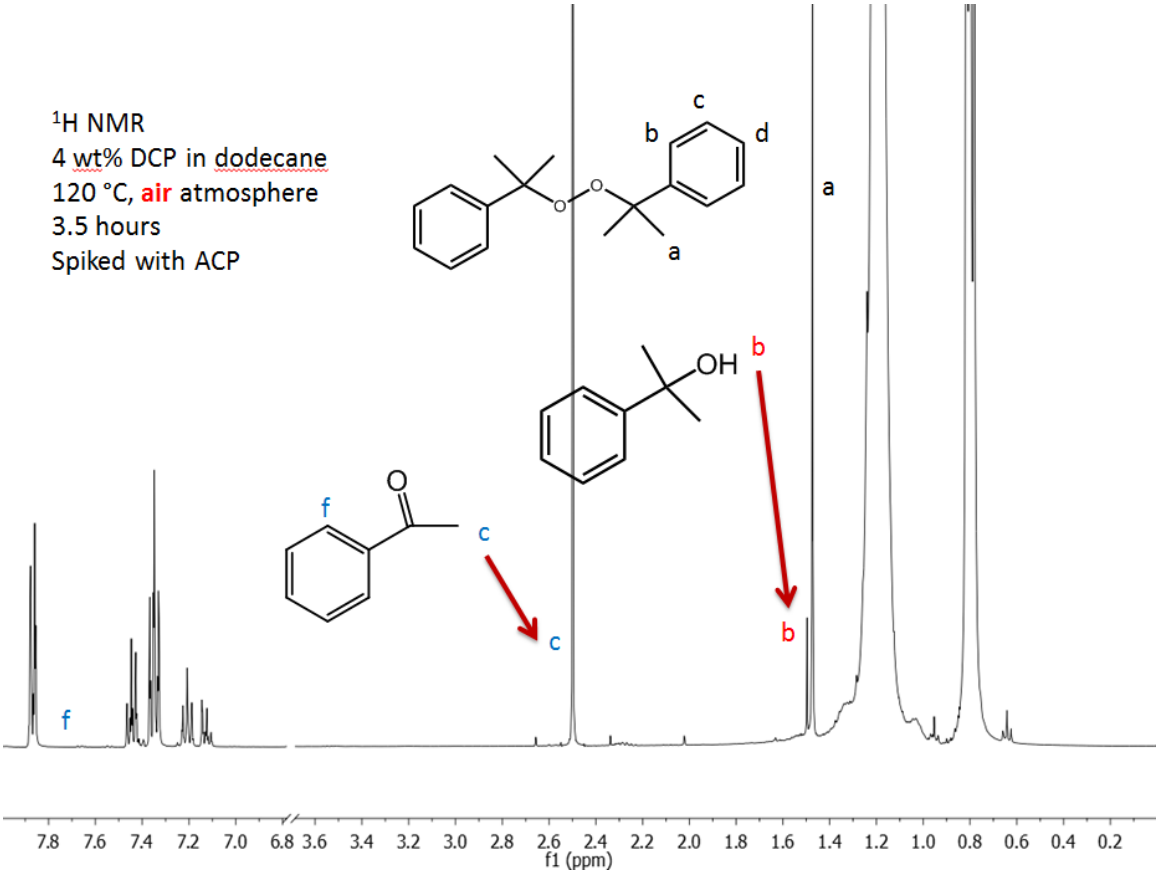

Figure 2.16. Proton NMR spectrum of a standard of acetophenone in dodecane.

Figure 2.15 shows a doublet at 7.75 ppm in the aromatic region, labeled with a blue 'f', and a peak at 2.35 ppm. Spiking the reaction sample with acetophenone (Figure 2.16) caused both of these peaks to increase in magnitude and did not produce any new peaks. This concretely demonstrates that acetophenone is observed from the thermal decomposition of DCP in dodecane.

The chemical shift of the methyl protons of cumyl alcohol (labeled with the red 'b' in Figure 2.15 and Figure 2.16) changes slightly between the two figures. This is due

to the fact that Figure 2.16 was obtained using $CDCl_3$ as the lock solvent (instead of a capillary of DMSO-d6. This slightly changes the chemical environment, resulting in a slightly different shift relative to DCP.

After identification of cumyl alchol and acetophenone via NMR, we quantified these species in reaction solutions as a function of time.

2.3.3 Quantification of DCP Thermal Decomposition Products

With the HPLC method described above, DCP elutes relatively quickly (under 3 minutes). However, acetophenone and cumyl alcohol elute at the same time, making quantification impossible. Therefore, for these experiments, a gradient HPLC method was employed.

The gradient method was used with a Waters 2960 HPLC and Waters 996 PDA detector. The column was a C-18 X Bridge Column with 2.1 mm internal diameter x 50 mm length and 3 micron particle size. The mobile phase started at a ratio of 70:30 methanol:water and increased to 85:15 methanol:water over the course of 8 minutes. This phase was sufficient to separate the peaks of cumyl alcohol and acetophenone on the chromatogram. Calibration curves were created for these species and concentrations were plotted as a function of time at various temperatures. The results are shown below in Figure 2.17 and in Figure 2.18.

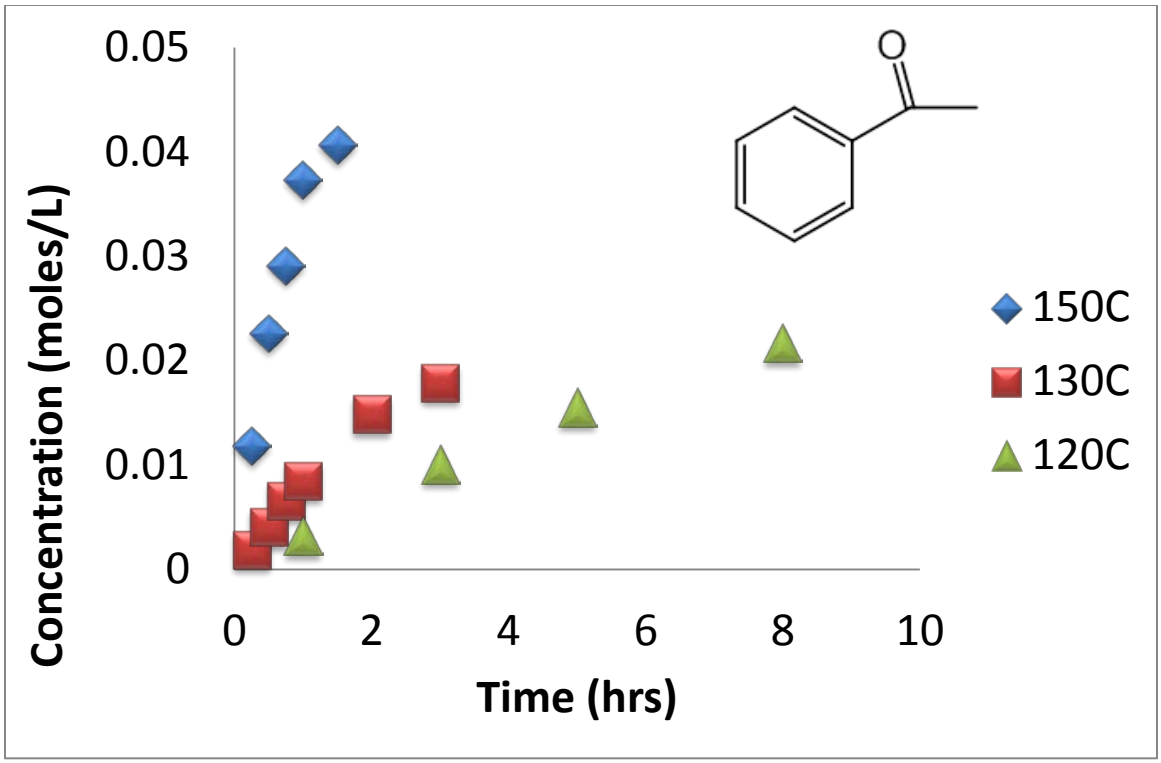

Figure 2.17. Concentration of acetophenone as a function of time for the reaction of 0.0589 M DCP in dodecane at various temperatures.

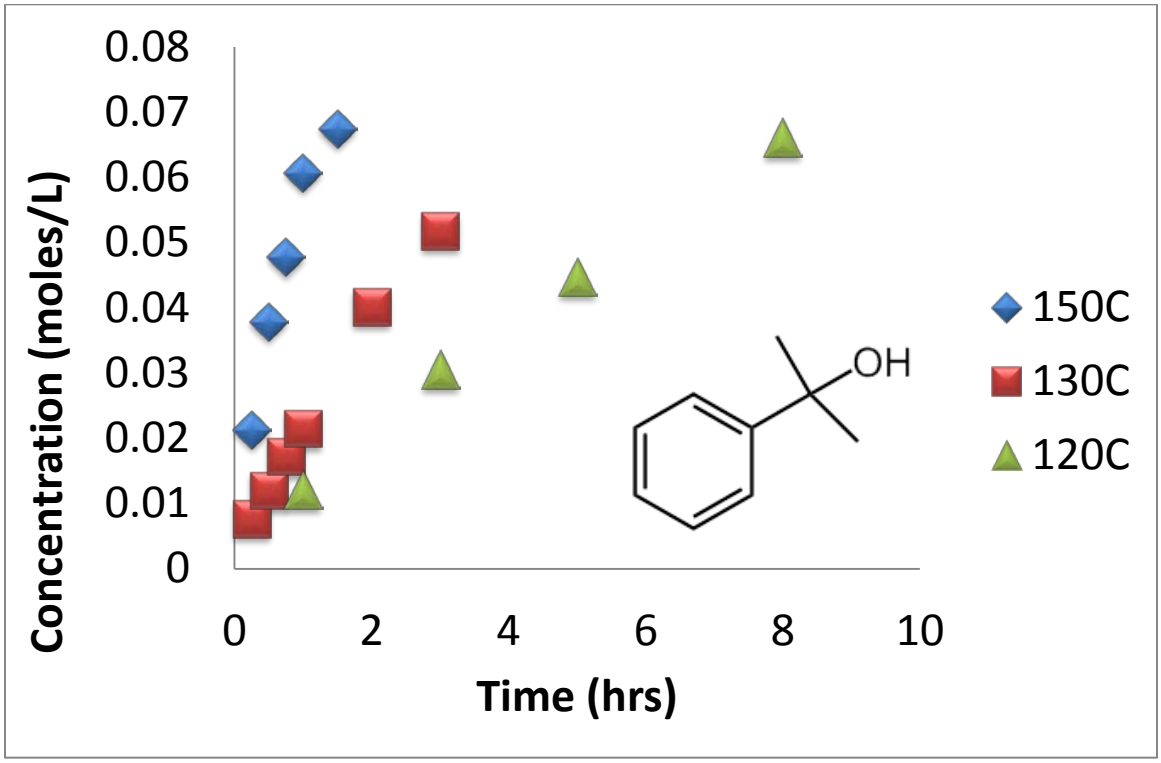

Figure 2.18. Concentration of cumyl alcohol as a function of time for the reaction of 0.0589 M DCP in dodecane at various temperatures.

Notice that the concentration of cumyl alcohol in Figure 2.18 reaches values higher than the starting DCP concentration of 0.0589 M. If the concentrations of acetophenone and cumyl alcohol are added together, the sum of the two species begins to approach double the starting concentration (0.1178 M). This is expected, as each mole of DCP can homolytically cleave to form 2 cumyloxy radicals. Each cumyloxy radical can form either of the two end products as shown in Figure 2.2. The ratios of the two products of thermal decomposition are plotted below in Figure 2.19.

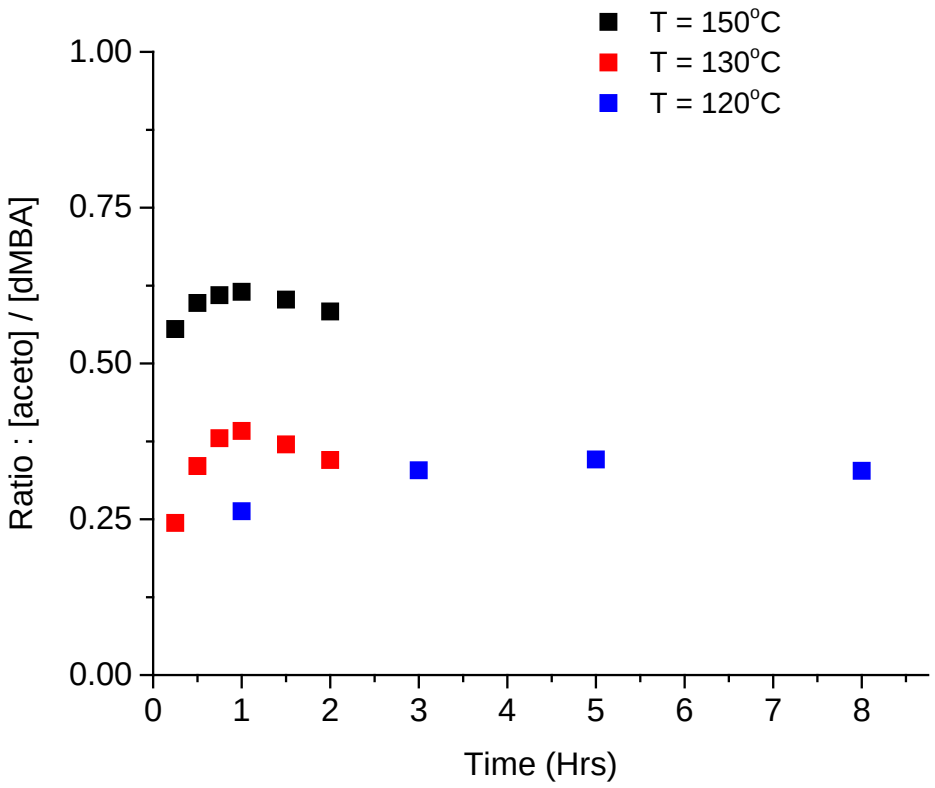

Figure 2.19. Concentration ratios of acetophenone:cumyl alcohol at various temperatures. The abbreviation dMBA stands for dimethyl benzyl alcohol, synonymous with cumyl alcohol.

As can be seen in Figure 2.19, the ratio of [acetophenone]:[cumyl alchohol] increases (particularly at early times) as temperature increases. This can easily be

explained by the mechanisms of formation for each of the two species shown in Figure 2.2. Formation of cumyl alcohol proceeds through hydrogen atom abstraction from any of the species in solution. Meanwhile, formation of acetophenone proceeds through an energetic rearrangement and liberation of a methyl radical. The formation of acetophenone is therefore expected to have a higher activation energy and require higher temperatures. This would account for the trend seen in Figure 2.19.

2.4 Thermal Decomposition of DCP Under Argon

The beneficial interaction of DCP with DSTDP only occurred when the two species were cured in air. That fact on its own does not provide much information. DCP and DSTDP may, separately, have distinct behaviors when heated in air or under inert atmosphere. Further, the interactions between the two species may be different in air and under inert atmosphere. It was therefore critical to examine the thermal decomposition of DCP under both air (in the previous section) and under an inert atmosphere.

To determine the effect of atmosphere on DCP thermal decomposition, many of the reactions from the previous section were repeated under argon.

2.4.1 Determination of DCP Thermal Decomposition Products Via NMR

Reactions of DCP in dodecane were carried out in the same vessels as the reactions described in the previous section. For these experiments, the vials were sealed with nylon lids and o-rings and the headspace was thoroughly purged with a flow of argon. Argon was also gently sparged through the liquid reaction medium. The reactors were kept under a positive pressure of argon with a needle during the course of reaction.

A proton NMR spectrum was measured of the reaction system before and after reaction at 120 °C for 3.5 hours. The spectrum before reaction looks identical to that shown in Figure 2.14. The spectrum after reaction is shown below in Figure 2.20.

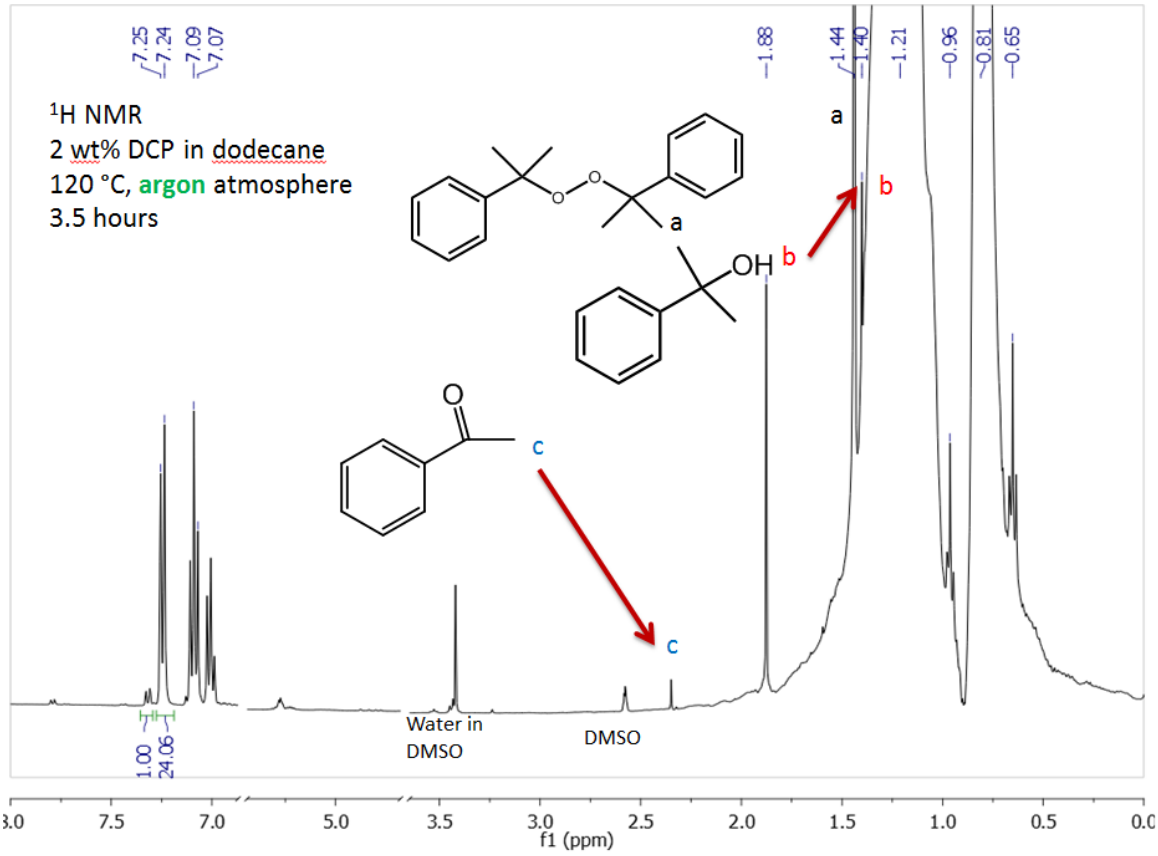

Figure 2.20. Proton NMR spectrum of 0.0589 M DCP in dodecane after 3.5 hours at 120 °C. Reaction was carried out under positive argon pressure after an argon purge. The two expected products, cumyl alcohol and acetophenone, are identified by their methyl proton shifts.

The most important observation regarding Figure 2.20 is that it looks identical to Figure 2.15. The same two expected products, cumyl alchol and acetophenone, are identifiable as shown previously. The large peak at 1.88 ppm is acetone introduced by washing our NMR tubes (confirmed by spiking the sample). No other significant products are observed. It is concluded that the product distribution from the thermal

decomposition of DCP is independent of atmosphere. The products were identical for the reactions open to air and those under argon.

2.4.2 Rate Determination of DCP Thermal Decomposition Using HPLC

The possibility had to be considered that although the products of thermal decomposition of DCP (cumyl alcohol and acetophenone) were identical, the presence of atmosphere oxygen could alter the rate of thermal decomposition. The concentrations of DCP in reaction samples were tracked using an isocratic HPLC method as discussed previously.

A sample of 0.0589 M DCP was thermally decomposed over the course of 5 hours at 120 °C under argon. The concentration of DCP as a function of time is reported below in Figure 2.21.

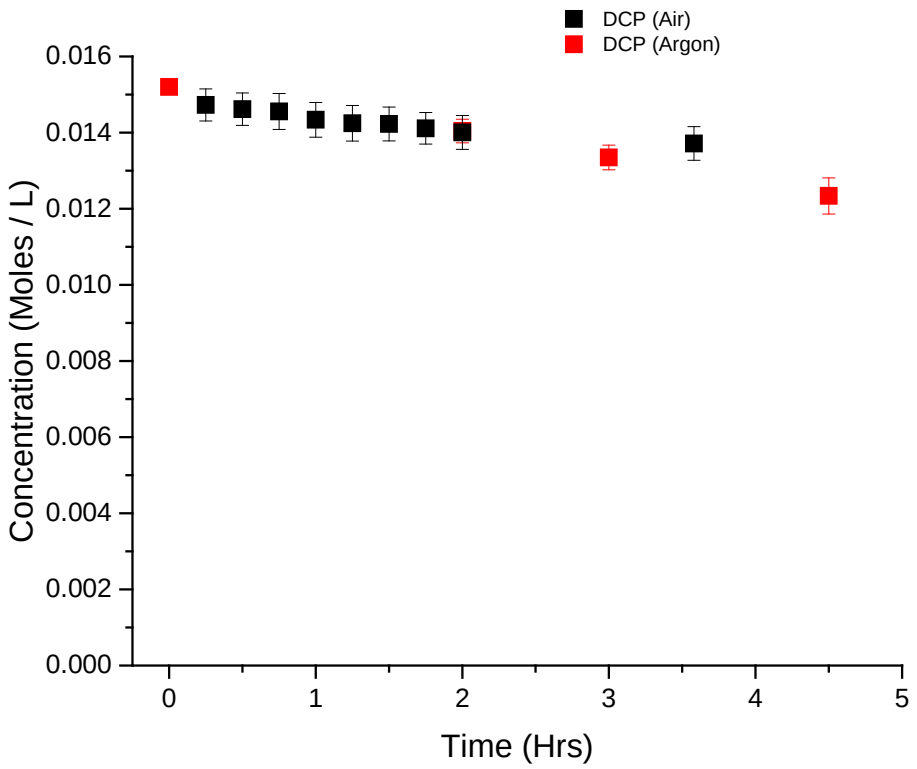

Figure 2.21. The concentration of DCP as a function of time for a sample of 0.0589 M DCP reacted at 120 °C under argon (red). For comparison, the same data gathered under air (black) are also shown.

The concentration data for the DCP decomposition reaction under argon are shown as the red data points in Figure 2.21. For comparison, data from a reaction of DCP in air (shown in black) are superimposed onto the data gathered under argon. The two sets of data exhibit very similar concentration profiles and rates of decomposition. As such, it is concluded that inert atmosphere has little to no effect on the rate of thermal decomposition of DCP. To reiterate: this study aims to observe a difference to account for the reduced crosslinking visible in Table 2.1. The difference in rate shown in Figure 2.21 (if there is a difference) is not sufficient to explain the dramatic reduction in crosslinking that is currently under investigation.

Both rates of decomposition and product analysis for the thermal decomposition of DCP for reactions conducted under air and under argon have been shown. There is no significant observable difference in either rate or products of degradation when the atmosphere is changed for thermal degradation. To determine the cause of the beneficial effects observed in Table 2.1, experiments to examine DSTDP and its chemical behavior were conducted.

2.5 Experiments With DSTDP

2.5.1 Purification of Stock DSTDP Material

DSTDP (CAS 693-36-7) was obtained from City Chemical, LLC. In accordance with the research goals stated previously, it was necessary to first examine any possible impurities contained within the chemical stock. A proton NMR of the raw stock material is included below in Figure 2.22. The peaks were identified in the figure and correspond to expectations.

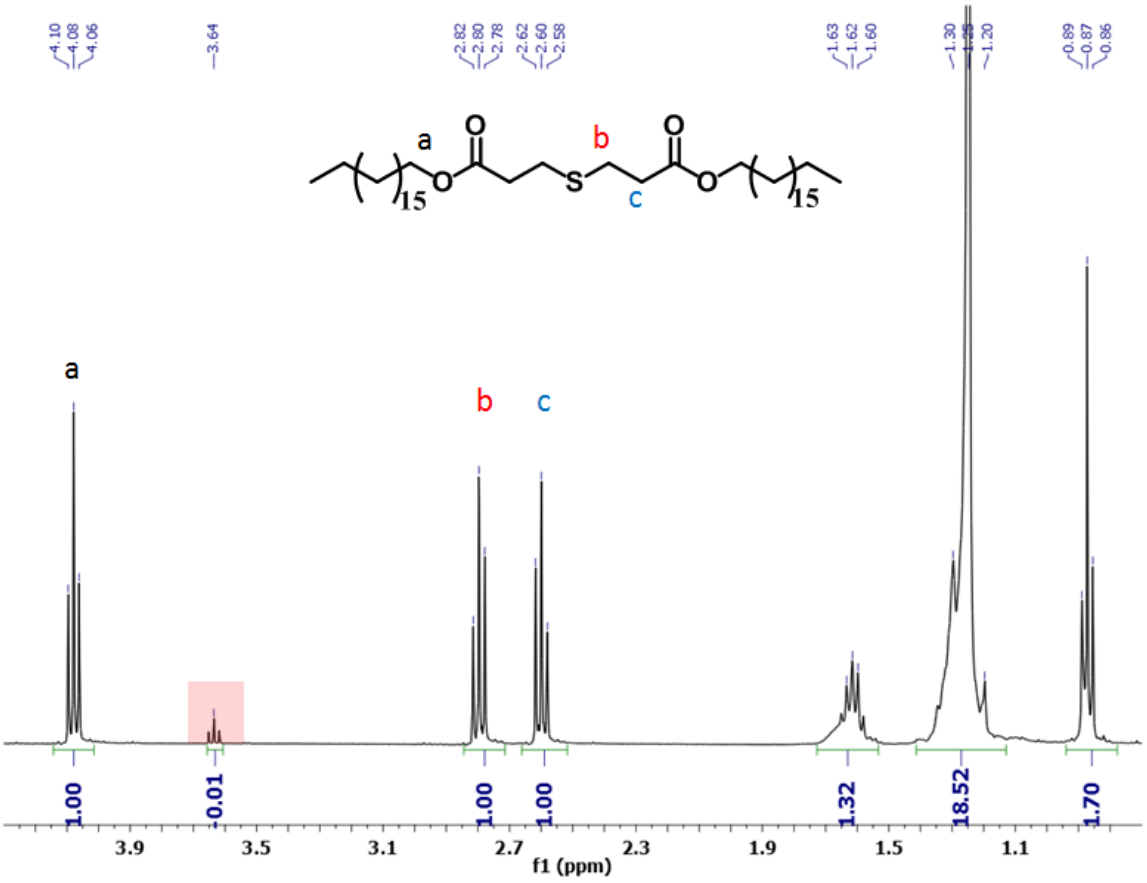

Figure 2.22. Proton NMR of stock DSTDP obtained from City Chemical. The most identifiable peaks are labled 'a', 'b', and 'c'. The peak highlighted in pink corresponds to an impurity in the sample.

Peak ratios are exactly as expected. Each of the peaks labeled 'a', 'b', and 'c' corresponds to two protons and therefore has the same integrated value. Other peaks integrate to expected values.

Several techniques were attempted to remove the impurity present in the DSTDP stock material. Initial attempts involved multiple heated, small washes of ethyl acetate over a filter and drying the remaining solid. It was later discovered (by accident) that the impurity is highly soluble in methanol while DSTDP is minimally soluble in methanol. The purification technique was therefore simplified to placing large amounts of DSTDP stock into a flask with excess methanol and a magnetic stir bar. This solution was then heated to a temperature of about 65°C (at which the DSTDP melts) and allowed to stir for

1 hr. After stirring, the suspension cooled to room temperature (to recrystallize DSTDP), was passed over a filter and the remaining solid was pure DSTDP. A proton NMR spectrum of purified DSTDP is shown below in Figure 2.23.

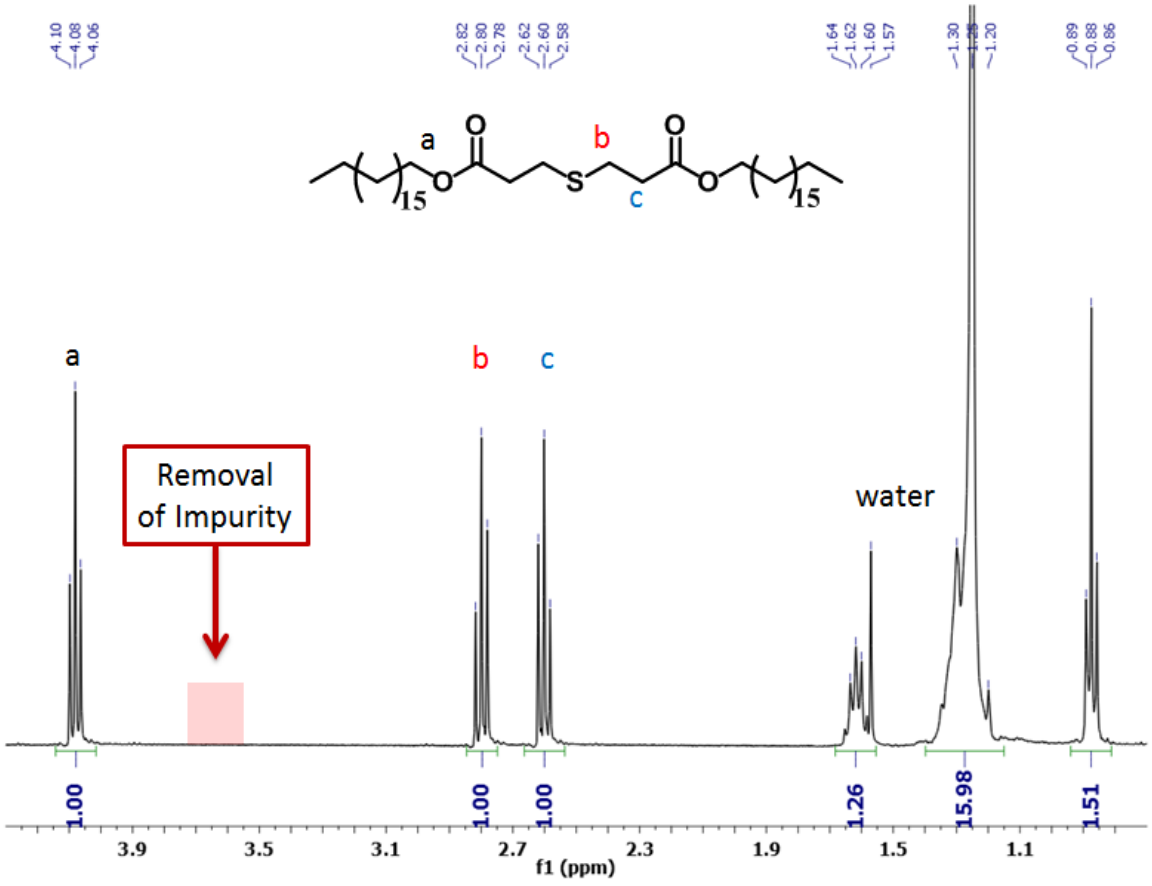

Figure 2.23. Proton NMR of purified DSTDP. Peaks are identified as in Figure 2.22. The large water peak is likely due to condensation during filtration. Evaporating methanol becomes cold in the vacuum filter, likely causing water condensation.

It can be clearly seen in Figure 2.23 that purification of DSTP was successful. From here, it is assumed that the DSTDP has been sufficiently purified to examine its chemistry without interference from impurities.

2.5.2 Thermal Treatment of DSTDP

The first step in examining the behavior of the reaction system with DSTDP is to examine the thermal stability of DSTDP on its own. It was shown that the combination of DCP and DSTDP produces beneficial reduction in premature crosslinking. As discussed before, the interactions from any possible products from thermal decomposition of DSTDP must be ruled out. With this in mind, DSTDP was heated at 110 °C in dodecane for 7 hours. The solution was prepared at the same concentration as 10 wt% DCP in dodecane (0.321 M). The reaction was left open to air to assess any possible products that could arise from interaction with oxygen. Anisole was added after reaction as an internal standard. The proton NMR spectrum is shown below in Figure 2.24.

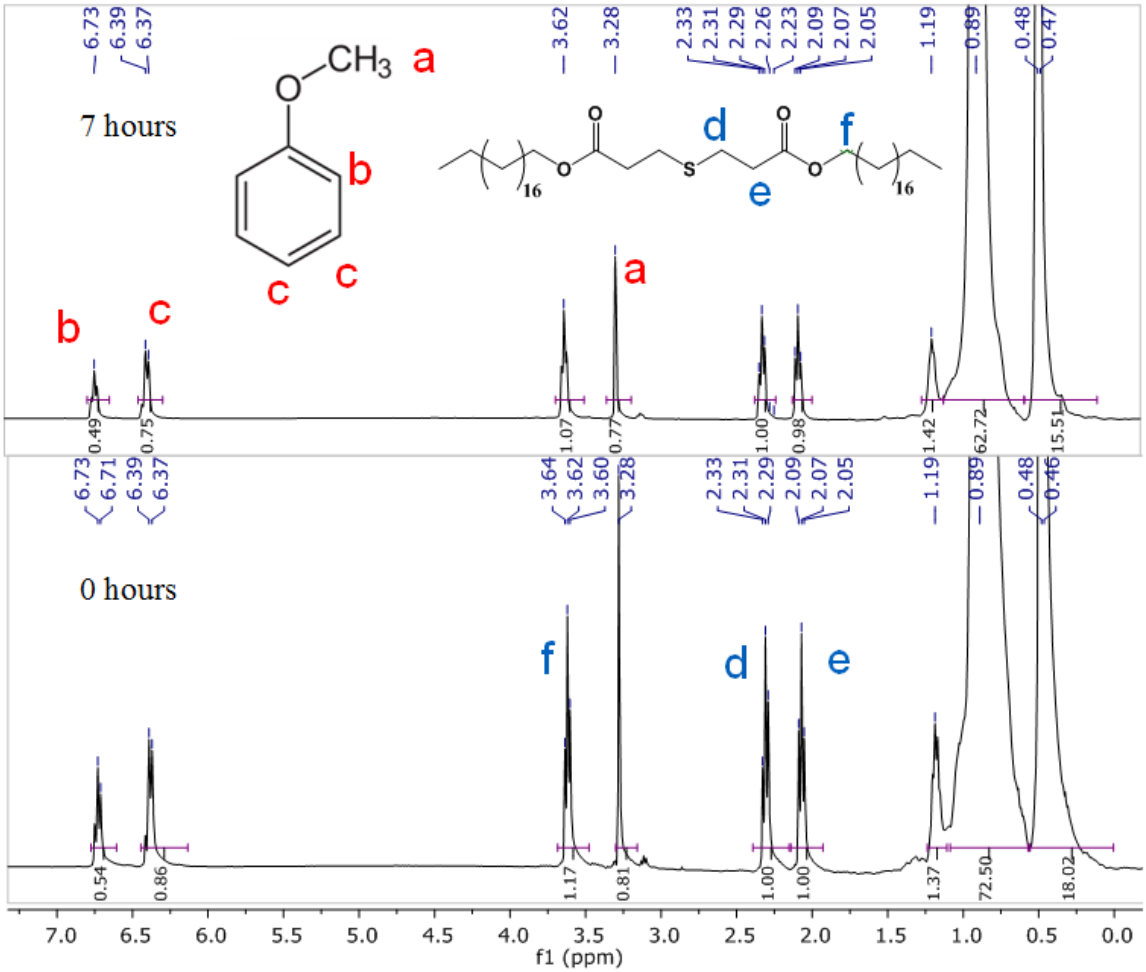

Figure 2.24. Proton NMR spectra of 0.321 M DSTDP in dodecane both before and after 7 hours of thermal treatment at 110 °C. Anisole was added as a standard after heating.

The spectra in Figure 2.24 show the high thermal stability of DSTDP on its own. There were no new peaks formed in the NMR spectrum to signify the formation of new species. The integral ratios also do not change significantly, further indicating thermal stability. For the temperatures and reaction times to be discussed, DSTDP is treated as completely thermally stable.

2.5.3 Reactions of DCP with DSTDP in Dodecane in Air

Thus far, two important experimental facts have been established:

1. The thermal decomposition of DCP is independent of air or inert atmosphere.
2. DSTDP is relatively pure and completely thermally stable.

With these two facts, the interactions of DCP with DSTDP can be examined to answer the research question posed earlier in this chapter. To reiterate, the aim is to learn why the beneficial crosslink prevention as shown in Table 2.1 is observed with blends of DCP and DSTDP.

2.5.3.1 Initial Product Identification with NMR in Air

The first step in examining the interactions of DCP and DSTDP is to identify the products formed from their reaction. To examine the reaction products, solutions of DCP with added DSTDP were placed into reactors identical to those used previously. For these initial studies, the reactors were left open to air. Stir bars were added to ensure homogeneity during the course of reaction. It is worthy to note that DSTDP is not soluble in dodecane at room temperature. However, the compound melts at approximately 65 °C and its liquid phase is soluble in dodecane. Stock solutions were homogenized by measuring the required weight of DSTDP solid into dodecane, heating the solution above the melting point while stirring, and allowing the solution to cool for storage. Since all of our reactions are conducted above the melting point, solubility has not yet been problematic.

The first set of reactions used 0.0589 M DCP with 1 full equivalent of DSTDP. Reactions were conducted at 120 °C for 3.5 hours. The proton NMR spectra for the initial DCP and DSTDP studies are below.

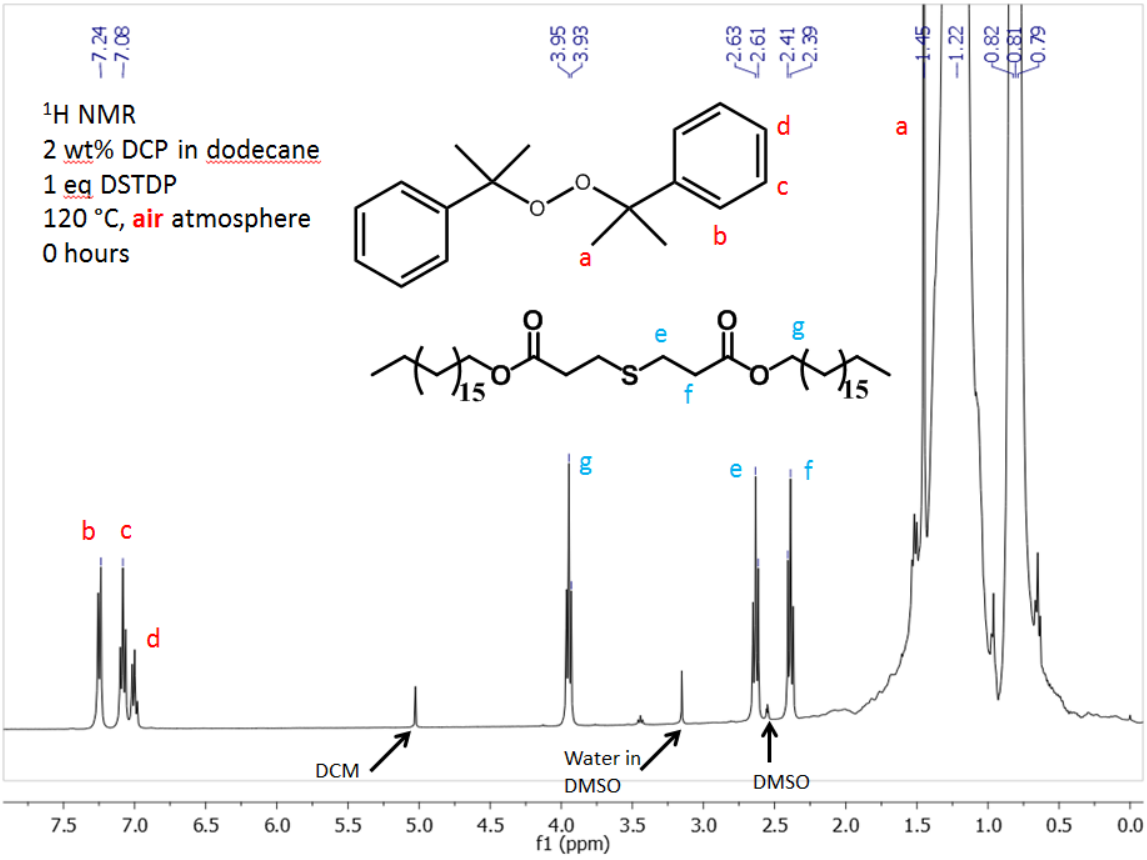

Figure 2.25. Proton NMR of the mixture of 0.0589 M DCP with 1 equivalent of DSTDP. A capillary of DMSO-D6 was used as the lock solvent.

As Figure 2.25 was measured before any heated reaction, the only notable peaks correspond to DCP, DSTDP, and dodecane. The peaks corresponding to DCP and DSTDP are labeled on the spectrum. The spectrum of the mixture after reaction is shown below in Figure 2.26.

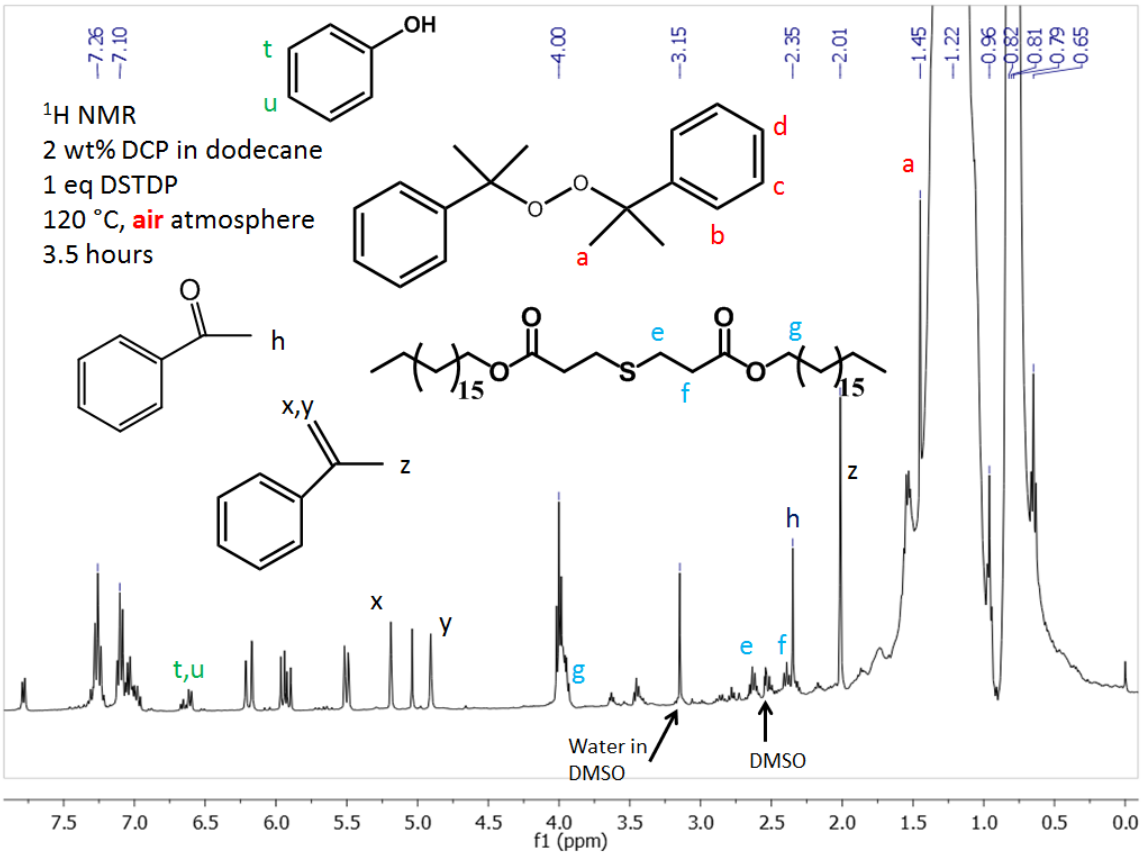

Figure 2.26. Proton NMR spectrum of the reaction of 0.0589 M DCP with 1 equivalent of DSTDP after 3.5 hours at 120 °C. The peaks corresponding to DCP and DSTDP are still labeled as on Figure 2.25.

The spectrum presented in Figure 2.26 shows the appearance of numerous new product peaks and the disappearance of peaks labeled ‘e’ and ‘f’ (corresponding to DSTDP). One peak was easy to identify, as it was observed before: peak ‘h’ corresponds to acetophenone, as seen previously. The peaks labeled ‘x’, ‘y’, and ‘z’ correspond to α-methyl styrene, as confirmed by NMR standards and literature. The peaks ‘t’ and ‘u’ correspond to phenol, also confirmed by NMR standards and literature.

We can see by the sizes of peaks ‘e’ and ‘f’ that almost all of the initial DSTDP was consumed in the reaction. This must mean that peak ‘g’ is overlapping with a peak from a new product species that happens to have a peak at the same proton shift. Also conspicuously absent is a peak corresponding to cumyl alcohol. Recall that for the

thermal decomposition of DCP, cumyl alchol (along with acetophenone) was observed as a product. Something in this system either (i) prevented the formation of cumyl alcohol, or (ii) consumed any cumyl alcohol as it formed.

The formation of phenol and α-methyl styrene, and a lack of cumyl alcohol in Figure 2.26, were observed. The best explanation to account for these 3 observations is the introduction of an acid species. The acidic decomposition of DCP has been studied in literature (and later in this thesis), and is known to produce α-methyl styrene and phenol.[14,17,18] It is hypothesized that the lack of cumyl alcohol is due to an acid-catalyzed dehydration reaction. This would convert cumyl alcohol to α-methyl styrene, consistent with experimental observations.

Also worthy of particular attention are the peaks that appeared between 5.5 ppm and 6.5 ppm after reaction. To confirm the identity of the species responsible for these peaks, a hypothesis was proposed. The peaks of interest are firmly in the vinyl region, and therefore correspond to a species with a double bond. It is hypothesized that the vinyl peaks corresponded to the acrylate species shown in the literature and in Figure 2.5. This species could form via the retro-Michael addition reaction of an oxidized derivative of DSTDP. The mechanism for such a reaction is shown below in Figure 2.27.

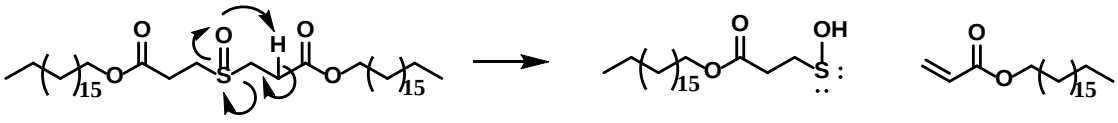

Figure 2.27. Mechanism for the retro-Michael addition to form an acrylate.

With this hypothesis in mind, the acrylate species was obtained from TCI America and a sample was prepared for proton NMR. The spectrum taken of the acrylate

sample, along with a zoomed in view of the spectrum in Figure 2.26, is shown below in Figure 2.28.

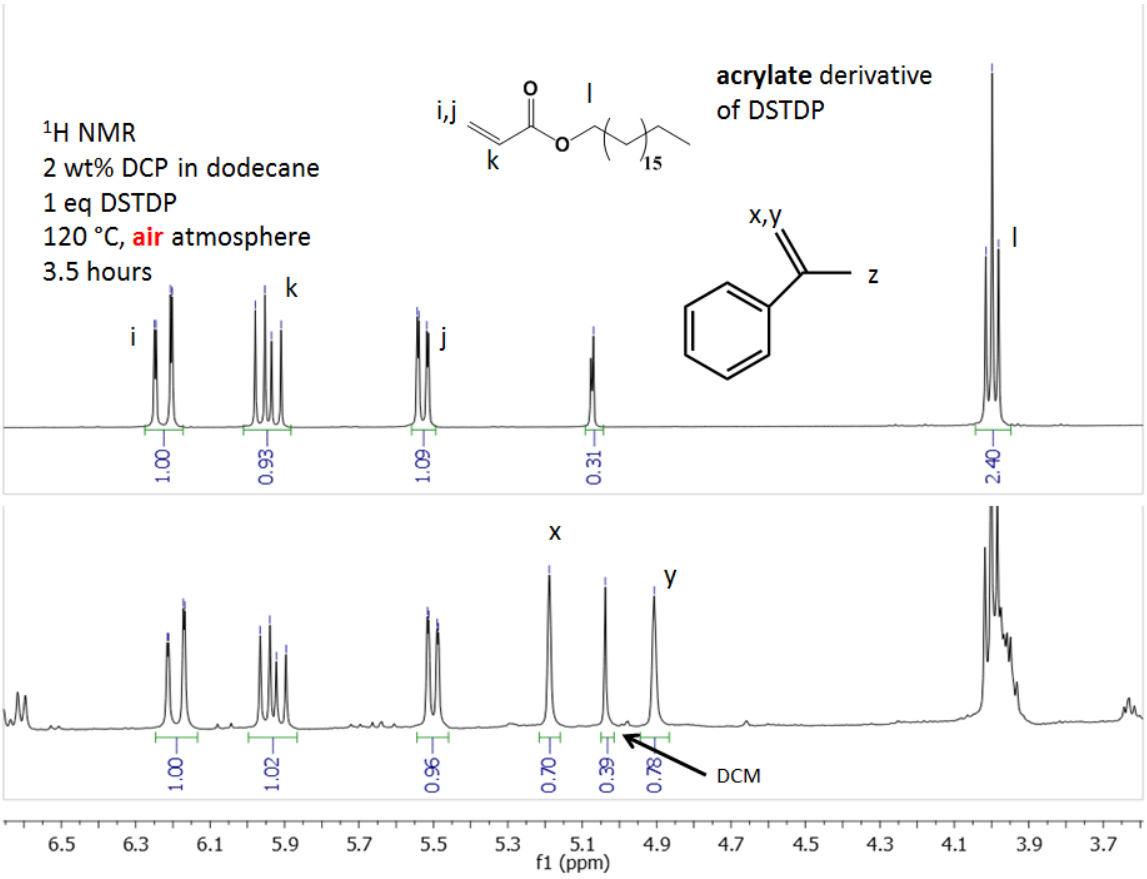

Figure 2.28. TOP: proton NMR spectrum of the acrylate species that could be formed via the mechanism in Figure 2.27. BOTTOM: zoomed view of the NMR spectrum in Figure 2.26 for comparison purposes.

The peaks between 5.5 ppm and 6.5 ppm are labeled ‘i’, ‘j’, and ‘k’, and correspond to the protons of the acrylate as shown. These are unequivocally the same peaks present in Figure 2.26, meaning the acrylate is a product of the interaction of DCP and DSTDP. It also appears that there is in fact a peak (labeled ‘l’) with the same proton shift as peak ‘g’ in Figure 2.26, which explains why that peak remains so large while the DSTDP was mostly consumed.

Several additional key observations were made from the product identification studies. First, the presence of α-methyl styrene and phenol indicate that an acid species is

formed during reaction. The acid must be strong enough to induce acidic decomposition of DCP. Second, the formation of an acrylate is observed which indicates that DSTDP is oxidized in solution to its sulfoxide form. The hypothesized answer to the research question must incorporate these observations.

2.5.3.2 HPLC Rate Studies of DCP and DSTDP Reactions in Air

Product identification is only part of the overall picture of DCP and DSTDP interaction. To progress the investigation, the rates of consumption of DCP in the presence of DSTDP were also studied in a variety of conditions. Solutions of 0.0589 M DCP with varying equivalents of DSTDP were reacted at 120 °C in the same reactors as used previously. The studies discussed here were reacted open to air to supplement the already discussed product identifications. HPLC was used as described above to track the concentration of DCP remaining in solution as a function of time. The results are shown below in Figure 2.29.

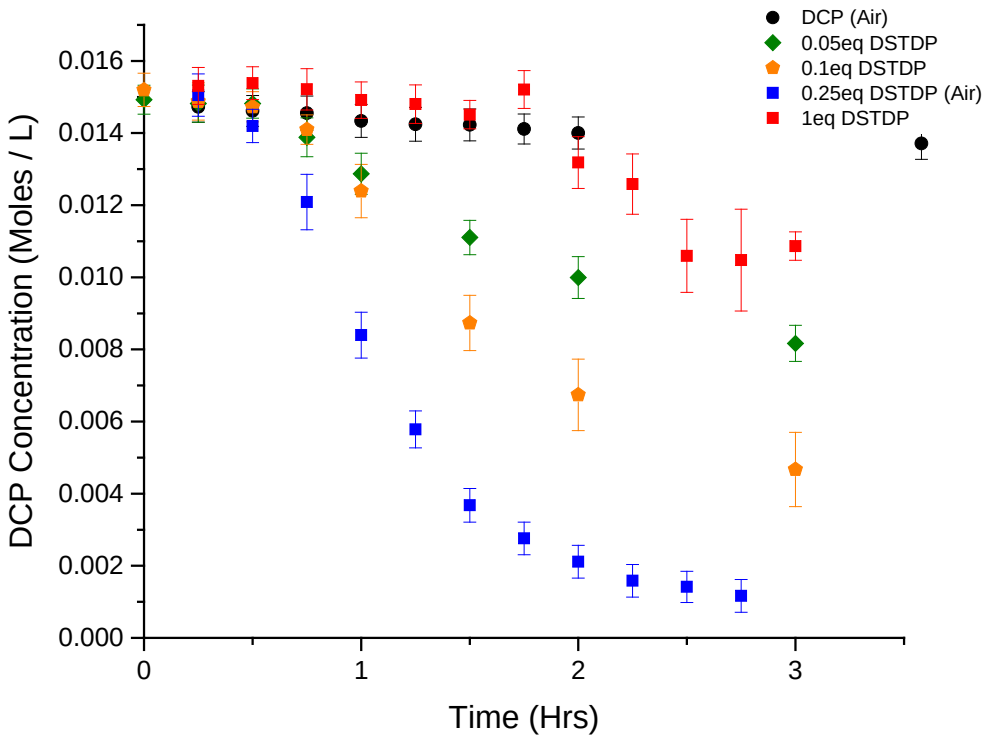

Figure 2.29. DCP concentrations as a function of time for the reactions of 0.0589 M DCP with varying amounts of DSTDP at 120 °C. Concentrations are plotted after a dilution of 1 part sample to 4 parts isopranol.

Some very interesting observations are made from Figure 2.29. The control reaction of just DCP in dodecane is shown as the black circles. The presence of DSTDP, in general, does affect the rate of disappearance of DCP in solution. Interestingly, there is not a straightforward relationship between DSTDP concentration and the rate of DCP consumption. The rate of DCP consumption increases as the DSTDP equivalents increase from 0.05, 0.10, and 0.25 equivalents. However, the rate of consumption decreases dramatically as the DSTDP concentration goes from 0.25 equivalents to 1 equivalent. It appears that at high concentrations of DSTDP, some interaction slows the consumption of DCP. Two possibilities are that at high enough concentrations, DSTDP

somehow stabilizes DCP or acts as a sink to consume another species that decomposes DCP.

To further demonstrate the unusual concentration dependence of DCP decomposition rate, a photograph was obtained of different reaction vials after reaction. The photograph is shown below as Figure 2.30.

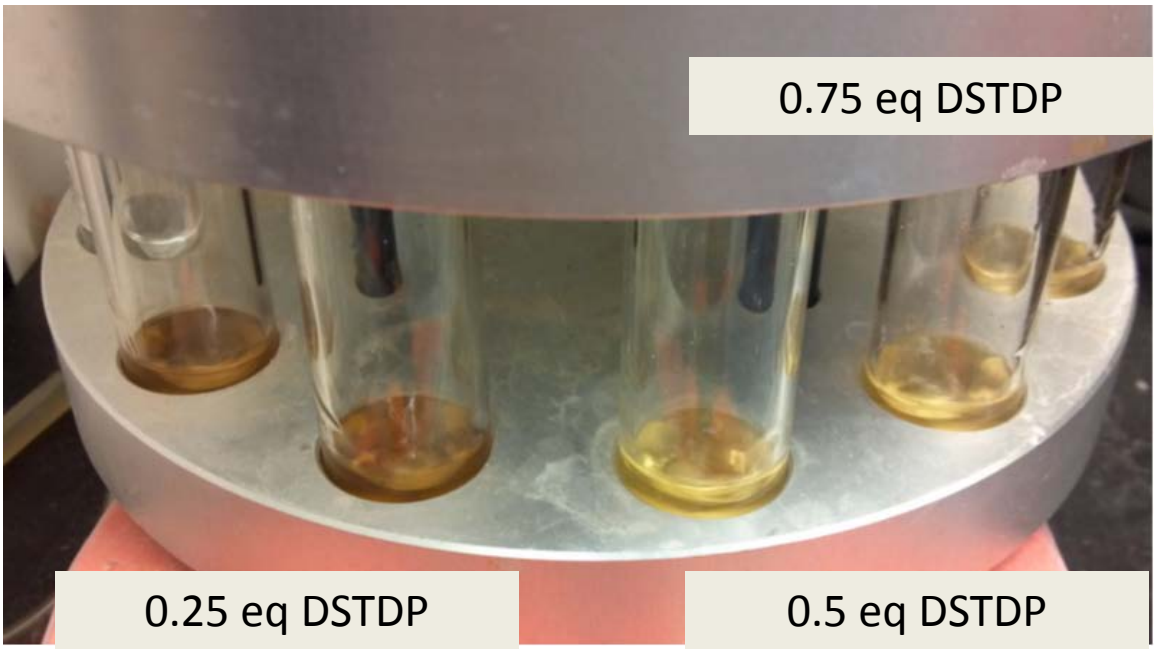

Figure 2.30. Photograph of 0.0589 M DCP + DSTDP reactions after reaction. The equivalents of DSTDP are labeled. Each reactor was subjected to the same temperature for the same amount of time.

During these reactions of DCP with DSTDP, reaction solutions begin colorless. As the reaction proceeds, the solutions progress from colorless to yellow and eventually to brown. A darker color of a solution signifies a greater extent of reaction. The colors shown in Figure 2.30 clearly demonstrate that the reactors with 0.25 equivalents of DSTDP exhibit the fastest reaction rates.

As a final piece of evidence for the unusual relationship of rate and DSTDP concentration, a proton NMR spectrum of the reaction of 0.0589 M DCP with 0.25 equivalents of DSTDP was gathered. This reaction was conducted open to air for 3.5

hours. The spectrum looks largely similar to that presented in Figure 2.26. The spectrum was zoomed to highlight a portion that shows the most dramatic difference between the spectra. The results are shown below in Figure 2.31.

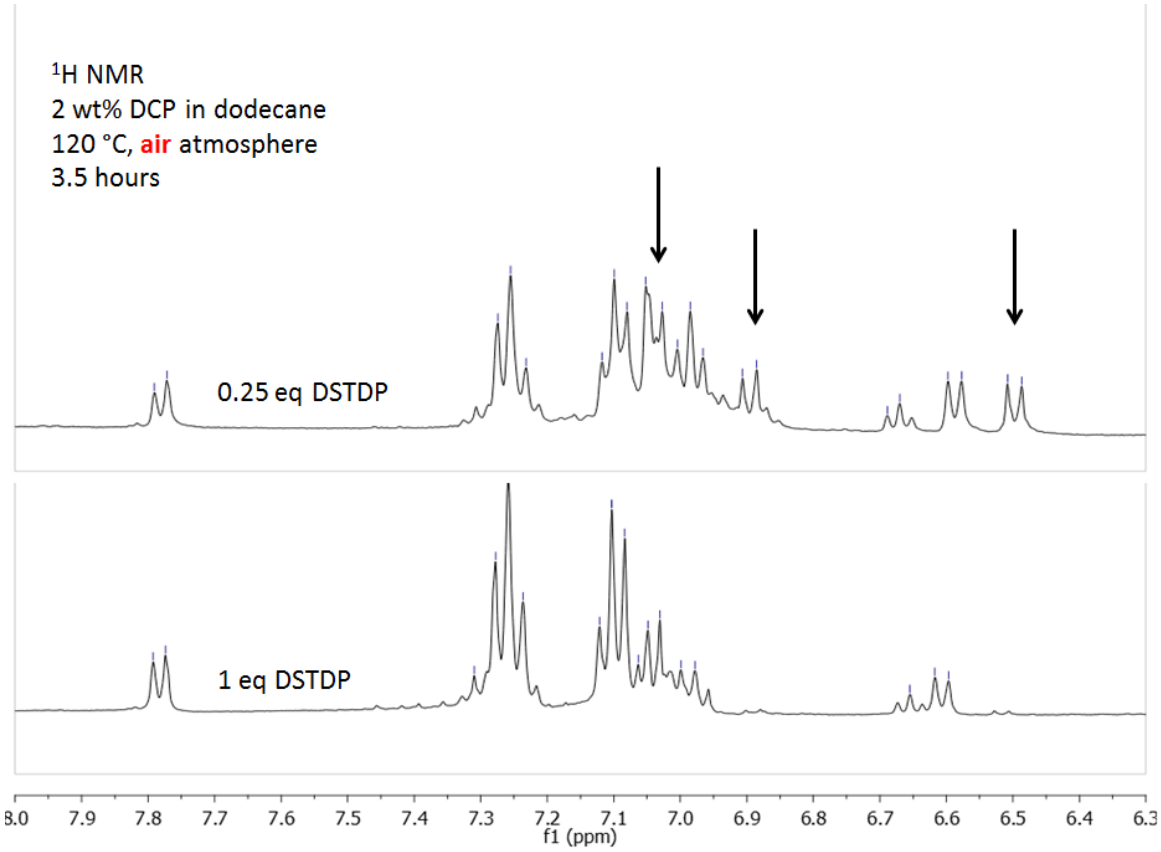

Figure 2.31. Proton NMR spectrum of the reaction of 0.0589 M DCP with 0.25 and 1 equivalent of DSTDP at 120 °C for 3.5 hours. Species formed during reaction are indicated with black arrows.

The spectra shown in Figure 2.31 clearly show the formation of new product peaks in the aromatic and vinyl regions. These peaks are much larger (e.g., these species form much more quickly) in the spectrum taken with 0.25 equivalents of DSTDP. This is one more demonstration that high concentrations of DSTDP slow down this reaction.

Another observation from the decomposition data is more obvious if the data in Figure 2.29 are shown more cleanly. The following plot is the exact same data as presented in Figure 2.29 with some data sets hidden.

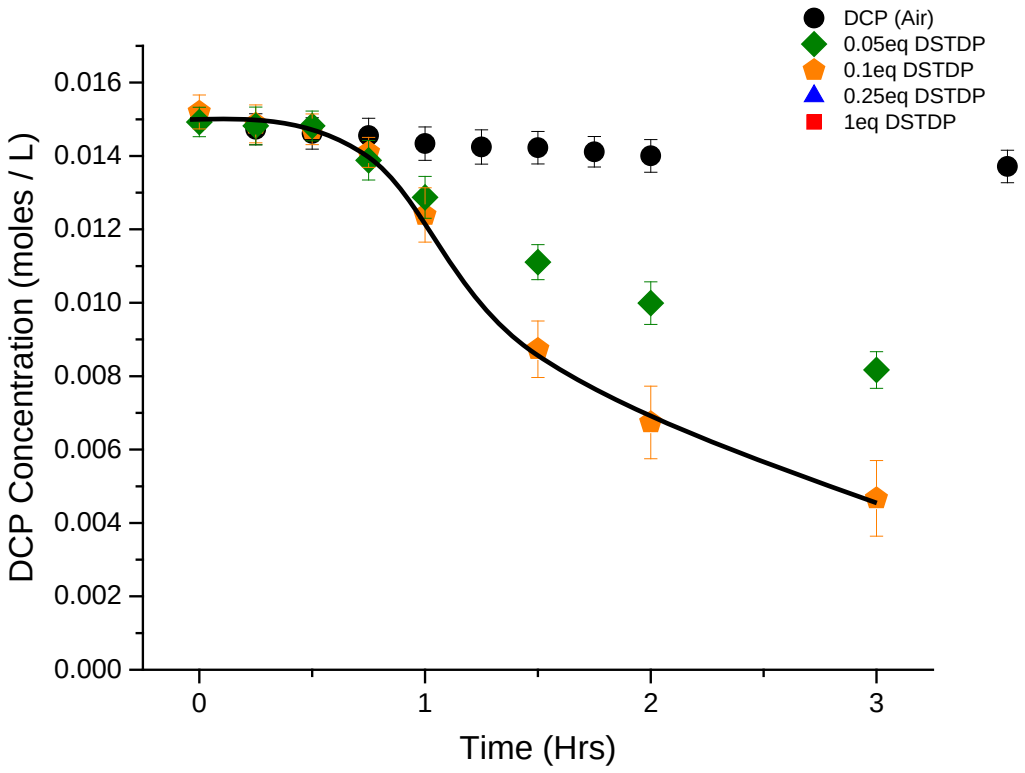

Figure 2.32. DCP concentrations as a function of time for the reactions of 0.0589 M DCP with varying amounts of DSTDP at 120 °C. Data have been manipulated for clarity. The black line is not a fit line, but added to highlight the shape of the data.

Figure 2.32 highlights another important observation from this data: the DCP decomposition follows an s-shaped curve. The s-shape of the data implies that the decomposition is somehow autocatalytic: during the early stages of reaction, a species that decomposes DCP accumulates. When the concentration of this new species is high enough, it begins to degrade DCP while continuing to accumulate. This would account for the accelerated decomposition during the middle stages of reaction.

From the HPLC rate data, some new observations were made. First, the relationship of the rate of DCP decomposition with the concentration of DSTDP is unusual and unexpected. A high concentration of DSTDP dramatically slows the rate of

DCP decomposition as compared to lower concentrations of DCP. Second, the DCP decomposition in the presence of DSTDP follows and s-shaped curve. This indicates autocatalysis. These observations must be incorporated into our answer to the research question.

2.5.4 Reactions of DCP with DSTDP in Dodecane Under Argon

Data from the thermal decomposition of DCP and the reactions of DCP with DSTDP in air have been presented and discussed. In the introduction, a stark difference in behavior was observed between experiments run exposed to air or reacted under inert atmosphere. It was also proven previously that the difference cannot come from the behavior of DCP itself. Therefore, to complete the data set and to answer the research question, reactions of DCP with DSTDP under argon must be examined. The methodology used was largely similar to those presented previously in this chapter.

2.5.4.1 Product Identification with NMR Under Argon

As for the cases under air, the products of the reaction of DCP with DSTDP under argon must be identified.

Reaction vials identical to those used previously were charged with solutions of 0.0589 M DCP and 1 equivalent of DSTDP. These reactors were heated at 120 °C for 3.5 hours. A proton NMR spectrum was taken of each reactor both before and after reaction. The spectrum taken before reaction looks entirely similar to previous spectra of DCP and DSTDP in dodecane, so it's been omitted. The spectrum of the reaction mixture after heating is shown below in Figure 2.33.

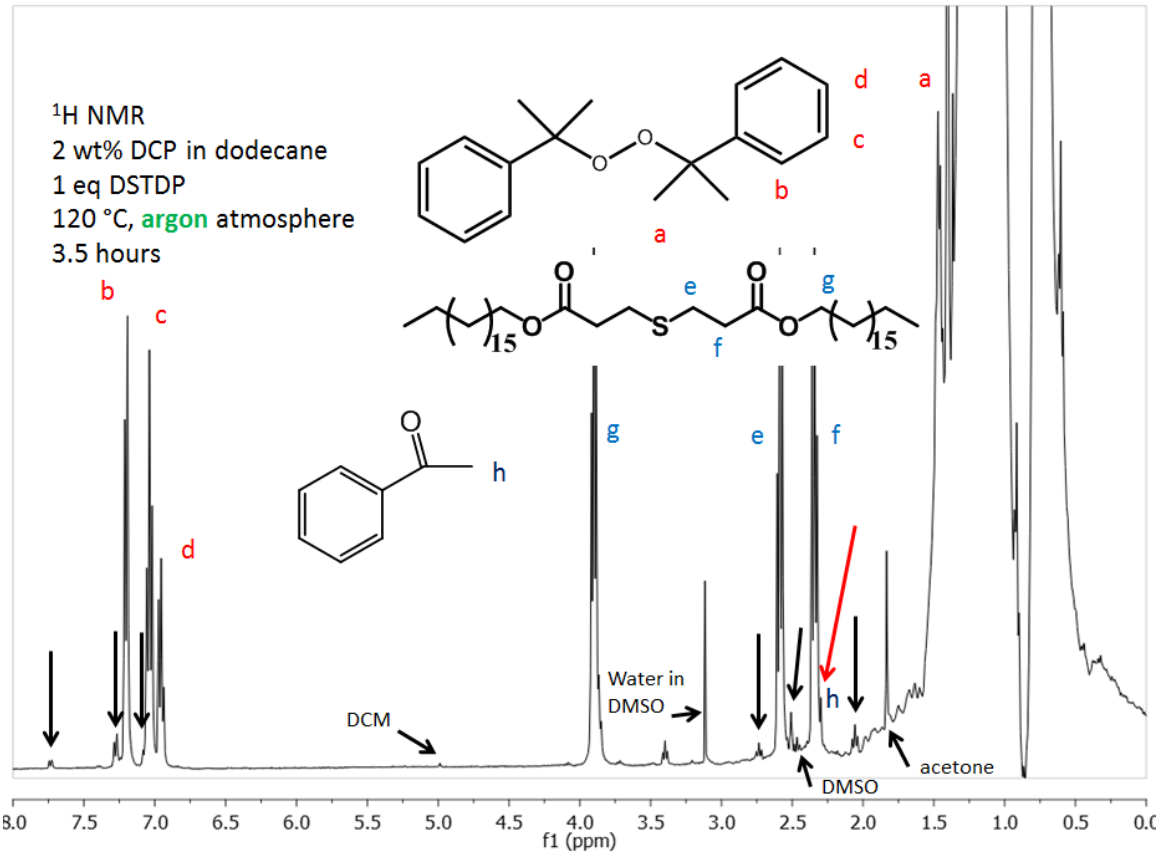

Figure 2.33. Proton NMR spectrum of 0.0589 M DCP with 1 equivalent DSTDP reacted at 120 °C for 3.5 hours. Black arrows are used to identify peaks of unidentified product species. The red arrow is simply used to highlight peak 'h', which is difficult to see otherwise.

The spectrum shown in Figure 2.33 shows a dramatic difference between DCP and DSTDP reactions under air and under argon. Figure 2.33 should be directly compared with Figure 2.26. With that in mind, it can be sees that Figure 2.33 does not exhibit any evidence of α-methyl styrene, phenol, or acrylate species. There is also little evidence of consumption of DSTDP. The magnitudes of the peaks labeled 'e', 'f', and 'g' are all similar, unlike the same peaks in Figure 2.26. These observations can be summarized to conclude that the DCP is likely not decomposing through an acidic mechanism in this case. Otherwise, phenol and α-methyl styrene would be observed. Additionally, the lack

of acrylate and retention of the DSTDP peaks means there is likely little (if any) oxidation of DSTDP.

A portion of the proton spectrum shown in Figure 2.33 was expanded to show the formation of cumyl alcohol. The zoomed spectrum is shown below in Figure 2.34.

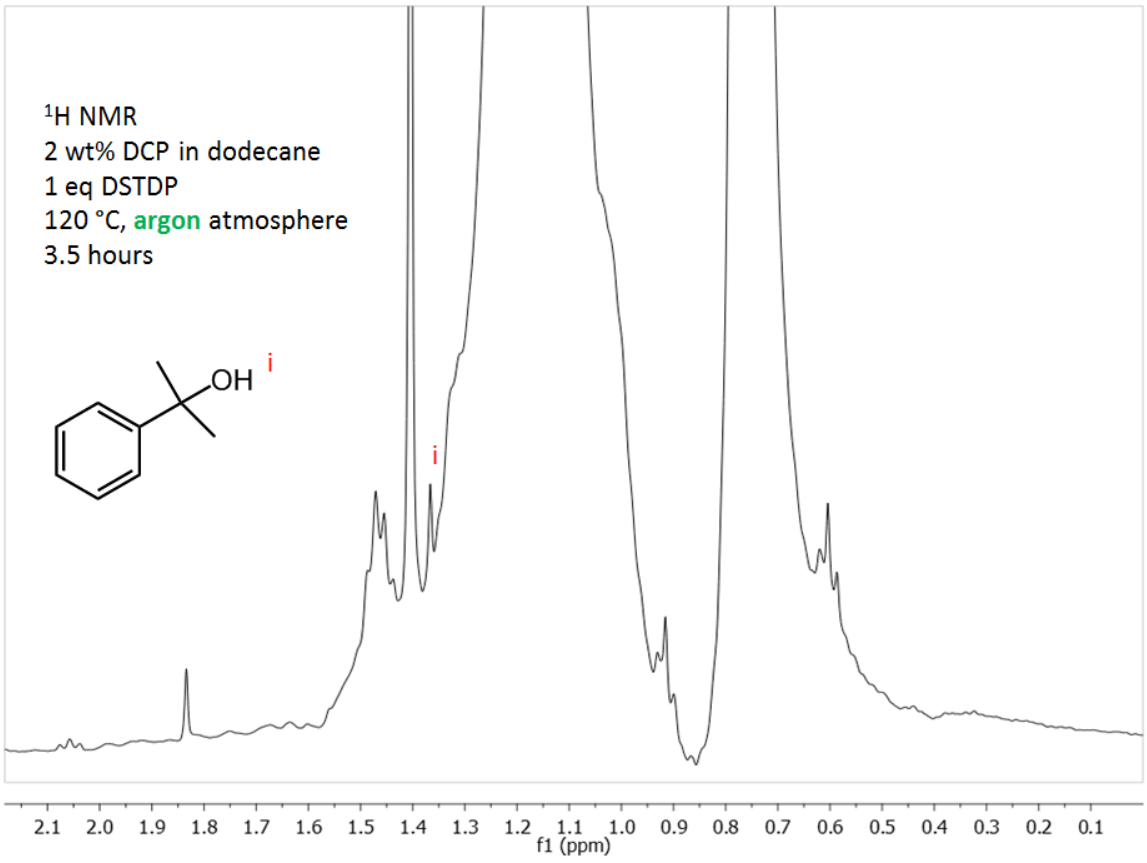

Figure 2.34. Proton NMR spectrum of 0.0589 M DCP with 1 equivalent DSTDP reacted at 120 °C for 3.5 hours, zoomed in to show the formation of cumyl alcohol.

The presence of cumyl alcohol (demonstrated in Figure 2.34) further shows that there is likely no acidic decomposition in this reaction. Otherwise, cumyl alcohol would be dehydrated to form α-methyl styrene.

As another piece of evidence of the difference between an air and argon atmosphere for this system, a photograph was obtained of a representative reaction from each case. The photograph is included below as Figure 2.35.

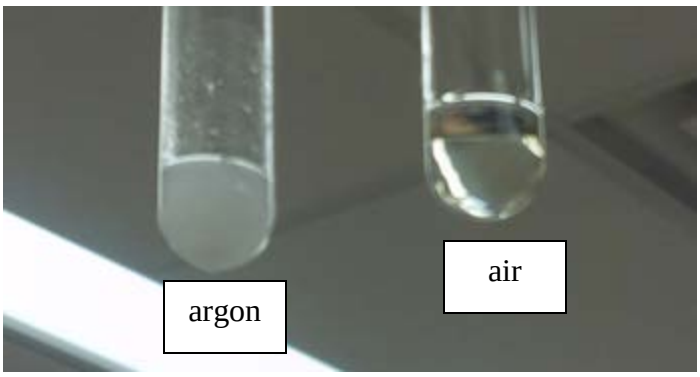

Figure 2.35. Photograph of reaction solutions of 0.0589 M DCP with 0.5 equivalents of DSTDP after 3.5 hours at 120 °C.

Figure 2.35 corroborates the information given by NMR analysis. The vial on the left (reacted under argon) is a cloudy white color. This is due to the presence of unreacted DSTDP, which is insoluble in dodecane. Figure 2.33 shows that there is remaining DSTDP when the system is reacted under argon. The vial on the right, meanwhile, is a transparent yellow color. The DSTDP has been largely consumed, matching what is expected based on Figure 2.26.

To summarize, the reaction of DCP with DSTDP under argon exhibits almost exactly the same behavior as the thermal decomposition of DCP. Aside from some low concentrations of products indicated by black arrows in Figure 2.33, the only major products formed are cumyl alcohol and acetophenone. This mimics the observations of the thermal decomposition of DCP. Again, product identification is only one part of the information required to assess this reaction. The rates of decomposition of DCP under argon were also examined.

2.5.4.2 HPLC Rate Studies of DCP and DSTDP Reactions Under Argon

HPLC peak integration was used to track the concentrations of DCP in reaction samples as described previously in this chapter. Reactor vials identical to those used in previous sections were charged with 0.0589 M DCP and varying equivalents of DSTDP. Reactions were conducted at 120 °C for varying times. Samples were extracted from the reactors at time intervals and examined via HPLC. The results are shown in the figures below.

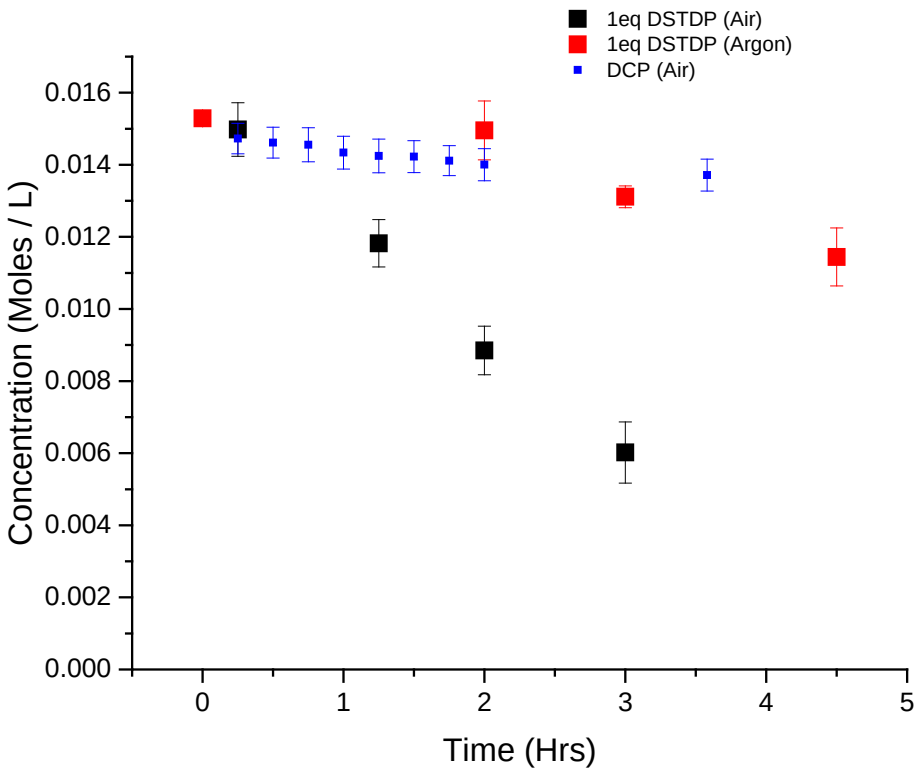

Figure 2.36. HPLC concentration data for the reactions of 0.0589 M DCP with 1 equivalent DSTDP at 120 °C as a function of time.

The plot in Figure 2.36 compares the rates of DCP decomposition for the cases of thermal decomposition, 1 equivalent DSTDP in air, and 1 equivalent DSTDP under argon. Note that there are fewer data points gathered for these experiments than were

shown previously. There is still enough information present to draw conclusions. It is clear that a difference exists between the rate of decomposition when under air or under argon. The red data set (under argon) exhibits a rate of decomposition only slightly faster than the control experiment of thermal decomposition. Meanwhile, the black data set (in air) exhibits a greatly accelerated decomposition when compared to either the control or the argon data. This data corroborates the information from the proton NMR studies and from Figure 2.35: the extent of reaction increases dramatically when the system is reacted under air as compared to argon.

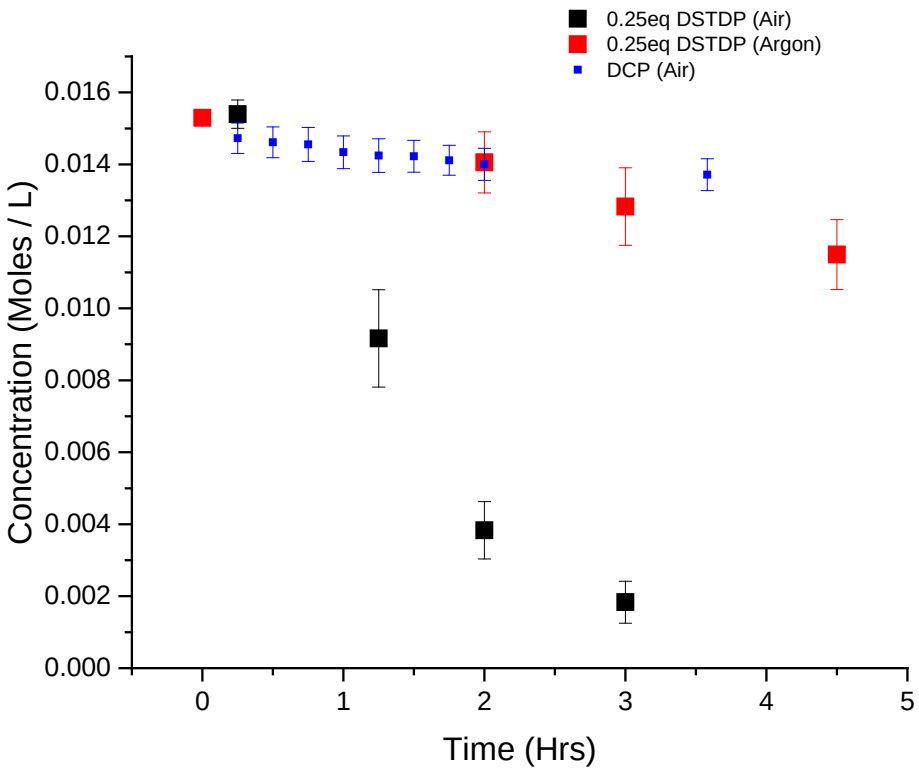

Figure 2.37. HPLC concentration data for the reactions of 0.0589 M DCP with 0.25 equivalent DSTDP at 120 °C as a function of time.

The plot in Figure 2.37 is the same as that in Figure 2.36, but the reactions included 0.25 equivalents of DSTDP instead of 1 equivalent. As in Figure 2.36, the data

in Figure 2.37 show that the rate of decomposition of DCP and DSTDP in air is much faster than the control experiment or the rate of the same reaction under argon. Furthermore, the rates of decomposition of DCP with 1 equivalent of DSTDP and DCP with 0.25 equivalents of DCP are effectively the same. The influence of DSTDP concentration is on the rate of this reaction is no longer present under argon.

To summarize the overall results of the reactions involving DCP to this point:

1. The thermal decomposition of DCP yields cumyl alcohol and acetophenone under both air and argon.
2. The rate of thermal decomposition of DCP is unaffected by the atmosphere.
3. The reaction of DCP with DSTDP in air yields phenol, α-methyl styrene, and stearyl acrylate.
4. The rate of DCP disappearance when reacted with DSTDP in air is greatly accelerated as compared with the thermal decomposition.
5. The rate of DCP disappearance exhibits and unexpected dependence on the concentration of DSTDP in air.
6. The reaction of DCP with DSTDP under argon yields the exact same products as the thermal decomposition of DCP.
7. The rate of DCP disappearance when reacted with DSTDP under argon is effectively the same as the thermal decomposition of DCP.

To make concrete conclusions about the nature of the interactions of DCP, DSTDP, and air, a few more experiments were carried out to examine the effects of the atmosphere.

2.5.5 Additional Experiments Regarding Experimental Atmosphere

So far, it has been demonstrated that reactions of DCP and DSTDP in air have dramatically different behavior from those conducted under argon. However, there is still another variable involved. If air is the cause of the difference in system behavior, then the difference could be caused by either atmospheric oxygen or atmospheric humidity. Experiments were conducted to deconvolute the effects of these species.

2.5.5.1. Reactions of DCP with DSTDP Under Wet Argon

The first experiment sought to determine the effect atmospheric water has on this reaction system. 0.0589 M DCP was reacted with 1 equivalent DSTDP in dodecane at 120 °C as described previously. To introduce humidity to the system but not oxygen, an argon line was flowed through a fritted glass diffuser tube. The diffused tube was connected to the argon line and placed into a bath of deionized water. The bubbles of argon rose through the water, humidified, and then flowed through another line into the reaction vessels. Reactors were purged and the reactor mixtures sparged with the humidified argon prior to reaction. During reaction, the reactors were kept under a positive pressure of humidified argon. The reactors were placed in heated oil at 120 °C for 3 hours and proton NMR spectra were recorded following reaction. The proton NMR spectra are shown below.

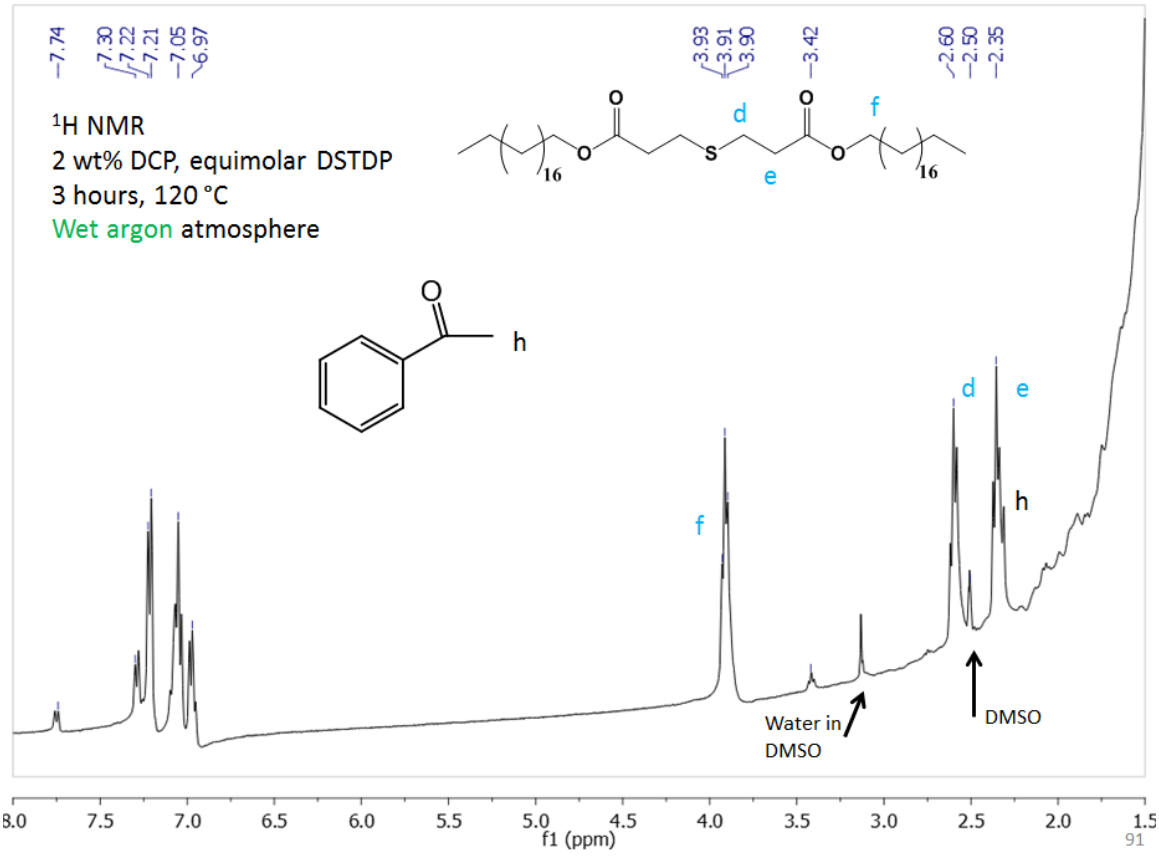

Figure 2.38. Proton NMR spectrum of the reaction of 0.0589 M DCP with 1 equivalent of DSTDP under humidified argon.

Figure 2.38 reveals that the products of the reaction of DCP with DSTDP under humidified argon are identical to those of the thermal decomposition of DCP. There is no evidence of phenol, α-methyl styrene, or acrylate. There is also no evidence of consumption of DSTDP, as demonstrated by the relative magnitudes of peaks 'd', 'e', and 'f'. These observations indicate that there is no formation of acid or oxidation of DSTDP. The presence of cumyl alcohol is shown in a zoomed portion of the spectrum shown in Figure 2.38. The zoomed spectrum is shown below in Figure 2.39.

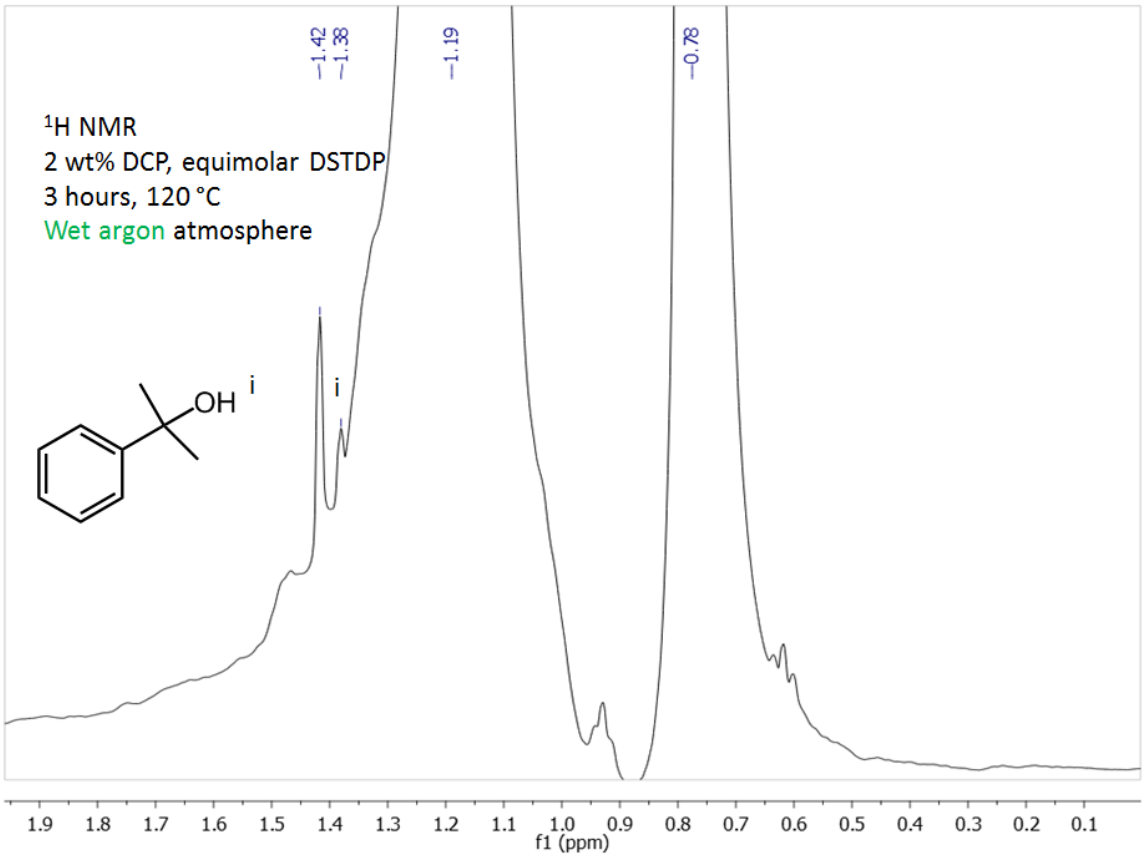

Figure 2.39. Zoomed proton NMR spectrum of the reaction of 0.0589 M DCP with 1 equivalent of DSTDP under humidified argon. Cumyl alcohol is observed, as shown with peak 'i'.

The presence of cumyl alcohol, when combined with observations discussed above, is enough to conclude that atmospheric humidity has little to no effect on the interactions of DCP with DSTDP. Specifically, atmospheric humidity cannot account for the observations made in Table 2.1.

2.5.5.2 Reactions of DCP with DSTDP Under Dry Air

Now that the effects of atmospheric humidity have been examined, the effects of atmospheric oxygen must be determined. Reaction solutions of 0.0589 M DCP with 1 equivalent of DSTDP in dodecane were loaded into glass reactors as described

previously. Reactors were purged with air sourced from a cylinder of compressed, bone-dry air from Airgas. Reaction solutions were also sparged with dry air. During the reaction, reactors were kept under a positive pressure of dry air from the compressed gas line. Reactions were carried out at 120 °C for 3 hours. Proton NMR spectra were measured after reaction and are shown below.

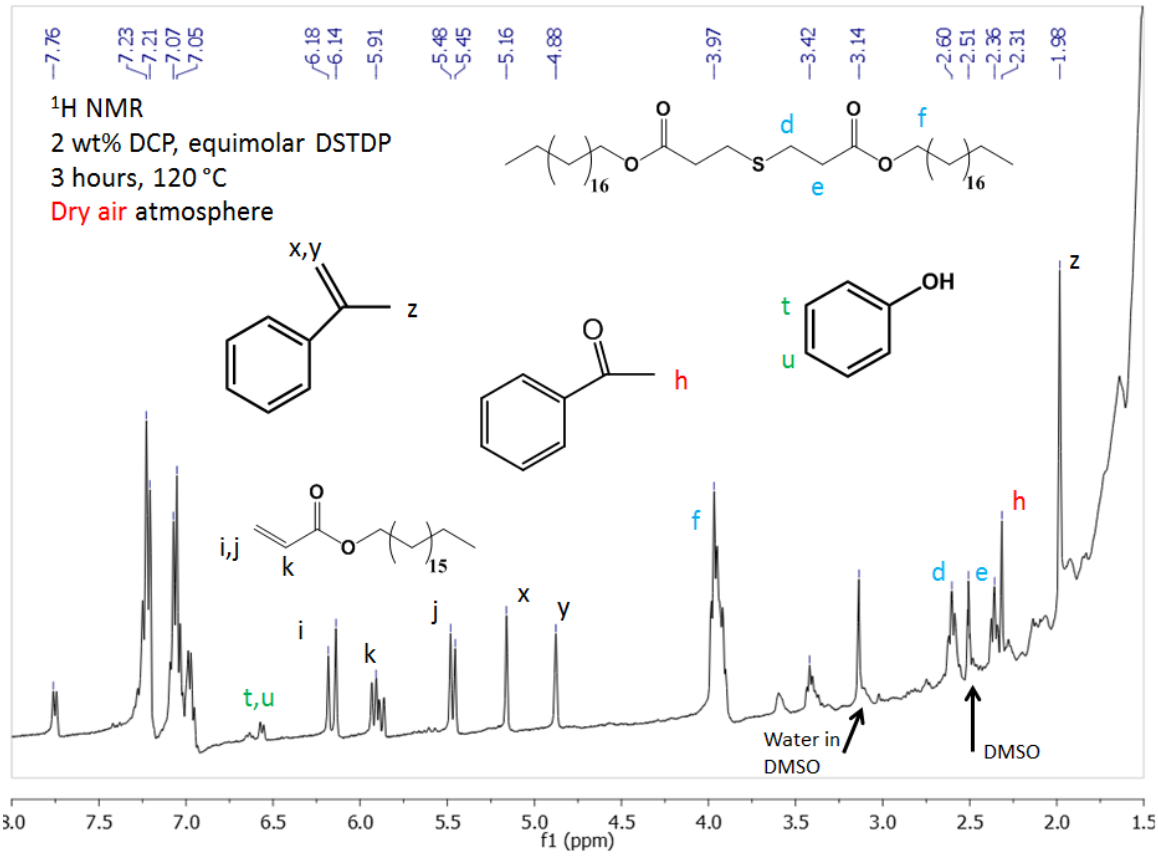

Figure 2.40. Proton NMR spectrum of the reaction of 0.0589 M DCP with 1 equivalent of DSTDP under dry air.

The peaks present in Figure 2.40 give us the answers we want immediately. It can be seen that when reacted under dry air, the reaction of DCP with DSTDP produces α-methyl styrene, phenol, and acrylate. There is also evidence of consumption of DSTDP as shown by the small peaks labeled ‘d’ and ‘e’. The portion of the spectrum that would reveal cumyl alcohol is shown below in Figure 2.41.

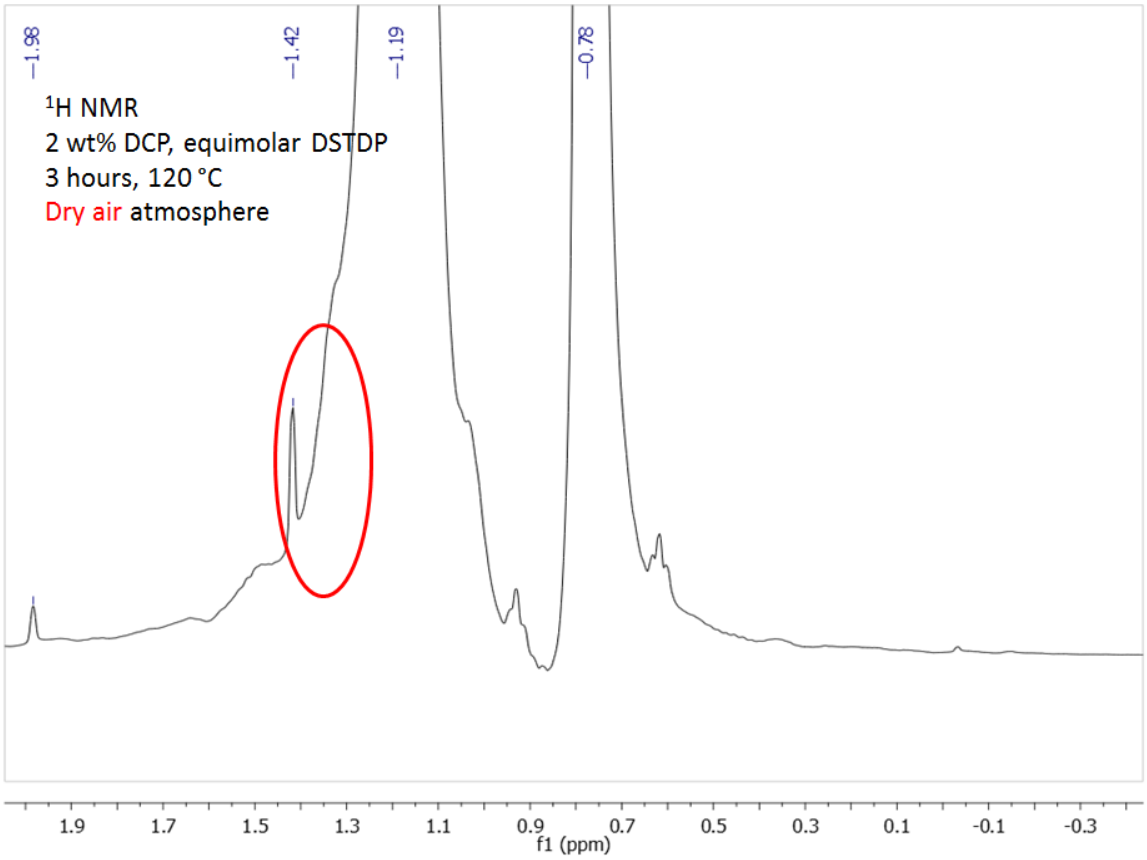

Figure 2.41. Proton NMR spectrum of the reaction of 0.0589 M DCP with 1 equivalent of DSTDP under dry air, zoomed to show the region where cumyl alcohol would be visible.

Figure 2.41 is lacking a peak corresponding to cumyl alcohol. Effectively, the data present in Figure 2.40 and Figure 2.41 combined reveal that atmospheric oxygen is responsible for the observations in Table 2.1 that formed our research question. With this information, combined with the 7 overall results listed earlier, a hypothesis can be proposed for the mechanism of interaction between DCP and DSTDP.

2.6 Hypothesized Mechanism for the Interaction of DCP with DSTDP

For clarity, the overall collection of experimental observations is listed here and updated to include all available information.

1. The thermal decomposition of DCP yields cumyl alcohol and acetophenone under both air and argon.
2. The rate of thermal decomposition of DCP is unaffected by the atmosphere.
3. The reaction of DCP with DSTDP in air yields phenol, α-methyl styrene, and stearyl acrylate.
4. The rate of DCP disappearance when reacted with DSTDP in air is greatly accelerated as compared with the thermal decomposition.
5. The rate of DCP disappearance exhibits and unexpected dependence on the concentration of DSTDP in air.
6. The reaction of DCP with DSTDP under argon yields the exact same products as the thermal decomposition of DCP.
7. The rate of DCP disappearance when reacted with DSTDP under argon is effectively the same as the thermal decomposition of DCP.
8. Experiments with wet argon and dry air revealed that oxygen, not humidity, is responsible for the different experimental results.

Below, a mechanism is proposed that can consistently explain all observations made in the list above. The mechanism is shown in Figure 2.42.

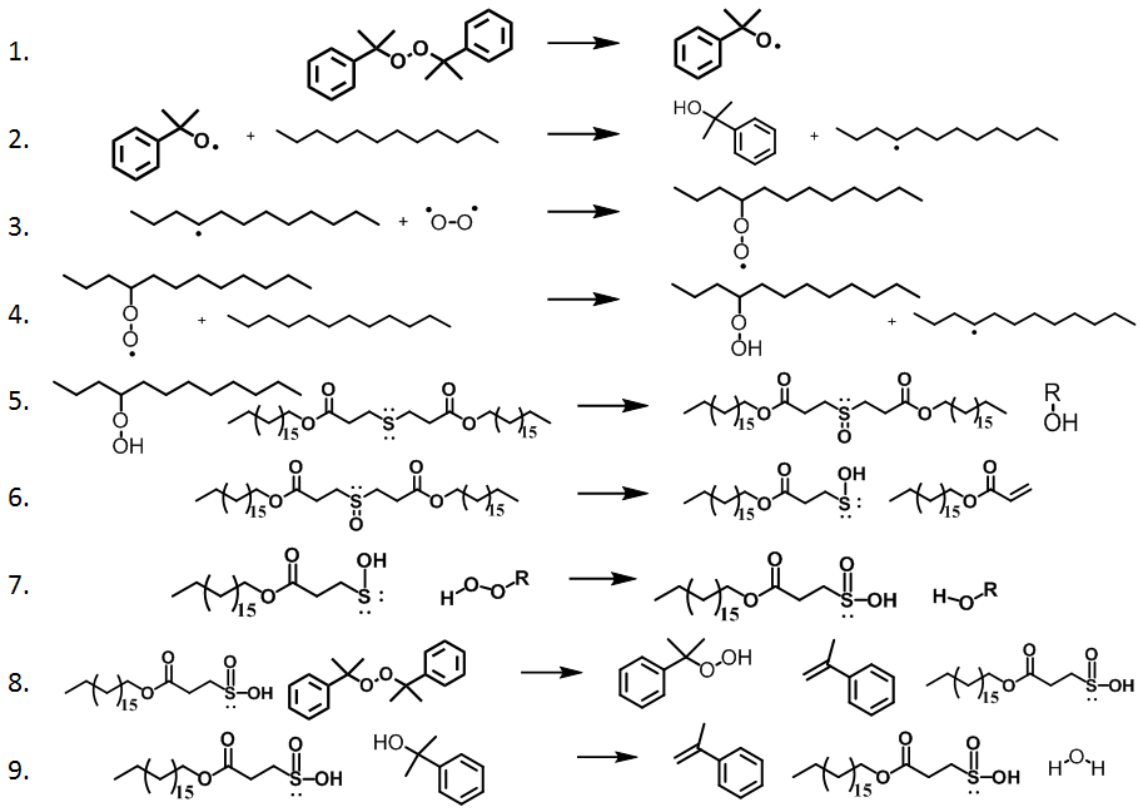

Figure 2.42. Hypothesized mechanism for the reaction of DCP with DSTDP in the presence of air.

The detailed mechanism is discussed here in a stepwise manner. Steps 1 and 2 are simply the thermal decomposition of DCP – the peroxide homolytically cleaves to form cumyloxy radicals. The cumyloxy radicals abstract hydrogen atoms from dodecane molecules, in turn forming alkyl radicals.

The absolutely critical nature of oxygen becomes apparent in step 3. Because oxygen exists as a ground-state di-radical, we propose that the collision of an oxygen molecule with an alkyl radical generates as hydroperoxy radical. This hydroperoxy radical can abstract a hydrogen atom from another dodecane molecule as shown in step 4, thereby forming an alkyl hydroperoxide.

It is proposed that these initial alkyl hydroperoxides are responsible for producing the sulfoxide derivative of DSTDP in step 5. The mechanism for such a reaction is shown below in Figure 2.43.

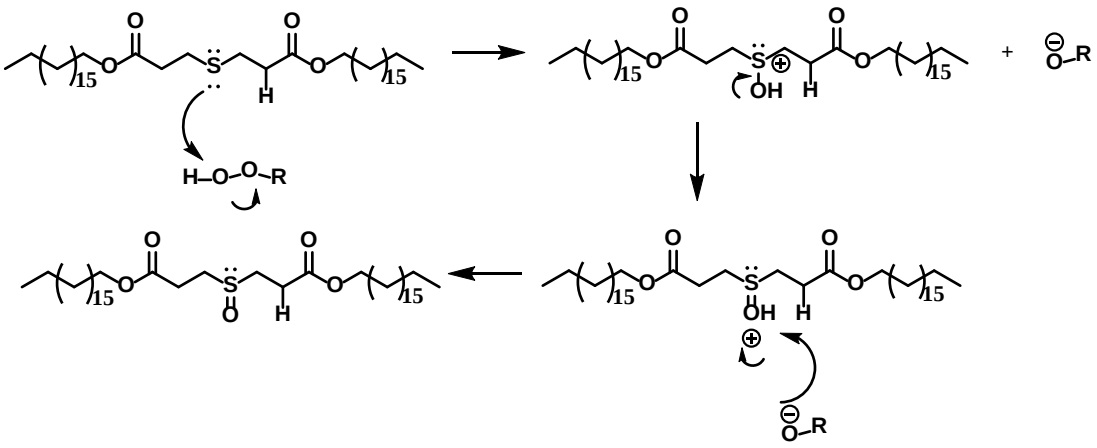

Figure 2.43. Possible mechanism of oxidation of DSTDP by a general hydroperoxide species.

Recall that oxygen alone cannot account for the oxidation of DSTDP inferred in our system. Figure 2.24 demonstrates that the DSTDP is thermally stable at the temperatures of interest. Any observed oxidation must be explained through another interaction. Also bear in mind that for our model system, these reactions take place in dodecane. In such a nonpolar solvent, the ions depicted in Figure 2.43 would be unlikely to transfer charge throughout the system. It's likely that the charged species will remain in close proximity.

Once a sulfoxide is formed, it is proposed that the next step (step 6) is a retro-Michael addition to form stearyl acrylate and a sulfenic acid. This step has been discussed in literature and the acrylate has been repeatedly observed in our reaction systems.

Step 7 is proposed to account for the strange relationship of DCP consumption rate with DSTDP concentration. It is hypothesized that the sulfenic acid formed via retro-Michael addition is too weak to rapidly decompose DCP. Therefore, it is suggested

that a hydroperoxide is needed to oxidize the sulfenic acid into a sulfinic acid. A possible mechanism for this step is shown below in Figure 2.44.

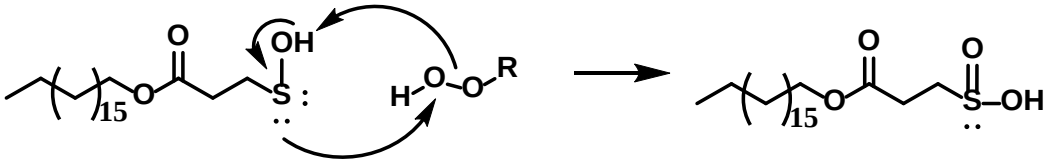

Figure 2.44. Possible mechanism of the oxidation of sulfenic acid to sulfinic acid by a hydroperoxide.

This consumption of hydroperoxides perfectly explains the fact that high concentrations of DSTDP decrease the rate of consumption of DCP. If hydroperoxides are required to convert DSTDP into a weak sulfenic acid, then it can be imagined that an excess of DSTDP will scavenge all available hydroperoxides in solution. There will thus be insufficient hydroperoxides available to oxidize sulfenic acid to sulfinic acid. Therefore, high concentrations of DSTDP prevent the oxidation of sulfenic acids to sulfinic acids, thereby reducing the rate of acid attack of DCP relative to lower concentrations of DSTDP.

Steps 8 and 9 of Figure 2.42 are the steps incorporating acid attack of species in solution. Step 8 accounts for the accelerated disappearance of DCP when reacted with DSTDP. Acid reacts with and consumes DCP at a faster rate than thermal decomposition alone. Step 9 accounts for the lack of cumyl alcohol when DCP is reacted with DSTDP. Acid attacks cumyl alcohol and converts it to α-methyl styrene. Notice in both steps 8 and 9 that the acid is regenerated. In this representation, the acid is presented as truly catalytic. A possible mechanism for catalytic acid degradation is shown below in Figure 2.45.

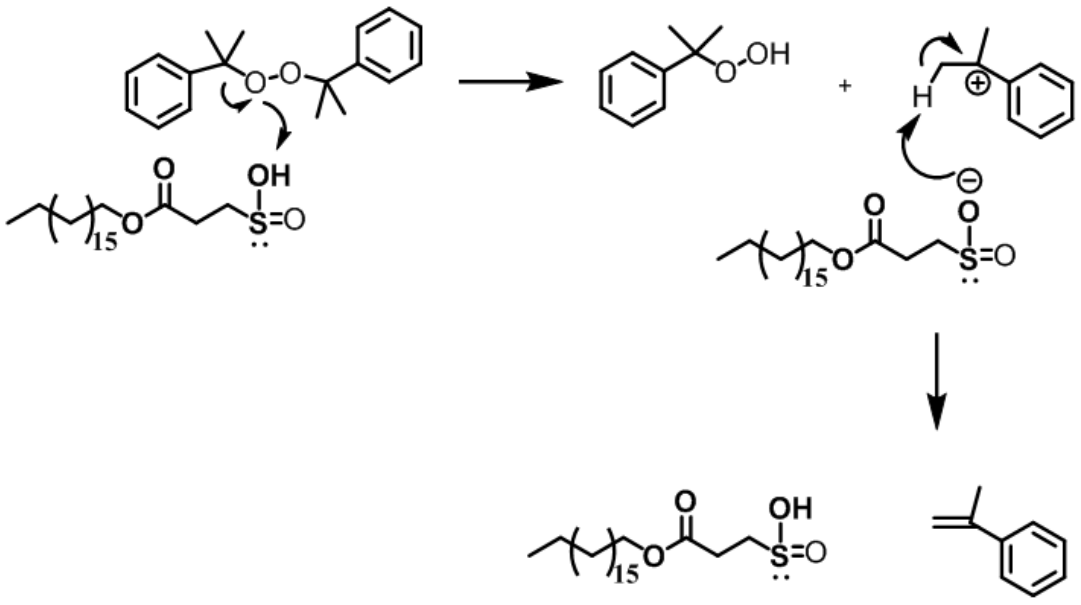

Figure 2.45. A possible mechanism for an acid-catalyzed decomposition of DCP. Acid is regenerated at the end of reaction.

The dehydration of cumyl alcohol can occur catalytically by an analogous reaction.

The catalytic nature of acid in steps 8 and 9 is necessary to account for the s-shaped curves shown during the reactions of DCP with DSTDP in air. Notice in the mechanism in Figure 2.42 that on the reactant (left) side, an acidic species appears 3 times (step 7, step 8, and step 9). However, an acidic species appears on the product (right) side 4 times (step 6, step 7, step 8, step 9). The continuous generation of acid with concurrent acid-catalyzed decomposition would provide the s-shaped curves observed during reactions. In other words, the mechanism accounts for the autocatalysis observed previously.

Step 8 in Figure 2.42 was, for a time, unproven. In fact, this single step is the topic of the entirety of Chapter 3 of this thesis. In literature, the acid-catalyzed decomposition of DCP produces α-methyl styrene (through cumyl alchol), phenol, and acetone. Here is proposed the formation of cumene hydroperoxide as an intermediate, as

shown in step 8. It was hypothesized that this additional hydroperoxide would be necessary to allow the mechanism to proceed at a rapid rate. As presented in Figure 2.42, there are 2 hydroperoxide species on the reagent side (step 5 and step 7) and 2 hydroperoxide species on the product side (step 4 and step 8). If the acid-catalyzed decomposition of DCP does not produce cumene hydroperoxide, there would thus be 2 moles of hydroperoxide consumed for every mole produced. It is hypothesized that this would drastically limit the rate of DCP consumption governed by this mechanism. Effectively, the rate-limiting step would be the generation of alkyl hydroperoxides via radical interactions. Chapter 3 documents the work proving that cumene hydroperoxide is in fact produced by the acid-catalyzed decomposition of DCP.

As presented, the mechanism in Figure 2.42 addresses every item on the list of experimental observations. It accounts for all of the observed products when DCP and DSTDP were reacted in air, accounts for the s-shaped curves observed in the DCP decomposition rates, and accounts for the importance of atmospheric oxygen. However, the fact that the mechanism has explanatory power is not enough to completely validate it. Therefore, further experiments were conducted to validate some of the individual mechanistic steps.

2.6.1 Thermal Treatment of Sulfoxide Derivative of DSTDP

Figure 2.42 and literature both propose that the sulfoxide derivative of DSTDP decomposes upon heating to form a sulfenic acid and stearyl acrylate. This reaction is step 6 in our proposed mechanism. The rate of this reaction was evaluated to determine

if this step is viable in the proposed mechanism. The first step in this study was to synthesize the sulfoxide derivative of DSTDP.

2.6.1.1 Synthesis of Sulfoxide Derivative of DSTDP

Literature is available regarding the relative proton NMR shifts of sulfides, sulfoxides, and sulfones.[19] A figure from literature is included for reference below.

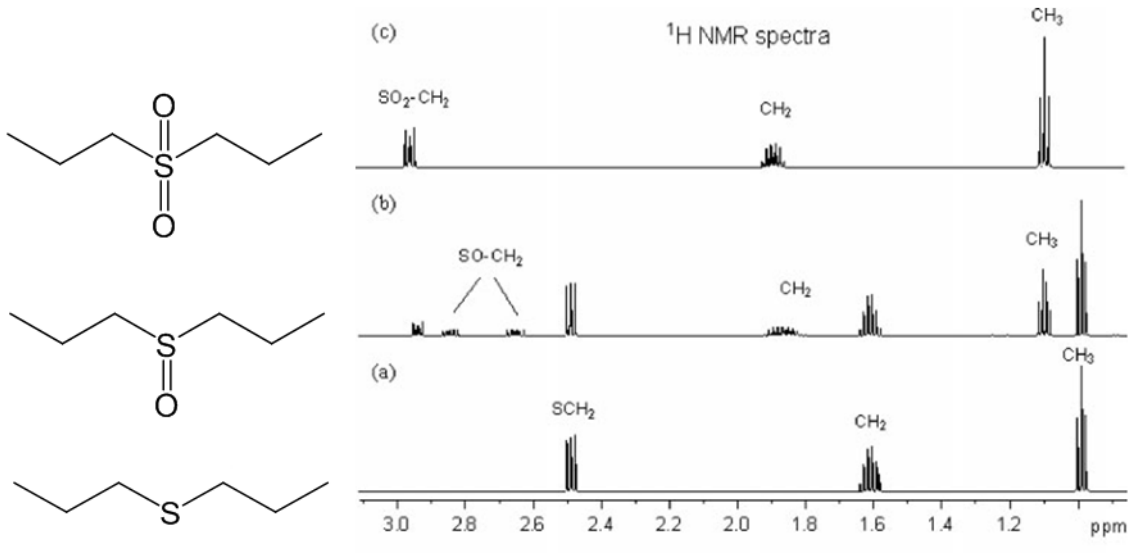

Figure 2.46. Literature proton NMR spectra highlighting the relative proton shifts of sulfides, sulfoxides, and sulfones.[19]

The spectra in Figure 2.46 show that there is an easy method for identifying sulfoxides and sulfides. For a sulfoxide, the protons on the carbon atoms immediately adjacent to the sulfur atom form two peaks instead of one. The lone pair on the sulfur atom makes the two protons enantiotopic, and they therefore have different proton NMR shifts. A sulfone should also be readily distinguishable since it has a peak shifted further downfield than either a sulfide or a sulfoxide.

To synthesize the sulfoxide derivative of DSTDP, DSTDP was reacted with meta-chloro-perbenzoic acid (mCPBA). This reaction is difficult because the sulfoxide can be

readily oxidized to form the sulfone. To prevent over-oxidation, the DSTDP was first dissolved in dichloromethane, stirred, and placed in an ice bath. 2 equivalents of mCPBA were slowly added dropwise from a solution of DCM over the course of 1 hour. The cold temperature, combined with the very slow method of addition, resulted in almost 100% yield of sulfoxide and minimal sulfone. After addition of mCPBA, the reaction was quenched with 5 wt% $NaHCO_3$ a total of 3 times and then extracted with dichloromethane. The resulting solution was dried in a rotary evaporator and was then ready for use. A proton NMR spectrum of the resulting solid is presented below.

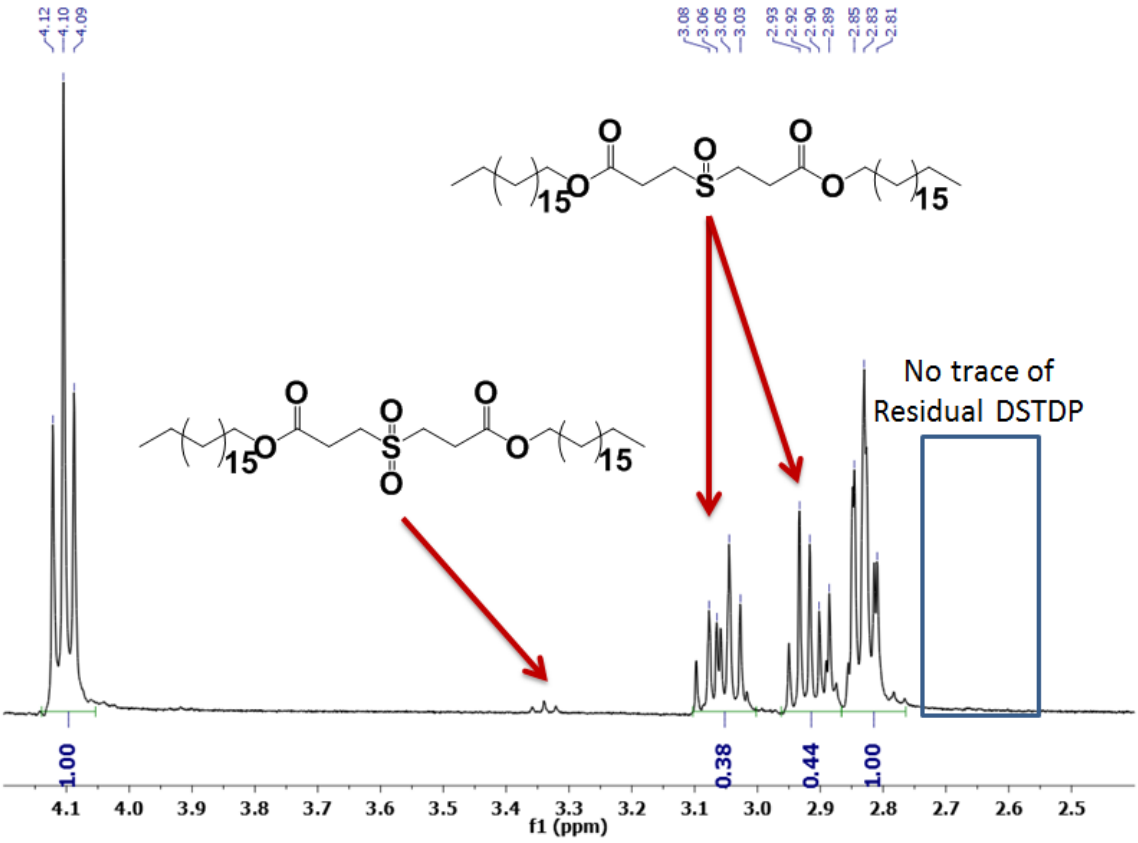

Figure 2.47. Proton NMR spectrum of our synthesized sulfoxide derivative of DSTDP. The sulfoxide exhibits the peak splitting observed in Figure 2.46.

The spectrum in Figure 2.47 shows almost 100% yield of sulfoxide. By comparing with the spectrum shown in Figure 2.23, we can see complete conversion of DSTDP. There is a minuscule peak corresponding to a small amount of sulfone.

The sulfone derivative was also synthesized using a similar, albeit much simpler, technique. DSTDP was reacted with 3.3 equivalents of mCPBA for 24 hours at room temperature. The resulting product was high-purity sulfone. The NMR spectrum of the synthesized sulfone is shown below in Figure 2.48. The peak at 3.64 ppm corresponds to a small amount of residual impurity. There are no observable peaks between 2.4 ppm and 3.2 ppm corresponding to either sulfide or sulfoxide.

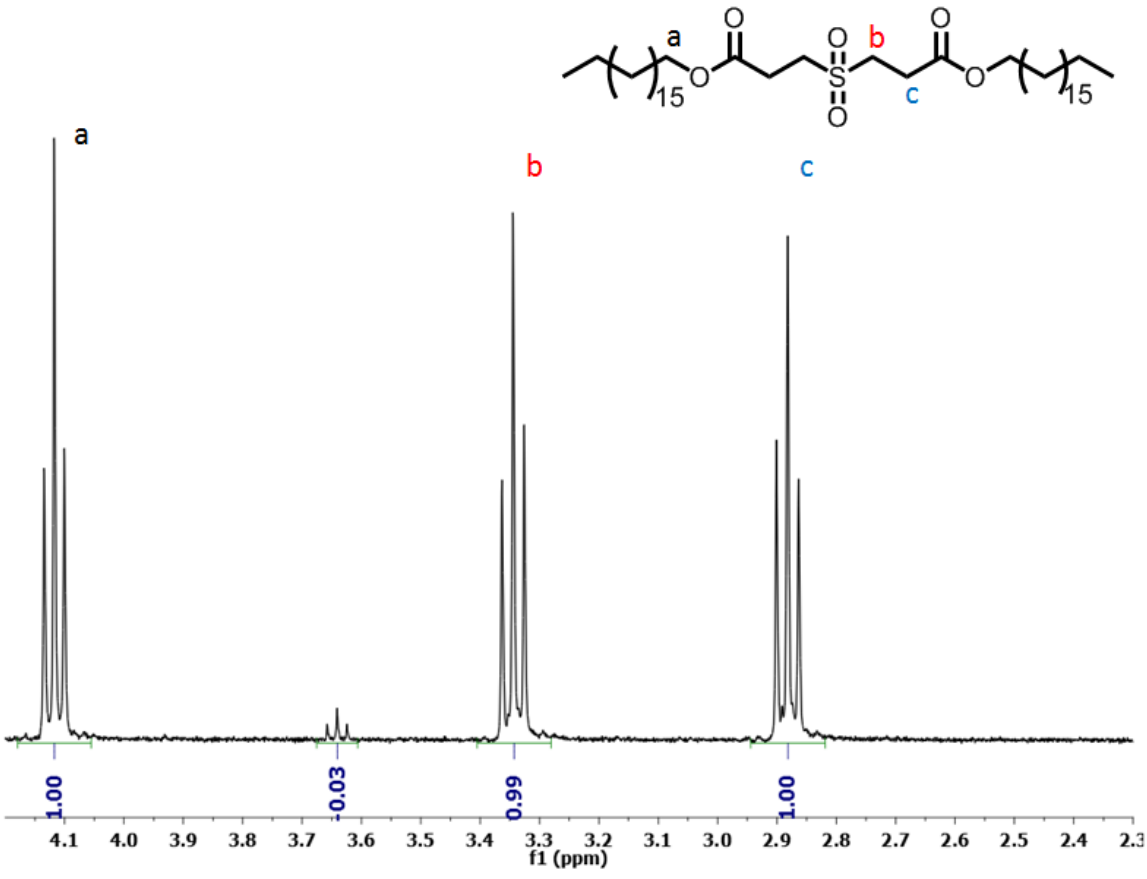

Figure 2.48. Proton NMR spectrum of synthesized sulfone derivative of DSTDP.

2.6.1.2 Verification of Step 6: Thermal Treatment of Sulfoxide Derivative of DSTDP

The rate of thermal decomposition of the sulfoxide derivative of DSTDP was measured using proton NMR. Samples of 0.0589 M sulfoxide were inserted into glass reactors and heated at various temperatures for 2 hours. Samples were extracted at time intervals and analyzed. The remaining proportion of sulfoxide was measured in each sample by determining the ratio of one peak with the total methyl protons on solution (which was assumed to be constant). The peak used for conversion measurements has a proton shift of 2.75 ppm. This peak does not overlap any other peaks either before or after reaction. A pair of representative NMR spectra is shown below in Figure 2.49.

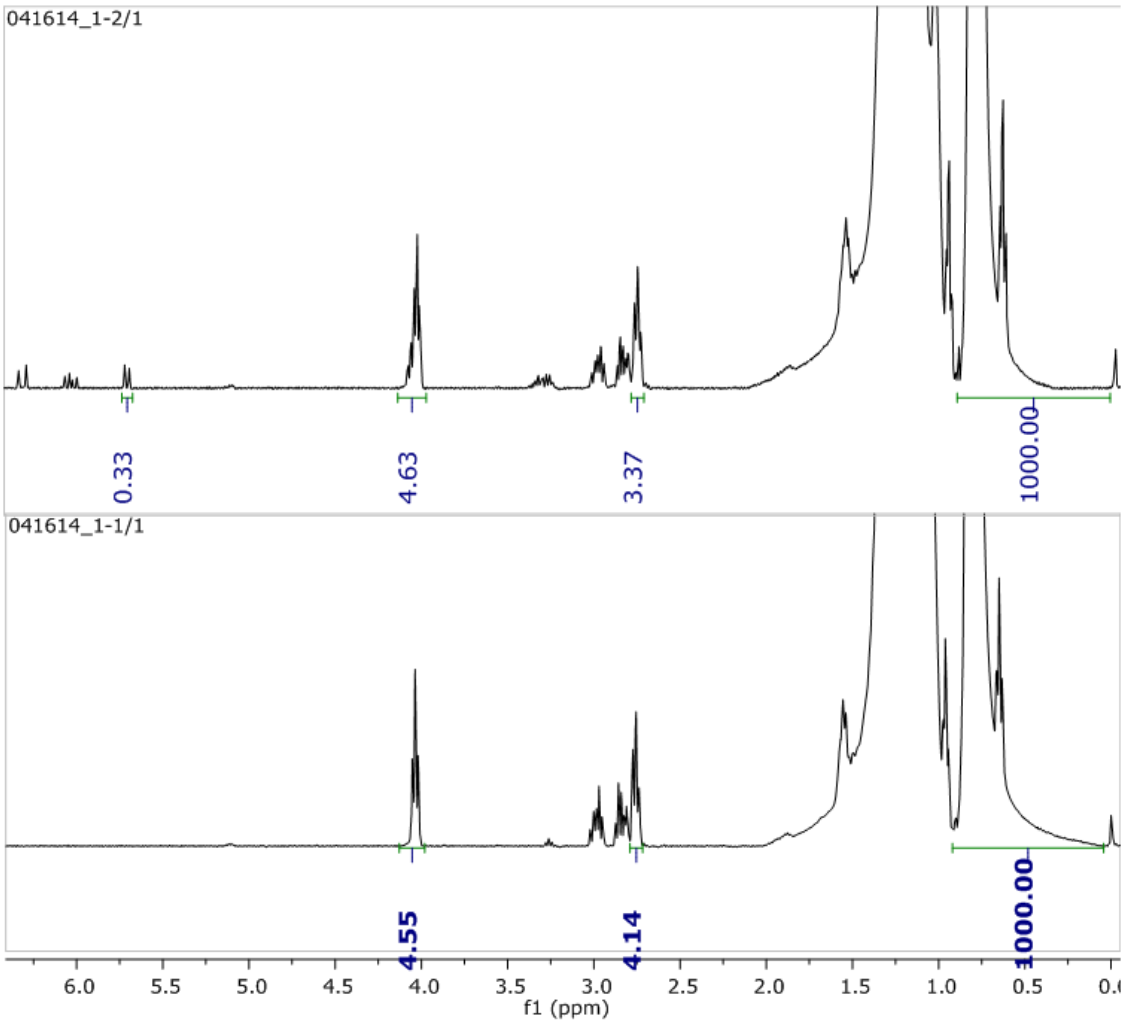

Figure 2.49. Proton NMR spectra of the thermal decomposition of 0.0589 M sulfoxide in dodecane at 102 °C. BOTTOM: prior to reaction. TOP: after 15 minutes of reaction. The peak at 2.75 ppm was compared with the methyl peak (set to 1000) to determine conversion.

As can be seen in Figure 2.49, the sulfoxide thermally decomposes at the temperature shown. The ratio of the peak at 2.75 ppm to the methyl peak decreases, and the peaks corresponding to the acrylate appear after heating.

Similar NMR spectra were measured every 15 minutes for 2 hours. The relative concentration data is plotted below for various temperatures below in Figure 2.50.

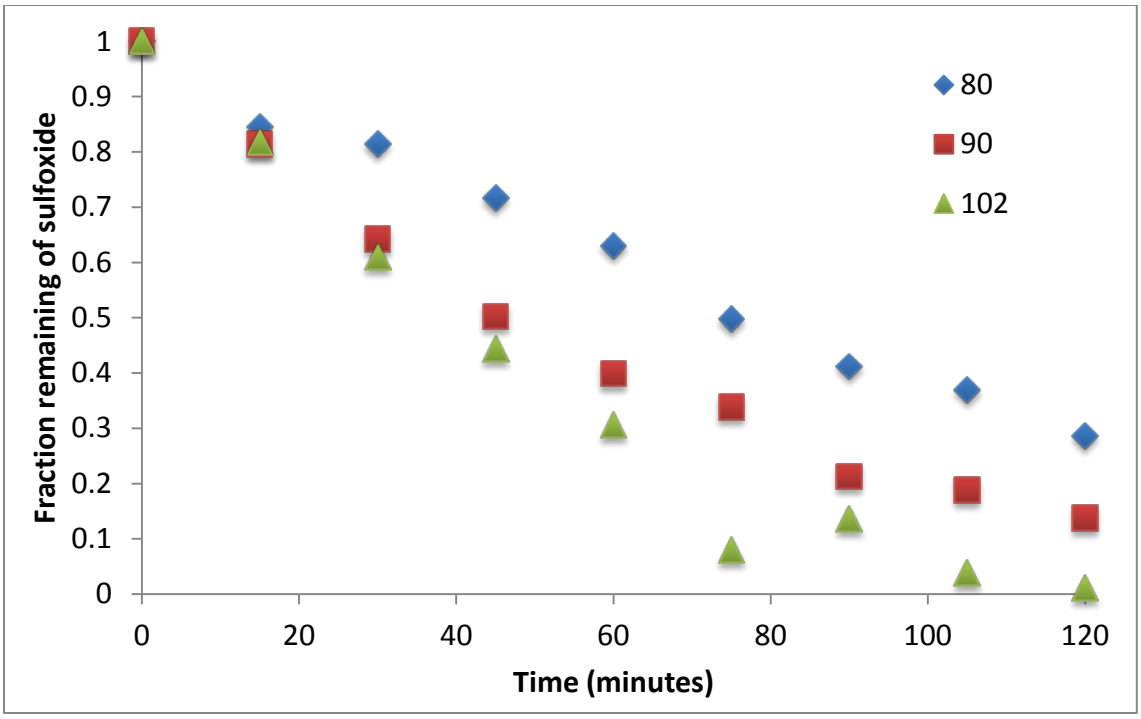

Figure 2.50. Conversion data for the thermal decomposition of 0.0589 M sulfoxide in dodecane over the course of 2 hours.

The data for the thermal decomposition of sulfoxide in Figure 2.50 give valuable insight. It appears that at the temperatures studied, sulfoxide has a fairly short half-life. At 102 °C, the half-life for this decomposition is approximately 40 minutes. This reveals that the retro-Michael addition and generation of sulfenic acid is fast enough to be relevant to the proposed mechanism. Step 6 in Figure 2.42 appears to be valid.

The sulfone derivative is not present in the proposed mechanism. This is because its rate of thermal decomposition was also examined using methods similar to those presented in Figure 2.49. The conversions for reactions of 0.0589 M sulfone in dodecane were measured over the course of 2 hours and are reported below in Figure 2.51.

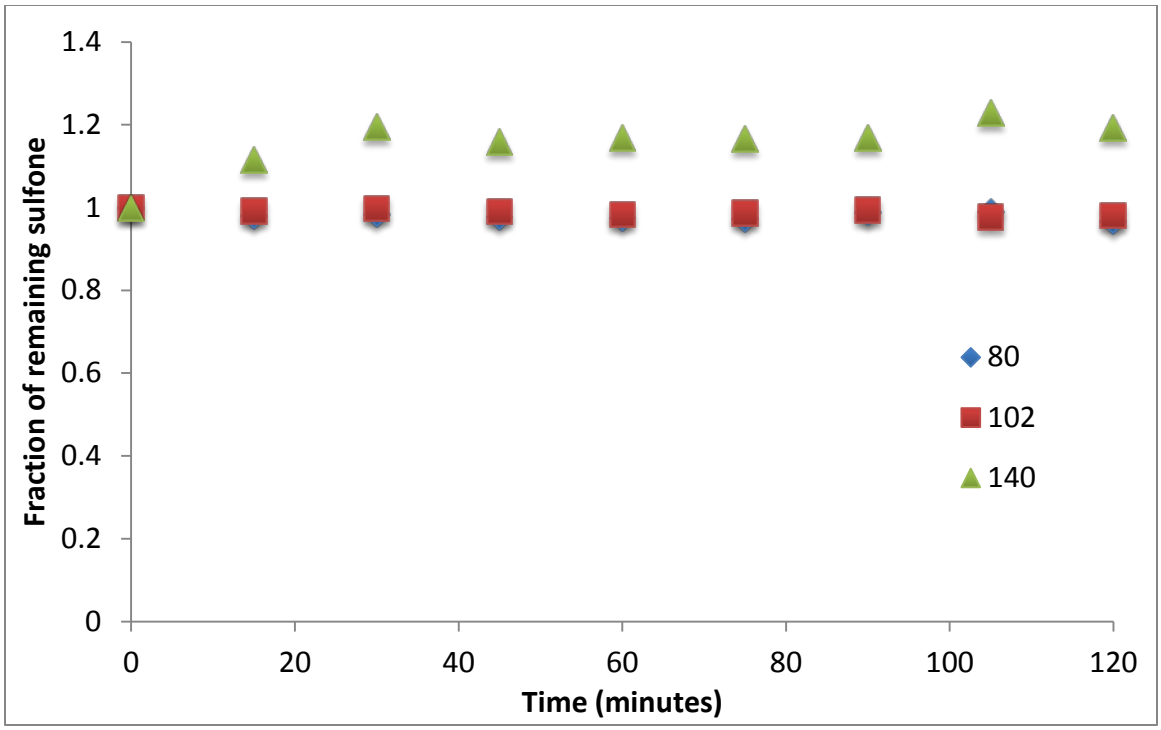

Figure 2.51. Conversion data for the thermal decomposition reactions of 0.0589 M sulfone in dodecane at various temperatures.

It is assumed that the initial increase reported in Figure 2.51 for the reaction at 140 °C is simply an error in the measurement technique. Regardless, it can be concluded that there is virtually no thermal decomposition of sulfone at any of the temperatures studied. For this reason, the sulfone derivative of DSTDP was neglected in the proposed mechanism. It's possible that the sulfone does form (at low concentrations) from oxidation via hydroperoxides; however, if it does form, it is essentially completely stable and no longer participates in the reaction.

2.6.2 Verification of Step 5: Reactions of DSTDP with CHP

Step 5 in Figure 2.41 proposes that hydroperoxides in solution are sufficient to oxidize DSTDP to the sulfoxide derivative. To prove the validity of this hypothesis,

0.1178 M DSTDP was reacted with 1 equivalent of CHP at 70 °C for 3 hours. The reaction mixture was loaded into glass vials as discussed and samples were taken periodically. The reaction was monitored using proton NMR, as shown below in Figure 2.52.

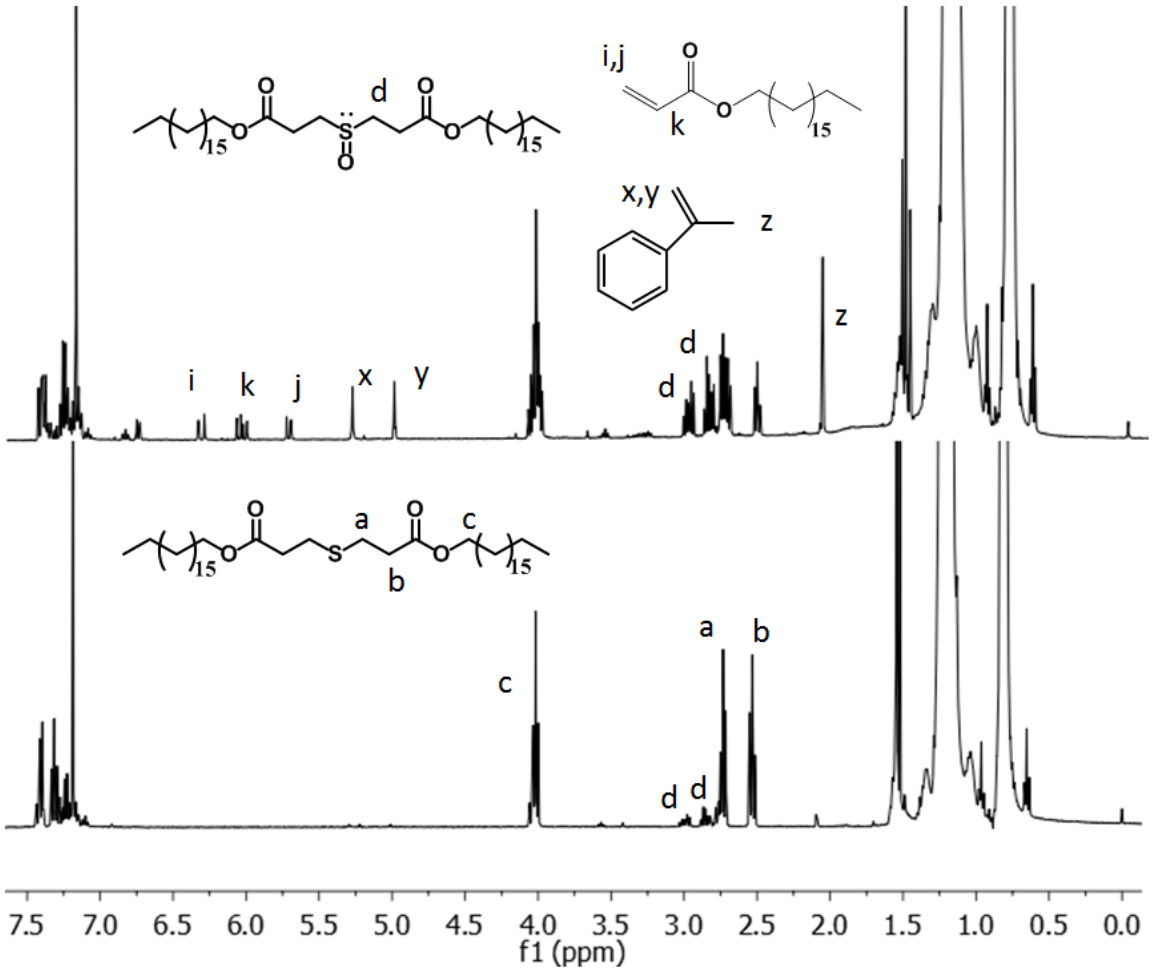

Figure 2.52. Proton NMR of the reaction of 0.1178 M DSTDP in dodecane with 1 equivalent of CHP. BOTTOM: reaction mixture after 1 minute at 70 °C. TOP: reaction mixture after 3 hours at 70 °C.

The spectra shown in Figure 2.52 demonstrate the oxidative power of hydroperoxides. A small amount of sulfoxide (as identified by peaks labeled 'd') was visible after only 1 minute at the relatively low temperature of 70 °C. After 3 hours at the same temperature,

substantial amounts of sulfoxide and acrylate are visible, concretely demonstrating the oxidation reaction. This experiment validates step 5 of the mechanism in Figure 2.41.

2.6.3 Reactions of DCP With the Sulfoxide Derivative of DSTDP

The thermal stability of the sulfoxide and sulfone derivatives of DSTDP have been examined. However, the impact of those derivatives on the rate of degradation of DCP has not been examined. This information would be a useful comparison to the rates of DCP decomposition with added DSTDP.

2.6.3.1 Verification of Step 7: Weakness of Sulfenic Acid

The consistency of the oxidation of sulfenic acid to sulfinic acid with the previous observations regarding DSTDP concentration and rate of DCP consumption has already been discussed. However, more concrete evidence for the necessity of step 7 in Figure 2.42 was needed. To verify the importance of the proposed step 7, 0.0589 M DCP was reacted with the sulfoxide derivative of DSTDP in dodecane at 120 °C. Glass reactors (similar to those used throughout this chapter) were charged with aliquots of this reaction mixture. Reactions with this composition were conducted both open to air and under argon pressure in argon-purged, sealed reactors. Reactors were submerged in heated oil baths for heating and samples were extracted at appropriate time intervals. The concentrations of DCP for each reaction mixture were determined using HPLC. Results are shown below in Figure 2.53.

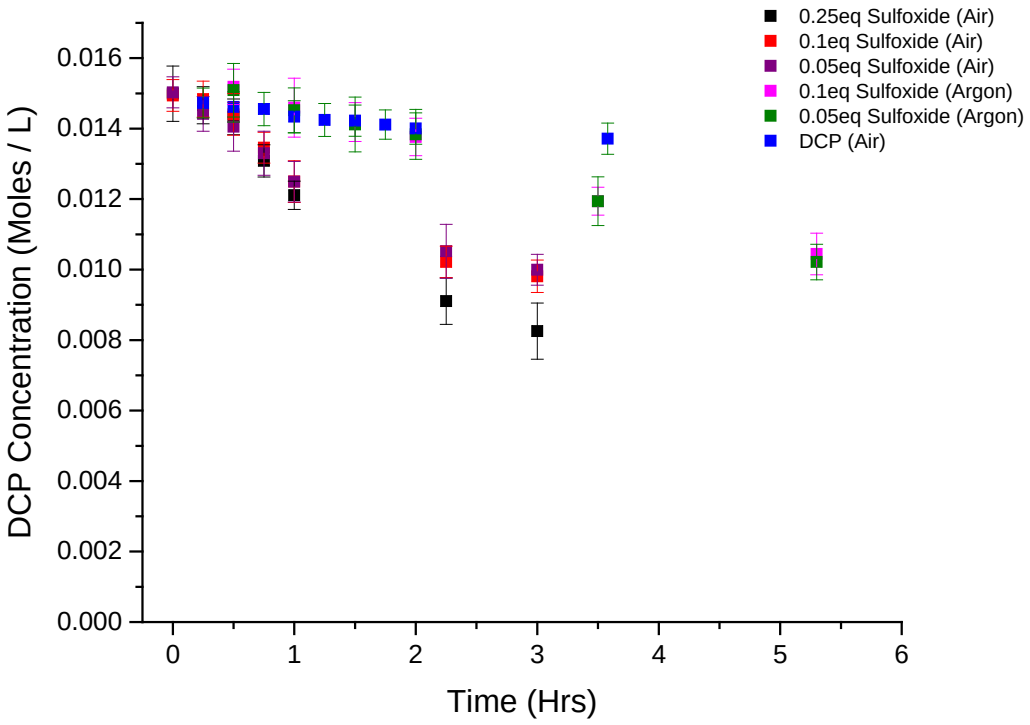

Figure 2.53. HPLC concentration data for the reactions of 0.0589 M DCP with the sulfoxide derivative of DSTDP in varying amounts at 120 °C for up to 5.5 hours.

The blue squares in Figure 2.53 are the control experiment: thermal decomposition of DCP. The remaining data sets all include some amount of sulfoxide. It can be seen that the remaining data are divided into two sets. The set of pink squares and green squares represent the reaction of DCP with 0.1 equivalents and 0.05 equivalents of sulfoxide, respectively, under argon. During the first 2 hours of reaction, these data sets appear to have the same rate of decomposition as the control experiment. This gives critical information about the nature of the acid species involved in our mechanism. Sulfoxide readily undergoes thermal degradation to form sulfenic acid. For the pink and green data sets, the reaction system immediately produces sulfenic acid. If the sulfenic acid were sufficiently strong to drive the decomposition observed in Figure 2.29, the pink

and green data sets would exhibit much faster degradation within 2 hours. Instead, they are largely indistinguishable from the control set. This strongly implies that sulfenic acid is not sufficiently strong to rapidly degrade DCP.

The black, red, and maroon data sets correspond to DCP reacted with 0.25 equivalents, 0.1 equivalents, and 0.05 equivalents of sulfoxide, respectively, open to air. Notice that these 3 data sets decompose much faster than the control and pink and green data sets. The data gathered for the reactions in air immediately display faster degradation rates. Recall that the proposed mechanism hypothesizes that oxygen is required to initially form hydroperoxides in the reaction system. It is therefore hypothesized that the sulfoxide present in the reactions immediately produces sulfenic acid and acrylate. Hydroperoxides formed by interaction with air then oxidize the sulfenic acid to sulfinic acid. This would explain the rapid degradation observed with the samples reacted in air but not observed with the samples reacted in argon.

Experimental evidence to confirm step 6 and step 7 of the proposed mechanism in Figure 2.42 has been presented. The rest of the steps in the mechanism are either uncontroversial or the subject of later study (acid-catalyzed decomposition in Chapter 3). At this point, the combination of a multitude of data has built and confirmed the proposed mechanism.

2.7 Explanation of Beneficial Reduction in Premature Crosslinking

Thus far, a comprehensive mechanism for the interaction of DCP with DSTDP when exposed to air has been proposed and supported. It seems that the proposed

mechanism is internally consistent and well supported with evidence so far. However, the beneficial observations in Table 2.1 have not yet been explained.

It is proposed that the reduction in premature crosslinking is caused by the formation of the radical sinks α-methyl styrene and stearyl acrylate. Both of these molecules can react with a radical to form a more stable radical due to the stabilizing electronics of the molecule. It is known that α-methyl styrene is an effective radical scavenger. Styrene is polymerized industrially using a radical mechanism.[20] An illustration of the possible stabilization mechanisms of both α-methyl styrene and acrylate is shown below in Figure 2.54.

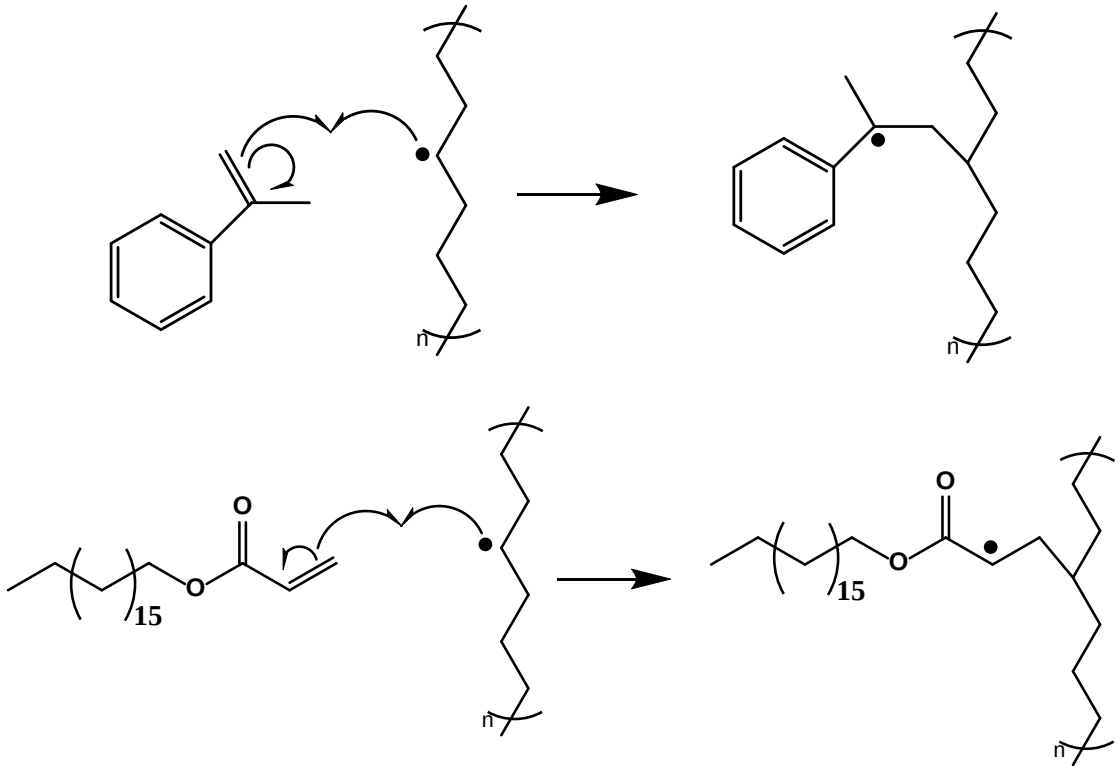

Figure 2.54. Proposed mechanism of radical stabilization by α-methyl styrene and stearyl acrylate, both of which are produced during reactions of DCP with DSTDP in air.

A logical question would be the following: if α-methyl styrene is an effective radical scavenger and stabilizer, why is it not used on its own as an additive to combat

premature crosslinking? The reason this is not feasible is because α-methyl styrene is vulnerable to radical-induced polymerization. A possible mechanism by which α-methyl styrene can be polymerized by radicals is shown below in

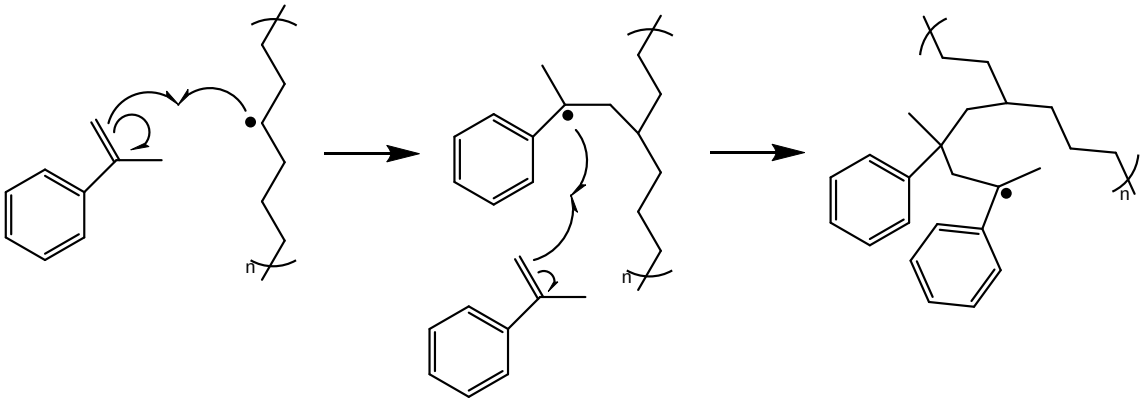

Figure 2.55. Possible mechanism of radical polymerization of α-methyl styrene. The polymerization can continue as long as methyl styrene is present in solution.

The reaction of DCP with α-methyl styrene in dodecane was examined. Reactors were charged with 0.0589 M DCP with 0.25 equivalents of α-methyl styrene and reacted at 120 °C. A proton NMR spectrum was taken after 15 minutes and 3 hours. The NMR spectra are shown below.

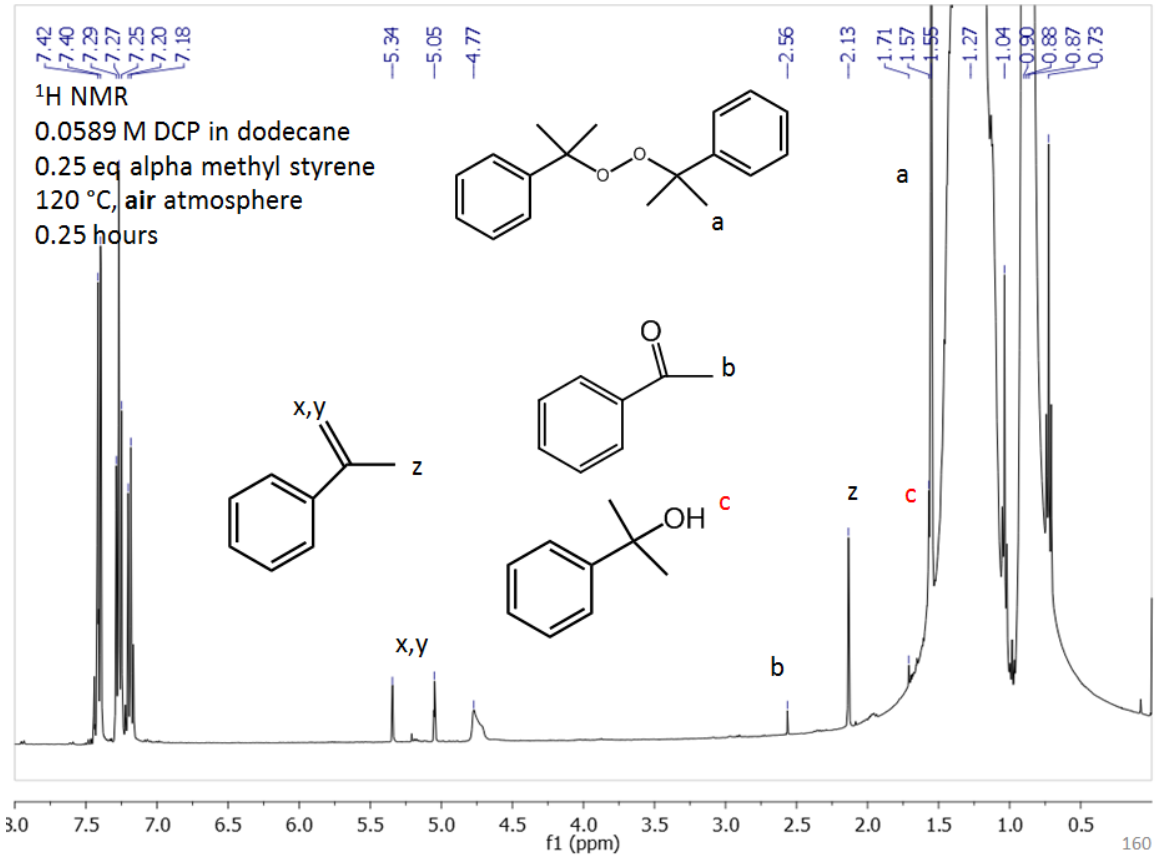

Figure 2.56. Proton NMR of the reaction of 0.0589 M DCP with 0.25 equivalents of α-methyl styrene after 15 minutes. Products are identified as labeled.

The reaction of DCP with α-methyl styrene after 15 minutes (Figure 2.56) shows expected product peaks. Peaks corresponding to DCP, acetophenone, cumyl alcohol, and α-methyl styrene are identified. There's also an unidentified peak that appears at 4.75 ppm that may correspond to polymerized styrene.

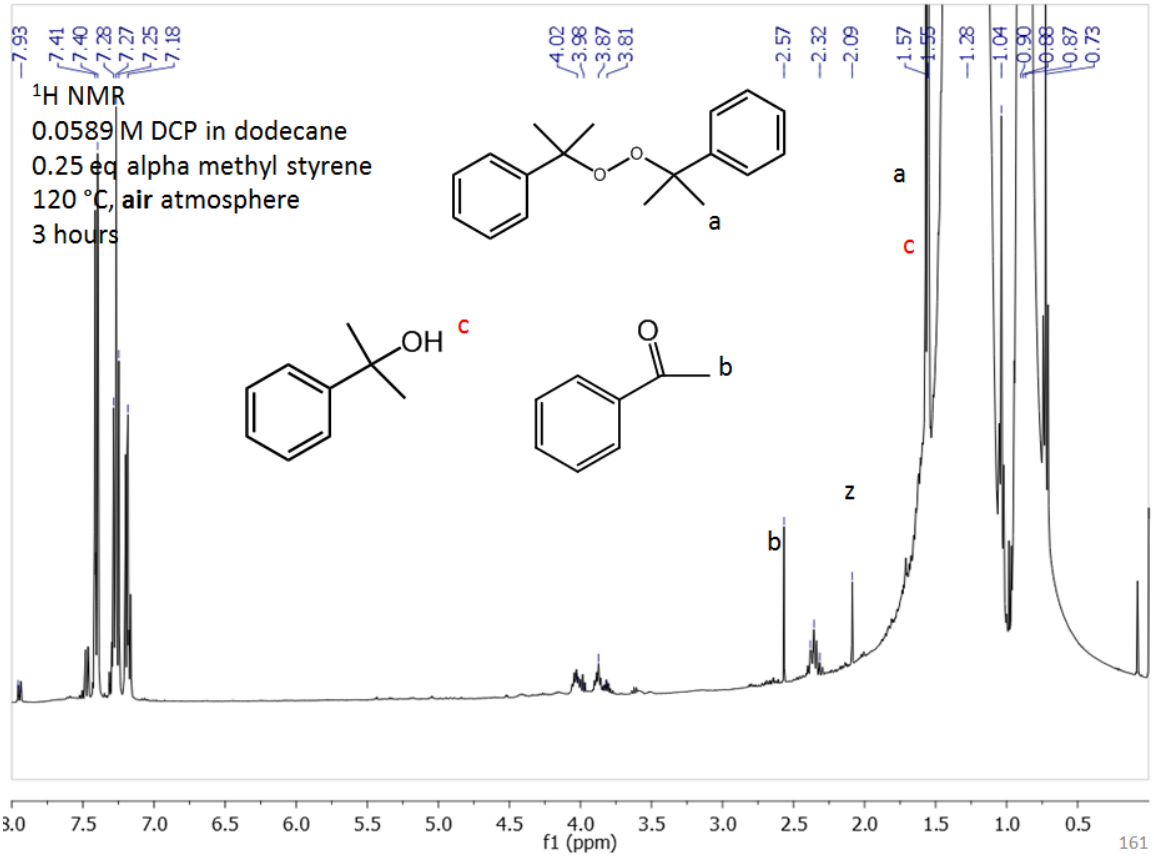

Figure 2.57. Proton NMR of the reaction of 0.0589 M DCP with 0.25 equivalents of α-methyl styrene after 3 hours. Products are identified when possible.

The reaction of DCP with α-methyl styrene after 3 hours shows the formation of several unidentified multiplets near 4.0 ppm on the proton NMR spectrum in Figure 2.57. It's likely that these peaks correspond to multiple different oligomers of α-methyl styrene.

This demonstrates the difficulty of using α-methyl styrene as a direct additive. It appears in Figure 2.57 that most of the initial α-methyl styrene was consumed while much of the DCP remained. Since the styrene can polymerize via radical propagation, it's possible for all the styrene to oligomerize without scavenging enough cumyloxy radicals. This would thereby render α-methyl styrene ineffective as a stabilizer when added alone.

Instead, the proposed mechanism hypothesizes that the α-methyl styrene and acrylate are both generated *in situ* near the reactive sites where they are necessary. If small amounts are present in solution at a given time, the likelihood is lessened that the radical scavengers will oligomerize prematurely.

2.7.1 Results With Other Peroxide Crosslinkers

Earlier it was mentioned that other peroxides have been used with DSTDP and exhibit a higher degree of premature crosslinking. The structures and names of these peroxides are shown below in Figure 2.58.

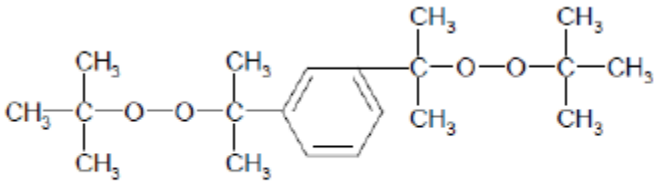

BIPB (di-(tert-butylperoxyisopropyl)benzene

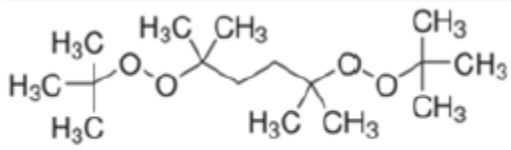

BTBPDMH (2,5-Bis(*tert*-butylperoxy)-2,5-dimethylhexane)

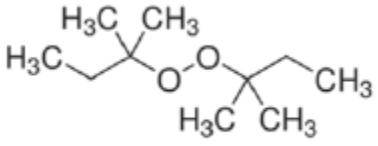

DTAP (Di-tert-amyl peroxide)

Figure 2.58. Structures and names of other peroxide crosslinkers examined in combination with DSTDP.

The relatively poor performance of the peroxides in Figure 2.58 is taken as weak supporting evidence for the hypothesis regarding the origin of premature crosslink reduction. If α-methyl styrene is responsible for scavenging radicals formed during processing, then the potential of each peroxide in Figure 2.58 to form α-methyl styene is worth examining.

Recall that in order of increasing premature crosslinking, the performance of the 4 peroxides was DCP<BIBP<BTBPDMH<DTAP. Among the 4 peroxides shown in this chapter, dicumyl peroxide is the only one capable of producing 2 moles of styrene per mole of peroxide (simply due to the symmetric structure containing 2 cumyl groups). BIBP is capable of producing only 1 mole of styrene, while the others can produce none. The prevention of crosslinking exhibited with each peroxide trends exactly with the ability of each peroxide to generate α-methyl styrene. This is taken as corroborating evidence suggesting that α-methyl styrene is important in reducing premature crosslinking.

2.8 Conclusions

This chapter presented our complete investigation of the kinetics and products of reactions of DCP with and without various additives. First discussed were the observations by Dow Chemical that motivated this study. A beneficial interaction was observed when DCP was blended with DSTDP in polyethylene and cured in air.

First, the thermal decomposition of DCP was examined as a baseline to contextualize later findings. The thermal decomposition of DCP was unaffected by the

presence of air. The products were cumyl alcohol and acetophenone under both air and argon, and the rate of decomposition was unaffected by atmosphere.

Reactions of DCP with DSTDP revealed several key pieces of information. The decomposition kinetics and products were vastly different under air and argon. Reactions under argon were largely identical to the thermal decomposition of DCP. The only new products of note were acetophenone and cumyl alcohol, and DCP decomposition was not notably accelerated. Reactions of DCP with DSTDP in air exhibited greatly accelerated decomposition of DCP and new products: phenol, α-methyl styrene, and stearyl acrylate.

It was hypothesized that the formation of acrylate was indicative of oxidation of DSTDP to its sulfoxide derivative. Using the accumulated information, a complete and consistent mechanism was proposed to explain the beneficial reduction in premature crosslinking observed with the combination of DCP and DSTDP. This chapter was concluded by providing further evidence for the proposed mechanism and relating it back to the reduction in premature crosslinking that motivated this investigation.

2.9 References

(1) Piringer, O. G.; Baner, A. L. *Plastic packaging: interactions with food and pharmaceuticals*; Wiley. com, 2008.

(2) Gugumus, F. Physico-chemical aspects of polyethylene processing in open mixers1: Review of published work. *Polymer degradation and stability* **1999**, *66*, 161.

(3) Khonakdar, H.; Morshedian, J.; Wagenknecht, U.; Jafari, S. An investigation of chemical crosslinking effect on properties of high-density polyethylene. *Polymer* **2003**, *44*, 4301.

(4) Mackevich, J.; Hoffman, J. Insulation enhancement with heat-shrinkable components. III. Shielded power cable. *Electrical Insulation Magazine, IEEE* **1991**, *7*, 31.

(5) Han, S. J.; Gross, L. Organic Peroxide-Initiated Crosslinking Study of Cable Compounds.

(6) Chaudhary, B.; Cogen, J.; Sun, Y. Dow Elastomers, Electrical and Telecommunications: Chemistry Options for Advanced Power Transmission Applications**2013**.

(7) RADO, R.; ZELENAK, P. CHEMICAL PROCESSES IN THE CROSS-LINKING OF POLYETHYLENE. *CHEMICKE LISTY* **1992**, *86*, 26.

(8) Hulse, G. E.; Kersting, R. J.; Warfel, D. R. Chemistry of dicumyl peroxide-induced crosslinking of linear polyethylene. *Journal of Polymer Science: Polymer Chemistry Edition* **1981**, *19*, 655.

(9) Di Somma, I.; Marotta, R.; Andreozzi, R.; Caprio, V. Dicumyl Peroxide Thermal Decomposition in Cumene: Development of a Kinetic Model. *Industrial & engineering chemistry research* **2011**, *51*, 7493.

(10) Bailey, H.; Godin, G. The thermal decomposition of dibenzoyl and di-α-cumyl peroxides in cumene. *Transactions of the Faraday Society* **1956**, *52*, 68.

(11) De Jonge, C. Synergism of antioxidants. *Pure and Applied Chemistry* **1983**, *55*, 1637.

(12) Grassie, N.; Scott, G. *Polymer degradation and stabilisation*; CUP Archive, 1988.

(13) Khonakdar, H.; Jafari, S.; Hässler, R. Glass-transition-temperature depression in chemically crosslinked low-density polyethylene and high-density polyethylene and their blends with ethylene vinyl acetate copolymer. *Journal of applied polymer science* **2007**, *104*, 1654.

(14) Dluzneski, P. R. Peroxide vulcanization of elastomers. *Rubber chemistry and technology* **2001**, *74*, 451.

(15) Chaudhary, B. I.; Chopin, L.; Klier, J. Nitroxyls for scorch suppression, cure control, and functionalization in free-radical crosslinking of polyethylene. *Polymer Engineering & Science* **2007**, *47*, 50.

(16) Arkema, I. Technical Decomposition Data for Assorted Proprietary Compounds.**2005.**

(17) Class, J. B. A review of the fundamentals of crosslinking with peroxides. *Rubber World* **1999**, *220*, 35.

(18) Ogunniyi, D. S. Peroxide vulcanisation of rubber. *Progress in rubber and plastics technology* **1999**, *15*, 95.

(19) Dračínský, M.; Pohl, R.; Slavětínská, L.; Buděšínský, M. Observed and calculated 1H and 13C chemical shifts induced by the in situ oxidation of model sulfides to sulfoxides and sulfones. *Magnetic Resonance in Chemistry* **2010**, *48*, 718.

(20) Hölderle, M.; Baumert, M.; Mülhaupt, R. Comparison of controlled radical styrene polymerizations in bulk and nonaqueous dispersion. *Macromolecules* **1997**, *30*, 3420.

CHAPTER 3 – FORMATION OF CUMENE HYDROPEROXIDE VIA THE ACID-CATALYZED DECOMPOSITION OF DICUMYL PEROXIDE

3.1 Introduction

In Chapter 2, the acid-catalyzed decomposition of dicumyl peroxide (DCP) was discussed in the context of the interaction of DCP with distearyl thiodipropionate (DSTDP). It was hypothesized that the acid-catalyzed reaction must generate a hydroperoxide to feed the mechanism presented in Chapter 2. Otherwise, the mechanism would proceed too slowly to account for the observations made of the reactions of DCP with DSTDP.

This chapter focuses on the detailed investigation of the reactions of a sulfur acid species with DCP. The investigation first seeks to simply prove that cumene hydroperoxide (CHP) is indeed an intermediate formed via the acid-catalyzed decomposition of DCP. Through the effort to prove this hypothesis, other experimental observations were made and are discussed herein. Additionally, substantial work will be discussed regarding the quantification of the amount of CHP formed during this acid-catalyzed reaction.

3.1.1 Reported Decomposition of Dicumyl Peroxide

As discussed in Chapter 2, DCP is a common radical initiator used for crosslinking polyethylene and other polymers.[1-4] The primary mechanism of crosslinking involves the thermal decomposition of DCP through homolytic cleavage to form two cumyloxy radicals. The cumyloxy radicals can then abstract hydrogen atoms from various species in a polymer blend, forming cumyl alcohol (CA). Alternatively,

cumyloxy radicals can undergo a beta-scission rearrangement to form acetophenone (ACP) and a methyl radical. This mechanism and the possible products are shown below in Figure 3.1.[5,6]

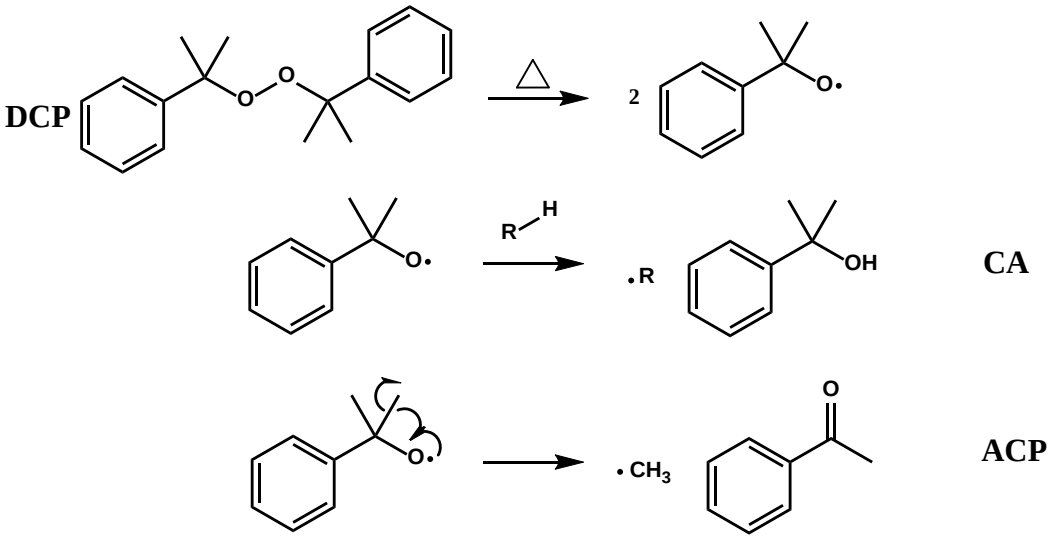

Figure 3.1. Mechanism of the thermal decomposition of DCP through homolytic cleavage.[6] Cumyloxy radicals can abstract hydrogen atoms to form CA or undergo beta-scission to form ACP.

In addition to thermal decomposition, DCP is vulnerable to reaction with acids. Acid reactions are relevant because common polyethylene compounding additives, such as clay fillers, can cause acidic decomposition.[7,8] The mechanism of acid-catalyzed decomposition of DCP is discussed in literature to some extent. It is suggested to follow an ionic mechanism giving rise to the end products phenol, acetone, and α-methyl styrene (AMS). The current literature mechanism is shown below in Figure 3.2.[1,8]

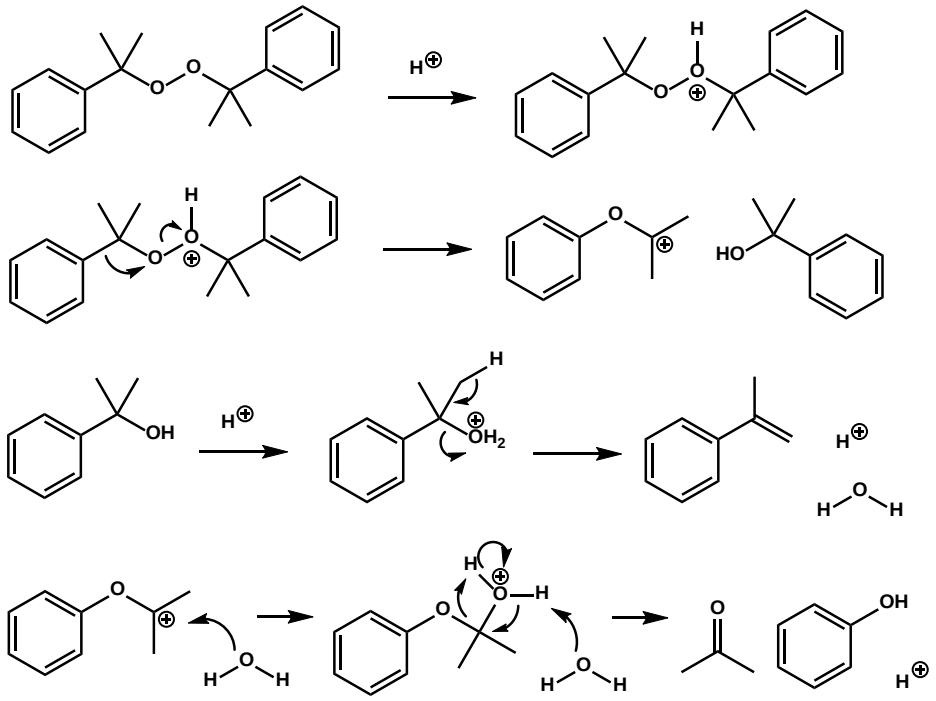

Figure 3.2. Literature mechanism for the acid-catalyzed decomposition of DCP.[1,8]

According to the literature mechanism shown in Figure 3.2, the products from this reaction are, per mole of DCP, 1 mole each of AMS, phenol, acetone, and water. Acid is proposed to be catalytic, as it is regenerated at the end of reaction. This corroborates the mechanism proposed in Chapter 2. The investigation presented herein aims to concretely demonstrate that the mechanism in Figure 3.2 is incomplete. It is hypothesized that instead of directly forming AMS, phenol, and acetone, a hydroperoxide intermediate is formed instead. The hydroperoxide then decomposes to form the observed end products of the reaction of DCP with acid. The current literature does not discuss the possibility of a hydroperoxide intermediate. As proposed in Chapter 2, the formation of a hydroperoxide intermediate could be vitally important and cause further reactions in a reaction system.

3.1.2 Phenol-Acetone Process

An industrial process called the "phenol-acetone" process uses the acid-catalyed decomposition of cumene hydroperoxide (CHP) to generate phenol and acetone.[9] In the phenol-acetone process, cumene is oxidized via a reaction with oxygen to form CHP. The resulting CHP is then reacted with a catalyst[10] or an acid[11] to generate the end products phenol and acetone. The phenol-acetone process is typically carried out using aqueous acid solutions. The mechanism of the aqueous acid-catalyzed decomposition of CHP is shown below in Figure 3.3.

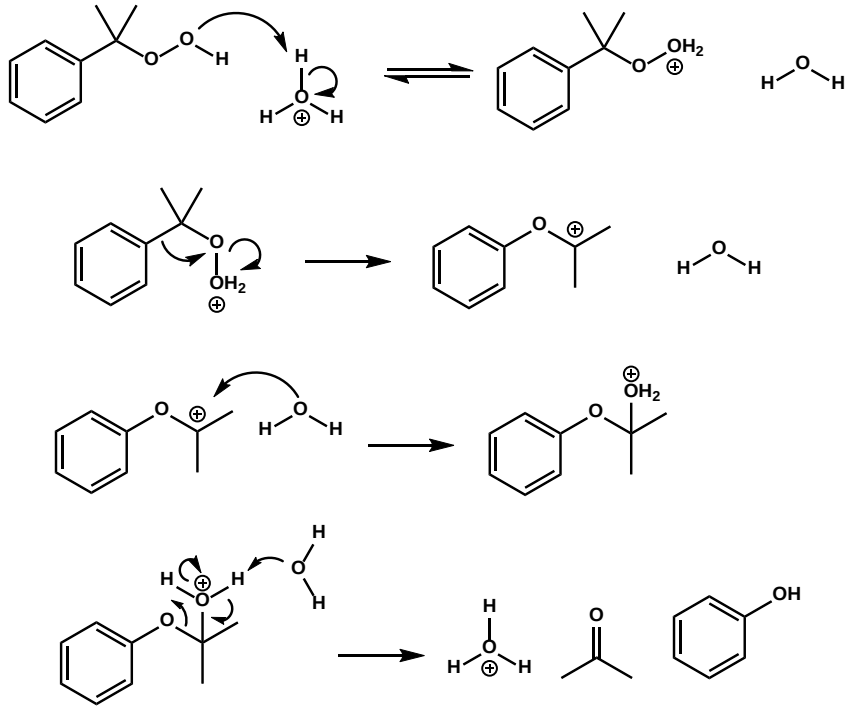

Figure 3.3. Aqueous acid-catalyzed decomposition of cumene hydroperoxide to form phenol and acetone.[12]

The details of the phenol-acetone process are well studied.[12-17] Furthermore, there are numerous patents describing the reaction systems relevant to the phenol-acetone process.[18-25] There are obvious similarities between the mechanisms shown in Figure 3.2 and Figure 3.3. The end products of the acid-catalyzed decompositions of DCP and CHP

are the same: 1 mole each of phenol and acetone per mole of reactant decomposed. In the case of DCP, the AMS comes from the second phenyl ring in the DCP structure. Despite the similarities in reaction products, none of the literature regarding DCP or CHP discusses the formation of CHP as an intermediate from DCP. One investigation discussed the possibility of the reverse reaction, wherein DCP is formed as a side product during the phenol-acetone process.[26] This is less significant than the production of CHP from DCP. In a detailed discussion of peroxide vulcanization chemistry, Leffler[27] proposed that reaction of t-butyl hydroperoxide with acid produced hydrogen peroxide. This discovery is significant and will be incorporated into the investigations herein. Finally, another author discussed the base-catalyzed decomposition of DCP to form phenol and acetone.[28] Still, there was no mention in the study of CHP. The hypothesis presented herein is therefore absent from the literature: the mechanisms presented in Figure 3.2 and Figure 3.3 actually represent different stages of the same process. Both are part of the acid-catalyzed decomposition of DCP.

3.2 Methodology

The goal of this chapter is to present a novel mechanism for the acid-catalyzed decomposition of DCP. As was the case in Chapter 2, this investigation attempts to relate the chemical behavior of DCP to polyethylene vulcanization. Thus, acid-catalyzed reactions were carried out in dodecane as a model solvent. The acid species discussed in Chapter 2 were sulfenic and sulfinic acids derived from the sulfoxide derivative of DSTDP. In this chapter, dodecylbenzenesulfonic acid (DBSA) was used as a model. Recall that the goal is to verify the presence of CHP as an intermediate, not to mimic the

kinetics shown in Chapter 2. The materials and analytical techniques used were as described below.

3.2.1 Materials

Dicumyl peroxide (DCP, 98%), dodecylbenzenesulfonic acid solution (DBSA, 70% in isopropanol), cumene hydroperoxide (CHP, 80%), tetrahydrothiophene (THTP, 99%), and dodecane (anhydrous, ≥99%) were all obtained from Sigma-Aldrich. DSTDP was purchased from City Chemical, LLC. With the exception of DBSA, all species were used as received. DBSA was purified using a Büchi Rotavapor R-210 and Vacuum Controller V-850. The solution was kept at approximately 30 psi and 50 °C for approximately 2 hours. The liquid phase was evaporated and the density was measured until it matched the reported value for DBSA (0.992 g/mL). The purified DBSA was promptly transferred to a dark freezer to prevent decomposition.

3.2.2 Reactions of DCP and Additives in Dodecane

Reactions typically contained 2 wt% DCP (or equivalent concentration of another reagent) in dodecane (0.0589 M). Reaction species (DCP and DBSA) were made into stock solutions in dodecane of double the required concentration (0.1178 M DCP, for example). Stock solutions could then be combined into the reaction vessel to reach the appropriate reaction volume. The mixtures were then diluted with dodecane, as necessary. Reaction solutions were prepared in cylindrical glass vials with stir bars. Vials were immersed in well-stirred baths of silicon oil set at the desired reaction temperature. Samples were removed at designated time intervals and worked up for

analysis with liquid chromatography, gas chromatography, or nuclear magnetic resonance.

3.2.3 Determination of the Critical Micelle Concentration of DBSA in Dodecane

DBSA has a sulfonic acid functionality as well as a long aliphatic tail. As such, it can form inverse micelles in dodecane. The sulfonic acid functionalities can hydrogen bond into clusters while the greasy tails orient outward into the bulk dodecane. To prevent any mass transfer effects, the critical micelle concentration (CMC) of DBSA in dodecane was determined using UV-Visible spectroscopy. Solutions of DBSA in dodecane were prepared at varying concentrations and analyzed with an Agilent Technologies Cary Series UV-Vis Spectrophotometer with quartz cuvettes of 1 cm path length. DBSA strongly absorbs UV-Visible radiation and its absorption spectrum and structure are shown below in Figure 3.4.

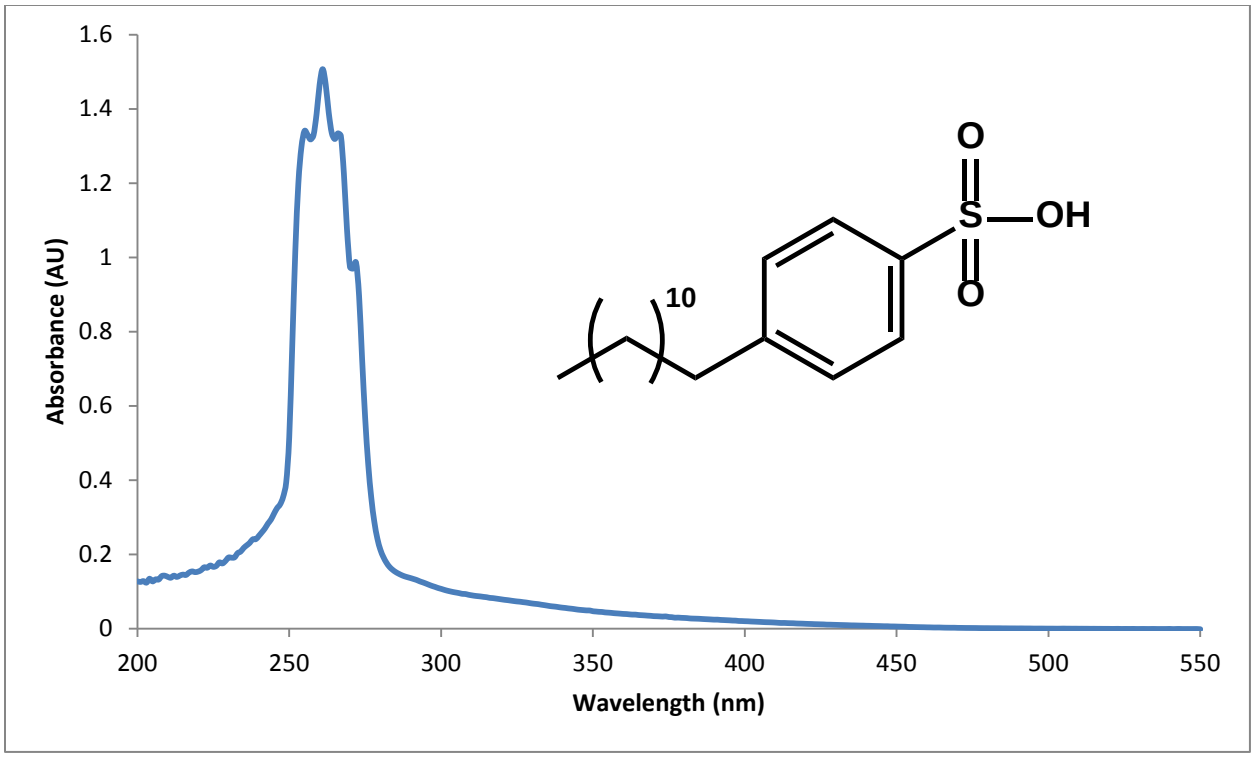

Figure 3.4. UV-visible absorption and structure of DBSA.

The maximum absorption was plotted against concentration to determine the CMC as shown below in Figure 3.5.

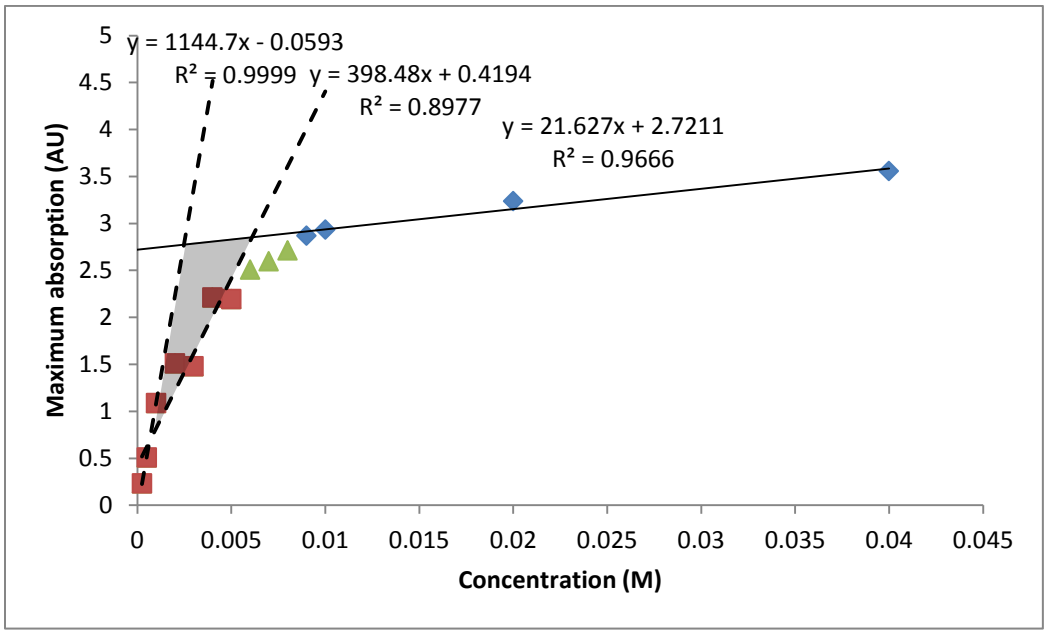

Figure 3.5. Maximum absorption of DBSA in dodecane plotted as a function of concentration. The gray area represents possible values of the CMC.

The maximum absorption of the DBSA solutions increases roughly linearly with increasing concentration below a certain threshold. After the threshold, higher concentrations of DBSA form inverse micelles and the absorbance does not increase with concentration at the same rate. The transition from rapid linear increase to a flat plateau is taken as the CMC.

Two dashed fit lines are observed on Figure 3.5 due to noisy data. The CMC is taken to be within the range shaded in dark grey, bounded by the 3 fit lines. Therefore, the CMC is between 0.0025 M and 0.006 M DBSA in dodecane. In this chapter, reaction mixtures measuring kinetics will contain concentrations of DBSA below this CMC to prevent any mass transfer effects from impacting the data. Some reactions will be run at higher concentrations for investigative purposes.

3.2.4 ^{1}H Nuclear Magnetic Resonance (NMR)

Some reactions were sampled and prepared for NMR analysis. Small aliquots were taken and diluted at approximately a 1:3 ratio with $CDCl_3$. Proton NMR spectra were gathered using a Brüker 400 MHz NMR instrument and Topspin processing software. Spectra were taken using 16 scans with 2-second relaxation time. NMR was used for product identification and quantification of sealed reaction products.

3.2.5 High Pressure Liquid Chromatography (HPLC)

Samples prepared for HPLC were diluted at exactly 1 part sample to 3 parts isopropanol, measured using a micropipette. HPLC spectra were gathered using a Shimadzu LC-20AD Liquid

Chromatograph with SPD-20A UV-Visible detector. The column was a Shimadzu C18 4.6 mm x 50 mm column with a 5 µm particle size. The mobile phase was 85% methanol / 15% water at a flow rate of 1 mL / minute. LC was used primarily for tracking the concentration of DCP and reaction products in the reaction mixture.

3.2.6 Gas Chromatography (GC)

Samples prepared for GC were diluted at exactly 1 part sample to 3 or 4 parts isopropanol. GC spectra were gathered using a Shimadzu GCMS-QP2010S with a Supelco PTA-5 column. The inlet temperature was 250 °C and a constant velocity method was used with a velocity of 40 cm / second. The oven used a variable temperature method starting at 150 °C for 5 minutes and ramping at 25 °C per minute to 250 °C for 6 minutes. The mass spectrometer ion source and interface were set at 225 °C. GC spectra aided in product identification and quantification.

3.3 Decompositions Reactions of DCP

3.3.1 Thermal Decomposition of DCP

Recall that in Chapter 2, solutions of 0.321 M DCP in dodecane were heated at temperatures between 110 °C and 150 °C for times of up to 8 hours. The results of these reactions are summarized here as a starting point for the acid-catalyzed reactions. The concentration of DCP during each reaction was tracked using HPLC and subjected to Arrhenius analysis. The experimental first-order rate constants are tabulated with reaction temperature below in Table 3.1.

Table 3.1. Reaction temperatures and first-order rate constants of the thermal decomposition of DCP.

Temperature (°C)	First-order rate constant
110	$6.05\ x\ 10^{-6}$
120	$4.64\ x\ 10^{-5}$
130	$8.38\ x\ 10^{-5}$
150	$5.57\ x\ 10^{-4}$

The Arrhenius analysis revealed that the thermal decomposition reaction had an experimental first-order activation energy of 146 kJ / mol, closely matching literature values of 144 kJ / mol.[5,29,30]

Products from the thermal decomposition of DCP were identified using proton NMR in Chapter 2. The products formed were CA and ACP, as reported by literature.[5] The agreement of the thermal decomposition kinetics and products with literature validates experimental techniques and are used as the starting point to investigate acid-catalyzed mechanisms.

3.3.2 Observation of CHP via the Acid-Catalyzed Decomposition of DCP

The primary goal of this chapter is to demonstrate that CHP is produced as an intermediate when DCP is decomposed by an acidic mechanism. However, directly measuring CHP in solution is difficult. As discussed previously in this chapter, both DCP and CHP are vulnerable to acid attack. CHP is expected to exist temporarily as an intermediate. To prove that CHP is formed from this acid-catalyzed reaction, a way to signify its presence was needed.

3.3.2.1 Reaction of DCP with DBSA in the Presence of DSTDP

The mechanism proposed in Chapter 2 suggests that CHP is capable of oxidizing DSTDP. As such, DSTDP was employed to determine whether or not CHP formed from the reaction of DCP with DBSA. If CHP is formed, some amount of DSTDP will be oxidized to form a sulfoxide. The sulfoxide will undergo retro-Michael addition to form stearyl acrylate. Therefore, the presence of stearyl acrylate in this reaction would be proof of the presence of hydroperoxides in solution.

DCP was reacted with DSTDP and a catalytic amount of DBSA. To mimic the catalytic nature of acid as proposed in our system, 0.05 molar equivalents of DBSA were added to decompose DCP. The reaction was conducted with 0.0589 M DCP, 0.0147 M DSTDP, and 0.00295 M DBSA. Stock solutions of 0.1178 M DCP and 0.1178 M DSTDP were combined and diluted with dodecane to reach final concentrations. DBSA was added neat at a volume of several microleters.

The 0.00295 M DBSA may be above the CMC as shown in Figure 3.5. To minimize the possibility of aggregation, reaction solutions were allowed to stir with stir bars for 30 minutes at room temperature prior to reaction.

To deconvolute the possible effects of CHP and atmospheric oxygen, the reaction solutions were sparged with argon and the reactors purged with argon prior to reaction. Reactors were also kept under positive argon pressure during reaction. The work in Chapter 2 demonstrated that this technique was sufficient to prevent interaction with atmospheric oxygen, so it is assumed to be an effective purging method. The reaction was conducted at 120 °C for 3 hours and analyzed via proton NMR. The first sample was taken after 15 minutes and is shown below in Figure 3.6.

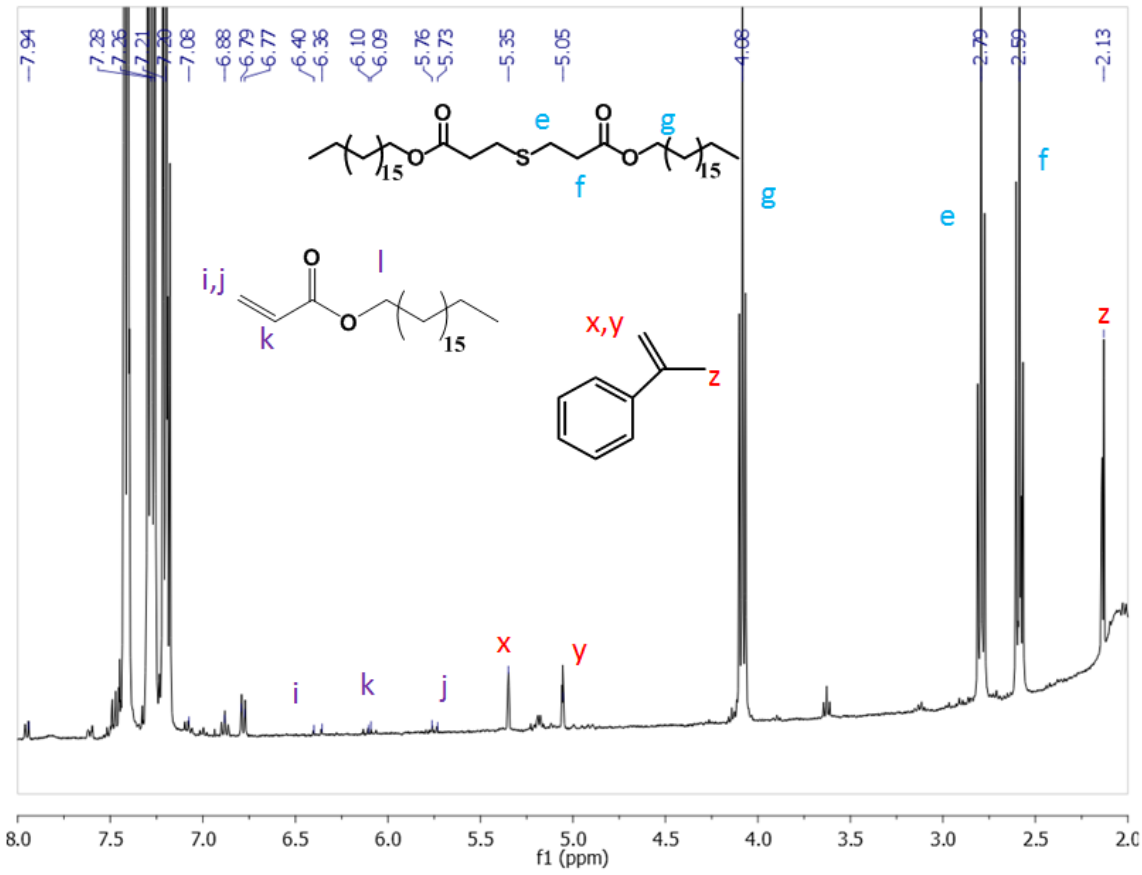

Figure 3.6. Proton NMR of the reaction of 0.0589 M DCP with 0.25 equivalents of DSTDP and 0.05 equivalents of DBSA in dodecane at 120 °C after 15 mintues.

The 15-minute sample is shown because it best demonstrates the presence of stearyl acrylate. The presence of acrylate, demonstrated by peaks labeled ‘i’, ‘j’, and ‘k’, indicates that hydroperoxides are formed during reaction. Since the reaction is purged with argon, any hydroperoxides must form via the acid-catalyzed decomposition of DCP. Proton NMR spectra recorded at later reaction times actually showed less acrylate. The low amount of acrylate shown in Figure 3.6 is weak evidence for the hypothesis that CHP is formed in this reaction. Since the main goal of this work is to concretely prove that CHP forms via acid-catalyzed decomposition of DCP, a more effective indicator was used.

3.3.2.2 Reaction of DCP with DBSA in the Presence of Tetrahydrothiophene

Like DSTDP, tetrahydrothiophene (THTP) is a symmetric sulfide. This mean that tracking its oxidation products is similar to tracking the oxidation products of DSTDP. In fact, the proton NMR spectra of THTP and its oxidized derivatives are available in literature and display a similar trend to DSTDP and its oxidized derivatives. The proton spectra of these species are shown below in Figure 3.7.

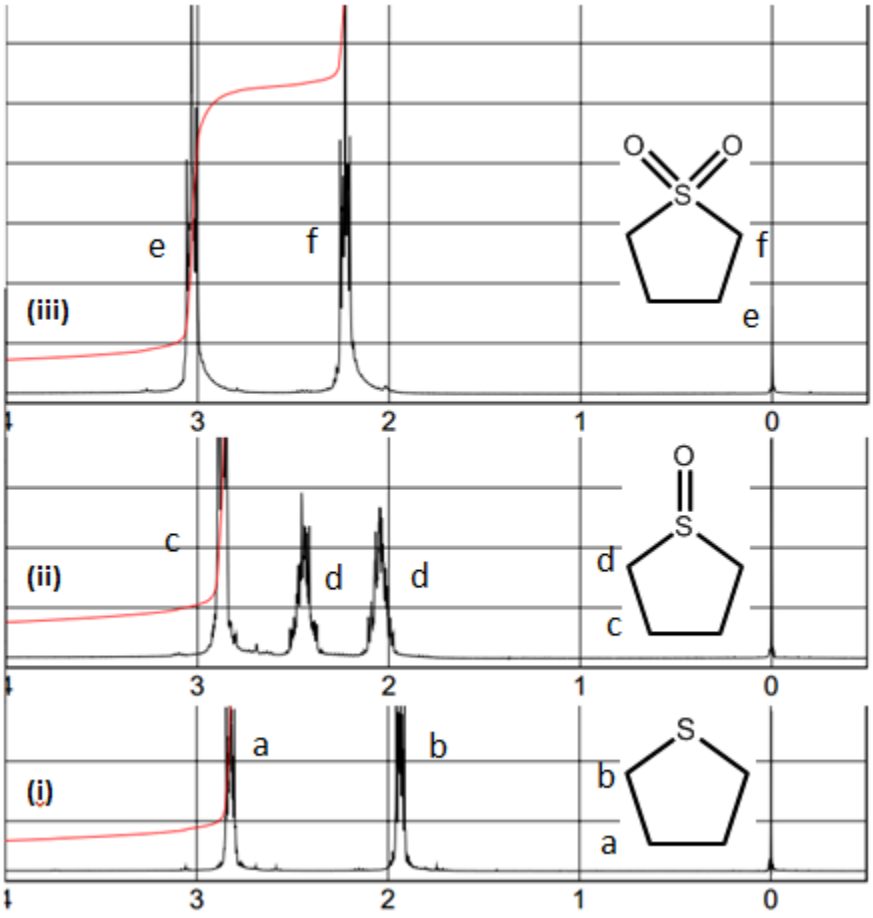

Figure 3.7. Proton NMR spectra of THTP and its oxidized derivatives in $CDCl_3$.

Similar to DSTDP, the sulfoxide form of THTP has enantiotopic protons (nearest the sulfur atom) labeled as 'd' in Figure 3.7. These two protons each have a different NMR

shift resulting in the spectrum shown. Fortunately, this means that the sulfoxide derivative will be readily identifiable if formed in a solution containing THTP.

Unlike DSTDP, THTP is a cyclic sulfide. As compared with DSTDP, which has two very long tails on each side of the sulfur atom, THTP has no steric hindrance around the sulfur atom. It is therefore expected that the rate of oxidation from a hydroperoxide would be much faster with THTP than with DSTDP.

To demonstrate the formation of CHP from the acid-catalyzed reaction, a suite of studies was conducted using THTP to deconvolute the possible variables influencing the reaction. Reaction mixtures were prepared analogously to those prepared with DSTDP. Initially, 0.0589 M DCP was reacted with 0.25 equivalents of THTP at 102 °C for 3 hours to show that DCP will not produce oxidized derivatives which would pollute the results. Second, 0.0589 M CHP was reacted with 1 equivalent of THTP at 120 °C for 30 minutes to show that CHP will oxidize THTP. Finally, 0.0589 M DCP was reacted with 0.25 equivalents of THTP and 0.03 equivalents of DBSA at 102 °C for 2 hours. The reactions were analyzed after heating via proton NMR as shown below in Figure 3.8.

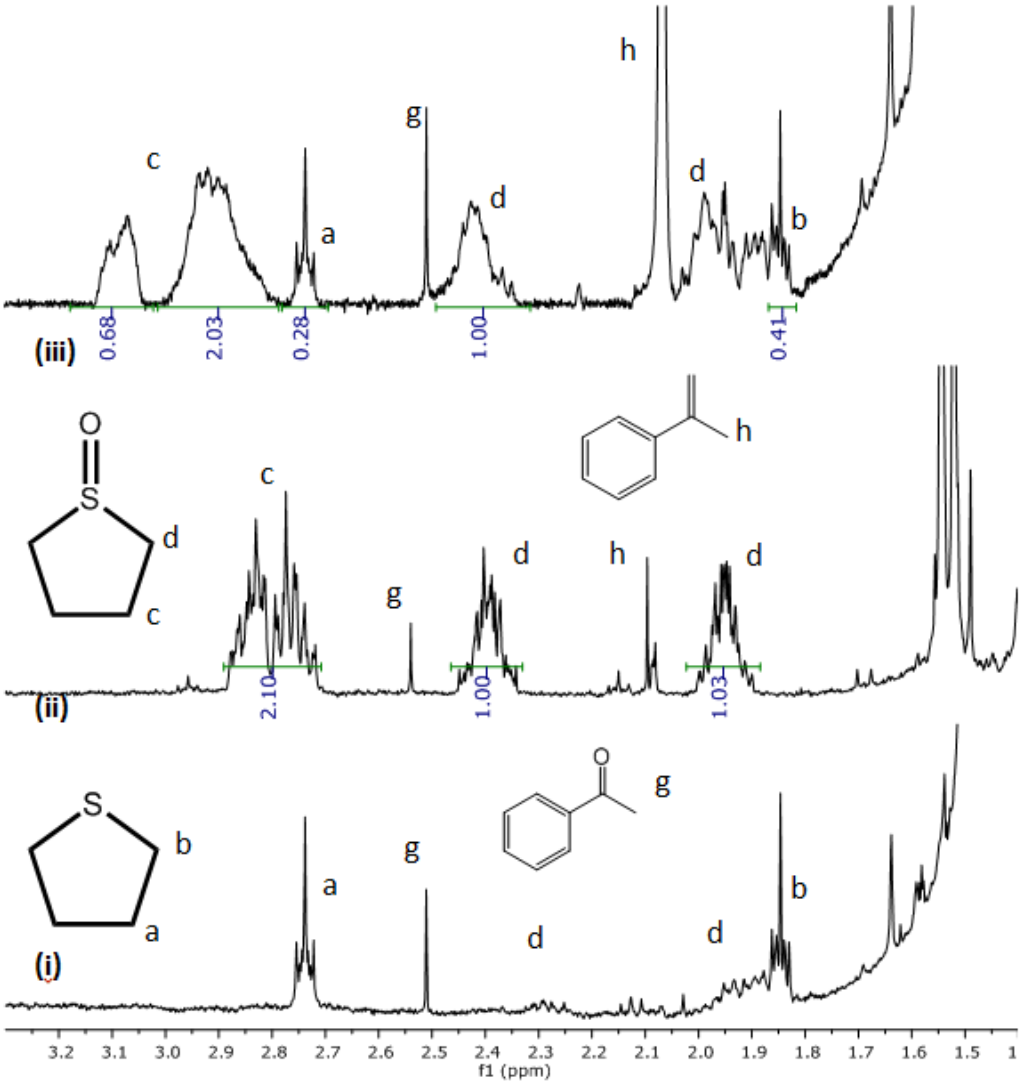

Figure 3.8. Reactions of THTP with peroxide species and acid. (i): 0.0589 M DCP + 0.25 molar equivalents of THTP at 102 °C for 3 hours. (ii): 0.0589 M CHP + 1 molar equivalent THTP at 120 °C for 30 minutes. (iii): 0.0589 M DCP + 0.25 molar equivalents THTP + 0.03 molar equivalents DBSA at 102 °C for 2 hours.

The results shown in Figure 3.8 demonstrate the formation of CHP. Spectrum (i) shows almost no interaction between DCP and THTP, even at long reaction times of 3 hours. Spectrum (ii) shows that CHP readily oxidizes THTP. Complete conversion was achieved after 30 minutes at 120 °C. The distinct peaks for the sulfide and sulfoxide species are made apparent: ‘a’ and ‘b’ correspond to the sulfide, while ‘c’ and ‘d’ correspond to the sulfoxide. No sulfone was observed.

Spectrum (iii) concretely demonstrates that the acid-catalyzed decomposition of DCP produced a hydroperoxide. The sulfoxide peaks are clearly visible in the NMR spectrum, which did not appear when DCP was mixed with THTP alone. The acid was necessary to produce a species that could oxidize THTP to the sulfoxide form.

The integrals in spectrum (iii) allow for a crude measurement of the extent of oxidation. The baseline of the NMR spectra were smoothed using the Whittaker smoother in MestreNova. In spectrum (iii), the ratio of peak 'a' to peak 'd' is 0.28:1.00. Peak 'a' corresponds to twice as many protons as peak 'd' (due to the enantiotopic protons), so the actual ratio of sulfide:sulfoxide is therefore 0.14:1.00. Therefore, approximately 88% of the initial sulfide was oxidized to form sulfoxide.

To determine how much DCP was consumed during the reaction in spectrum (iii) of Figure 3.8, the NMR spectrum was shifted to view the protons corresponding to DCP and dodecane. The ratio of the integral of the methyl peaks of DCP to the methyl peaks of dodecane was measured both before and after the acid-catalyzed reaction. The relative values were compared to determine the conversion of DCP. An example proton NMR spectrum of a solution of 0.0589 M DCP in dodecane is shown below.

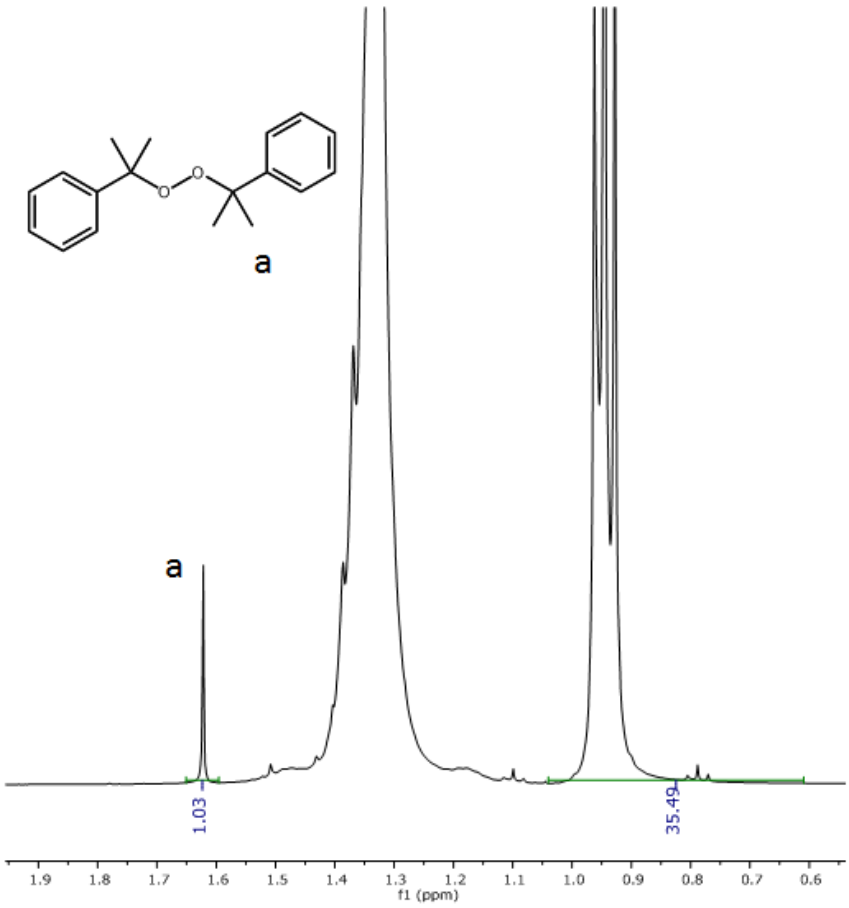

Figure 3.9. Proton NMR spectrum of 0.0589 M DCP in dodecane, zoomed to show the methyl peaks of DCP and the methyl peaks of dodecane.

The ratio of the DCP peak to the dodecane peak as shown in Figure 3.9 is roughly 1:35 for 0.0589 M DCP. After the reaction shown in spectrum (iii) of Figure 3.8, the ratio was roughly 1:49. This change represents a DCP conversion of 29%. It was established above that 88% of the 0.25 equivalents of THTP were oxidized during the reaction of DCP with DBSA. A conversion of 29% of DCP was able to oxidize 88% of 0.25 equivalents of THTP. By simple mathematics, this means that approximately 75% of the consumed DCP produced CHP that was able to oxidize the THTP to the sulfoxide form.

As part of the investigation of the reaction of DCP with DBSA, kinetics data were also gathered.

3.3.3 Kinetics Analysis of the Reaction of DCP with DBSA

For the reactions of DCP with DBSA, DCP was reacted at 2 wt% in dodecane (0.0589 M). To emulate a catalytic amount of acid, 0.03 molar equivalents of DBSA (0.001767 M) were typically added to solutions of DCP.

Stock solutions were again prepared at double the required concentration and combined at equal volume to obtain the desired concentrations. DCP was prepared at 0.1178 M in dodecane and DBSA was prepared at 0.003534 M. According to Figure 3.5, 0.003534 M may be above the CMC of DBSA in dodecane. Once again, to account for this possibility and to minimize any possible aggregation, reaction solutions were allowed to stir for 30 minutes at room temperature prior to reaction. Reactions were conducted between 60 °C and 130 °C. The concentrations of DCP were measured using HPLC. A sample HPLC chromatogram is included below in Figure 3.10.

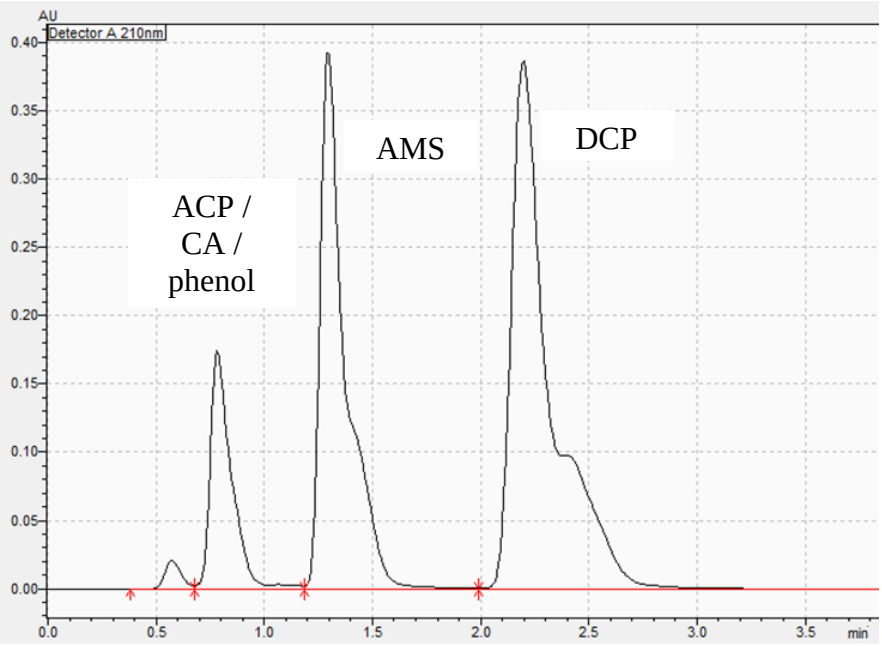

Figure 3.10. Representative chromatogram from the HPLC analysis of reactions of DCP with DBSA.

Species in Figure 3.10 were identified by retention time using standards of the pure compounds run using the HPLC using the same method. The concentration of DCP was easily trackable using the area under the DCP curve in the chromatogram. The DCP concentration data for all reactions are shown below in Figure 3.11.

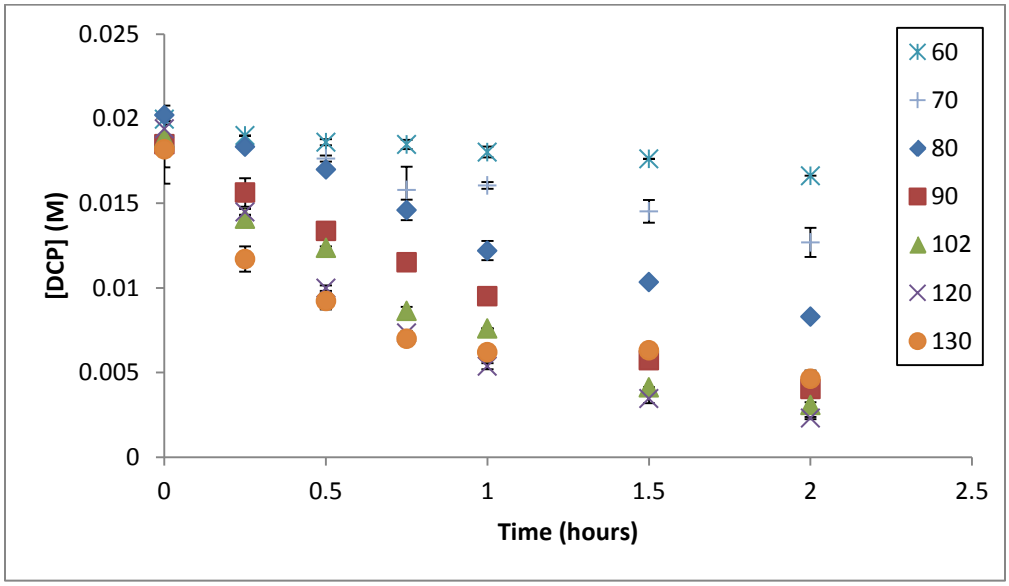

Figure 3.11. Concentrations of DCP as a function of time for the reactions of 0.0589 M DCP with 0.03 equivalents of DBSA in dodecane. All reactions were run for 2 hours.

The decomposition rates in Figure 3.11 show the expected trend. In general, higher temperatures induce faster rates of decomposition. However, significant overlap is observed at later reaction times at the higher temperatures (90 °C and higher). In particular, the curve for the 130 °C data flattens out more than the other sets of data after 1 hour. This may be caused by poisoning of the acid catalyst by water generated via the reaction (through dehydration of cumyl alcohol). Water molecules in solution could hydrogen bond with DBSA and inhibit the acid's ability to attack DCP.

As with the thermal decomposition of DCP, the data in Figure 3.11 were subjected to Arrhenius analysis. It was assumed that the DBSA behaved catalytically and

the reaction of DCP with DBSA is pseudo-first order. The data sets in Figure 3.11 were linearized on a first-order plot. In the case of the 130 °C data set, only the first 3 data points were used as the rest were possibly influenced by poisoning of the acid catalyst. The first-order plot is shown below as Figure 3.12.

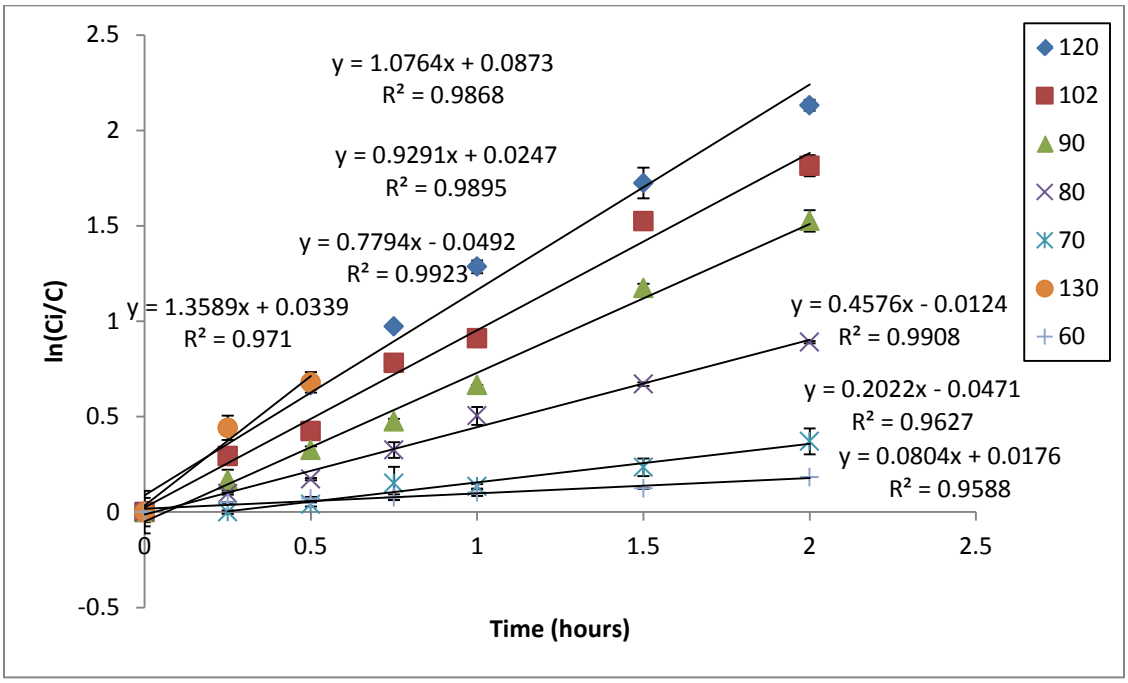

Figure 3.12. First-order plot of the concentration profiles from the reactions of 0.0589 M DCP with 0.03 equivalents DBSA in dodecane.

The slopes of the lines in Figure 3.12 were taken as first-order rate constants for the reaction of DCP with DBSA. The rate constants were plotted on an Arrhenius plot as shown below in Figure 3.13.

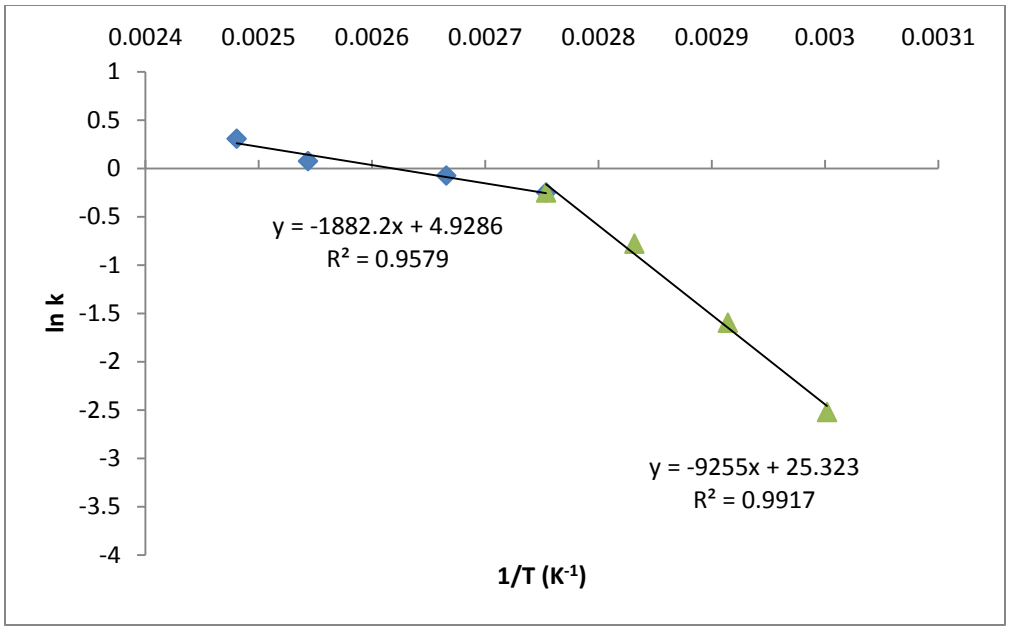

Figure 3.13. Arrhenius plot for the reactions of 0.0589 M DCP with 0.03 equivalents of DBSA in dodecane.

A remarkable discovery is apparent from Figure 3.13. The Arrhenius plot exhibits two distinct regimes with different activation energies. At low temperatures (up to 90 °C), the activation energy is observed to be 76.9 kJ / mol. At higher temperatures (measured up to 130 °C), the activation energy was measured at 15.6 kJ / mol. Both of the measured activation energies are considerably lower than that of the thermal decomposition of DCP (140 kJ / mol), which accounts for the much faster decomposition rates in the presence of acid.

A convex Arrhenius plot (as shown in Figure 3.13) can be explained by an equilibrium reaction during the attack of acid on DCP.[31] It's possible that instead of a truly ionic protonation step, DCP and DBSA instead form a hydrogen-bonded complex that can readily reverse to starting materials. This is another difference from the mechanism reported in literature. A visual presentation of the hydrogen-bonding mechanism is shown below in Figure 3.14.

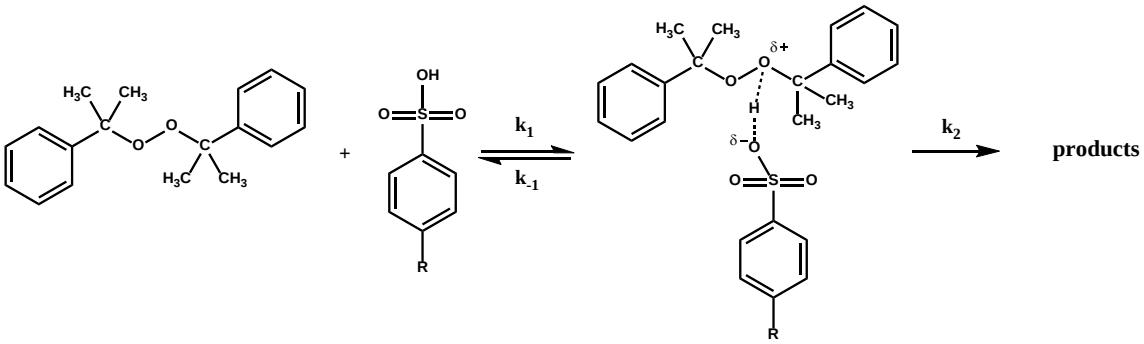

Figure 3.14. Proposed mechanism involving a hydrogen-bonded complex during the reaction of DCP with DBSA. The large complex could break apart via several pathways, including the reverse reaction.

It is possible to develop a straightforward analytical expression for the concentration of DCP as a function of time if several assumptions are applied. First, the concentration of DBSA in solution is assumed constant (e.g., DBSA acts as a true catalyst). This assumption is likely valid for at least the initial stages of reaction. Second, the steady-state assumption is applied to the concentration of the intermediate complex. If both assumptions are applied, the rate expression for the consumption of DCP can be developed as below in Figure 3.15.

$$C = [complex]$$

$$\frac{dC}{dt} = k_1[DCP][DBSA] - k_{-1}C - k_2C$$

$$set\ \frac{dC}{dt} = 0$$

$$C = \frac{k_1[DCP][DBSA]}{k_{-1} + k_2}$$

$$\frac{d[DCP]}{dt} = -k_1[DCP][DBSA] + k_{-1}C$$

$$\frac{d[DCP]}{dt} = -k_1[DCP][DBSA] + k_{-1}\left[\frac{k_1[DCP][DBSA]}{k_{-1} + k_2}\right]$$

$$-\frac{d[DCP]}{dt} = \frac{k_2k_1}{k_2 + k_{-1}} * [DBSA] * [DCP]$$

$$-\frac{d[DCP]}{dt} = k_{eff} * [DCP]$$

$$k_{eff} = \frac{k_2k_1}{k_2 + k_{-1}} * [DBSA]$$

Figure 3.15. Derivation of an analytical expression for the rate of consumption of DCP when reacted with DBSA.

With the form of the effective first-order rate constant k_{eff} expressed in Figure 3.15, two kinetic regimes are possible. The lower temperature regime in Figure 3.13 has the higher activation energy (76.9 kJ / mol). This magnitude of activation energy is usually associated with bond formation. As a result, it is proposed that at low temperatures, the following simplification is possible in Figure 3.16.

$$k_2 \gg k_{-1}$$

$$-\frac{d[DCP]}{dt} = k_1[DBSA][DCP]$$

Figure 3.16. Proposed form of the rate expression for the reaction of DCP with DBSA in dodecane at low temperatures.

The expression in Figure 3.16 assumes k_2 is much larger than k_{-1}. In such a case, the reaction is driven strongly in the forward direction and the influence of the equilibrium step is effectively eliminated. Essentially, the complex reacts in the forward direction as quickly as the initial hydrogen bond is made. The rate expression therefore looks like a strictly first-order expression.

The higher temperature regime of Figure 3.13 exhibits the lower activation energy of 15.6 kJ / mol. Such low activation energies are typically associated with hydrogen bonding phenomena. Therefore, the following simplification is proposed for high temperatures in Figure 3.17.

$$k_{-1} \gg k_2$$

$$-\frac{[DCP]}{dt} = \frac{k_1}{k_{-1}} k_2[DBSA][DCP] = K_{eq} k_2[DBSA][DCP]$$

Figure 3.17. Proposed form of the rate expression for the reaction of DCP with DBSA in dodecane at high temperatures.

The expression in Figure 3.17 assumes k_{-1} is much larger than k_2, corresponding to a weakening of hydrogen bonding at high temperatures. In such a case, the reaction would be limited by the backward equilibrium step. Indeed, the simplified rate expression now contains the equilibrium constant, K_{eq}, signifying the importance of the backward step.

The derived rate expression in Figure 3.15 and simplifications in Figure 3.16 and Figure 3.17 can explain the appearance of the convex Arrhenius plot. The formation of a

hydrogen-bonded complex instead of simple protonation can be easily understood by the fact that the reaction solvent is dodecane. In such a nonpolar solvent, the formation of ionic species (via protonation) is highly unfavorable. It's possible that in a more traditional solvent, the Arrhenius plot would be linear.

3.3.3.1 Proton NMR Analysis of Reactions of DCP with DBSA

In addition to purely kinetic analysis, the products of reaction were examined using proton NMR. Spectra were recorded for the reaction of 0.0589 M DCP with 0.03 equivalents of DBSA at 120 °C. The results are shown below in Figure 3.18.

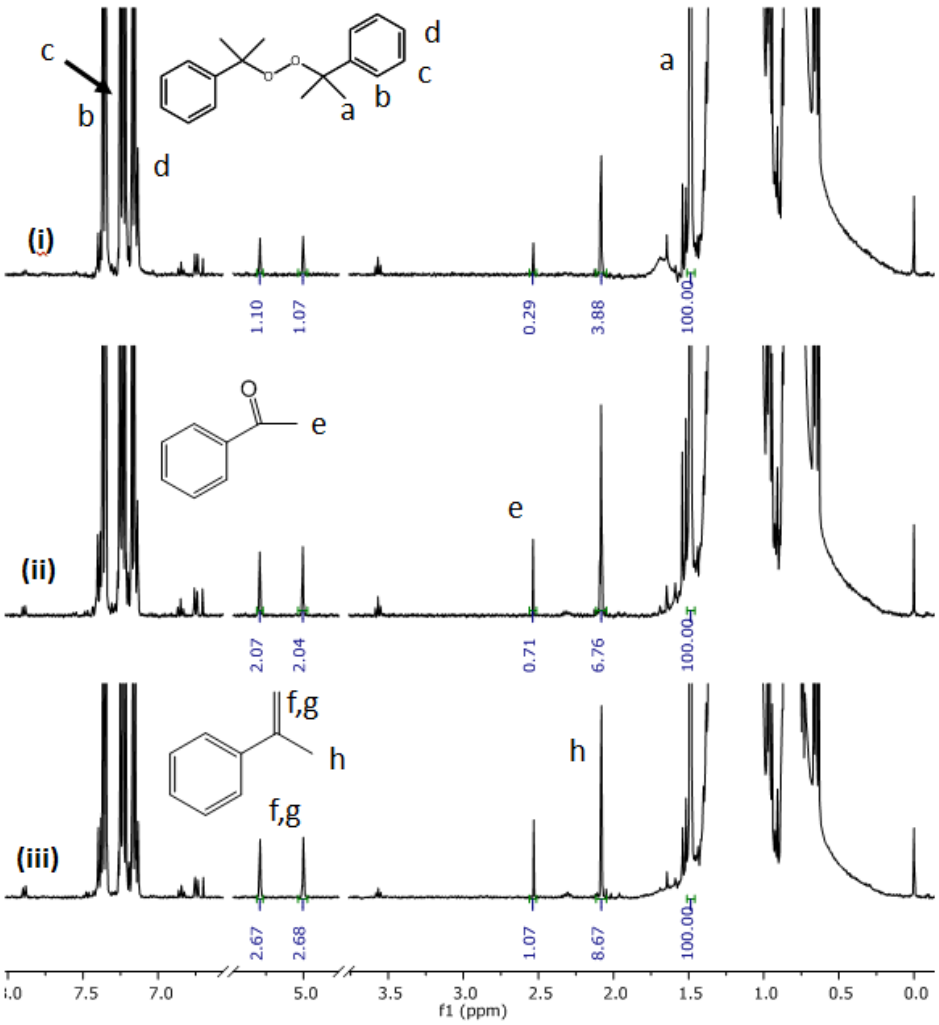

Figure 3.18. Proton NMR spectra of the reaction of 0.0589 M DCP with 0.03 equivalents of DBSA at 120 °C. (i): spectrum after 15 minutes of reaction. (ii): spectrum after 30 minutes of reaction. (iii): spectrum after 45 minutes of reaction.

The spectra in Figure 3.18 show products consistent with literature reports. Specifically, phenol and AMS are both observed as products. Additionally, ACP is observed, likely due to the thermal degradation of DCP. No CA is observed as expected, as CA would be dehydrated by DBSA to form AMS.

3.4 Mechanism of Reaction of DCP with DBSA in Dodecane

Combining the kinetics analysis and product identification discussed in this chapter, a complete mechanism of the reaction of DCP with DBSA in dodecane was proposed. The complete mechanism is shown below in Figure 3.19.

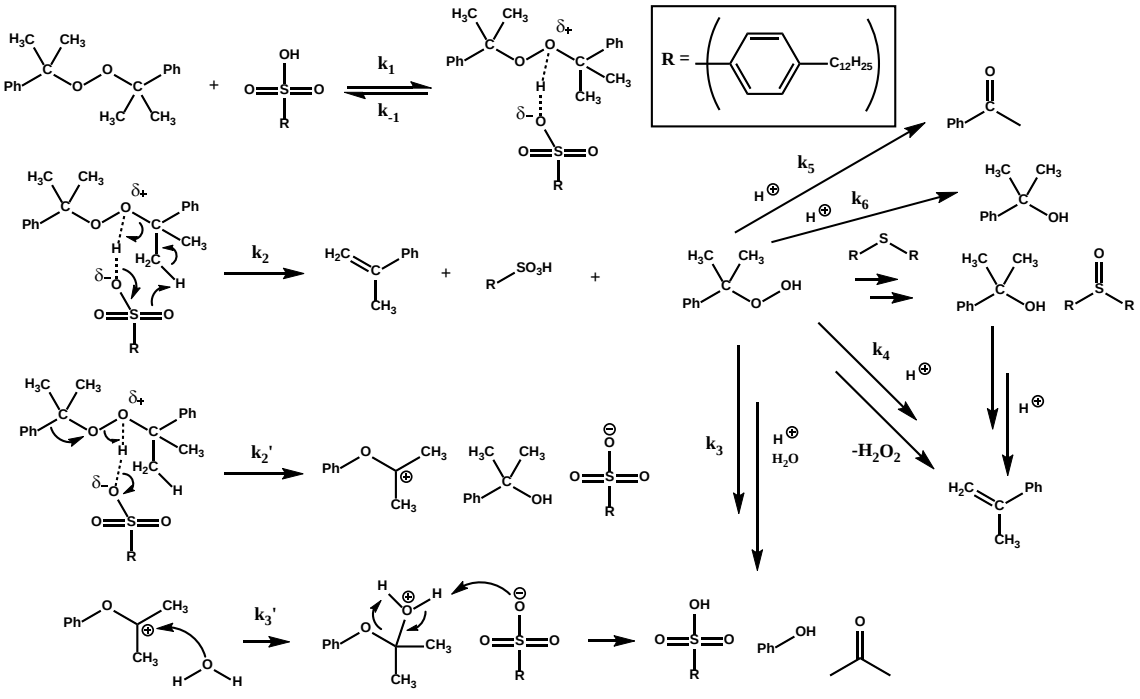

Figure 3.19. Proposed mechanism of the acid-catalyzed decomposition of DCP.[27]

As discussed, after the initial formation of a hydrogen-bonded complex, several possible pathways are available. The complex can break apart to form the starting materials, DCP and DBSA. Alternatively, the reaction can progress via either the k_2 pathway to form AMS and CHP or through the k_2' pathway to form phenol and acetone. Notice that this mechanism does not attempt to supersede the current literature understanding; rather, it is an addendum to provide a more complete understanding of this acid-catalyzed reaction.

Any CHP formed can be rapidly degraded with acid to form a variety of products including phenol and acetone. Notice that up to two moles of AMS can be formed per mole of DCP degraded. AMS can form through the k_2 pathway and also subsequently through the k_4 pathway.

As shown in Figure 3.18, phenol was observed in the reaction system. The proposed mechanism shows two possible pathways to form phenol: via k_2' followed by k_3', or by k_2 followed by k_3. The origin of the observed phenol cannot be conclusively determined at this point.

While it does substantially alter current literature understanding, the mechanism presented in Figure 3.19 accounts for all observations made regarding the acid-catalyzed decomposition of DCP.

3.5 Quantification of Acid-Catalyzed DCP Decomposition Products

The formation of CHP was concretely shown earlier in this chapter. The amount formed was also crudely calculated using proton NMR. A more rigorous analysis of the amount of CHP produced is presented here. The goal of this analysis is to determine the

ratio of $k_2'/(k_2 + k_2')$ shown in Figure 3.19. This ratio expresses exactly how much CHP is formed during the acid-catalyzed decomposition.

To close the mass balance for the acid-catalyzed reaction, it was assumed that all cations produced from the k_2' pathway also proceed through the k_3' pathway to form phenol. In other words, it is assumed that no side products are formed from the cationic species. No unidentified species were identified in significant concentrations to invalidate this assumption.

From examination of Figure 3.19, a mass-balance expression for the selectivity of phenol is possible. This expression is shown below in Figure 3.20.

$$phenol\ selectivity = \frac{k_2'}{k_2 + k_2'} + \left[1 - \frac{k_2'}{k_2 + k_2'}\right] X_{CHP} \frac{k_3}{k_3 + k_4 + k_5}$$

Figure 3.20. Expression for the selectivity of phenol during the acid-catalyzed decomposition of DCP. The selectivity of phenol is defined as $(\boldsymbol{moles\ phenol\ produced})/(\boldsymbol{mole\ DCP\ consumed})$. 'X' represents conversion of the relevant species.

The aim is to obtain phenol selectivity on the basis of DCP consumption, so X_{DCP} can be set to 1. The full derivation of Figure 3.20 is shown below as Figure 3.21.

$$[phenol\ produced] = \int_0^t \frac{d[phenol]}{dt} dt = \int_0^t [phenol]' dt$$

$$[phenol\ produced] = \int_0^t [phenol]'_{DCP} dt + \int_0^t [phenol]'_{CHP} dt$$

where [phenol]'$_{DCP}$ is the rate of phenol produced directly from DCP and [phenol]'$_{CHP}$ is the rate of phenol produced directly from CHP.

$$[phenol\ produced] = \frac{k_2'}{k_2 + k_2'} \int_0^t \frac{d[DCP]}{dt} dt + \int_0^t [phenol]'_{CHP} dt$$

$$[phenol\ produced] = \frac{k_2'}{k_2 + k_2'} * X_{DCP} * [DCP]_0 + \int_0^t [phenol]'_{CHP} dt$$

$$[phenol\ produced] = \frac{k_2'}{k_2 + k_2'} * X_{DCP} * [DCP]_0 + \frac{k_3}{k_3 + k_4 + k_5} \int_0^t (rate\ of\ consumption\ of\ CHP) dt$$

$$[phenol\ produced] = \frac{k_2'}{k_2 + k_2'} * X_{DCP} * [DCP]_0 + \frac{k_3}{k_3 + k_4 + k_5} * X_{CHP} * [CHP]_0$$

where $[CHP]_0$ is taken to be the total amount of CHP produced during the course of reaction (not the initial amount of CHP), and is therefore expressed as below.

$$[phenol\ produced] = \frac{k_2'}{k_2 + k_2'} * X_{DCP} * [DCP]_0 + \frac{k_3}{k_3 + k_4 + k_5} * X_{CHP} * X_{DCP} * [DCP]_0 * \frac{k_2}{k_2 + k_2'}$$

To rearrange and simplify,

$$[phenol\ produced] = X_{DCP} * [DCP]_0 * \left\{ \frac{k_2'}{k_2 + k_2'} + \frac{k_3}{k_3 + k_4 + k_5} * X_{CHP} * \left[1 - \frac{k_2'}{k_2 + k_2'} \right] \right\}$$

$$phenol\ selectivity = \frac{k_2'}{k_2 + k_2'} + \left[1 - \frac{k_2'}{k_2 + k_2'} \right] X_{CHP} \frac{k_3}{k_3 + k_4 + k_5}$$

Figure 3.21. Full derivation of Figure 3.20.

To obtain the relative kinetic parameters and selectivity needed to solve for $k_2'/(k_2 + k_2')$, the final product distributions of acid-catalyzed reactions were determined using GC-MS and HPLC. The Arrhenius plot in Figure 3.13 shows two distinct temperature regimes. Therefore, the ratio $k_2'/(k_2 + k_2')$ was determined for one temperature in each regime.

To obtain phenol selectivity, solutions of 0.0589 M DCP with 0.03 equivalents of DBSA were reacted in flame-sealed glass ampules at 110 °C for 1 hour and 70 °c for 2 hours. The flame sealed ampules were employed to completely prevent volatilization of any species. After reaction, solutions were diluted with acetone. HPLC was used to determine concentrations of DCP and AMS. GC-MS was used to determine the concentration of phenol. The reaction of DCP + DBSA produces other products (i.e., ACP), but these products are difficult to quantify for two reasons. First, several products elute at the same retention time in the HPLC as shown in Figure 3.10. Second, DCP decomposes into ACP and CA (and only these products) during GC analysis. Phenol concentration is easily obtained via GC as it is stable and DCP does not form phenol during analysis.

A sample GC-MS chromatogram and mass spectra are included below in Figure 3.22.

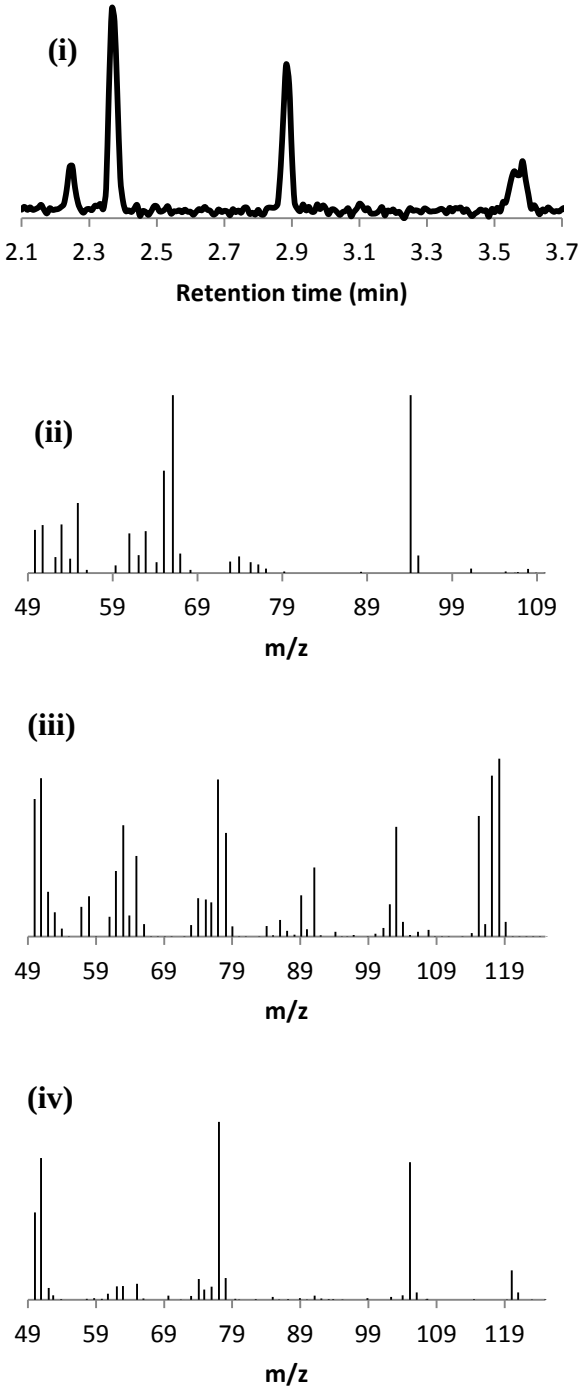

Figure 3.22. (i) GC chromatogram for the reaction of 0.0589 M DCP with 0.00177 M DBSA at 90 °C for 60 minutes. (ii) mass spectrum of the first (2.25 min) GC peak. Molecular ion of 94 m/z. Corresponds to phenol. (iii): mass spectrum of the second (2.37 min) GC peak. Molecular ion of 118 m/z. Corresponds to α-methyl styrene. (iv): mass spectrum of the third (2.9 min) GC peak. Molecular ion of 120 m/z. Corresponds to acetophenone.

The combined analysis technique described here produced the phenol selectivity as shown below in Table 3.2.

Table 3.2. Select species concentrations and selectivities ($moles\ product/mole\ DCP\ consumed$) and DCP conversion after sealed reactions of 0.0589 M DCP with 0.03 equivalents of DBSA in dodecane at 70 °C for 2 hours and 110 °C for 1 hour. Samples were diluted by a factor of 3 prior to analysis.

Temperature		[DCP]	[αMS]	[phenol]	conversion
70 °C	final concentration	0.01161 ± 0.00025	0.00859 ± 0.00007	0.00544 ± 0.00007	0.409
	selectivity	N/A	1.0710	0.6775	
110 °C	final concentration	0.00658 ± 0.00012	0.01310 ± 0.00026	0.00796 ± 0.00017	0.665
	selectivity	N/A	1.0035	0.6098	

These reactions of DCP with DBSA were deliberately not run to completion. At long reaction times, a viscous brown liquid is observable in the reaction vessels. It is hypothesized that the brown liquid corresponds to dimerized and polymerized AMS. AMS is vulnerable to acid-catalyzed oligomerization.[32] As the goal of these studies was to close the mass balance, the formation of the brown liquid was minimized by shortening reaction times.

To obtain the relative kinetic parameters and the ratio $k_3/(k_3 + k_4 + k_5 + k_6)$ as shown in Figure 3.1, 0.0589 M CHP was reacted in flame-sealed ampules with 0.03 equivalents of DBSA at 110 °C for 25 minutes and at 70 °C for 45 minutes. At these reaction times, CHP was completely consumed by the acid. This was convenient, as it allowed for X_{CHP} to be set to 1 in Figure 3.20. Final concentrations of AMS, phenol, CA, and ACP were determined using GC-MS after reaction. The results are shown below in

Table 3.3. Final species concentrations and selectivities ($moles\ product/mole\ CHP\ consumed$) for the sealed reactions of 0.0589 M CHP with 0.03 equivalents of DBSA at 70 °C for 45 minutes and 110 °C for 25 minutes (complete conversion). The 'mass balance' is calculated by $[products] * 3/0.0589$. The factor of 3 comes from the dilution prior to analysis.

Temperature		[ACP]	[αMS]	[CA]	[phenol]	Mass balance
70 °C	final concentration	0.00367 ± 0.00001	0.00295 ± 0.000002	0.0000 ± 0.0000	0.01305 ± 0.00025	1.00
	selectivity	0.1868	0.1506	0	0.6648	
110 °C	final concentration	0.00282 ± 0.00004	0.00715 ± 0.00011	0.0000 ± 0.0000	0.01003 ± 0.00012	1.02
	selectivity	0.1434	0.3642	0	0.5111	

The reactions of CHP with DBSA reached complete conversion much more quickly than reactions with DCP.

The equation in Figure 3.20 and the data in Table 3.2 and Table 3.3 were used to determine the ratio of $k_2'/(k_2 + k_2')$. The results are tabulated below in Table 3.4.

Table 3.4. Relative kinetic parameters from Figure 3.19 as determined from acid-catalyzed reactions of DCP and CHP.

Temperature	$\frac{k_3}{k_3 + k_4 + k_5 + k_6}$	$\frac{k_2'}{k_2 + k_2'}$
70 °C	0.6648	0.0410
110 °C	0.5111	0.2019

At the lower examined temperature (70 °C), 96% of DCP decomposition results in the formation of CHP. At 110 °C, 80% of DCP decomposition results in the formation of CHP. In both cases, the majority of DCP decomposition produces CHP which is

capable of oxidizing other species in solution. It's possible that at the higher temperature of 110 °C, the cation formed via the k_2' pathway is more stable than at 70 °C. This could account for more of the DCP decomposition proceeding through that pathway. It's also possible that the difference in reaction pathways reported in Table 3.4 is directly related to the different activation energies reported in Figure 3.13. A more rigorous set of studies with more temperatures examined could clarify the relationship between $k_2'/(k_2 + k_2')$ and reaction temperature.

Also of note is the selectivity of AMS reported in Table 3.2. At 70 °C, the selectivity of AMS is reported at 1.07. Recall that the literature mechanism only predicts a maximum AMS selectivity of 1. At 70 °C for 2 hours, 0.03% of the initial DCP will thermally degrade according to literature models. This amount is insignificant, and therefore unable to account for the 1.07 selectivity. The more likely explanation is that CHP is formed as an intermediate which then generates AMS via acid-catalyzed liberation of hydrogen peroxide.[27]

It also appears that the AMS selectivities in Table 3.2 and Table 3.3 are inconsistent. Since a large majority of DCP produces CHP, and CHP has AMS selectivities of 0.15 and 0.36 at 70 °C and 110 °C, respectively, the AMS selectivities for DCP reactions should be substantially higher than reported. A hypothesis to explain this discrepancy is the acid-catalyzed oligomerization of AMS.[32] Oligomerization of AMS would reduce the reported AMS concentrations. Possible AMS dimers are shown below in Figure 3.23.

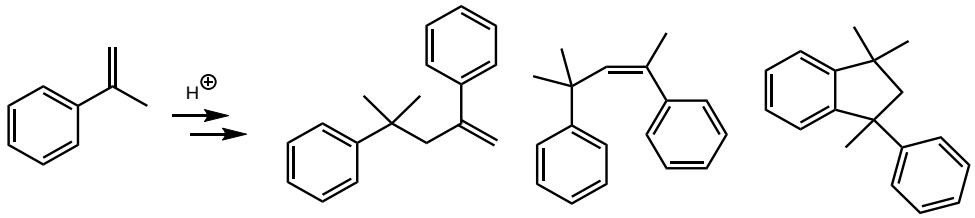

Figure 3.23. Reported structures of AMS dimers when AMS was reacted with pTSA.[32]

Unfortunately, the mass balance could not be closed for the reactions of DCP with DBSA. The acid-catalyzed AMS dimerization is the best available hypothesis to explain low reported selectivities of AMS.

3.6 Conclusions

In this chapter, the acid-catalyzed decomposition of DCP in dodecane has been thoroughly examined. First, reactions of DCP and DBSA in the presence of DSTDP or THTP concretely demonstrated the production of CHP from this reaction.

Next, the kinetics of acid-catalyzed DCP decomposition were examined. A convex Arrhenius plot was observed. This unusual Arrhenius plot was discussed in the context of an equilibrium hydrogen-bonding step and a simple rate expression was derived. The rate expression was able to account for the unusual kinetic behavior.

Finally, a complete mechanism for the reaction of DCP with DBSA in dodecane was proposed. The products of acid-catalyzed decomposition of DCP and of CHP were quantified. This quantification allowed for the precise calculation of exactly how much CHP is formed during acid-catalyzed degradation of DCP.

The evidence presented herein is sufficient to justify the mechanism proposed in Chapter 2.

3.7 References

(1) Ogunniyi, D. S. Peroxide vulcanisation of rubber. *Progress in rubber and plastics technology* **1999**, *15*, 95.

(2) Hulse, G. E.; Kersting, R. J.; Warfel, D. R. Chemistry of dicumyl peroxide-induced crosslinking of linear polyethylene. *Journal of Polymer Science: Polymer Chemistry Edition* **1981**, *19*, 655.

(3) Class, J. B. A review of the fundamentals of crosslinking with peroxides. *Rubber World* **1999**, *220*, 35.

(4) Cogen, J. M.; Gross, L. H.; Keogh, M. J.; Obal, J. A.; Polyethylene crosslinkable composition; Google Patents: 2001.

(5) Di Somma, I.; Marotta, R.; Andreozzi, R.; Caprio, V. Dicumyl peroxide thermal decomposition in cumene: development of a kinetic model. *Industrial & engineering chemistry research* **2011**, *51*, 7493.

(6) Naskar, K.; Kokot, D.; Noordermeer, J. Influence of various stabilizers on ageing of dicumyl peroxide-cured polypropylene/ethylene-propylene-diene thermoplastic vulcanizates. *Polymer degradation and stability* **2004**, *85*, 831.

(7) Grassie, N.; Scott, G. *Polymer degradation and stabilisation*; CUP Archive, 1988.

(8) Dluzneski, P. R. Peroxide vulcanization of elastomers. *Rubber chemistry and technology* **2001**, *74*, 451.

(9) Fortuin, J.; Waterman, H. Preparation of cumene hydroperoxide. *Chemical Engineering Science* **1954**, *3*, 60.

(10) Fortuin, J.; Waterman, H. Production of phenol from cumene. *Chemical Engineering Science* **1953**, *2*, 182.

(11) Andrigo, P.; Caimi, A.; Cavalieri d'Oro, P.; Fait, A.; Roberti, L.; Tampieri, M.; Tartari, V. Phenol-acetone process: cumene oxidation kinetics and industrial plant simulation. *Chemical Engineering Science* **1992**, *47*, 2511.

(12) Seubold Jr, F. H.; Vaughan, W. E. Acid-catalyzed decomposition of cumene hydroperoxide. *Journal of the American Chemical Society* **1953**, *75*, 3790.

(13) Levin, M.; Gonzales, N.; Zimmerman, L.; Yang, J. Kinetics of acid-catalyzed cleavage of cumene hydroperoxide. *Journal of hazardous materials* **2006**, *130*, 88.

(14) Matsui, S.; Fujita, T. New cumene-oxidation systems: O2 activator effects and radical stabilizer effects. *Catalysis today* **2001**, *71*, 145.

(15) Kozhevnikov, I.; Mastikhin, V.; Matveev, K.; Kirichenko, G.; Churkin, Y. V.; Glazunova, V. Kinetics of decomposition of isopropylbenzene hydroperoxide catalyzed by dodecamolybdophosphoric acid. *Reaction Kinetics and Catalysis Letters* **1977**, *7*, 291.

(16) Beltrame, P. L.; Carniti, P.; Gamba, A.; Cappellazzo, O.; Lorenzoni, L.; Messina, G. Side reactions in the phenol/acetone process. A kinetic study. *Industrial & engineering chemistry research* **1988**, *27*, 4.

(17) Kharasch, M.; Fono, A.; Nudenberg, W. THE CHEMISTRY OF HYDROPEROXIDES I. THE ACID-CATALYZED DECOMPOSITION OF α, α-

DIMETHYLBENZYL (α-CUMYL) HYDROPEROXIDE1. *The Journal of Organic Chemistry* **1950**, *15*, 748.

(18) Dykman, A. S.; Grebenshchikov, I. N.; Nelson, M. E.; Pinson, V. V.; Zhukov, D. N.; Zinenkov, A. V.; Method for producing phenol and acetone; Google Patents: 2011.

(19) Griaznov, A. K.; Vassilieva, I. I.; Zakoshansky, V. M.; High selective method of phenol and acetone production; Google Patents: 2000.

(20) Knifton, J. F.; Sanderson, J. R.; Method for production of phenol/acetone from cumene hydroperoxide; Google Patents: 1990.

(21) Koff, F. W.; Sifniades, S.; Tunick, A. A.; Decomposition of cumene oxidation product; Google Patents: 1982.

(22) Langley, P. E.; Process for the production of phenol and acetone; Google Patents: 1982.

(23) Nelson, M.; Sederel, W. L.; Dyckman, A. S.; Grebenshchikov, I. N.; Pinson, V. V.; Zinenkov, A. V.; Method for the production of phenol and acetone; Google Patents: 2009.

(24) Nelson, M. E.; Dykman, A. S.; Zinenkov, A. V.; Pinson, V. V.; Grebenshchikov, I. N.; Method for producing phenol and acetone; Google Patents: 2011.

(25) Zakoshansky, V. M.; Method for the decomposition of cumene hydroperoxide by acidic catalyst to phenol and acetone; Google Patents: 1993.

(26) ZAKOSHANSKII, V. FORMATION OF DICUMENYL PEROXIDE AS SIDE PRODUCT OF ACID-CATALYTIC DECOMPOSITION OF ISOPROPYLBENZENE HYDROPEROXIDE. *ZHURNAL OBSHCHEI KHIMII* **1989**, *59*, 1122.

(27) Leffler, J. E. Cleavages and Rearrangements Involving Oxygen Radicals and Cations. *Chemical Reviews* **1949**, *45*, 385.

(28) Kornblum, N.; DeLaMare, H. E. The base catalyzed decomposition of a dialkyl peroxide. *Journal of the American Chemical Society* **1951**, *73*, 880.

(29) "Dialkyl Peroxides," Arkema, Inc., 2007.

(30) Sigma-Aldrich "Applications: Free Radical Initiators."

(31) Truhlar, D. G.; Kohen, A. Convex Arrhenius plots and their interpretation. *Proceedings of the National Academy of Sciences* **2001**, *98*, 848.

(32) SONG, G.; JIN, X.; HU, C.; CHEN, X. Synthesis and application of α-methyl styrene dimer. *Chemical Industry and Engineering Progress* **2012**, *9*, 041.

CHAPTER 4 – MECHANISTIC INVESTIGATION OF POLYVINYL CHLORIDE DEGRADATION AND STABILIZATION

4.1 Introduction

4.1.1 Thermal Decomposition of Polyvinyl Chloride

Thermal degradation of polyvinyl chloride (PVC) negatively affects polymer performance after processing.[1] Particularly at high temperatures, PVC degradation involves the elimination of hydrogen chloride from the polymer chain to form allylic chlorides. The allylic chlorides have increased vulnerability to further dehydrochlorination, creating a chain reaction of increasing rates of dehydrochlorination. This chain reaction is known as "chain-unzipping" in reference to the way the PVC chain "unzips" as it liberates HCl. Ultimately, the degradation process forms an extended system of conjugated double bonds along the PVC chain. If degradation is initiated at high temperature, the process continues (at a slower rate) when the polymer is brought to lower temperatures. To combat the thermal degradation of PVC, various additives have been explored. These additives include epoxidized oils, phthalates, and various stearate salts. The mechanisms by which PVC interacts with these additives, and their modes of stabilization, are complex and not entirely understood. The work in this chapter focuses on the investigation of the stabilization mechanism of a common industrial stabilizer system.

The ideal PVC structure is constructed of vinyl chloride units – chlorine atoms are located at secondary carbons beta to one another. The stereochemical arrangements of the chlorine atoms can be isotactic, syndiotactic, or atactic, as shown below in Figure 4.1. Unlike the "ideal" polymer, real PVC contains various structural irregularities known as

"defects." Defects include chlorine atoms at vinylic, allylic, and tertiary carbons, as well as chlorine atoms with a vicinal relationship. The most important structural defects are also shown below in Figure 4.1. The structural defects are inevitable; they arise at low concentrations during the polymerization process and are believed to be the weak points at which the degradation process begins.[2-4] Vinylic chlorines are generally accepted to be relatively unreactive. However, allylic and tertiary chlorines are expected to be highly vulnerable to thermal elimination. Thus, current literature proposes that PVC thermal degradation is initiated at these sites. The problem of thermal elimination is exacerbated by the fact that liberated HCl acts as a catalyst for further elimination of HCl. The degradation process is therefore autocatalytic. The elimination produces large degrees of polyunsaturation, creating undesirable color in the polymer.

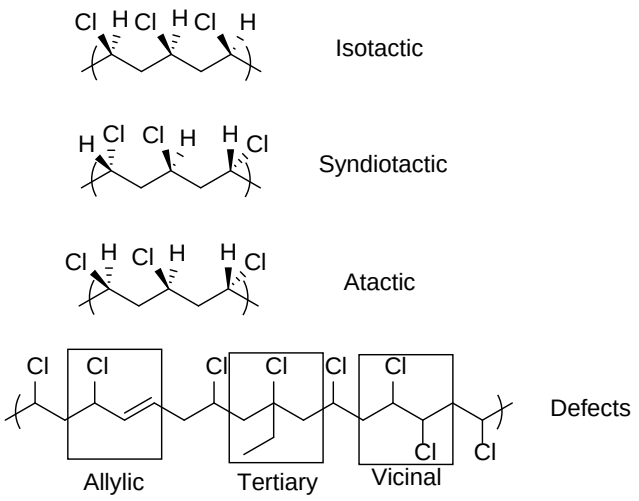

Figure 4.1. Tacticities and defects that affect the thermal degradation and stabilization of PVC.

4.1.2 Use of PVC Model Compounds

The mechanistic details of PVC degradation are inherently difficult to analyze. The reactions involved in degradation and stabilization can correspond to minuscule

structural changes relative to the chain length of individual polymer molecules. As such, the relevant reactions can be difficult to observe and analyze. To overcome the difficulties in examining the actual polymer, model compounds are used to replicate the important structural features of real PVC and to mimic the fundamental reactions related to PVC stabilization. The use of model compounds is a common approach in PVC investigation.[5-13] Studies of model compounds provide useful insight on the relative kinetics of various structures in PVC degradation. However, previous studies of model compounds are not comprehensive. Some used dilute solutions of model compounds in solvents which may not replicate the polymer system. Others did not investigate Zn/Ca stabilizer systems that are commonly implemented in commercial processes.[14,15]

4.1.3 Thermal Stabilization of PVC

As mentioned above, various additives are commonly introduced to PVC to mitigate thermal degradation. A common industrial approach is the combination of zinc stearate and calcium stearate. Zinc stearate ($ZnSt_2$) is thought to stabilize PVC by two mechanisms: first, $ZnSt_2$ is thought to sequester HCl to prevent autocatalysis. Second, $ZnSt_2$ is hypothesized to substitute at allylic chloride sites, thereby decreasing the lability of neighboring chlorine atoms.[2-4]

The sequestration process produces stearic acid and zinc chloride from the reaction of ZnSt2 and HCl. Stearic acid is far less capable of catalyze dehydrochlorination than HCl. However, zinc chloride is an active catalyst that promotes the loss of HCl. This is the main function of calcium stearate ($CaSt_2$). Zinc chloride, when reacted with $CaSt_2$, undergoes a thermodynamically favored ion-exchange to

regenerate $ZnSt_2$ and produce calcium chloride.[16-18] Calcium chloride is much less capable of catalyzing dehydrochlorination; the ion exchange is thereby a necessary component of stabilization.

The substitution process involves the substitution of allylic chlorine by $ZnSt_2$. The substitution reaction produces an ester, which is much less capable of elimination and thus provides a barrier to the "chain-unzipping" process. The activity of both $CaSt_2$ and $ZnSt_2$ and their interactions provide thermal stabilization of PVC. A mechanistic representation of the stabilization process is shown below in Figure 4.2.

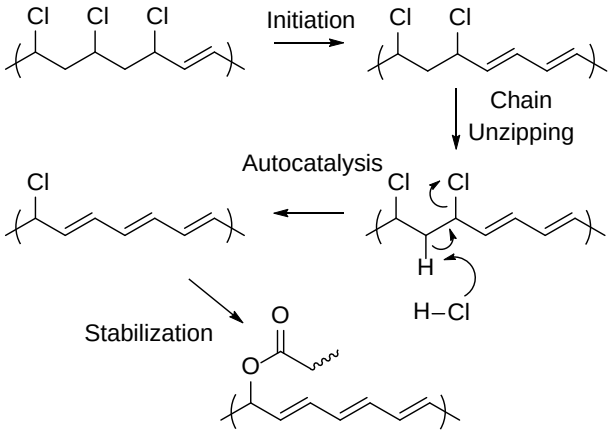

Figure 4.2. Mechanism of initial thermal degradation, "chain-unzipping," autocatalysis, and stearate substitution of PVC.

4.1.4 Overall Experimental Approach

The studies presented herein focus on three related investigations: (i) the kinetics analysis for the reactions of neat model compounds with metal acetates in the presence of the phase-transfer catalyst (PTC) tetra-n-butylammonium acetate (thereby simulate a nucleophile/base without a coordinating metal cation); (ii) the qualitative reaction rates and product identification for the reactions of Zn and Ca stearates with 2,4-

dichloropentane; and (iii) study of the rates of weight loss from the thermal analysis of plasticized PVC containing blends of Zn and Ca stearates.

Model compounds were selected to simulate particular PVC structural defects of interest. The models include:

1. 1,3-dichlorobutane, simulating a primary chloride.
2. meso- and D,L-2,4-dichloropentane, simulating different tacticities of secondary chlorides.
3. 3-chloro-3-ethylpentane, simulating a tertiary chloride.
4. meso- and D,L-3,4-dichlorohexane, simulating vicinal chlordies.
5. 3-chloro-1-butene, simulating an allylic chloride.
6. (E)-6-chloronon-4-ene, simulating an allylic chloride on a longer carbon chain.

The structures of all model compounds examined are shown in Figure 4.3.

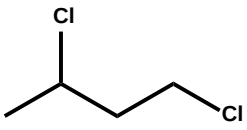

1,3-dichlorobutane

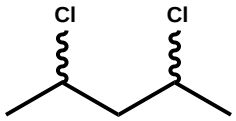

2,4-dichloropentane

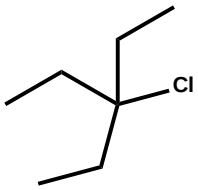

3-chloro-3-ethylpentane

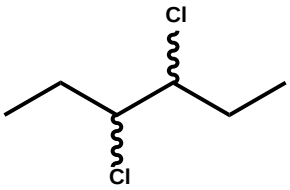

3,4-dichlorohexane

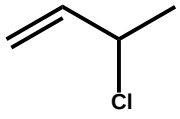

3-chlorobutene

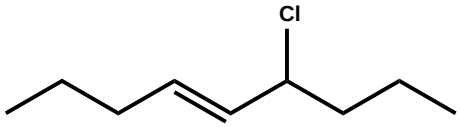

(E)-6-chloronon-4-ene

Figure 4.3. Structures of model compounds used for determination of relative kinetics of PVC defects.

All reactions involving the PVC models were conducted neat (without solvent) to closely approximate the chemical environment of the PVC polymer system.

The kinetics studies in this chapter used metal acetates (in the presence of a PTC) as a simpler model of stearates. Rates of reaction of model compounds were compared using this methodology to determine relative reactivities of various defects and tacticities found in PVC polymer. This method provides for the direct and simple investigation of factors influencing PVC degradation. The reactivity studies with stearates used a similar methodology, replacing acetates and a PTC with real stearates. Experiments were still conducted neat, unlike most studies in the literature.

Model compound studies were ultimately compared, as directly as possible, to corresponding studies with actual PVC resin. The combined techniques provided a complete investigation of multiple aspects of PVC thermal degradation and stabilization, allowing for a unified mechanistic hypothesis thereof.

4.2 Methodology and Materials

4.2.1 Materials

Calcium acetate ($Ca(OAc)_2$), *o*-dichlorobenzene (anhydrous), 1,3-dichlorobutane, diisodecyl phthalate (DIDP), deuterated dimethylsulfoxide (d_6-DMSO), sodium acetate (NaOAc, anhydrous), tetradecane, tetrahydrofuran (THF, anhydrous, inhibitor-free), tetra-*n*-butylammonium chloride (TBAC), zinc acetate ($Zn(OAc)_2$), and zinc stearate ($ZnSt_2$, purum, 10-12% zinc metal basis) were obtained from Sigma-Aldrich. Calcium

stearate ($CaSt_2$) was obtained from Alfa Aesar. The grade of PVC powder used was Oxyvinyls 240F.[19] Helium and nitrogen were obtained from Airgas. All materials were >97% purity or ultra-high purity unless otherwise stated and used as received from the manufacturers.

4.2.2 Experimental

Detailed syntheses and characterization of the non-commercial model compounds are presented here.

4.2.2.1 Synthesis of 2,4-dichloropentane[20]

2,4-Pentanediol (I). A solution of sodium borohydride ($NaBH_4$, 2.5 g, 0.066 mol) and sodium hydroxide (NaOH, 0.050 g, 0.0013 moles) in water (25 mL) was prepared and kept at approximately 20°C. A solution of acetylacetone (10 g, 0.099 moles) in methanol (MeOH, 30 mL) was added dropwise and stirred for 15 minutes. The solvent was removed *in vacuo*, yielding a white solid. The solid was then extracted into glycerol (50 mL). The extract was distilled at 60-70°C (0.45 mmHg) and, subsequently, fractionally distilled at 70-75°C (3.5 mmHg) in order to remove trace amounts of glycerol. 6.024 g (60% yield) of 2,4-pentanediol (colorless liquid) was obtained. ^{1}H NMR (400 MHz, acetone-d_6) δ 1.12 (t, J = 6.3 Hz, 6H), 1.47 (m, 2H), 3.97 (m, 2H), 4.06 (d, J = 4.68 Hz, 1H), 4.40 (d, J = 3.32 Hz, 1 H); ^{13}C NMR (100 MHz, acetone-d_6) δ 23.5 (2C), 47.1, 47.3, 64.1, 67.1.

2,4-Dichloropentane (II). Thionyl chloride ($SOCl_2$, 27.9 mL, 0.384 moles) was added drop wise to a solution of 2,4-pentanediol (10. g, 0.096 moles) in pyridine (1.17 mL,

0.0146 moles) at 0°C under argon atmosphere. The mixture was refluxed for 3 hours. After being cooled to room temperature, ice was added to quench any unreacted $SOCl_2$. The mixture was extracted twice with diethyl ether (50 mL). The combined organic layers were dried over magnesium sulfate ($MgSO_4$) and the solvent removed *in vacuo* (75 mmHg). Distillation (140-150°C, atm. pressure) yielded 5.558 g (41% yield) of 2,4-dichloropentane as a colorless liquid. ^{1}H NMR (400 MHz, $CDCl_3$) δ 1.52 (2d, J = 10.8, 7.5 Hz, 6H), 1.98 (m, 1.3H), 2.28 (dt, J = 14.2, 7.7 Hz, 0.6H), 4.13 (m, 1.2H), 4.30 (m, 0.7H); ^{13}C NMR (100 MHz, $CDCl_3$) δ 24.5, 25.5, 50.1, 50.4, 54.7, 55.8.

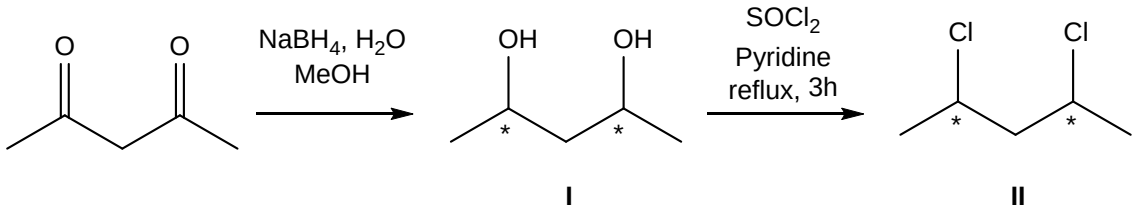

Figure 4.4. Overview of the synthesis of 2,4-dichloropentane.

4.2.2.2 Synthesis of 3-chloro-3-ethylpentane[21]

3-Chloro-3-ethylpentane (III). Hydrochloric acid (HCl, 12 M, 40 mL) was added to 3-ethyl-3-pentanol (40 mL, 0.289 mol). The biphasic mixture was stirred at room temperature for 2 hours. The organic layer was then separated, dried over magnesium sulfate and purified over a silica plug with hexanes as the eluent. The solvent was removed under vacuum at 75 mmHg, 25°C to yield 40 mL (90% yield) of 3-chloro-3-ethylpentane as a clear liquid. ^{1}H NMR (400 MHz, $CDCl_3$) δ 0.95 (t, J = 7.4 Hz, 9H), 1.77 (q, J = 7.4 Hz, 6H); ^{13}C NMR (100 MHz, $CDCl_3$) δ 8.6, 22.6, 79.8.

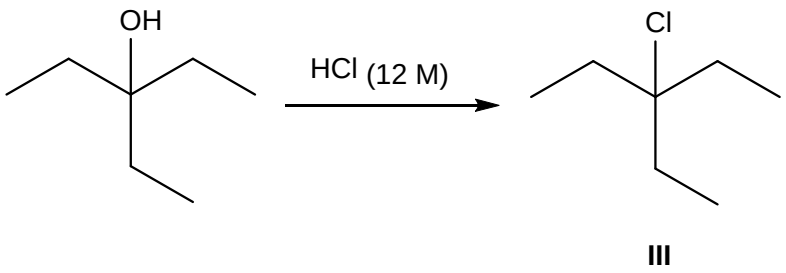

III

Figure 4.5. Overview of the synthesis of 3-chloro-3-ethylepentane.

4.2.2.3 Synthesis of 3,4-dichlorohexane[22]

3,4-Dichlorohexane (IV). Phosphorus pentachloride (PCl_5, 12.37 g, 60 mmol) was suspended in carbon tetrachloride (CCl_4, 23 mL) and heated to 50°C. 3-Hexene (5 g, 60 mmol) was slowly added to the suspension and stirred overnight at 50ºC. The PCl_5 and CCl_4 were removed by distillation. The 3,4-dichlorohexane was purified by distillation at 12-14 mmHg and 40°C to yield 1.72 g (20% yield) of 3,4-dichlorohexane as a clear liquid. ^{1}H NMR (400 MHz, $CDCl_3$) δ 1.05 (m, 6H), 1.58-1.81 (m, 2 H), 1.96-2.07 (m, 2H), 3.91-3.96 (m, 2H); ^{13}C NMR (100 MHz, $CDCl_3$) δ 10.4, 11.4, 27.9, 28.0, 66.9, 67.1.

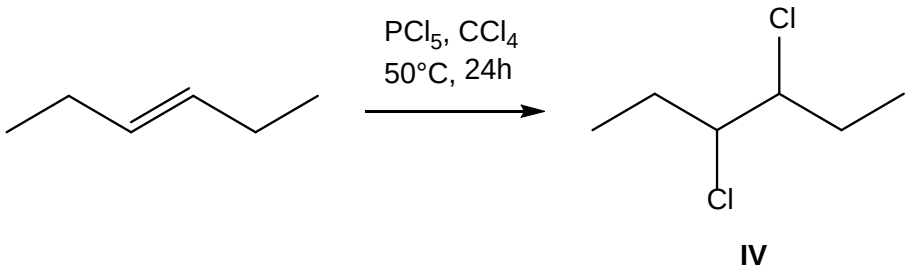

IV

Figure 4.6. Overview of the synthesis of 3,4-dichlorohexane.

4.2.2.4 Synthesis of (E)-6-chloronon-4-ene[23]

(*E*)-Non-4-ene-6-ol (V). To a solution of *trans*-2-hexen-1-al (11.8 mL, 10.0 g, 0.102 mol) in anhydrous diethyl ether (Et_2O, 148 mL) was added, drop wise, a solution of n-propylmagnesium bromide (nPrMgBr, 51 mL, 0.102 mol) in anhydrous diethyl ether (25 mL) over the course of 30 min at 0°C. The resulting pale yellow mixture was stirred for 1 hour at room temperature. After 1 hour, the reaction mixture was quenched with a saturated aqueous ammonium chloride solution (NH_4Cl, 100 mL). The organic layer was separated and the aqueous layer was extracted twice with Et_2O (50 mL). The combined organic layer was dried over $MgSO_4$ and the solvent was removed to yield 12.8 g (88% yield) of (*E*)-non-4-ene-6-ol as a pale yellow oil. ^{1}H NMR (400 MHz, $CDCl_3$) δ 0.80 (m, 6H), 1.18-1.50 (m, 4H), 1.79 (q, 2H), 1.90 (q, 2H), 2.40 (s, 1H), 3.64 (m, 1H), 5.32 (m, 1H), 5.55 (m, 1H); ^{13}C NMR (100 MHz, $CDCl_3$) δ 13.48, 13.85, 18.58, 22.25, 34.18, 39.44, 67.73, 131.23, 133.36.

(*E*)-6-Chloronon-4-ene (VI). (*E*)-Non-4-ene-6-ol (12.8 g, 0.091 mol) and anhydrous pyridine (1.43 mL, 1.4 g, 0.018 mol) were combined and cooled to 0°C. Phosphorous trichloride (PCl_3, 2.9 mL, 7.2 g, 0.034 mol) was added drop wise over the course of 20 min at 0 °C. The resulting pale yellow mixture was stirred for 3 hours at 0 °C. After 3 hours, the upper layer was separated and distilled at reduced pressure (31 °C, 0.3 mmHg) to yield 10.1 g (70% yield) of (*E*)-6-chloronon-4-ene as a pale yellow oil. ^{1}H NMR (400 MHz, $CDCl_3$) δ 0.9 (t, 6H), 1.4 (m, 4H), 1.79 (m, 2H), 2.0 (m, 2H), 4.37 (m, 1H), 5.5 (m, 1H), 5.59 (m, 1H); ^{13}C NMR (100 MHz, $CDCl_3$) δ 13.45, 13.57, 19.84, 22.18, 33.98, 40.93, 63.43, 131.22, 133.25.

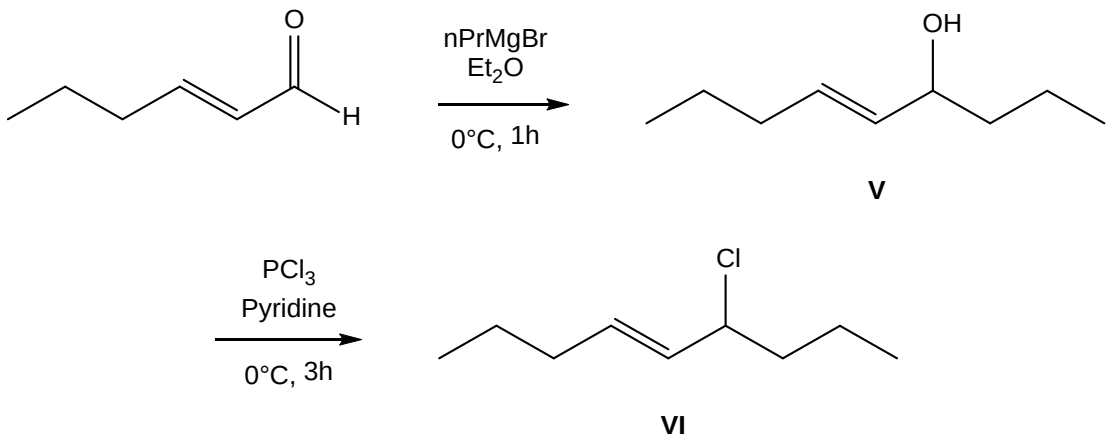

Figure 4.7. Overview of the synthesis of (E)-6-chloronon-4-ene.

4.2.2.5 Kinetics Studies with Acetates

Kinetics studies were performed on all of the model compounds with various metal acetates (NaOAc, $Ca(OAc)_2$, or $Zn(OAc)_2$). As an procedural example, a solution of the phase transfer catalyst (PTC) tetra-*n*-butylammonium chloride in THF (3.0 mL of a 0.1 M solution, 0.0003 mol, 0.05 eq) was added to the acetate salt (0.003 mol $^-$OAc, 0.5 eq) under an argon atmosphere with a condenser, heated to 60°C, and stirred overnight to allow the PTC to condition the acetate salt. The THF was then evaporated and tetradecane (0.001 mol) was added as an internal standard and heated to 100°C. 1,3-dichlorobutane (0.006 mol, 1 eq) was then added and the resulting slurry was stirred throughout the reaction. Aliquots were taken periodically, filtered to remove any solids, and quantitatively diluted in THF for analysis. As the procedure was repeated with other model compounds, other volumes were used. However, the ratio of the model compound to the acetate ion to the PTC was maintained constant at 1 : 0.5 : 0.05.

4.2.2.6 Mechanistic Studies with Stearates

Mechanistic studies using 2,4-dichloropentane with various stearates (e.g., $ZnSt_2$ and $CaSt_2$) at the parts per hundred resin (phr, grams of additive per 100 grams of polymer or model) scale were performed in sealed glass reaction vessels. For example, 2,4-dichloropentane (5.655 mmol) was added to zinc stearate (0.0315 mmol, 2.5 phr) and calcium stearate (0.0328 mmol, 2.5 phr). The resulting slurry was transferred to the reaction vessel (thick walled NMR tube or Ace Glass pressure tube #8648-03) which was subsequently purged with argon and sealed (i.e., the NMR tube was flame sealed or the glass pressure tube capped). The reaction vessel was then heated *via* an oil bath for the desired reaction time then cooled. Higher concentration studies were also performed with 0.10 equivalents of additive (to 1 eq of 2,4-dichloropentane).

4.2.2.7 Thermal Studies of PVC Blends

PVC and blends with additives were prepared for thermogravimetric analysis. Blends consisted of 3 g of PVC powder, 30 phr (0.9 g) plasticizer (DIDP), and 5 phr (0.15 g) additional additives ($ZnSt_2$, $CaSt_2$, or 1:1 $ZnSt_2$: $CaSt_2$). The PVC powder and one-half of the plasticizer (0.45 g) were physically combined in a glass vial, heated to 95°C in an oil bath, and thoroughly mixed by hand. Separately, the remaining plasticizer and all other additives were combined and heated to 95°C. The two mixtures were then combined and heated to 95°C and thoroughly mixed. The temperature of 95°C was chosen since it was above the 83°C glass transition temperature of the PVC resin,[19] which allowed for a more complete uptake of the stabilizer into the polymer matrix. Blending

the plasticizer with the PVC in two separate steps allowed the most uniform uptake and distribution of the additives which do not blend well with PVC otherwise.

4.2.2.8 Analysis Techniques

Model compounds reactions were monitored via gas chromatography-mass spectroscopy (GC-MS) using a Shimadzu GCMS-QP2010P fitted with a Supelco PTA-5 (30m x 0.32 mm x 1.00 µm, length x inside diameter x film thickness) capillary column and/or nuclear magnetic resonance (NMR) using a Bruker DSX 300MHz NMR spectrometer fitted with a 5mm probe. Reaction samples were quantitatively diluted in THF and injected into the GC at 250°C with a mobile phase of helium (70.1 kPa, 40 cm/sec). The oven temperature was ramped from 50°C to 250°C at a rate of 15°C/min. The MS was operated in electron impact mode with an ion source and interface temperature of 225°C. For NMR, a 1 mm d_6-DMSO capillary was used as the lock solvent. NMR spectra were gathered at 100°C to ensure homogeneity of the reaction mixture.

Thermogravimetry of the bulk PVC and associated blends was performed on a TA Instruments Thermogravimetric Analyzer Q50 under a flow of nitrogen at 100 mL / min. After the sample was loaded onto a platinum pan, the mass loss was monitored while the temperature was brought to 170°C within 8 minutes and held isothermally for 2 hours.

4.3 Kinetics Studies with Acetates

The literature contains several examples of previous studies that have used a variety of model compounds in solvents. A study by Klemchuk investigated 4-chloropent-2-ene and 2-chloro-2-methyl butane in solution with chlorobenzene.[24] The reactivities of these models were examined in the presence of dibutyltin dilaurate, dibutyltin maleate, and other dibutyltin compounds. Boughdady et al. examined various chloroalkanes and chloroalkenes, such as 1,4,7-thichloroheptane, 2,4-dichloropentane, 8-chlorohexadecane, 4-chlorohex-2-ene, and 7-chloronona-3,5-diene.[14] The models were thermally decomposed neat and in solutions with 2-chloropropane/n-heptane, dioctyl phthalate, or o-dichlorobenzene. This study neglected to examine the effects of any nucleophiles on the decomposition of the model compounds. Varma et al. examined 1-chlorododecane, 2-chlorododecane, 1,1,3-thrichlorononane, and dichlorononene as models for various PVC structures.[5] Similar to the work by Boughdady, models were thermally degraded with no nucleophiles present. The experiments were conducted in the solvents methyl salicylate and eugenol. Ayrey et al. examined the model compounds tert-butyl chloride and 3-chlorobut-1-ene.[8] This study contained used a similar methodology to that presented in this chapter: model compounds underwent substitution from dialkyltin mercaptides, thioglycollates, and carboxylates in the absence of solvents. However, the materials examined are significantly different than those discussed herein and the results are not applicable. Baum et al. investigated 4-chlorohex-2-ene in solution with di-2-ethylhexyl phthalate and no added nucleophiles, separating the work from that discussed here.[25]

As mentioned above, model compounds reacted in this chapter were conducted neat, eliminating the effects of solvents.[5] Stearates are common substances used in the

stabilization of PVC. However, experimental results using stearates would be difficult to interpret due to the complexity and size of stearates. Therefore, these kinetics experiments use acetates to model the important functionality of stearates. It is hypothesized that the relative reaction rates of model compounds with acetates will reflect the relative reaction rates of model compounds with stearates. Literature suggests that ligand size in these systems does not substantially affect substitution rates.[9]

PVC stabilizers employ a variety of metal cations. To better understand the role of the cationic portion of carboxylate salts in stabilization, calcium, zinc, and sodium acetates were examined. These acetates were used to determine relative reactivities of the defects represented in the model compounds investigated herein. Figure 4.8 below shows the hypothesized reaction pathways expected of the model compounds in the presence of metal acetates.

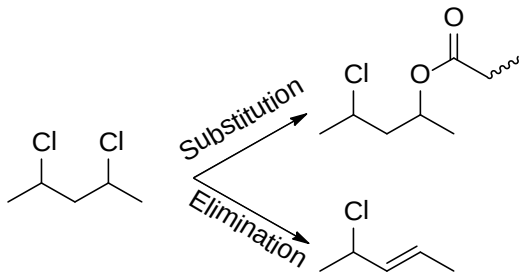

Figure 4.8. Expected reaction pathways of model compounds reacted with metal carboxylates. The substitution pathway is analogous to stabilization; the elimination pathway is representative of thermal degradation.

As briefly discussed above, previous studies have investigated various metal stabilizers. Ayrey et al investigated the organotin stabilizers dibutyltin diacetate and dibutyltin dilaurate.[8,9] Klemchuck used organic salts of cadmium, zinc, lead, and barium.[24] In such works, carboxylates have only been examined as accompanied by coordinating metal cations. In contrast, the current study makes use of a quaternary

ammonium salt as a phase transfer catalyst. Effectively, the PTC isolates the acetate anion, allowing investigation of its effects without coordination of the cation.

First, the relative reactivities of the three acetates were determined via reaction with 1,3-dichlorobutane. Initial reaction of 1,3-dichlorobutane with NaOAc, $Ca(OAc)_2$ or $Zn(OAc)_2$ at 100°C after two days showed no reaction. This result was unsurprising as the acetate salts have limited solubility in the neat model compounds. Solubility was improved by employing tetra-n-butylammonium chloride as a phase transfer catalyst. Reactions of all three acetates with 1,3-dichlorobutane were repeated in the presence of PTC. A representative GC chromatograph from the reaction mixtures is shown below in Figure 4.9.

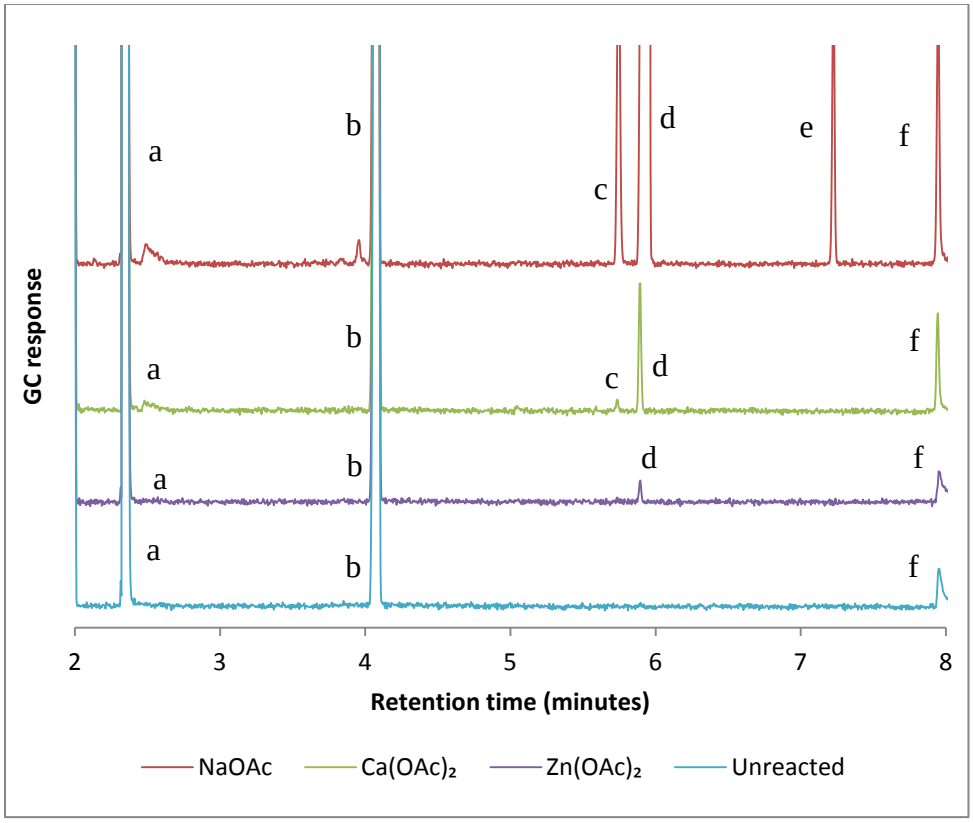

Figure 4.9. GC chromatograph of the reaction of 1,3-dichlorobutane (0.006 mol) with NaOAc, $Ca(OAc)_2$, and $Zn(OAc)_2$ (0.003 mol $^-$OAc) in the presence of PTC (0.0003 mol) at 100 °C with added tetradecane (0.001 mol) as internal standard. Reaction was run for 20 hours. Peaks were identified using mass spectroscopy and are assigned as follows: 'a' – THF; 'b' – 1,3-dichlorobutane; 'c' 4-chlorobutan-2-yl acetate; 'd' – 3-chlorobutyl

acetate; 'e' – butane-1,3-diyl diacetate; 'f' - PTC. The small extents of reaction for the calcium and zinc acetate can be attributed to the poor solubility of divalent acetate species, even in the presence of PTC.

The peaks in Figure 4.9 reveal that the reaction of sodium acetate with 1,3-dichlorobutane produces both mono- and disubstituted products. No elimination products were observed at all. The complete mechanism of 1,3-dichlorobutane reaction with acetate salts is shown below in Figure 4.10.

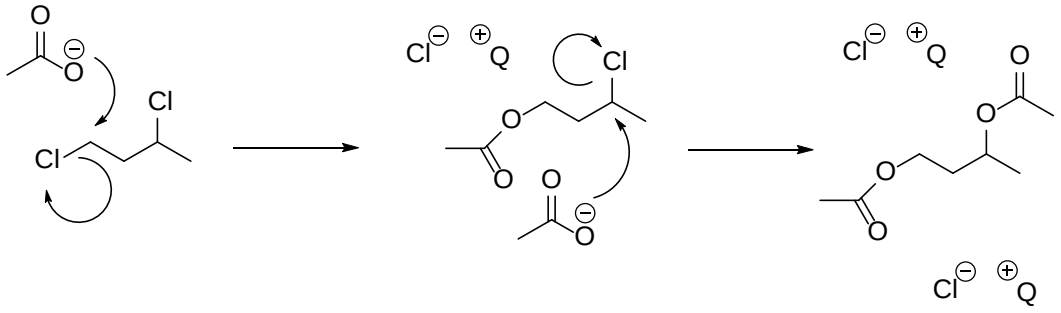

Figure 4.10. Reaction mechanism of 1,3-dichlorobutane with acetate salts. 'Q+' denotes the quaternary ammonium salt. It is expected that there is almost no coordination between the metal cation and chloride anion.

The concentration of 1,3-dichlorobutane in reaction samples was determined via integration of the peak in the GC chromatogram ('b' in Figure 4.9). Concentration data was transformed into conversion data, as shown below in the representative plot Figure 4.11.

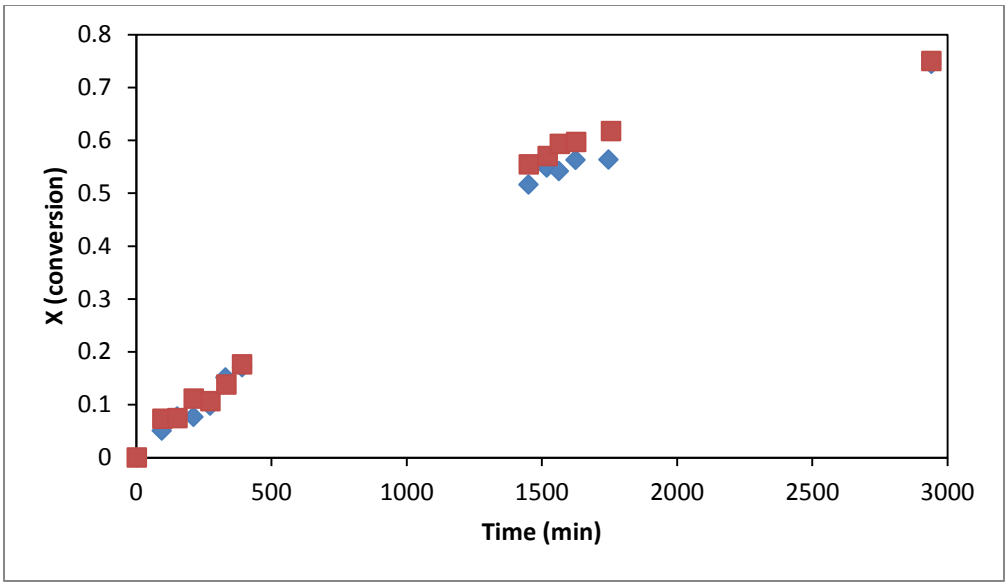

Figure 4.11. Conversion as a function of time for the reaction of 1,3-dichlorobutane with NaOAc at 100 °C with PTC. The multiple data sets represent different trials of the same reaction.

Pseudo-first-order rate constants were calculated by making the assumption that the concentration of acetate ion in solution is constant. This assumption is made due to the interaction of the phase transfer catalyst.[26] With that assumption, the rate expression for the consumption of model compound is shown below.

$$-\frac{dC_1}{dt} = kC_1C_{MOAc} = k_{eff}C_1$$

Figure 4.12. Rate expression for the consumption of model compound when reacted with metal acetate salts in the presence of PTC. C_1 is the concentration of model compound, C_{MOAc} is the concentration of acetate, and k_{eff} is the effective first-order rate constant.

The rate expression was solved to give a simple expression for conversion, shown below in Figure 4.13.

$$(1 - X) = e^{-k_{eff}t}$$

Figure 4.13. Expression for conversion of model compounds when reacted with metal acetates in the presence of PTC. k_{eff} is as expressed in Figure 4.12.

The expression for conversion in Figure 4.13 was linearized and plotted into a first-order plot. The slopes of the lines in the first-order plot were taken to be the effective first-order rate constants for the reaction of each model compound. The first-order plot for the reaction of 1,3-dichlorobutane with NaOAc in the presence of PTC is shown below in

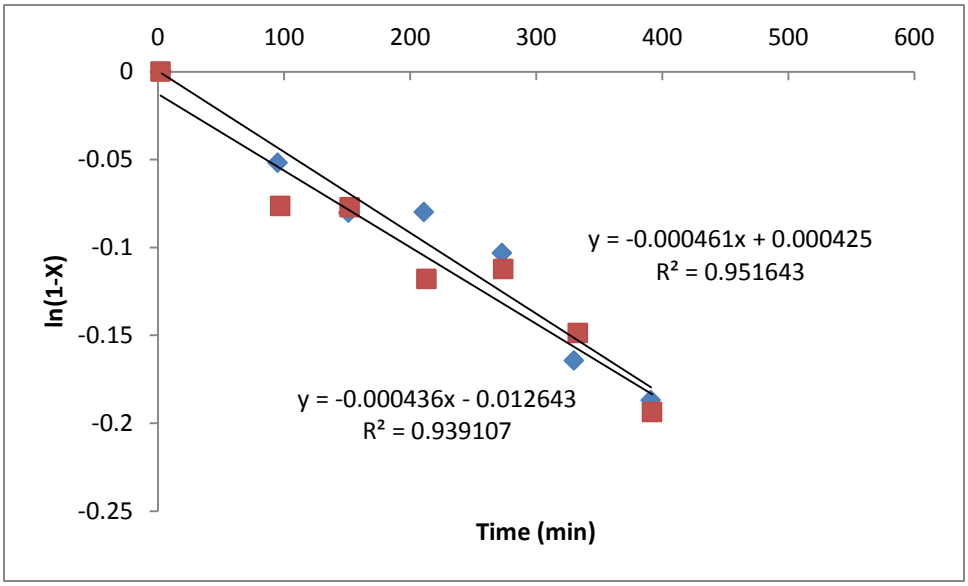

Figure 4.14. First-order plot for the reaction of 1,3-dichlorobutane with NaOAc in the presence of PTC at 100 °C. The slopes are taken to be the values of the effective first-order rate constant of the reaction.

The reaction rate of 1,3-dichlorobutane with acetate changes as a function of metal cation. The rate decreases as the metal cation is changed from NaOAc to $Ca(OAc)_2$ to $Zn(OAc)_2$. The effect of rate on cation is clearly demonstrated in Figure 4.9. The reaction rate constants were quantified using first-order plots and the results are tabulated below in Table 4.1. From a cursory analysis of Figure 4.9, the selectivities of the major products do not appear to change significantly.

Table 4.1. Effective first-order reaction rate constants from reactions with 1,3-dichlorobutane at 100 °C. Metal acetates were used at 0.5 eq $^{-}$OAc. Tetra-n-butylammonium chloride (the PTC) was used at 0.05 eq.

Metal Acetate	k_{app} ($\cdot 10^{-4}$ min^{-1})
NaOAc	4.49 ± 0.13
$Ca(OAc)_2$	1.35 ± 0.22
$Zn(OAc)_2$	0.510 ± 0.102

The differences in apparent first-order reaction rates can likely be attributed to the varying solubility of the metal acetates in the presence of PTC. The PTC is more effective on monovalent ions; thus, NaOAc exhibits the highest apparent rate constant. With the relative rate constants in mind, NaOAc was selected for all further kinetics studies simply because it facilitates the fastest reactions.

The following set of figures contains the data for the reactions of all remaining model compounds studied with NaOAc. Both conversion data and first-order plots (and lines of best fit relating to rate constants) are presented.

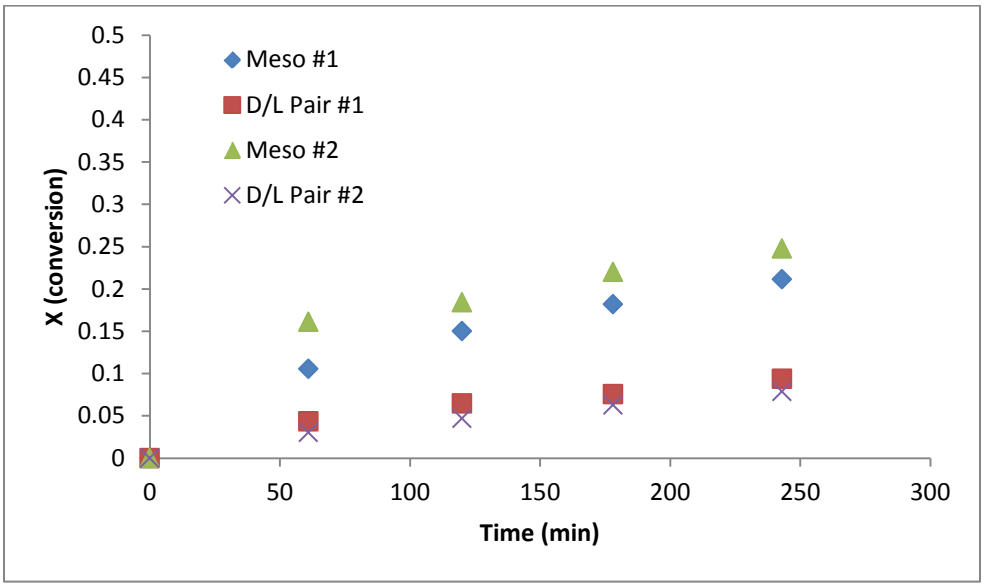

Figure 4.15. Conversion data for the reaction of 2,4-dichloropentane with NaOAc at 100 °C in the presence of PTC.

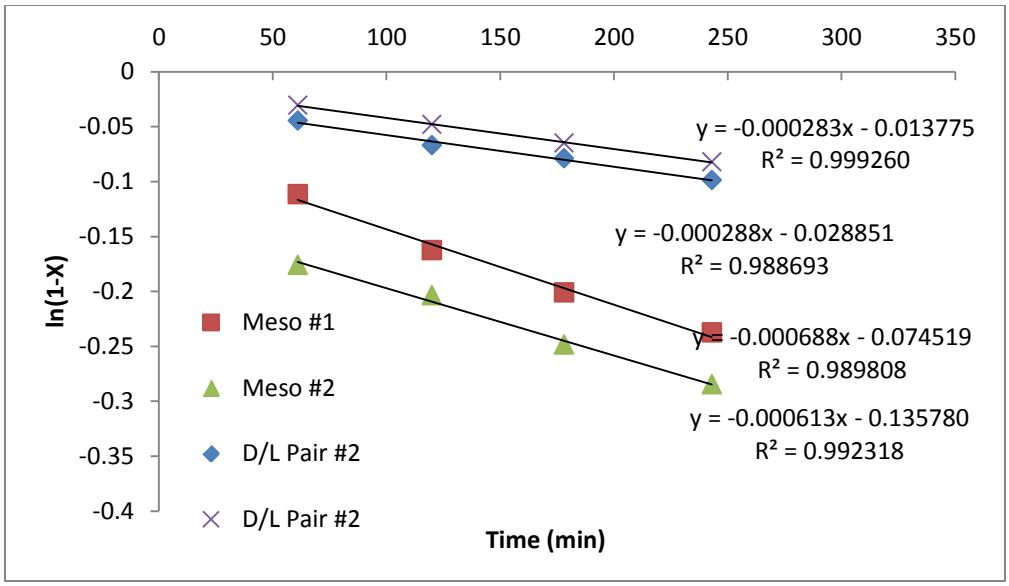

Figure 4.16. First-order plot for the reaction of 2,4-dichloropentane with NaOAc at 100 °C with PTC. The value of the rate constant, k, for each stereoisomer is the average of the negative of the slopes of the two fit lines.

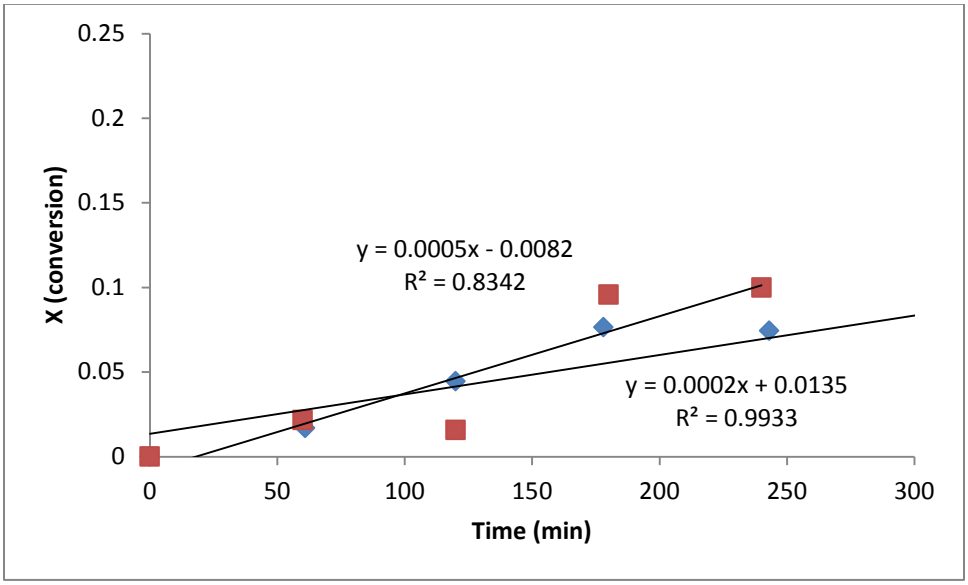

Figure 4.17. Conversion data for the reaction of 3-chloro-3-ethylpentane with NaOAc at 100 °C in the presence of PTC.

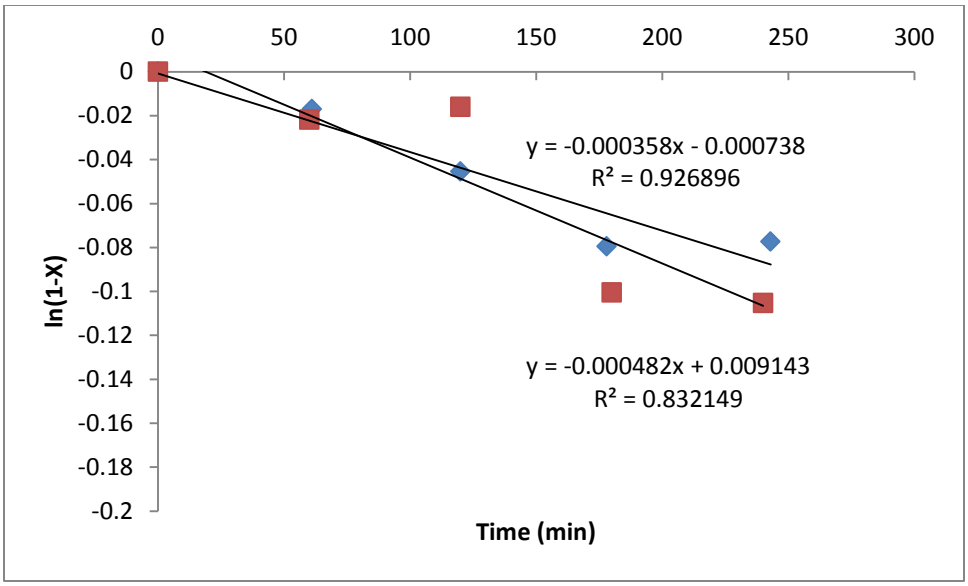

Figure 4.18. First-order plot for the reaction of 3-chloro-3-ethylpentane with NaOAc at 100 °C with PTC. The value of the rate constant, k, is the average of the negative of the slopes of the two fit lines.

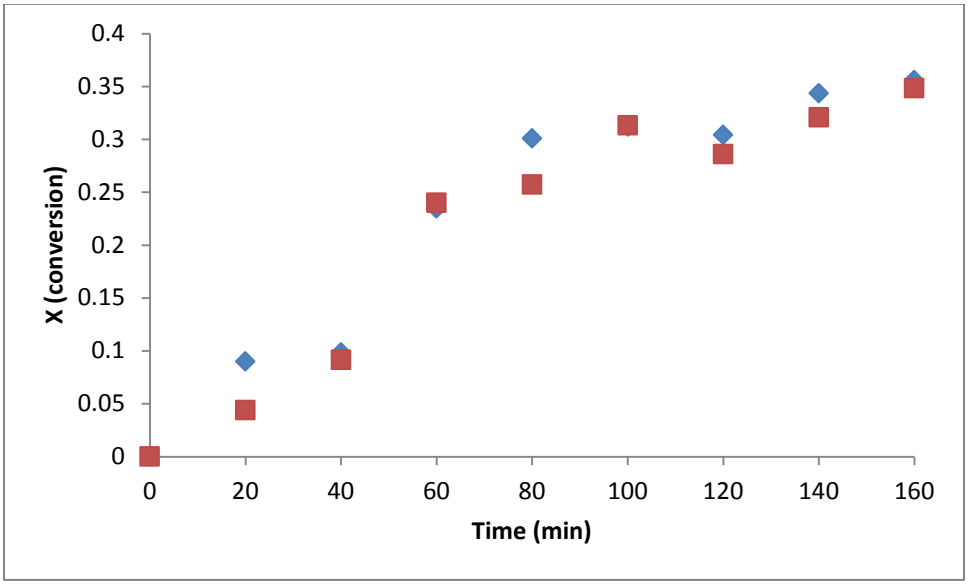

Figure 4.19. Conversion data for the reaction of 3-chloro-1-butene with NaOAc at 100 °C in the presence of PTC.

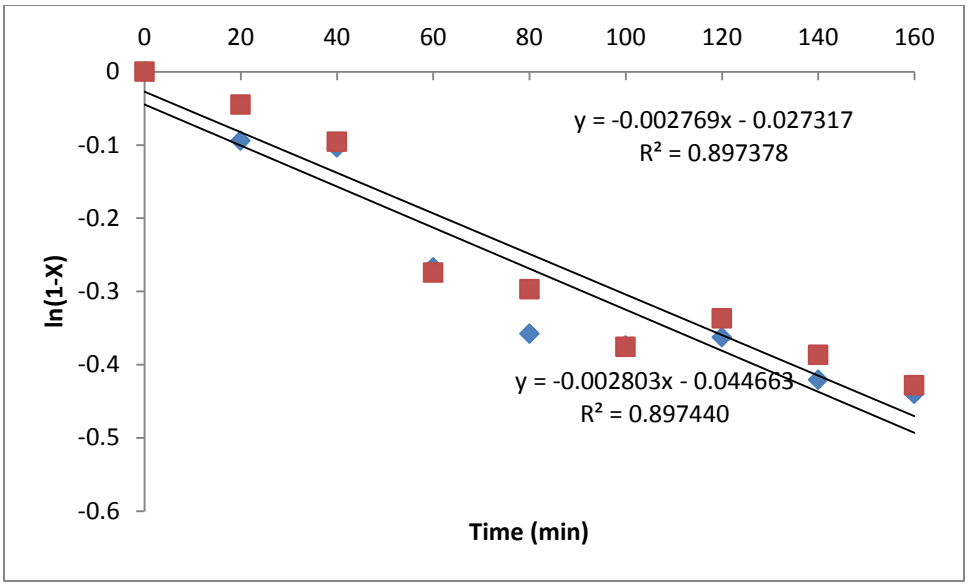

Figure 4.20. First-order plot for the reaction of 3-chloro-1-butene with NaOAc at 100 °C with PTC. The value of the rate constant, k, is the average of the negative of the slopes of the two fit lines.

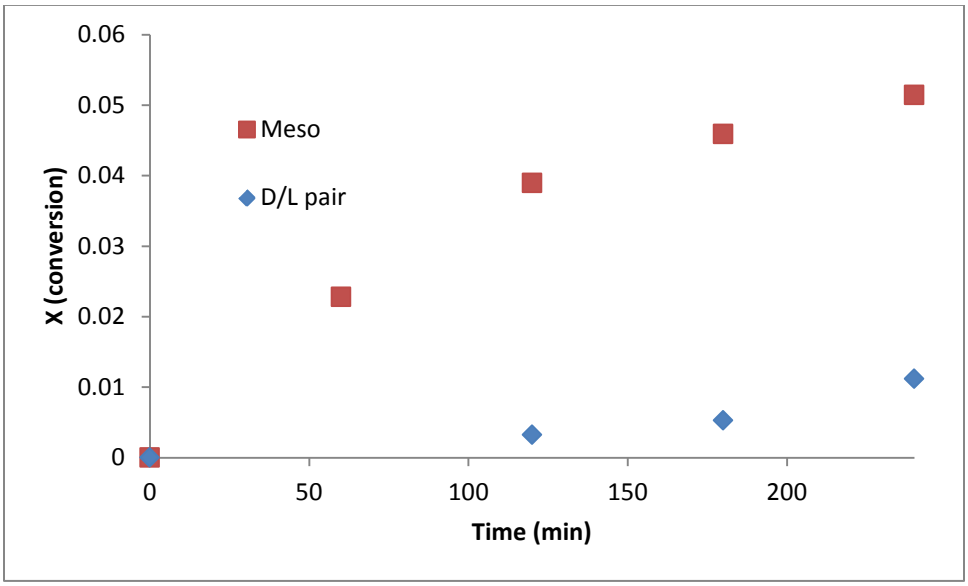

Figure 4.21. Conversion data for the reaction of 3,4-dichlorohexane with NaOAc at 100 °C in the presence of PTC.

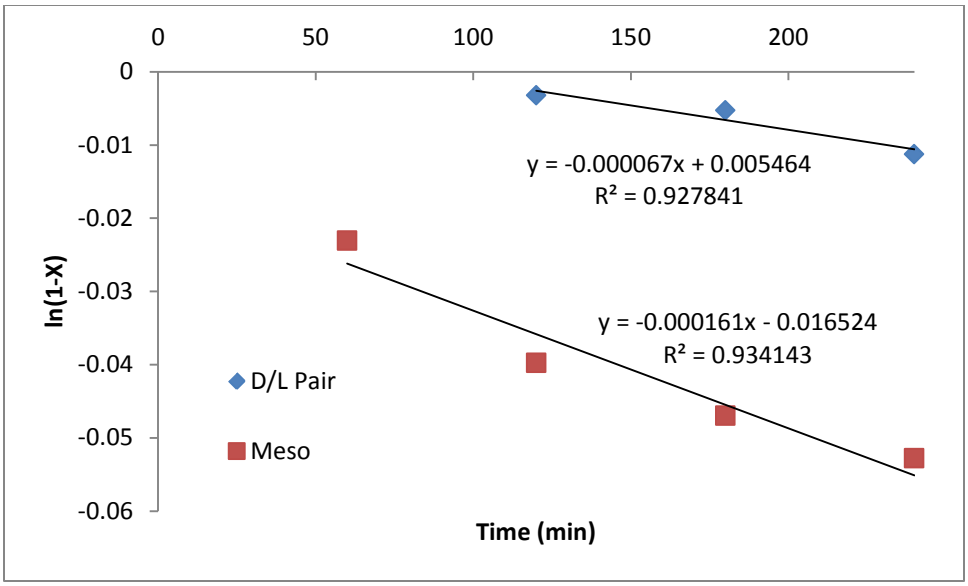

Figure 4.22. First-order plot for the reaction of 3,4-dichlorohexane with NaOAc at 100 °C with PTC. The value of the rate constant, k, for each stereoisomer is the negative of the slope of the corresponding fit lines.

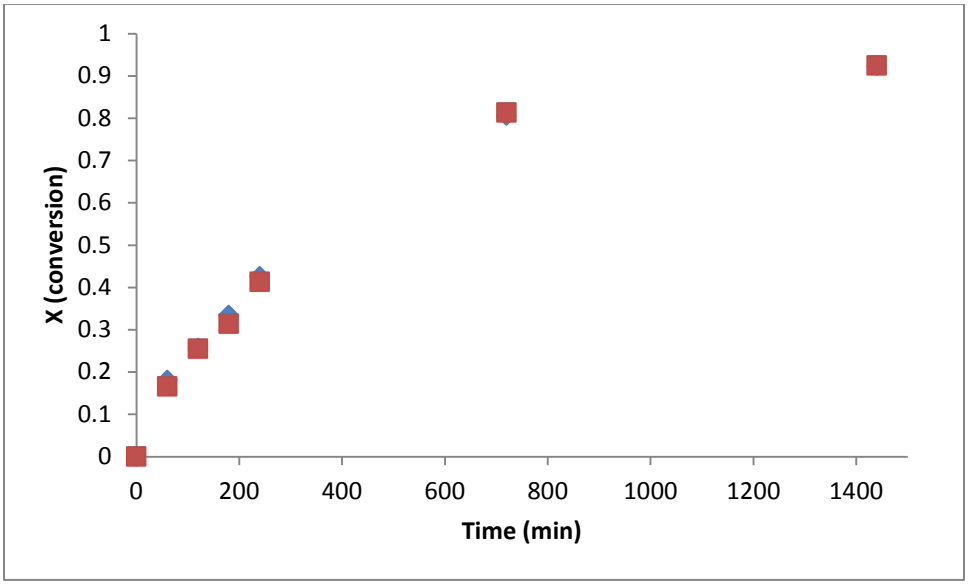

Figure 4.23. Conversion data for the reaction of 6-chloro-4-nonene with NaOAc at 100 °C in the presence of PTC.

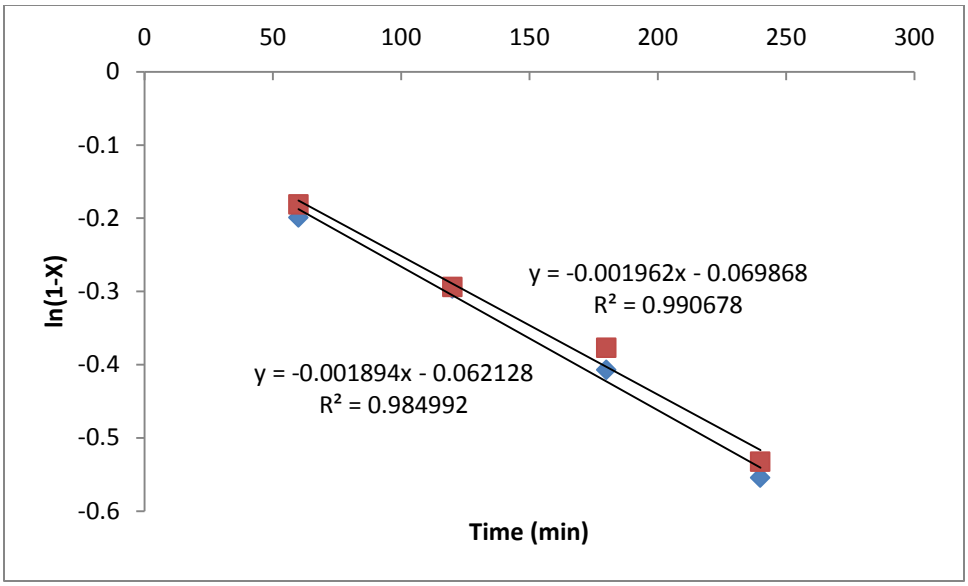

Figure 4.24. First-order plot for the reaction of 6-chloro-4-nonene with NaOAc at 100 °C with PTC. The value of the rate constant, k, is the average of the negative of the slopes of the two fit lines.

The reaction rate constants (determined from first-order plots) for all model compounds reacted with NaOAc are all tabulated below in Table 4.2 for detailed comparison and discussion.

Table 4.2. Summary of effective reaction rate constants of model compounds reacted with 0.5 eq NaOAc and 0.05 eq tetra-n-butylammonium chloride at 100 °C.

#	Structure	$k_{effective}$ ($\cdot 10^{-4}$ min^{-1})	Major Products
(1)	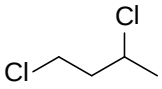	4.49 ± 0.13	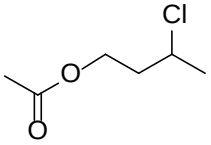
(2a)	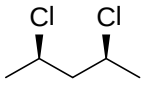	6.51 ± 0.38	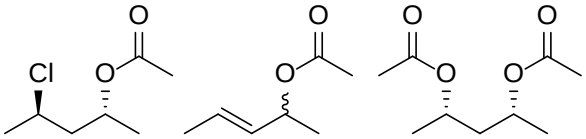
(2b)	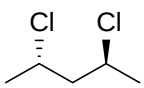	2.86 ± 0.25	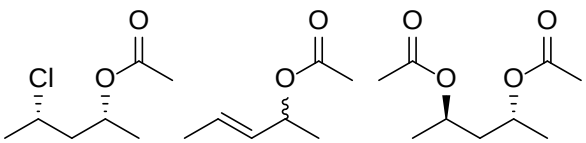

(3)[I]	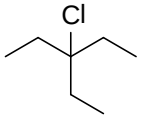	4.20 ± 0.62	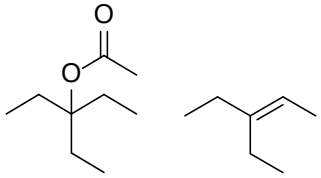
(4a)	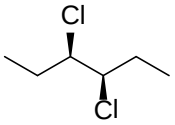	1.61	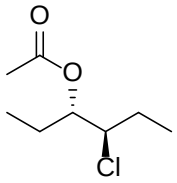
(4b)	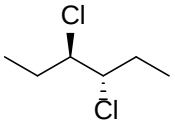	0.67	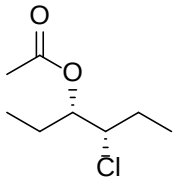
(5)[II]	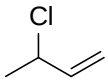	27.86 ± 0.17	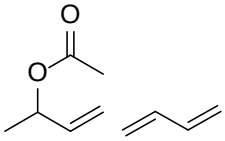
(6)[III]	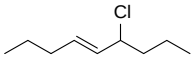	19.28 ± 0.34	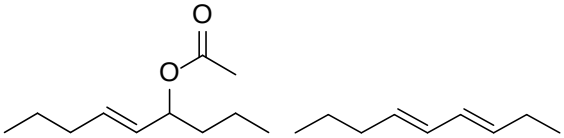

[I]Substitution product only seen during first hour; disappeared by end of reaction
[II]Butadiene is not actually observed due to volatility; it is conjectured for this reaction
[III]Substitution product was observed through 4 hours; disappeared by end of reaction

The examination of 2,4-dichloropentane (**2**) allows exploration of the effects of stereochemistry on reaction rates. The *meso* stereoisomer (**2a**) models isotactic PVC. The enantiomeric pair (**2b**) models syndiotactic PVC. The diasteromeric ratio is roughly 1.6:1 *meso*:enantiomeric pair; the two isomers can be readily discerned by GC-MS and NMR.

As a representation of the analysis techniques, the GC chromatograms and MS spectra of 2,4-dichloropentane both before and after reaction are included below.

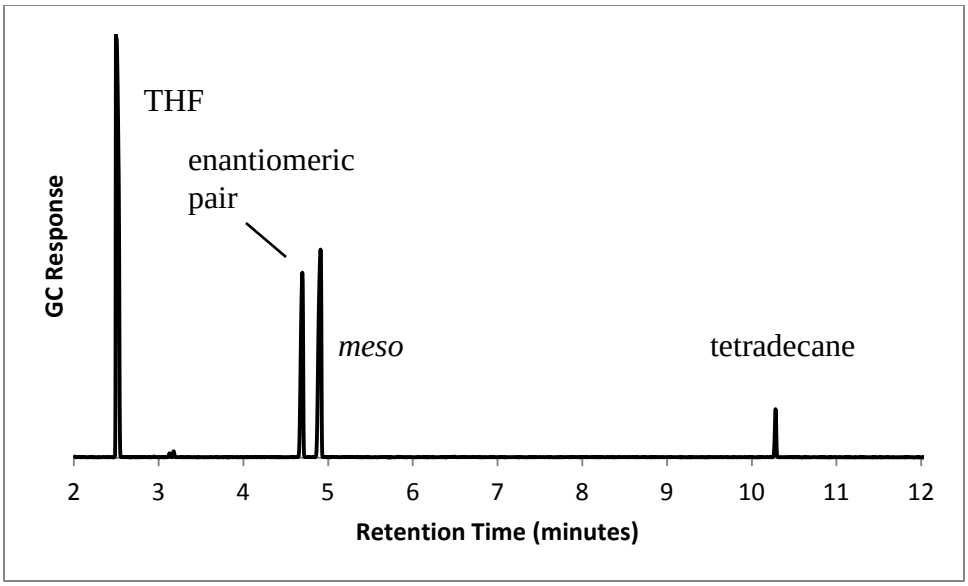

Figure 4.25. GC chromatogram of 2,4-dichloropentane in THF. The 2 peaks reveal the 2 stereoisomers. All peaks were identified using MS.

Before reaction, the only major species are 2,4-dichloropentane, the solvent THF, and added tetradecane. Recall that solids (such as acetate salts and PTC) were filtered before analysis using GC-MS.

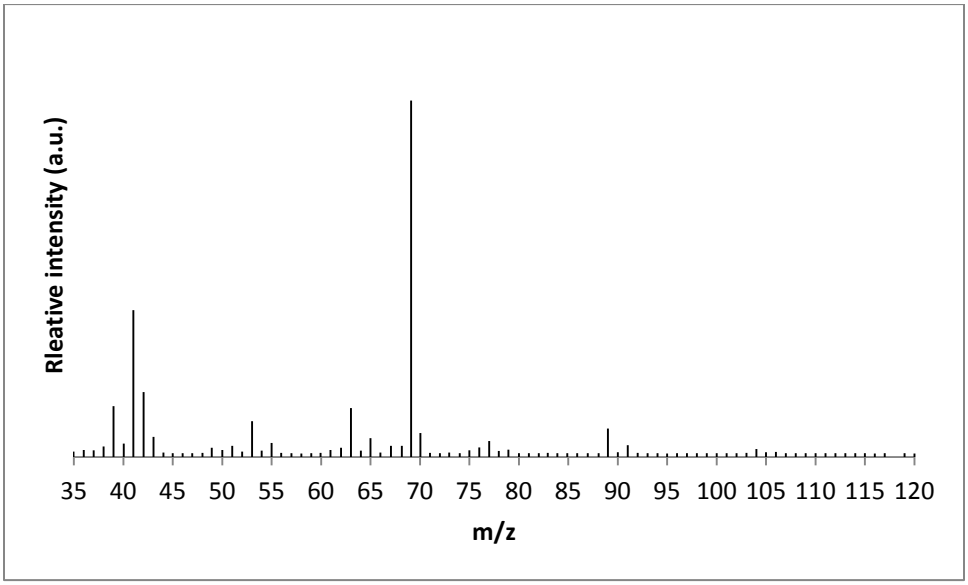

Figure 4.26. Mass spectrum of the peak at 4.9 minutes in Figure 4.25. The spectrum corresponds to 2,4-dichloropentane.

Only the mass spectrum for 2,4-dichloropentane is provided here, just for verification of the species identity. The other species in the chromatogram are of little interest. The analysis of the solution after reaction is shown in the figures below.

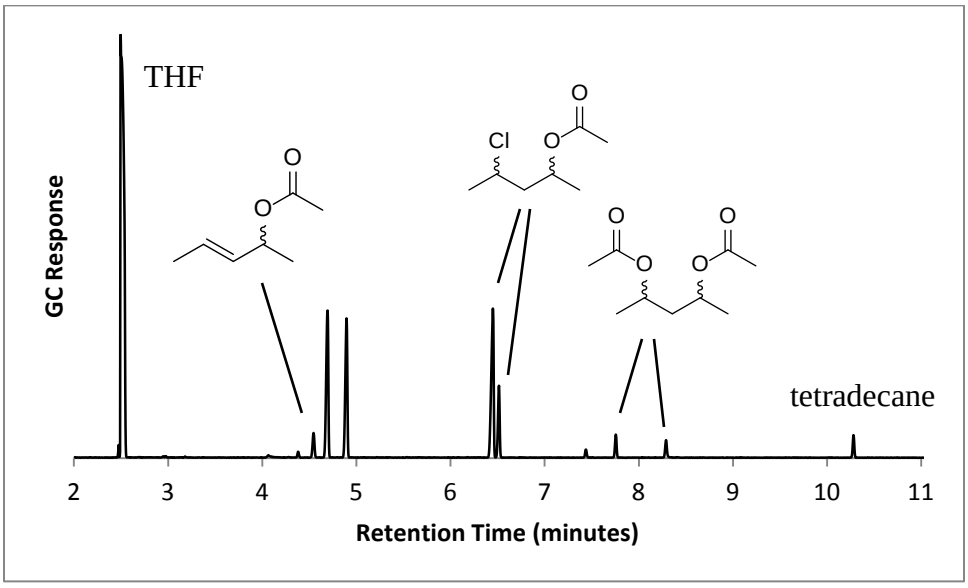

Figure 4.27. Gas chromatogram of the reaction of 2,4-dichloropentane after reaction at 100 °C with NaOAc in the presence of PTC. All peaks were identified using MS.

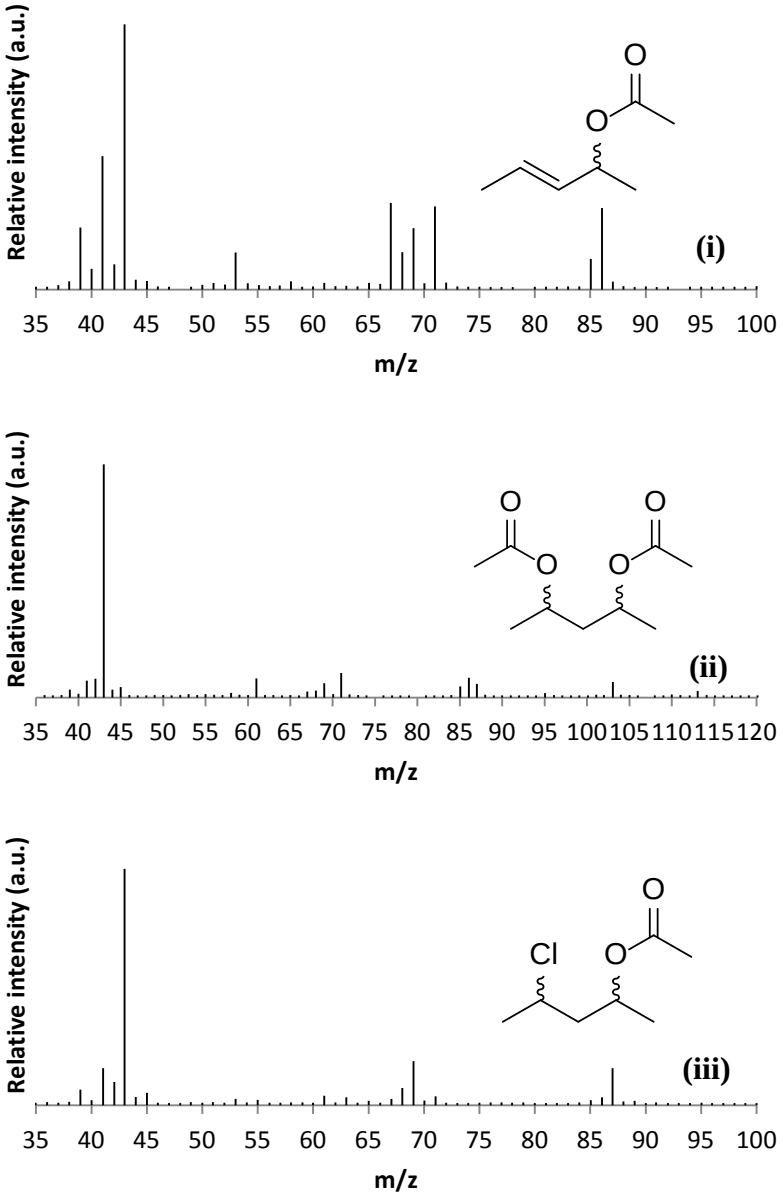

Figure 4.28. Mass spectra of the products seen in Figure 4.27. (i): spectrum of the peak at 4.54 minutes. Corresponds to pent-3-en-2-yl acetate. (ii): spectrum of the peak at 7.75 minutes. Corresponds to pentan-2,4-diyl acetate. (iii): spectrum of the peak at 6.44 minutes. Corresponds to 4-chloropentan-2-yl acetate.

As shown by the ratio of peaks after reaction in Figure 4.27, the reaction rate of (**2a**) is faster than that of (**2b**) with 0.1 equivalents of NaOAc at 100 °C in the presence of PTC. This is likely due to the steric hindrance of (**2b**) slowing the substitution reaction. The primary product formed from this reaction is 4-chloropentan-2-yl acetate.

Eventually, the second substitution takes place and pentan-2,4-diyl diacetate is also formed. The faster rate of reaction of the *meso* stereoisomer agrees with findings in literature that isotactic PVC is more easily stabilized than syndiotactic PVC.[27,28]

The fact that substitution is observed with 2,4-dichloropentane suggests that carboxylates could substitute onto random sites in the polymer backbone. Such random substitution would be entirely beneficial as it would provide limits to the extent of "chain-unzipping." Unlike the reactions of 1,3-dichlorobutane, the elimination product (specifically pent-3-en-2-yl acetate) is also formed. The elimination product formed at a ratio of 4:1 monosubstituted:eliminated products. As seen in Figure 4.27, there is no evidence of any significant amount of the pentadiene elimination product.

Unlike typical carboxylate systems used for PVC, the inclusion of a PTC in these reactions produced uncoordinated acetate anions (e.g., acetate anions that are largely independent of their metal cations). Thus, compared with ordinary carboxylates, the acetate used in these studies has increased nucleophilicity and basicity. An increase in nucleophilicity (and absence of coordinating cation) means that the models in these studies can substitute through an S_N2 mechanism. This hypothesis accounts for the faster reaction rate of the *meso* isomer of 2,4-dichloropentane as compared with the enantiomeric pair. Additionally, elimination products can also form via bimolecular mechanisms. Such a bimolecular elimination is shown below in Figure 4.29.

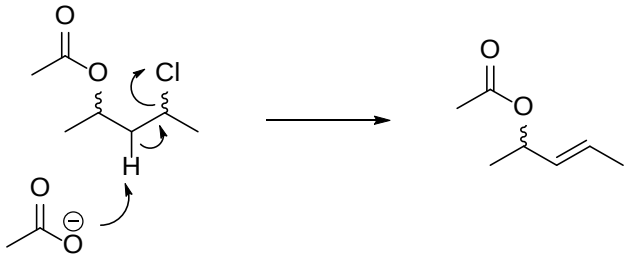

Figure 4.29. Bimolecular basic elimination to form the substituted alkene pent-3-en-2-yl acetate from the reaction of 2,4-dichloropentane with NaOAc at 100 °C with added PTC.

Note that Figure 4.29 is drawn to show substitution occurring prior to elimination. There was no evidence in Figure 4.27 of 4-chloro-2-pentene, which would be a necessary precursor for the substitution following elimination.

The model for the tertiary chloride (**3**) showed small amounts of the substitution product (pentan-3-yl acetate) at short reaction times (up to 1 hour). When the reaction was complete (after 1 day), however, the only observable product was the elimination product (3-ethylpen-2-ene). It is hypothesized that the substitution must have occurred via an S_N1 mechanism due simply to the steric hindrance surrounding the chlorine atom. The elimination product likely also occurred via a unimolecular mechanism for the same reason. The presence of the elimination product signifies that even in the nonpolar environment examined, the dissociation of chloride is rapid enough to occur measurably.

The models of the vicinal chloride defect (**4a**) and (**4b**) (*meso* and enantiomeric pair, respectively) have *slower* reaction rates than 2,4-dichloropentane, which represents defect-free PVC. Meanwhile, the product distributions of (**4a**) and (**4b**) are analogous to those of (**2a**) and (**2b**): the *meso* isomer reacts faster in both cases. Both models yield primarily a substitution product. The relatively slow reaction rates of (**4a**) and (**4b**) imply that vicinal defects likely do not play a significant role in the stabilization process.

Both models with allylic defects (**5**) and (**6**) react to form substitution products. No elimination product was observed for (**5**); however, this certainly does not signify that no elimination occurred. Rather, this is likely due to the extreme volatility of 1,3-butadiene, preventing its retention in the heated reaction solution. Nonetheless, the concentration of the substitution product increased steadily during the entire reaction (2.5

hours), signifying the susceptibility of allylic chlorides to substitution. (**6**) forms its substitution product during only the first 4 hours of reaction. Samples taken after this point exhibit a rapid conversion to the elimination product nona-3,5-diene. The last reaction sample (24 hours) showed almost complete conversion to the diene. No visible substitution product remained. This result is different from that observed with (**5**) in that elimination was ultimately the dominating process.

The three models (**3**), (**5**), and (**6**) all contain relatively labile chlorides. The tertiary model (**3**) exhibited the least amount of substitution and the lowest reaction rate among the labile models. This was discussed above in context of the uncoordinated acetate ions generated by the PTC. There is simply too much steric hindrance with the tertiary model to measure meaningful reaction rates.

Models (**5**) and (**6**) both mimic allylic defects. Of the two allylic models, (**5**) demonstrates the greater reaction rate and the greater degree of substitution. It's probable that (**5**) undergoes elimination and substitution simultaneously; this would account for the higher reaction rate. Additionally, this discrepancy highlights the profound impact of steric effects in the reaction system discussed herein. The uncoordinated acetate ions produced by the PTC likely react via bimolecular mechanisms. The substitution observed with (**5**) (but not with (**6**)) is hypothesized to be due to the smaller size (and thereby lack of steric hindrance) of (**5**). To extrapolate on these results, it's likely that as the size of a model more closely approximates PVC (via increasing chain size), elimination products will begin to dominate.

The results of the kinetics investigation discussed above provide valuable insight. The use of a PTC produced uncoordinated acetate ions, thereby simplifying the reaction

system. Reactions of models with these uncoordinated ions provide a very clear picture of relative reactivities via different mechanisms of the defects being examined. Through this methodology, the trends present in Table 4.2 are conjectured to be strongly representative of the trends in actual PVC.

The results reported in Table 4.2 are also supported by literature. Various references report early substitution with elimination becoming important later in reactions.[3,4] The products observed herein agree with literature reports. The observed products are, again, likely due to the influence of sterics. It was observed that elimination became more favorable and substitution less favorable as steric hindrance surrounding the chlorine atoms increased. This is likely due to the bimolecular mechanisms carried out by the uncoordinated acetate ions in the system examined.

To form a better picture of the behavior of real PVC systems, 2,4-dichloropentane was reacted with zinc and calcium stearates.

4.4 Mechanistic Investigations with Stearates

To more directly relate to industrial PVC systems, 2,4-dichloropentane (the model of defect-free PVC) was reacted with combinations of zinc and calcium stearates at 140 °C. The metal stearates are soluble in 2,4-dichloropentane, thereby eliminating the need for a PTC. The mixture of stereoisomers (*meso* and enantiomeric pair) was employed for these studies. All reactions in this section were carried out in sealed vessels.

Reactions were monitored by noting the evolution of color as a function of heat and time. The reaction solutions all began colorless. The formation of color is indicative

of conjugated polyene sequences as such sequences are active in the visible wavelengths of light. In actual PVC, polyene sequences can readily form on the PVC backbone via "chain-unzipping."[29-31] However, in the model system with 2,4-dichloropentane, the maximum length of conjugated double bond sequence is seemingly 2. Color change is observed, however, and is attributed to oligomerization of eliminated species. The proposed oligomerization process is discussed later.

When heated at 140 °C, the colorless reaction solutions would run through a color profile of yellow, brown, and eventually black as shown in Figure 4.30 below. The amount of time to reach each color was measured as a function of carboxylate mixture. The results are tabulated below in Table 4.3.

Figure 4.30. Color appearance of a representative reaction of 2,4-dichloropentane with 2.5 phr $ZnSt_2$ and 2.5 phr $CaSt_2$ at 140 °C. Samples were selected to clearly demonstrate the color definitions.

Table 4.3. Times required to reach the defined colors for the reactions of 2,4-dichloropentane with various compositions of carboxylates at 140 °C. "NR" means no reaction within 180 minutes. "NA" means color was not visible (change was too rapid).

		Time to Color Change (minutes)		
Additive 1	**Additive 2**	**Yellow**	**Brown**	**Black**
None	None	NR	NR	NR
$ZnSt_2$ (5 phr)	None	NA	8±2	11±1
$ZnSt_2$ (2.5 phr)	$CaSt_2$ (2.5 phr)	102±10	131±6	159±20

$ZnSt_2$ (5 phr)	$CaSt_2$ (2.5 phr)	85±5	100±0	119±12
$ZnCl_2$[1]	None	NA	5±2	8±2
$ZnCl_2$[1]	$CaSt_2$ (2.5 phr)	21±0	27±2	43±2

[1]Equimolar in Zn to 5 phr of $ZnSt_2$

2,4-Dichloropentane with no additives exhibited no color change after 3 days. In other words, the model compound on its own is completely thermally stable for the purposes of this study. The addition of 5 ph $ZnSt_2$ caused the color of the reaction mixture to become brown within 8 minutes. This short time frame suggests a rapid degradation, thereby implying that $ZnSt_2$ may contribute detrimentally to PVC degradation. This result is unsurprising as $ZnSt_2$ can act as a Lewis acid to facilitate dehydrochlorination and yield stearic acid and $ZnCl_2$, an even stronger Lewis acid. As shown in Table 4.3, when $ZnSt_2$ was replaced with $ZnCl_2$, the color change was accelerated *despite* the much lower solubility of $ZnCl_2$ in 2,4-dichloropentane.

Zinc stearate is almost never used as the only stabilizer in a PVC blend (due largely to its known effects as a Lewis acid). Instead, it is often used in combination with other metal stearates, such as calcium stearate.[32] In all cases reported in Table 4.3, the presence of $CaSt_2$ mitigated the rapid degradation caused by $ZnSt_2$. The reaction of $ZnCl_2$ with $CaSt_2$ is enthalpically favored and produces $ZnSt_2$ and $CaCl_2$. Since $CaCl_2$ is a much less potent Lewis acid than $ZnCl_2$, the combination of the two stearates should logically exhibit less degradation than a blend with $ZnSt_2$ on its own. Interestingly, the presence of any stearates at all induced the degradation of 2,4-dichloropentane.

In addition to the qualitative color change studies, NMR was used to monitor structural changes associated with the stearate reactions. Higher concentrations of reactants were reacted at 140 °C for 3 hours. ^{1}H NMR spectra of zinc stearate and 2,4-dichloropentane are included below in Figure 4.31. Proton NMR spectra were measured

at 100 °C to ensure sample homogeneity. The *meso* stereoisomer (**2a**), indicated by primes " ' " in Figure 4.31, are distinguished from the enantiomeric pair (**2b**) using the signal from the protons on the same carbons as the chlorides ("b" and "b' "). The long chain of aliphatic protons in the stearate (labeled "f" in Figure 4.31) can be used as an internal standard to track disappearance of 2,4-dichloropentane. The total number of these aliphatic protons is not expected to change over the course of reaction.

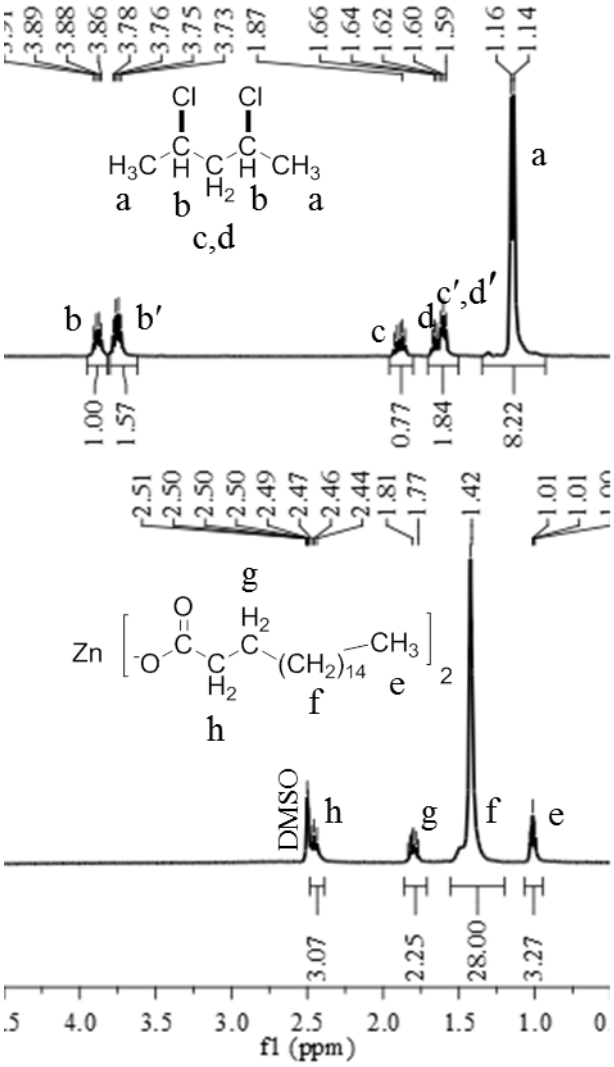

Figure 4.31. Proton NMR spectra of reactants measured at 100 °C. TOP: Proton NMR of neat meso-2,4-dichloropentane (denoted by ') and (2S*,4S*)-dichloropentane with DMSO capillary. BOTTOM: Proton NMR of zinc stearate in o-dichlorobenzene with a DMSO capillary.

The ratios of the stereoisomers of 2,4-dichloropentane and the conversions of 2,4-dichloropentane with various mixtures of stearates are reported below in Table 4.4. Representative NMR spectra of the reaction mixtures after heating are shown below in Figure 4.32.

Table 4.4. Stereoisomer ratios and conversion of 2,4-dichloropentane for reactions of 2,4-dichloropentane with various compositions of stearates at 140 °C for 3 hours.

Additive 1	Additive 2	*Meso*:Enantiomeric Pair	2,4-Dichloropentane Conversion (%)
PRIOR TO REACTION		1.57	--
NONE	NONE	1.57	0
$ZnSt_2$ (0.1 eq)	NONE	0.71	75
$ZnSt_2$ (0.05 eq)	$CaSt_2$ (0.05 eq)	0.99	42
$ZnSt_2$ (0.1 eq)	$CaSt_2$ (0.05 eq)	0.74	56

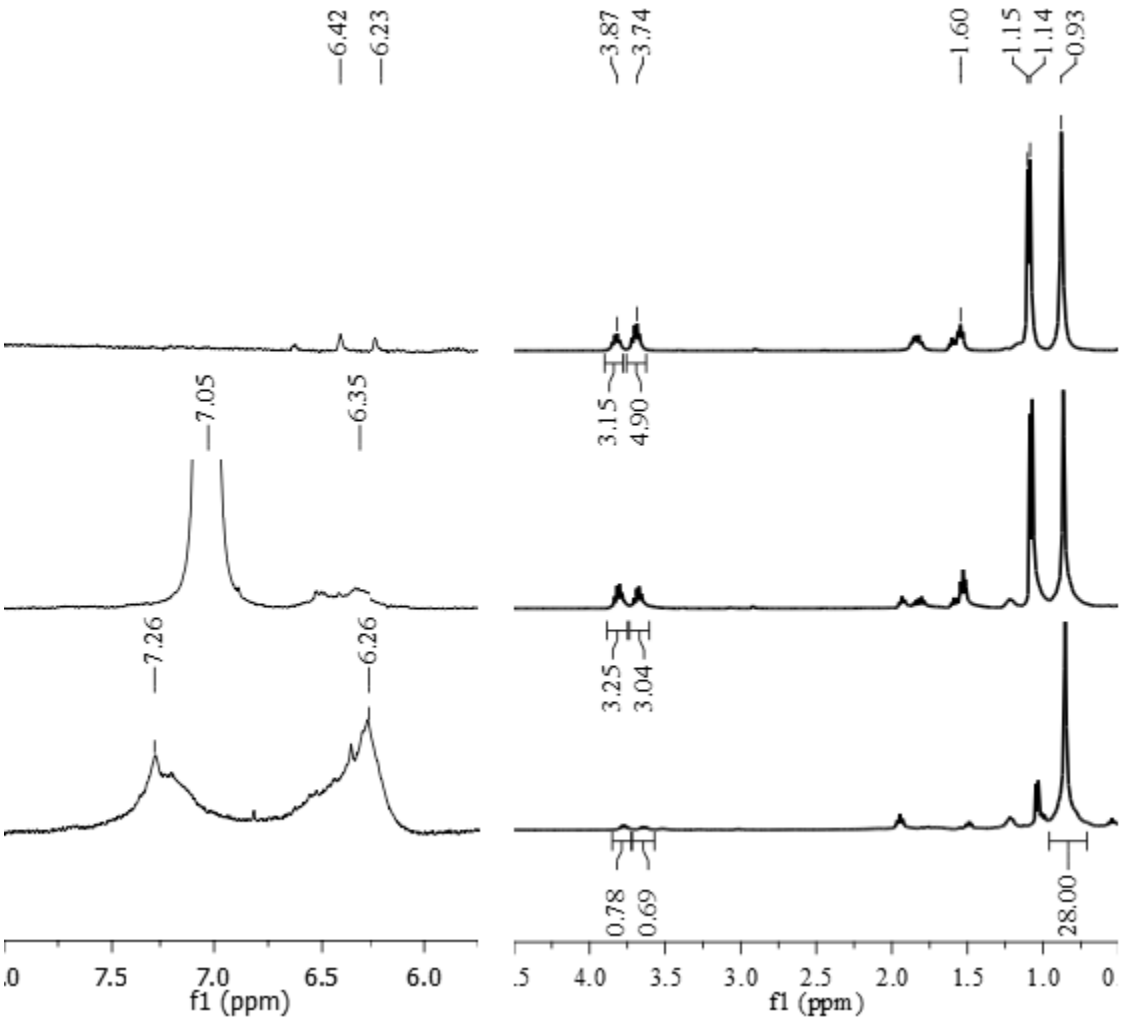

Figure 4.32. Proton NMR spectra of the reaction of 2,4-dichloropentane with $ZnSt_2$ at 140 °C. TOP: Spectrum measured prior to reaction. MIDDLE: Spectrum measured after 1.5 hours of reaction time. BOTTOM: Spectrum measured after 3 hours of reaction time. Spectra are normalized by setting the aliphatic protons of the stearate (labeled "f" in Figure 4.31) to 28. The left portion of the spectrum is greatly zoomed in to emphasize the appearance of species with protons in the aromatic and vinyl regions.

An important observation from Table 4.4 is possible: the *meso* (isotactic) model of PVC (**2a**) reacts much faster than the enantiomeric pair (syndiotactic) model (**2b**). The only new product peaks observed in Figure 4.32 are several peaks in the aromatic and vinyl regions (albeit with low concentration) and those corresponding to stearic acid. The presence of stearic acid is confirmed below in Figure 4.33.

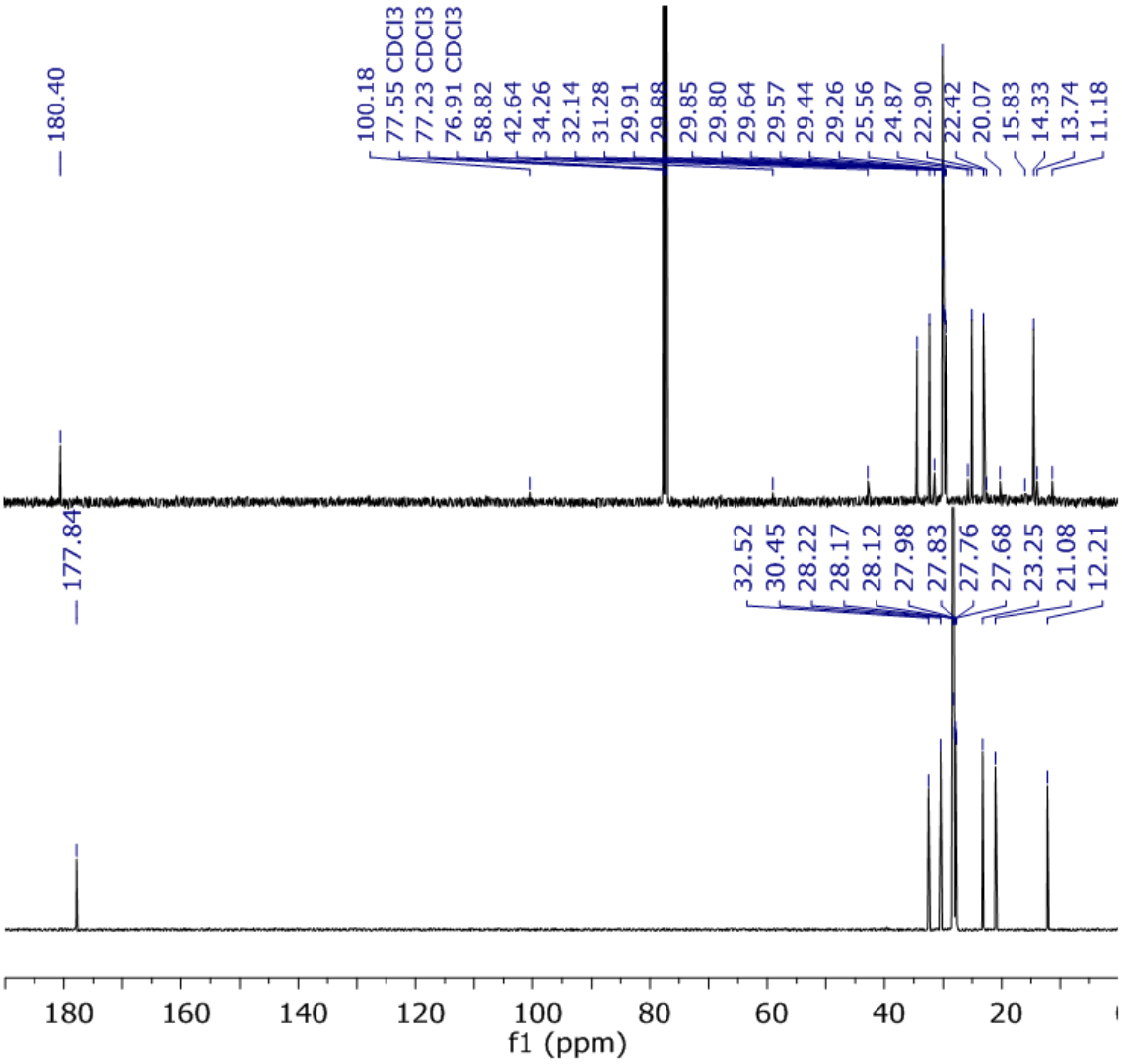

Figure 4.33. ^{13}C NMR confirming the presence of stearic acid in reaction solutions of 2,4-dichloropentane with stearates after 3 hours at 140 °C. BOTTOM: Spectrum of stearic acid in DMSO. TOP: Spectrum of the reaction mixture of 2,4-dichloropentane after reaction with $ZnSt_2$ at 140 °C for 3 hours.

The largest peaks in Figure 4.33 are confirmation of the presence of stearic acid. The slight difference in chemical shifts are due to the difference in solvent used to gather the two carbon NMR spectra.

Other than stearic acid and vinylic species, only disappearance of the starting material was observed. Additionally, the rate results corroborate what was shown in

Table 4.3: zinc stearate causes degradation of the model compound. Increasing amounts of calcium stearate mitigate this degradation.

The product distribution from these stearate reactions differs greatly from that observed with the acetate models in Table 4.2. Reactions of 2,4-dichloropentane with acetate models produced almost exclusively substitution products. The reactions with stearates produced no products observed via NMR. The lack of substitution illustrates the importance of steric hindrance: bulky stearate groups were much less able to react than the small, uncoordinated acetate ions.

The peaks in the proton NMR are hypothesized to correspond to the species responsible for the color changes observed in Figure 4.30. The formation of conjugated polyenes (with proton peaks in the vinyl region) is attributed to the polymerization of 2,4-pentadiene as catalyzed by $ZnCl_2$. The possible polymerization of 2,4-pentadiene is investigated below.

4.4.1 Investigation of Color Change in Reactions with 2,4-dichloropentane

To investigate the origin of color change in the reactions of 2,4-dichloropentane with stearates, 5.655 mmol (1.2 M) piperylene (2,4-pentadiene) were reacted with 10 phr $ZnCl_2$ in 5 mL of ortho-dichlorobenzene (o-DCB) at 140 °C. $ZnCl_2$ proved difficult to weigh both quickly and accurately (due to its hygroscopic nature), but its solubility in o-DCB is highly limited regardless. The color change of the reaction and proton NMR spectra were monitored. The color change is shown below in Figure 4.34. The associated NMR spectra are shown below in Figure 4.37.

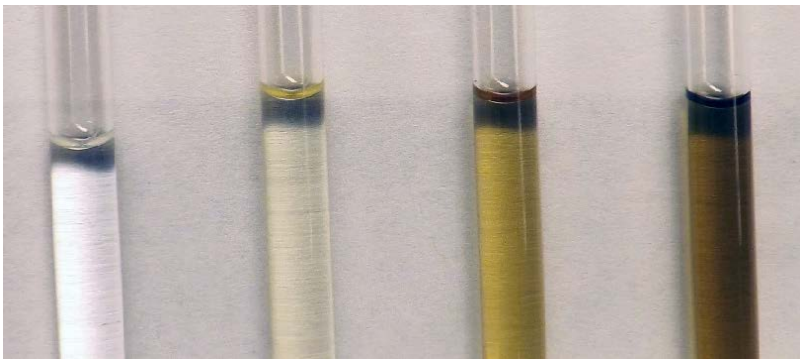

Figure 4.34. Color change of the reaction of 1.2 M 2,4-pentadiene with 10 phr $ZnCl_2$ in o-DCB at 140 °C. Samples shown were taken from the same reaction mixture at different times. The reaction times are, from left to right: 0 minutes, 30 minutes, 60 minutes, 120 minutes. The dark coloration at the top of each sample is a shadow made more prominent by the contrast adjustment of the images.

The color change exhibited in Figure 4.34 progresses similarly to that shown in Figure 4.30. Reaction solutions began transparent and progressed through yellow, brown, and dark brown colors. It is clearly evident that $ZnCl_2$ can induce color formation in normally transparent species. It is hypothesized that the color change in Figure 4.30 is caused by the catalytic polymerization of 2,4-pentadiene by $ZnCl_2$. The resulting polymerized species contain conjugated double bond sequences of sufficient length to develop visible color. A control experiment was conducted of 2,4-pentadiene heated in o-DCB at the same temperature and time as the experiment shown in Figure 4.34. The control study is shown below in Figure 4.35.

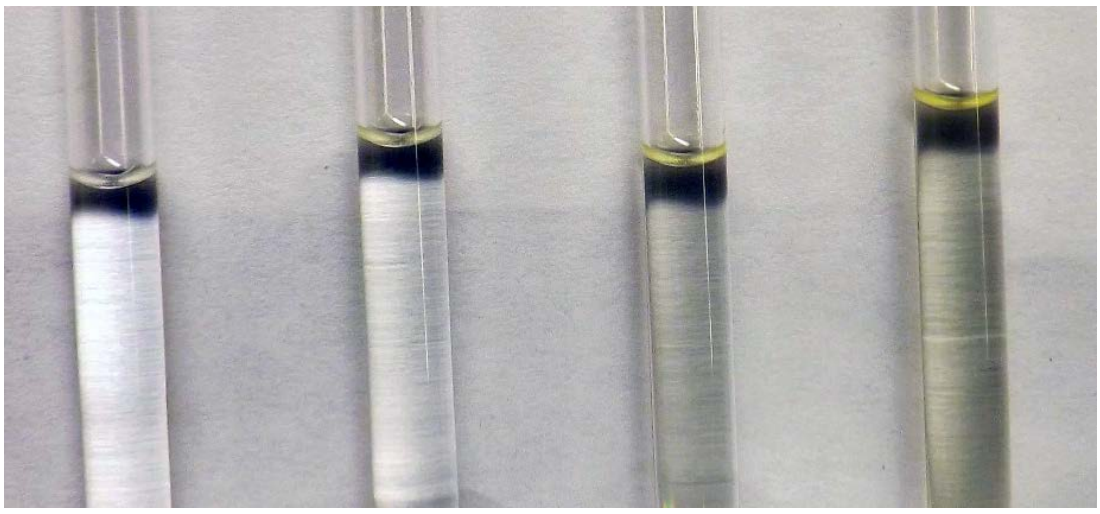

Figure 4.35. Reaction of 1.2 M 2,4-pentadiene in o-DCB at 140 °C. Samples were extracted from the same reaction mixture at different times. The image times are, from left to right: 0 minutes, 30 minutes, 60 minutes, 120 minutes. The dark coloration at the liquid / atmosphere interface is a shadow made more obvious by contrast adjustment.

The control study in Figure 4.35 does not produce nearly as much color change as the reaction shown in Figure 4.34. However, some color change is observed. This even further supports the hypothesis that 2,4-pentadiene can react to form color change at elevated temperatures.

The hypothesized mechanism by which conjugated double bond sequences can form from 2,4-pentadiene involves catalytic reaction with the Lewis acid $ZnCl_2$. The actual mechanism as hypothesized is shown below in Figure 4.36.

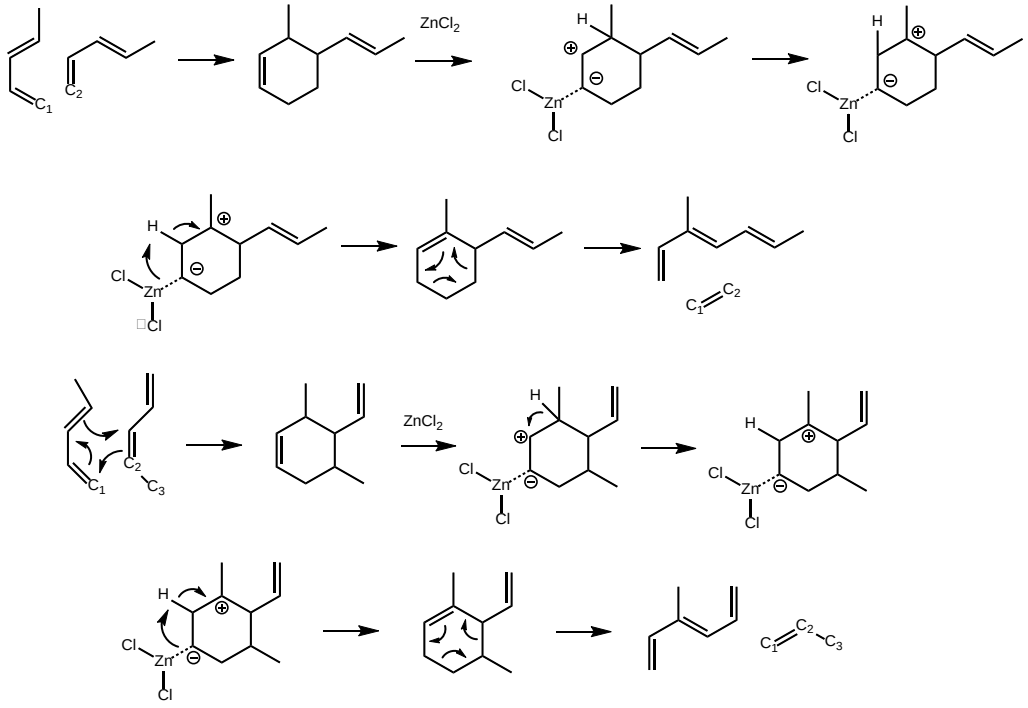

Figure 4.36. Hypothesized mechanisms for the formation of colored conjugated double bond systems via reaction of 2,4-penadiene with $ZnCl_2$. The mechanism involves a combination of Diels-Alder, hydride/proton shift, and retro-Diels-Alder steps to increase the length of conjugated chains. The process can repeat to form longer conjugated double bond sequences.

As drawn, the mechanism in Figure 4.36 can form either ethane (if the dienophile is terminal) or propene (if the dienophile is an internal double bond).

The reaction of 2,4-pentadiene with $ZnCl_2$ was also monitored via proton NMR. The NMR spectra from the reaction are shown below.

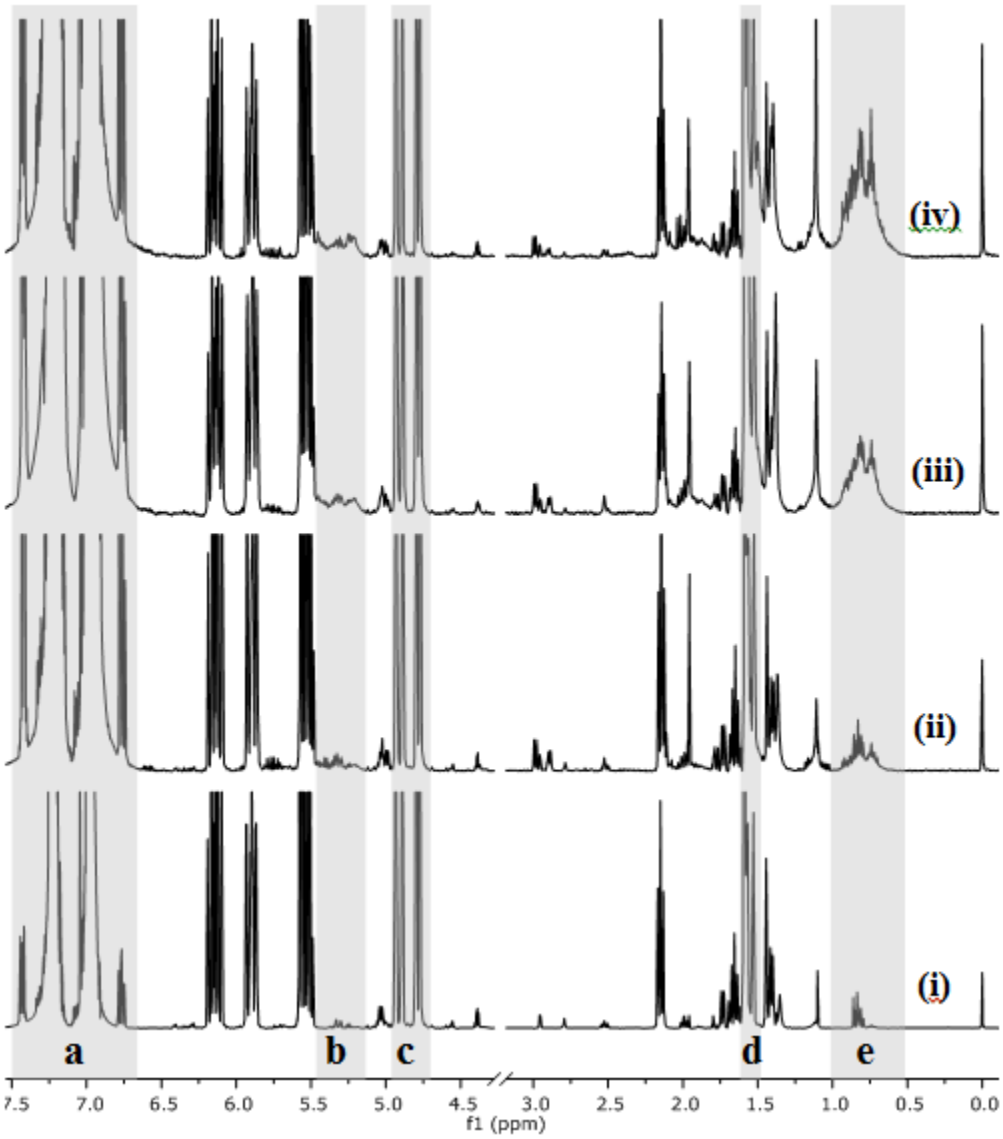

Peak	a	b	c	d	e
(i)	10000	7.22	415.65	677.8	11.45
(ii)	10000	10.9	136.01	234.54	21.19
(iii)	10000	11.22	76.69	142.38	38.94
(iv)	10000	14.15	60.38	130.46	73.19

Peak ratio	b : c	e : c
(i)	0.017	0.028
(ii)	0.080	0.156
(iii)	0.146	0.508
(iv)	0.234	1.212

Figure 4.37. Proton NMR spectra for the reaction of 1.2 M 2,4-pentadiene with 10 phr ZnCl2 in o-DCB at 140 °C. The spectra correspond to the following reaction times: (i) 0 minutes; (ii) 30 minutes; (iii) 60 minutes; (iv) 120 minutes. Peaks are labeled along the x-axis with letters corresponding to the columns shown in the tables.

In a qualitative sense, Figure 4.37 demonstrates the formation of new vinyl (polymerized) species. Regions "c" and "d" correspond to the starting material, 2,4-pentadiene. Region "b" corresponds to new species with protons in the vinyl region. The peaks that appear in this region are broad, likely indicating several species with similar chemical shifts in this region. Region "e" corresponds to the formation of new species with methyl protons. Once again, peaks in this region are broad and overlapping; it's likely that multiple new species contain protons with peaks in this region. The new peaks in regions "b" and "e" are believed to correspond to species responsible for the color change in Figure 4.34.

If the assumption is made that minimal new species will form with peaks in the aromatic region, o-DCB can be used as an internal standard for quantification. Under this assumption, the region from 6.7 ppm to 7.5 ppm (e.g., the region corresponding to o-DCB, labeled "a") was set to 10000 in all spectra. The integrals of the other highlighted regions (relative to this reference) are reported in the first table in Figure 4.37. As the reaction progresses, the areas of regions "b" and "e" (corresponding to new products formed) increase. Meanwhile, the areas of regions "c" and "d" (corresponding to 2,4-pentadiene) decrease.

Unfortunately, meaningful conclusions cannot be drawn from the rate of decrease of the areas of the regions corresponding to 2,4-pentadiene. The diene is highly volatile, and much of the decrease in peak integration is likely due to evaporative losses.

As another method of quantification, peak ratios were compared in the second table of Figure 4.37. Both ratios "b:c" and "e:c" increase as a function of reaction time. This is probably due to both volatilization of the starting material and the formation of new species. A similar examination of proton NMR spectra was conducted for the control experiment of 2,4-pentadiene in o-DCB. The spectra are reported below in Figure 4.38.

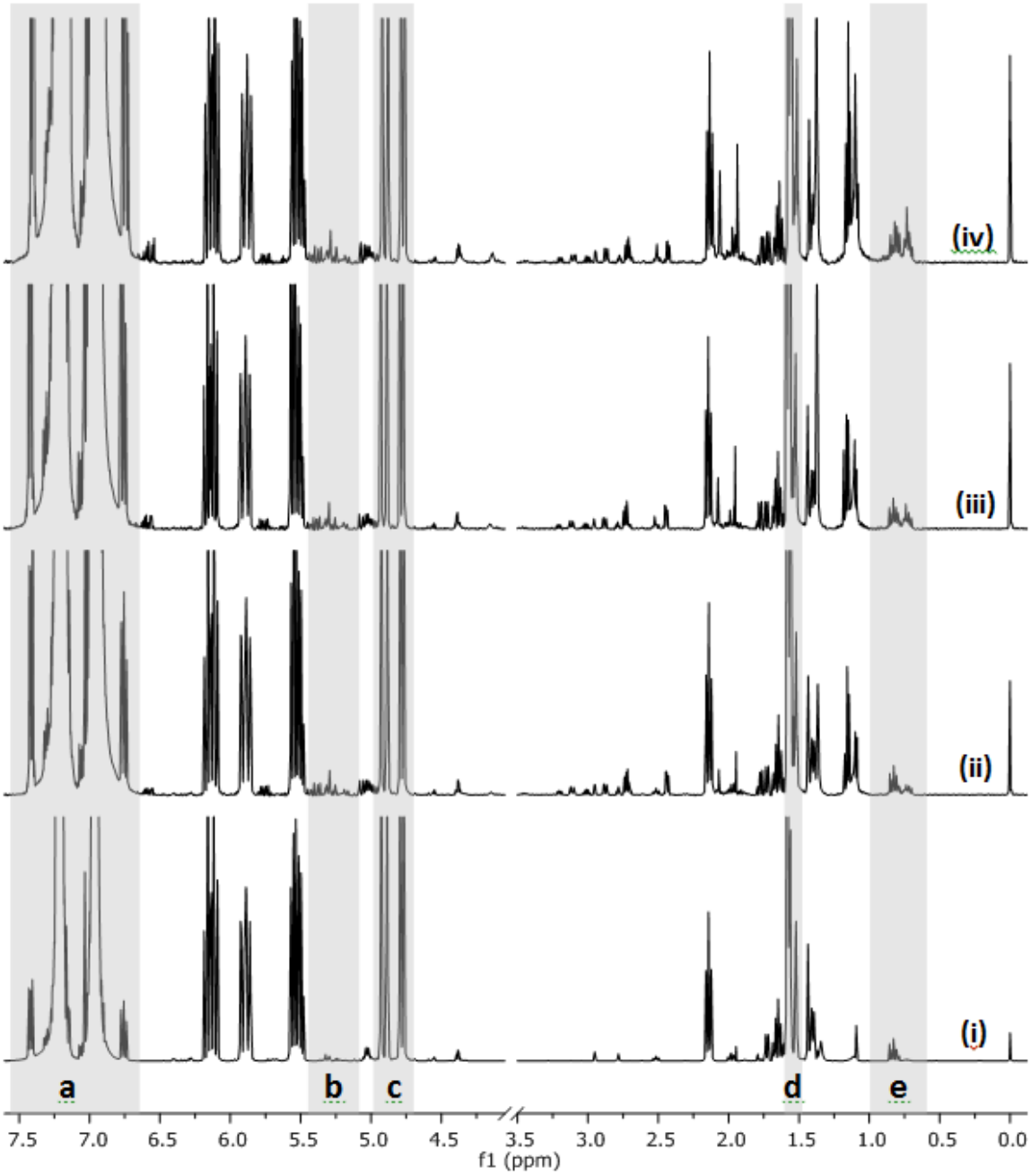

Peak	a	b	c	d	e
(i)	10000	6.04	387.44	630.76	10.73
(ii)	10000	5.13	122.52	211.95	7.46
(iii)	10000	3.64	77.55	136.69	7.50
(iv)	10000	5.06	69.10	121.25	11.69

Peak ratio	b / c	e / c
(i)	0.016	0.028
(ii)	0.042	0.061
(iii)	0.047	0.097
(iv)	0.073	0.169

Figure 4.38. ^{1}H NMR spectra for the reaction of 1.2 M 2,4-pentadiene in o-DCB at 140 °C. Spectra are presented in order from top to bottom: (i) 0 minutes; (ii) 30 minutes; (iii) 60 minutes; (iv) 120 minutes. Peaks are labeled along the x-axis and correspond to the columns in the tables below the spectra. Integrals are given in the table.

Figure 4.38 is an excellent comparison to Figure 4.37. Regions "b" and "e" in the NMR spectra visibly show much less increase in area in Figure 4.38 as compared with Figure 4.37. The different rates of appearance of these regions are also visible in the first table of Figure 4.38. Finally, the peak ratios discussed previously (shown in the second tables of Figure 4.37 and Figure 4.38) show a much slower rate of increase in Figure 4.38. It is clear that the presence of $ZnCl_2$ has a strong influence on the appearance of species with peaks in the vinyl region.

It has been concretely demonstrated with the reactions of 2,4-pentadiene with $ZnCl_2$ that $ZnCl_2$ induces the formation of color and peaks in the proton NMR in the vinyl region. Recall that on its own, 2,4-pentadiene did not exhibit nearly as much color change. It can be concluded that in the reactions of 2,4-dichloropentane, it's likely that both $ZnCl_2$ and 2,4-pentadiene were formed during reaction. The subsequent polymerization of 2,4-pentadiene is responsible for inducing the color change shown in Figure 4.30. The mechanism of formation of 2,4-pentadiene and $ZnCl_2$ in the reaction system is discussed below.

4.4.2 Analysis of Headspace Over Reactions of 2,4-dichloropentane with Stearate

Figure 4.32 showed the disappearance of large amounts of starting material and the appearance of stearic acid and of minor amounts of vinyl peaks. To determine where

the remainder of the mass went, the headspace above the reaction of 2,4-dichloropentane with zinc stearate was analyzed. The gas chromatograph of the vapor phase is shown below in Figure 4.39.

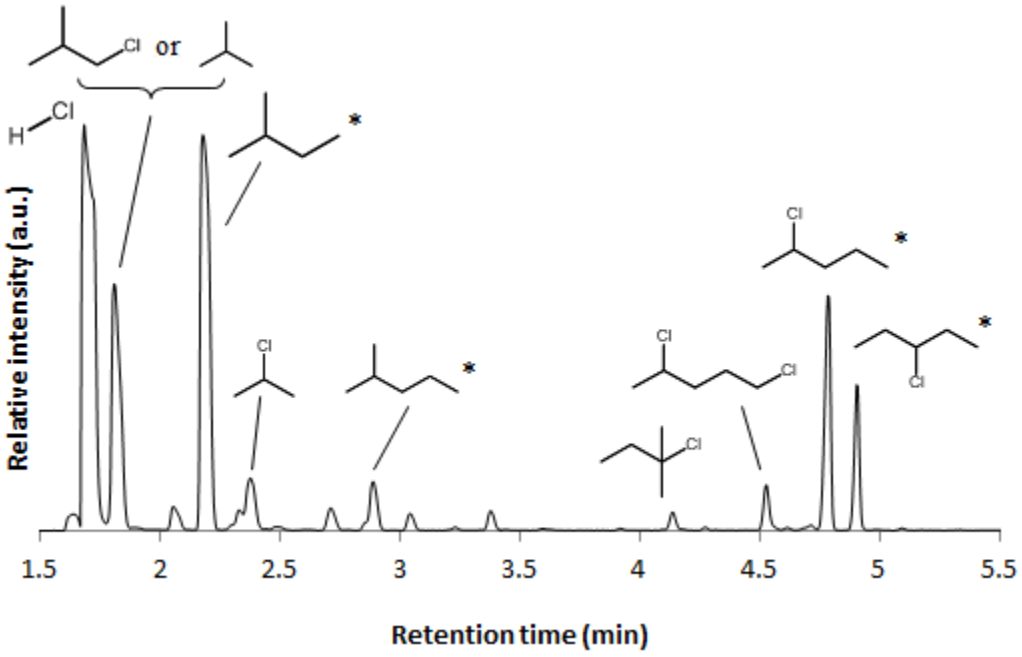

Figure 4.39. Gas chromatograph and associated species of the vapor phase above the reaction of 2,4-dichloropentane with $ZnSt_2$ at 140 °C for 3 hours. The "*" symbols denote those species whose mass spectra matched exactly with those predicted by Shimadzu similarity search. A small peak corresponding to 2,4-dichloropentane eluted at 7.2 minutes (not shown).

As can be seen in Figure 4.39, numerous peaks at various retention times were observed in the analysis of the headspace. Peaks were identified using mass spectrometry and the corresponding species are labeled in Figure 4.39. The mass spectra used in identifying the species are all shown below in Figure 4.40.

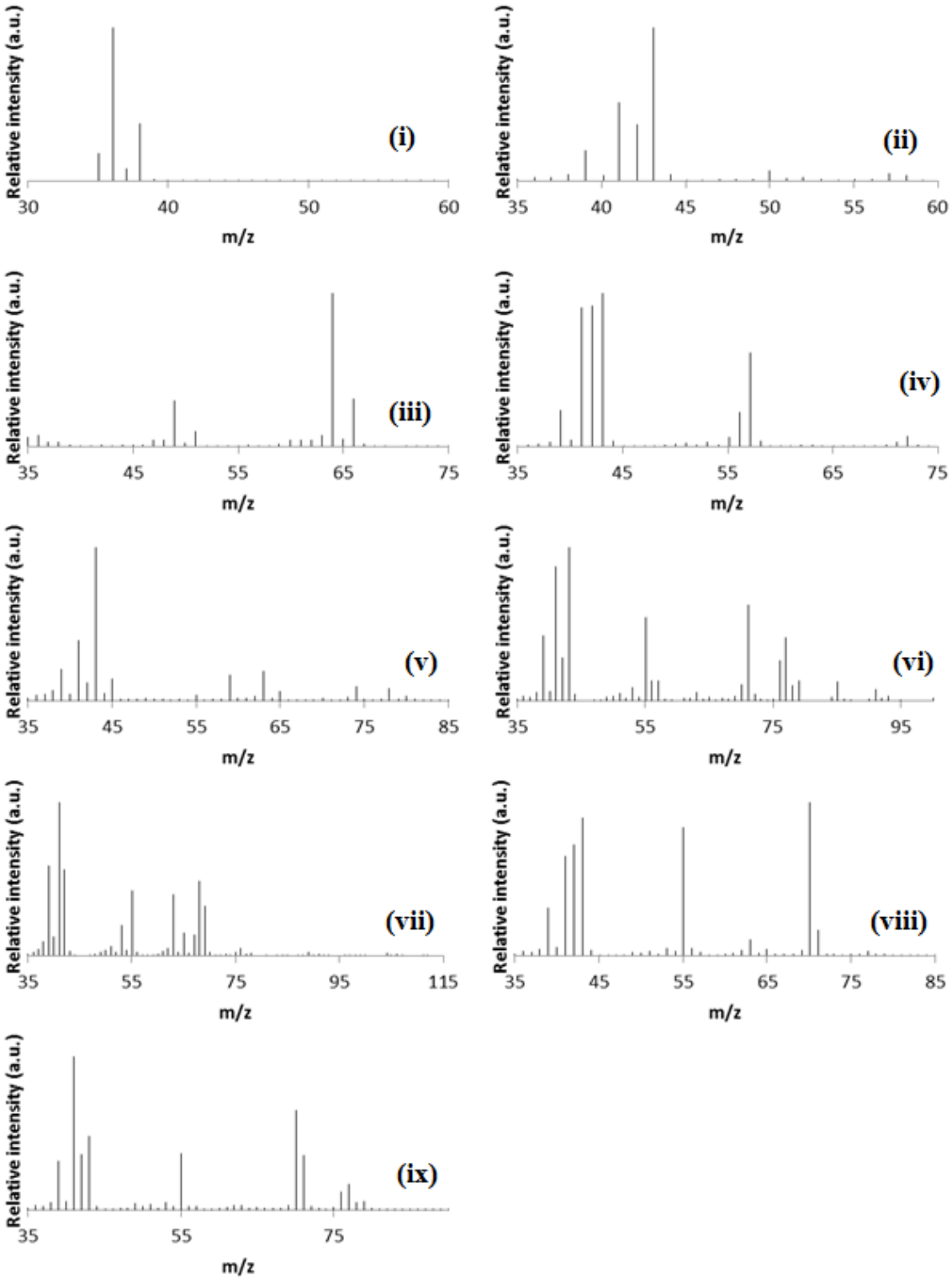

Figure 4.40. Mass spectra used in identification of the GC peaks in Figure 4.39. The spectra correspond to: (i) peak at 1.705 minutes; (ii) peak at 1.820 minutes; (iii) peak at 2.060 minutes; (iv) peak at 2.175 minutes; (v) peak at 2.380 minutes; (vi) peak at 4.140 minutes; (vii) peak at 4.530 minutes; (viii) peak at 4.785 minutes; (ix) peak at 4.915 minutes.

The largest peak in Figure 4.39 corresponds to (as expected) HCl. HCl is liberated via the elimination of 2,4-dichloropentane. Since no substitution products were observed in Figure 4.32 and starting material disappeared, the only option left for products result from elimination. The other species in Figure 4.39 are likely formed via complexation with ZnCl2. Hypothesized mechanisms for formation of the species in Figure 4.39 with retention times of 2.2 minutes and 4.6 minutes are shown below in Figure 4.41. The remaining species in the GC chromatogram are likely formed analogously.

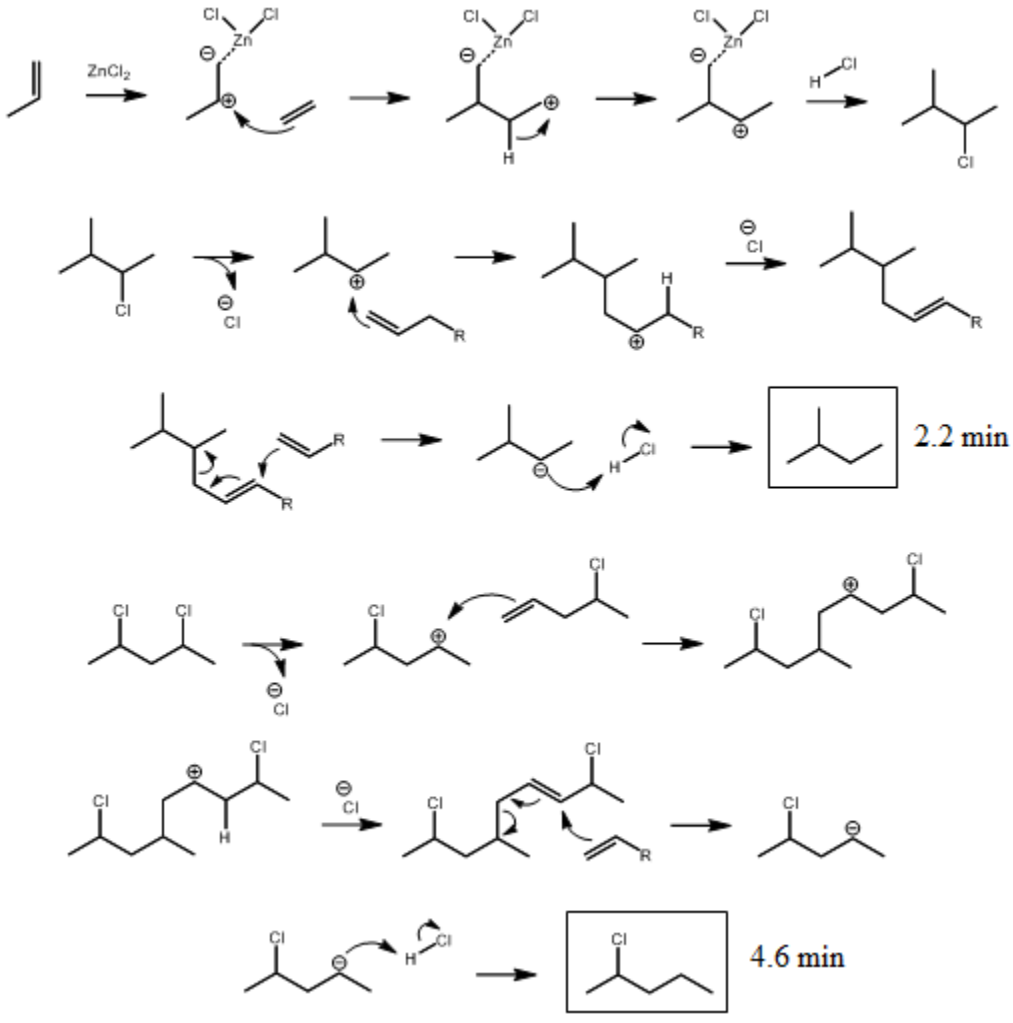

Figure 4.41. Proposed mechanisms for the formation of species with retention times of 2.2 minutes and 4.6 minutes in Figure 4.39.

Strong evidence has been presented supporting the formation of volatile elimination species from the reaction of 2,4-dichloropentane with zinc stearate at 140 °C. The elimination products illustrate the profound difference between the reaction behavior of 2,4-dichloropentane in the presence of (i) a non-coordinating carboxylate anion and (ii) a carboxylate with a coordinating metal. The acetate anion, in the presence of a PTC, was nucleophilic and sterically unhindered, resulting in large extents of substitution onto 2,4-dichlorpentane. The stearates appear to have facilitated only elimination reactions via carbocations when reacted with 2,4-dichloropentane.

The qualitative color studies of 2,4-dichloropentane revealed that calcium stearate can mitigate the degradation effects induced by zinc stearate. It was thus useful to study similar stearate reactions using proton NMR. As shown in Table 4.4, the addition of $CaSt_2$ to blends containing $ZnSt_2$ reduced the rate of consumption of 2,4-dichloropentane. This result is consistent with the results of the color studies.

4.4.3 Mechanism of Zn/Ca Stearates Interaction with PVC

All mechanistic studies in this section were used to propose an overall mechanism of the interaction between PVC and metal carboxylates. The mechanism is shown below in Figure 4.42. As shown in the figure, zinc stearate is proposed to complex with a chloride on the backbone to promote its abstraction and form a cation (supported by the study of 2,4-pentadiene with $ZnCl_2$). The carbocation then likely undergoes elimination (recall no substitution was seen of stearates onto 2,4-dichloropentane). The stearate in

the zinc complex formed in step 1 could then abstract a proton as shown in step 2 in Figure 4.42. This proton abstraction forms stearic acid, ZnClSt, and an alkene. This process can repeat, converting ZnClSt to $ZnCl_2$.[33] Once $ZnCl_2$ is formed, it can ion exchange with $CaSt_2$ as shown in step 3 (supported by the color change and NMR studies with stearates). The ion exchange would prevent accumulation of $ZnCl_2$ and regenerate $ZnSt_2$ by forming $CaCl_2$. The regenerated $ZnSt_2$ could proceed through the cycle again, reacting with more PVC or PVC model.

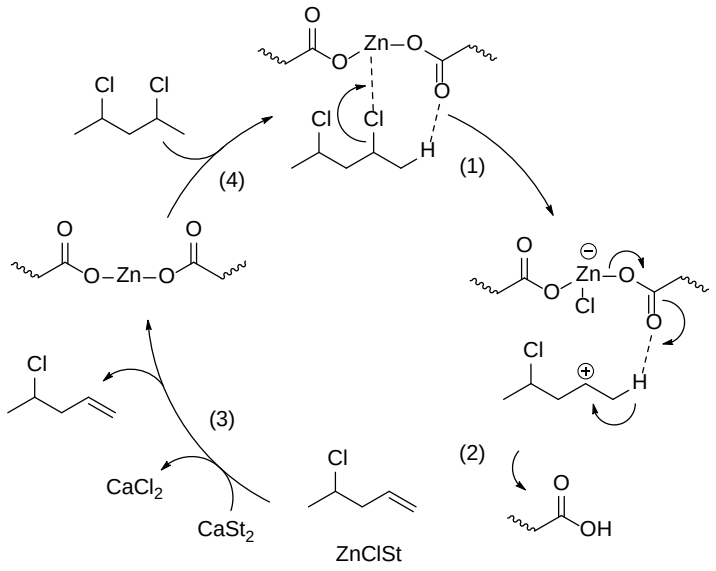

Figure 4.42. Proposed mechanism of interaction of metal stearates with PVC.

It is noteworthy that the mechanism presented in Figure 4.42 does not represent stabilization. It is possible that $ZnSt_2$ can stabilize PVC by simple acting as a base. By scavenging HCl to form $ZnCl_2$ (and exchanging with $CaSt_2$ to form $ZnSt_2$ and $CaCl_2$), the synergistic stearate pair could prevent autocatalysis.

Based on all the evidence used to produce Figure 4.42, stearates cannot substitute to stabilize defect-free PVC. Stearates therefore do not likely act as barriers to the "chain-unzipping" process. The scavenging of HCl is likely the method of stabilization.

4.5 Comparison to Studies of PVC Polymer

Thus far, the work in this chapter has examined reactions of PVC model compounds. To provide a comparison to real PVC systems, PVC blends plasticized with di-isodecyl phthalate (DIDP) were studied with stearate additives. Blends of PVC, DIDP, and stearates were prepared. Blends consisted of 3 g PVC, 30 phr DIDP, and 5 phr total metal stearates (divided into 2.5 phr Ca/2.5 phr Zn when combined). The blends were heated at 170 °C over the course of 2 hours. Mass loss was recorded as a function of time and photographs of each sample were taken after heating. The mass loss of each blend is shown in Figure 4.43. The color change of each blend is shown in Figure 4.44. Each blend was prepared and heated at least twice to ensure repeatability. The figures below are representative.

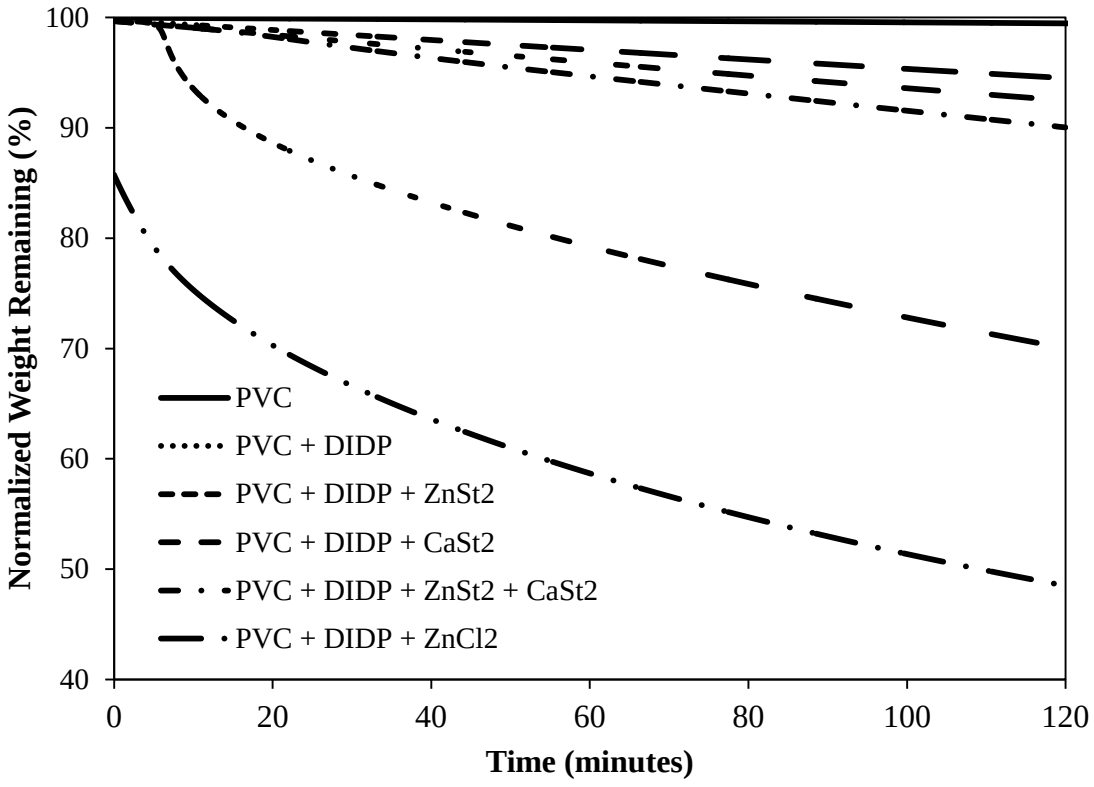

Figure 4.43. Mass loss of PVC blends during thermogravimetric analysis at 170 °C. Remaining mass is normalized against the mass of PVC in each blend, discounting additives. The ratio of $CaSt_2$:$ZnSt_2$ was 1:1 in the blended sample.

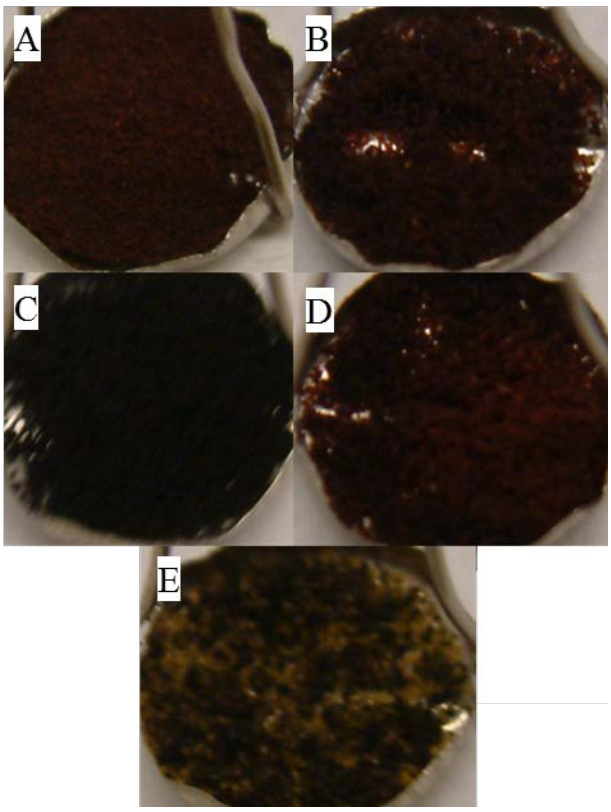

Figure 4.44. Photographs of PVC blends after thermal treatment at 170 °C for 2 hours. (A) PVC; (B) PVC + DIDP; (C) PVC + DIDP + $ZnSt_2$; (D) PVC + DIDP + $CaSt_2$; and (E) PVC + DIDP + $ZnSt_2$ + $CaSt_2$.

The PVC sample without any additives lost the least mass when thermally treated. Its weight profile is almost parallel to the top of Figure 4.43: it loses 0.81% of its original mass after 2 hours at 170 °C. From examination of the weight profile alone, it would seem that stabilizers are unnecessary. However, PVC with no additives displays terrible color retention, shown in Figure 4.44A. Additionally, PVC alone is too rigid and brittle for use in most consumer applications. Plasticizers are therefore necessary for any PVC product.

DIDP was chosen as a plasticizer for this study; DIDP does not exhibit any confounding thermal stabilization effects and is commonly used in industry.[34] As shown in Figure 4.43, PVC plasticized with DIDP exhibits more degradation than PVC, losing

5.5% of its mass over the heat treatment. It also displays the poor color retention exhibited by PVC alone.

Addition of stearates induces interesting weight loss performance. PVC with DIDP and added $ZnSt_2$ shows a flat curve during the first 7 minutes of heating. However, after this period, a catastrophic weight loss is observed. A total of 30% of the original mass is lost during heating. This blend also displayed terrible color retention (Figure 4.44C). PVC with DIDP and added $CaSt_2$ did not display the catastrophic weight loss observed with $ZnSt_2$; instead, it lost 7.5% of its original mass. This is further evidence of the extraordinary degradation induced by $ZnCl_2$. It is hypothesized that the initial flat region of the blend containing of PVC and DIDP with $ZnSt_2$ corresponds to an accumulation of $ZnCl_2$. The catastrophic weight loss occurs once $ZnCl_2$ has accumulated to a sufficient extent. To test this hypothesis, a blend of PVC and DIDP with $ZnCl_2$ was prepared. The shape of the curve of this blend closely matches that exhibited by the blend of PVC and DIDP with $ZnSt_2$. This is evidence that the degradation in the blend with $ZnSt_2$ is in fact caused by $ZnCl_2$.

Interestingly, the blend of PVC with DIDP and a mixture of both $ZnSt_2$ and $CaSt_2$ exhibited fairly poor weight retention. It lost 9.9% of its original mass, more than either blend containing the individual stearates. However, the color retention of this blend (Figure 4.44E) was by far superior to any other blend examined. It was the only blend to have any portion that did not appear black or dark brown.

Color change is an important metric in these polymer systems. As discussed above, color change is observed due to the formation of conjugated double bond sequences on the PVC backbone. The portions of Figure 4.44E with lighter color

represent regions with lesser degrees of double bond conjugation. Somehow, the number or length of conjugated sequences in these regions was lower than in the other blends. In other words, this blend was stabilized by synergistic action between zinc and calcium stearates. Since $ZnSt_2$ has not demonstrated an ability to substitute onto PVC, it's likely that the two stearates are acting as base and ion exchange system. Calcium stearate is not a strong enough base to significantly scavenge HCl, or the blend of PVC and DIDP with $CaSt_2$ should exhibit better color retention or weight loss.

These color change and weight loss studies correlate to the model studies. Zinc stearate exhibits an especially negative effect on PVC stability when used on its own in both cases. In the model studies, adding calcium stearate to the zinc stearate blend reduced the rate of reaction and improved color retention. In the polymer studies, weight loss with added calcium stearate was not improved, but color retention was vastly superior to any other blend.

It seems that the interaction of zinc and calcium stearates is the major influence driving thermal stability in these PVC systems. Under the conditions studied, calcium stearate alone did not significantly affect polymer degradation. Zinc stearate had a catastrophic effect on polymer weight loss. The combination of the two stearates showed excellent color retention with both model systems and polymer blends. The ion exchange of $ZnCl_2$ and $CaSt_2$ is likely responsible for this synergistic effect.

4.6 Conclusions

A library of model compounds was selected to simulate various structural components of PVC. Both defect-free PVC and various defect models were studied. Model compounds were reacted with metal acetates in the presence of PTC to isolate the effects of the carboxylate anion uncoordinated with a cation. These studies produced relative first-order rate constants for each model. Substitution reactions of both defect-free PVC and allylic defect models were sufficiently rapid to suggest they both play a significant role in PVC stabilization and degradation.

In particular, the relative rate constants highlight the hugely important role of steric hindrance in model compound interaction with acetates. The reaction rate constant of chlorobutene is 50% greater than that of chlorononene. The increased steric hindrance of the chlorononene likely reduces reaction rate. Of all models containing labile chlorides, the tertiary model demonstrated the lowest reaction rate, once again demonstrating the constraining effects of sterics. Even the defect-free model, 2,4-dichloropentane, exhibits the effects of sterics. The *meso* model showed 127% faster reaction rates than the enantiomeric pair model. Sterics, it seems, play a powerful role in reactions with small model species.

The reactions with acetates showed significant amounts of substitution onto the PVC models. In the reactions of 2,4-dichloropentane with stearates, substitution was not observed at all. Instead, stearic acid was formed and various elimination products were observed in the reaction headspace. Evidence was presented to suggest that the Lewis acid $ZnCl_2$ was formed in sufficient concentrations to induced polymerization of elimination products. This revelation inspired a proposed mechanism of the interaction of stearates with PVC. The proposed mechanism suggests that stearate stabilization takes

the form of sequestration of HCl by zinc stearate, followed by ion exchange with calcium stearate.

The polymer weight loss and color studies confirmed what was revealed by the stearate model studies. Zinc stearate induces a catastrophic effect when introduced to a PVC blend on its own. The addition of calcium stearate mitigates the effect of the damaging zinc stearate. By the metric of color retention, the PVC blend with both stearates demonstrated by far the best stabilization.

The studies discussed in this chapter represent an all-encompassing approach to the study of PVC interactions with carboxylates. The techniques employed and the results discussed here allowed for the fabrication of novel stabilizer systems in future chapters.

4.7 References

(1) Wypych, G.; PVC Degradation & Stabilization; ChemTec Publishing.

(2) Frye, A. H.; Horst, R. W. The Mechanism of Poly(Vinyl Chloride) Stabilization by Barium, Cadmium, and Zinc Carboxylates .1. Infrared Studies. *Journal of Polymer Science* 1959, *40*, 419.

(3) Frye, A. H.; Horst, R. W. The mechanism of polyvinyl chloride stabilization by barium, cadmium, and zinc carboxylates. II. Radioactive tracer studies. *Journal of Polymer Science* 1960, *45*, 1.

(4) Frye, A. H.; Horst, R. W.; Paliobagis, M. A. The chemistry of poly (vinyl chloride) stabilization. III. Organotin stabilizers having radioactively tagged alkyl groups. *Journal of Polymer Science Part A: General Papers* 1964, *2*, 1765.

(5) Varma, I. K.; Grover, S. S. Thermal degradation of some model compounds of PVC. *Die Makromolekulare Chemie* 1974, *175*, 2515.

(6) Asahina, M.; Onozuka, M. Thermal decomposition of model compounds of polyvinyl chloride. II. Gaseous thermal decomposition of unsaturated chain end model compounds. *Journal of Polymer Science Part A: General Papers* 1964, *2*, 3515.

(7) Asahina, M.; Onozuka, M. Thermal decomposition of model compounds of polyvinyl chloride. I. Gaseous thermal decomposition of model compounds having secondary and tertiary chlorine. *Journal of Polymer Science Part A: General Papers* 1964, *2*, 3505.

(8) Ayrey, G.; Siddiqui, I. H.; Poller, R. C. Use of Organotin Compounds in Thermal Stabilization of Polyvinyl-Chloride) .3. Reactions of Dialkyltin Mercaptides, Thioglycollates, and Carboxylates with Chlorohydrocarbons. *Journal of Polymer Science Part a-1-Polymer Chemistry* 1972, *10*, 725.

(9) Ayrey, G.; Poller, R. C.; Siddiqui, I. H. Mechanism of stabilization of poly(vinyl chloride). *Journal of Polymer Science Part B: Polymer Letters* 1970, *8*, 1.

(10) Klemchuk Peter, P. In *Stabilization of Polymers and Stabilizer Processes*; AMERICAN CHEMICAL SOCIETY: 1968; Vol. 85, p 1.

(11) Bacaloglu, R.; Fisch, M. Degradation and stabilization of poly(vinyl chloride). III. Correlation of activation enthalpies and entropies for dehydrochlorination of chloroalkanes, chloralkenes and poly(vinyl chloride). *Polymer degradation and stability* 1994, *45*, 325.

(12) Bacaloglu, R.; Fisch, M. Degradation and stabilization of poly (vinyl chloride). V. Reaction mechanism of poly(vinyl chloride) degradation. *Polymer degradation and stability* 1995, *47*, 33.

(13) Bacaloglu, R.; Fisch, M. Degradation and stabilization of poly (vinyl chloride). IV. Molecular orbital calculations of activation enthalpies for dehydrochlorination of chloroalkanes and chloroalkenes. *Polymer degradation and stability* 1995, *47*, 9.

(14) Boughdady, N.; Chynoweth, K.; Hewitt, D. Thermal Dehydrochlorination of Poly (vinyl chloride) Model Compounds. I. *Australian Journal of Chemistry* 1991, *44*, 567.

(15) Blazso, M.; Jakab, E. Effect of metals, metal oxides, and carboxylates on the thermal decomposition processes of poly (vinyl chloride). *Journal of Analytical and Applied Pyrolysis* 1999, *49*, 125.

(16) Atakul, S.; Balköse, D.; Ülkü, S. Synergistic effect of metal soaps and natural zeolite on poly (vinyl chloride) thermal stability. *Journal of Vinyl and Additive Technology* 2005, *11*, 47.

(17) Bensemra, N.; Tran Van, H.; Guyot, A.; Gay, M.; Carette, L. Thermal dehydrochlorination and stabilization of poly(vinylchloride) in solution: Part IV—Synergistic effects of β-diketone compounds and metal soap stabilizers. *Polymer degradation and stability* 1989, *24*, 89.

(18) Ureta, E.; Cantú, M. E. Zinc maleate and zinc anthranilate as thermal stabilizers for PVC. *Journal of applied polymer science* 2000, *77*, 2603.

(19) Sun, B.; Chaudhary, B. I.; Shen, C. Y.; Mao, D.; Yuan, D. M.; Dai, G. C.; Li, B.; Cogen, J. M. Thermal stability of epoxidized soybean oil and its absorption and migration in poly (vinylchloride). *Polymer Engineering & Science* 2013, *53*, 1645.

(20) Pritchard, J.; Vollmer, R. The meso and Racemic Forms of 2, 4-Pentanediol and Certain of Their Derivatives. *The Journal of Organic Chemistry* 1963, *28*, 1545.

(21) Peters, R. H.; Crowe, D. F.; Tanabe, M.; Avery, M. A.; Chong, W. K. Steroidal silicon side-chain analogs as potential antifertility agents. *Journal of medicinal chemistry* 1987, *30*, 646.

(22) Marker, R. E.; Rohrmann, E. Sterols. LVIII. The Position of the Nuclear Hydroxyl Groups in Chlorogenin. *Journal of the American Chemical Society* 1939, *61*, 946.

(23) Mayer, Z.; Obereigner, B.; Lim, D. In *Journal of Polymer Science Part C: Polymer Symposia*; Thermal dehydrochlorination of poly (vinyl chloride) models in the liquid phase; Wiley Online Library: 1971; Vol. 33, p 289.

(24) Klemchuck, P. Stabilization Mechanisms. *ACS Advances in Chemistry Series* 1968, *85*.

(25) Baum, B.; Wartman, L. Structure and mechanism of dehydrochlorination of polyvinyl chloride. *Journal of Polymer Science* 1958, *28*, 537.

(26) Starks, C. M.; Liotta, C. L.; Halpern, M. *Phase-transfer catalysis : fundamentals, applications, and industrial perspectives*; Chapman & Hall: New York, 1994.

(27) Martínez, G.; Mijangos, C.; Millán, J. Selective Substitution Reactions on PVC. Lability of Some "Normal" Structures. *Journal of Macromolecular Science: Part A - Chemistry* 1982, *17*, 1129.

(28) Mijangos, C.; Martínez, G.; Millán, J. L. New approaches to the study of labile structures in poly(vinyl chloride) by phenolysis. *European Polymer Journal* 1982, *18*, 731.

(29) Bacaloglu, R.; Fisch, M. Degradation and Stabilization of Poly(Vinyl Chloride) .1. Kinetics of the Thermal-Degradation of Poly(Vinyl Chloride). *Polymer degradation and stability* 1994, *45*, 301.

(30) Fisch, M. H.; Bacaloglu, R. Kinetics and mechanism of the thermal degradation of poly(vinyl chloride). *Journal of Vinyl Technology* 1995, *1*, 233.

(31) Fisch, M. H.; Bacaloglu, R. Mechanism of poly(vinyl chloride) stabilisation. *Plastics Rubber and Composites* 1999, *28*, 119.

(32) Kaseler, T. G. Nonlead Stabilizer Systems for Pvc Wire and Cable Extrusion - (an Update). *Antec 93 : Be in That Number, Vols 1-3* 1993, *39*, 717.

(33) Wypych, J. PVC thermal degradation. III. On the mechanism of action of metal carboxylates. *Journal of Polymer Science: Polymer Letters Edition* 1984, *22*, 425.

(34) González-Ortiz, L. J.; Arellano, M.; Sánchez-Peña, M. J.; Mendizábal, E.; Jasso-Gastinel, C. F. Effect of stearate preheating on the thermal stability of plasticized PVC compounds. *Polymer degradation and stability* 2006, *91*, 2715.

CHAPTER 5 – USE OF EPOXIDIZED LINOLENIC ACID SALTS AS MULTIFUNCTIONAL STABILIZERS IN PLASTICIZED PVC BLENDS

5.1 Introduction

As was briefly discussed in Chapter 4, polyvinyl chloride (PVC) is almost always produced with an added plasticizer. PVC, on its own, is far too hard and brittle for use in most consumer applications.[1] Plasticizers are used to improve the mechanical properties of PVC end products. Plasticizers increase the flexibility and workability of PVC systems.

PVC plasticizers can belong to one of several classes based on molecular structure. One such class of plasticizers is phthalate esters synthesized from long-chain branched alcohols. These can include diisodecyl phthalate (DIDP) and bis(2-ethylhexyl) phthalate. The combination of dipolar and nonpolar components of these plasticizers allow for their compatibility in PVC. Effectively, they act as an internal lubricant or binding agent that allows for greater mobility and flexibility of PVC polymer chains.

Unfortunately, phthalates are derived from surplus material produced during petroleum processing. They are also damaging to the environment and exhibit negative health effects. For these reasons, interest in industry has grown in the development of alternative bio-based plasticizers to replace the harmful and unsustainable phthalates.[2,3] One such bio-based plasticizer of particular interest to this study is epoxidized soybean oil (ESO). The structure of ESO is shown below in Figure 5.1.

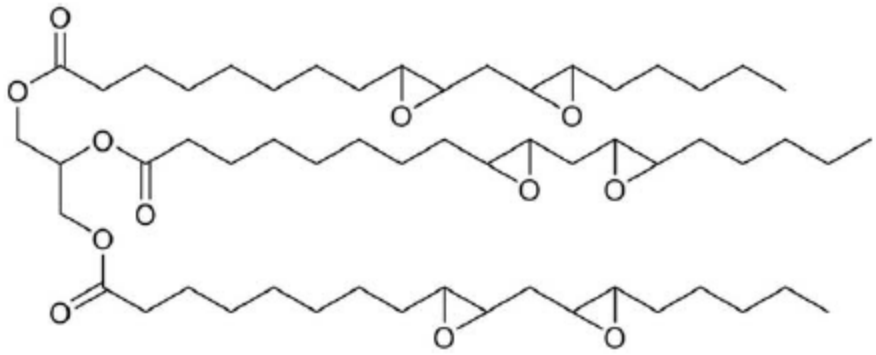

Figure 5.1. Chemical structure of epoxidized soybean oil (ESO).

The synthesis of ESO from soybean oil is straightforward. Soybean oil contains a large amount of nonconjugated double bonds which are easily epoxided to form oxirane rings using common and inexpensive reagents. The compatibility of ESO as a plasticizer in PVC has been demonstrated. Generally, it is at least as good a plasticizer as traditional phthalates.[4-6]

5.1.1 Plasticizer Selection Considerations

There are several criteria that must be considered when selecting a plasticizer for a PVC product. These criteria include the solubility of the plasticizer in the PVC matrix, the plasticizers UV-Visible absorption profile (as this can influence the color of the final product), and the tendency of the plasticizer to migrate out of the polymer. ESO is, ordinarily, highly soluble in PVC and unlikely to migrate out of the polymer. However, ESO is vulnerable to attack by HCl liberated from PVC during thermal degradation. HCl can open the oxirane rings to form the corresponding chlorohydrins.[2,7-9] A representation of this HCl attack of oxirane rings in ESO is shown below in Figure 5.2.

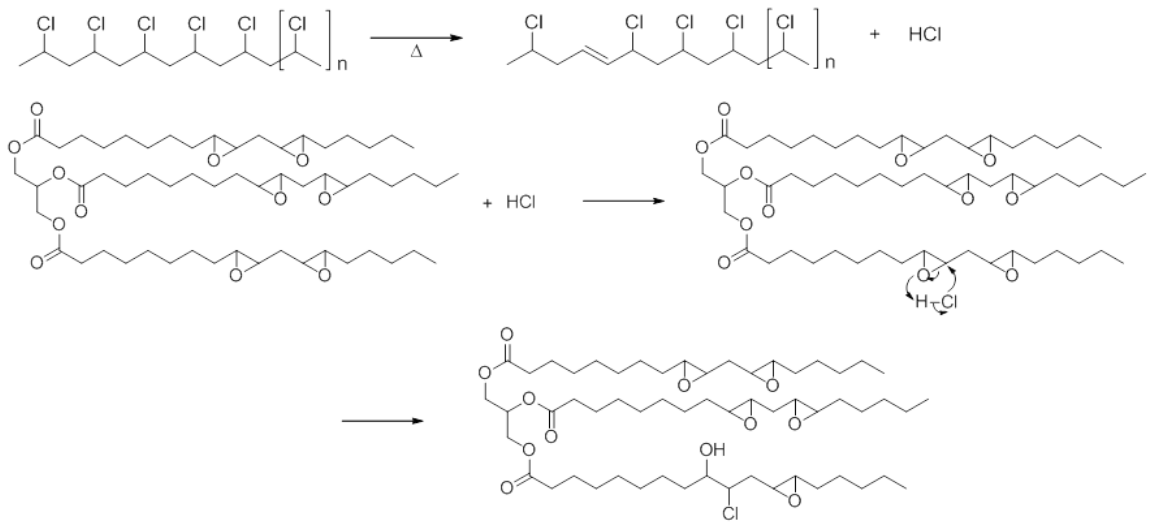

Figure 5.2. Mechanism of the attack of ESO by HCl to open oxirane rings and to form a chlorohydrin.

The mechanism shown in Figure 5.2 can continue beyond a single attack by HCl. Multiple HCl molecules can attack a single ESO molecule, forming multiple chlorohydrins on each molecule of plasticizer. Unfortunately, the chlorohydrin derivatives of ESO are much less soluble in PVC. They therefore have a tendency to migrate out of the PVC matrix. The thermal degradation of PVC can directly cause loss of ESO compatibility through generation of chlorohydrins.

Production of PVC products with ESO as a plasticizer is therefore reliant on methods of thermal stabilization. Common stabilization techniques are often employed in conjunction with ESO. One common industrial stabilization system (zinc and calcium stearates) was discussed at length in Chapter 4. With proper stabilization, the release of HCl from PVC can be minimized, thereby increasing the effectiveness of ESO as a stabilizer.[6]

5.1.2 PVC Stabilization

Much of the details of PVC thermal degradation and stabilization were discussed previously in Chapter 4. As such, the summary here will be relatively brief.

Ideally, PVC is formed of multiple vinyl chloride monomers: a carbon-chain backbone with chlorine atoms located at alternating secondary carbons. Unfortunately, defect sites are invariably introduced to the polymer during the manufacturing process. While these defects are uncommon in the perspective of the bulk polymer, they are thought to be initiation sites of thermal degradation of PVC.[10,11] The structures of ideal PVC and the most common defects are shown below in Figure 5.3.

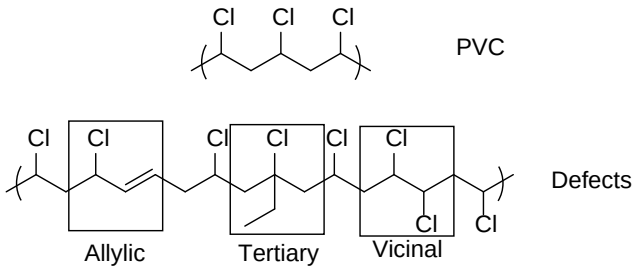

Figure 5.3. Structure of ideal, defect-free PVC. Structures of several of the most common defects are also shown.

Once thermal degradation is initiated, liberated HCl is capable of inducing further degradation. The process is therefore autocatalytic. Additionally, once several chlorides are liberated to form a conjugated double bond sequence, the process can accelerate. The longer the conjugated sequence becomes, the more labile neighboring chlorine atoms become. This phenomenon is known as "chain-unzipping," so-called for the rapid, consecutive liberation of chlorides down the PVC backbone. Increasing conjugation causes discoloration of the PVC polymer. The degradation of PVC is shown below in Figure 5.4.

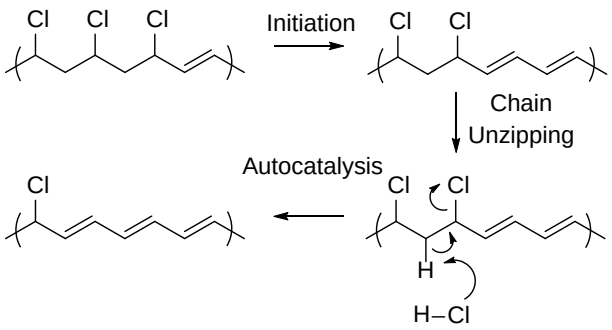

Figure 5.4. Initiation of PVC thermal degradation (at an allylic site), "chain-unzipping," and autocatalysis of degradation.

A variety of additive systems have been employed for thermal stabilization of PVC and reported in the literature. With the mode of degradation discussed in Figure 5.4, stabilization approaches generally attempt to either (i) minimize the amount of dehydrochlorination via substitution onto the PVC backbone, or (ii) sequester liberated HCl to prevent autocatalytic behavior.[12-20]

Additives used for these stabilization techniques include metal salts of fatty acids and molecules with epoxide functionalities.[4-6,21,22] The mechanistic behaviors of stearates, particularly calcium and zinc stearates, were examined in detail in Chapter 4. Benanbiba et al.[2] examined epoxidized sunflower oils as plasticizers and found that they exhibited a stabilization effect. Specifically, the study found that (i) epoxides increase the induction time until initiation of rapid dehydrochlorination, and (ii) epoxides decrease the rate of dehydrochlorination after the induction time. It is hypothesized that this effect is due to the scavenging of HCl by oxirane functionalities as shown in Figure 5.2. Any HCl scavenged by epoxides is unavailable for autocatalytic thermal degradation of PVC.

Other studies examined epoxides as stabilizers alongside more traditional stabilizers, including studies by Iida et al.,[12,13] Odilora,[23] Okieimen,[15] and Worschech et

al.[24] These studies found that, as a trend, as the number of epoxy groups within a stabilizer increases, the stabilization effects also increase (e.g., the rate and extent of dehydrochlorination decrease).

Importantly, the results confirming the success of epoxides as stabilizers suggest that epoxides can be used as HCl scavengers. This revelation is the main motivation for the work in this chapter. Sequestration of liberated HCl will ideally protect ESO employed as a plasticizer from acidic attack.

The results of C hapter 4 and the literature suggest beneficial synergistic interactions of zinc and calcium stearates. Literature discussed in this section suggests that the inclusion of epoxide rings in stabilizer compounds increases thermal stability. These two insights were used to propose a novel stabilizer system.

5.2 Methodology

In this chapter, a novel approach to PVC stabilization and plasticizer protection is introduced and investigated. The novel stabilizers take the form of the zinc and calcium salts of epoxidized linolenic acid. This stabilizer system combines dual functionalities: (i) the epoxide functionalities capable of sequestering HCl liberated from PVC thermal degradation, thereby protecting ESO; and (ii) metal carboxylate functionalities which should mimic the behavior of zinc and calcium stearates. The zinc and calcium salts of epoxidized linolenic acid (abbreviated “ZnEp” and “CaEp”, respectively) were synthesized according to Figure 5.5 below.

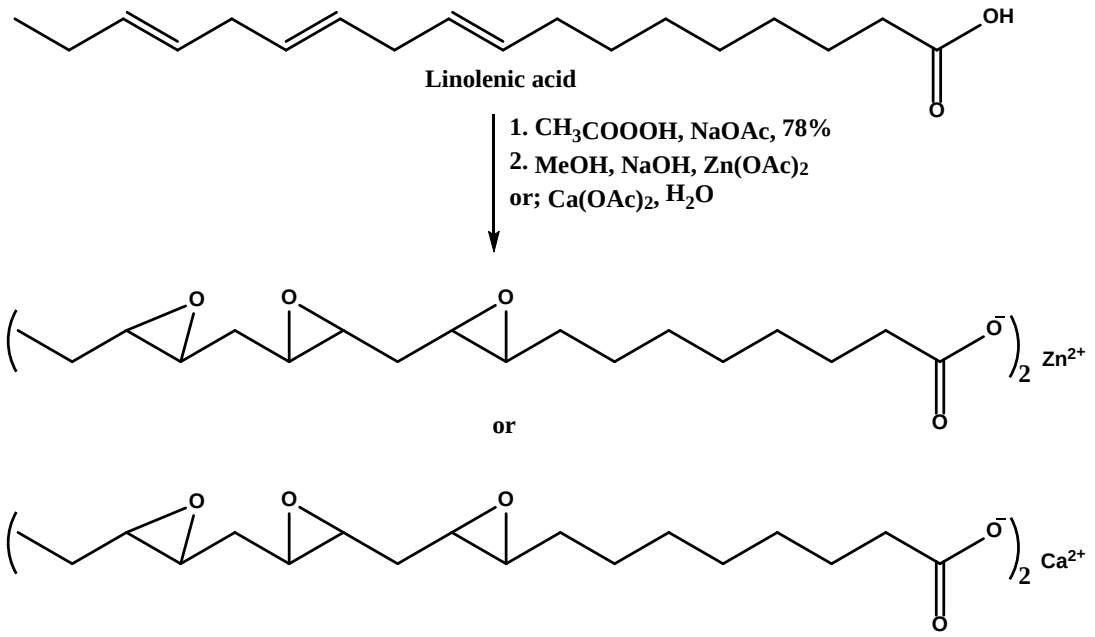

Figure 5.5. Method of synthesis of the zinc and calcium salts of 9,12,15-triepoxylinolenic acid.

Once synthesized, ZnEp and CaEp were studied for their viability as PVC thermal stabilizers. They were used in thermal studies of PVC plasticized with both ESO and DIDP (as a non-stabilizing control). Stabilizer performance was examined by mass loss (analyzed via thermogravimetry) and color examination after heating. To supplement the studies of actual PVC polymer, studies of epoxide ring opening by HCl were analyzed via nuclear magnetic resonance.

5.2.1 Materials

Diisodecyl phthalate (DIDP) and zinc stearate ($ZnSt_2$, purum grade) were obtained from Sigma-Aldrich. Calcium stearate ($CaSt_2$) was purchased from Alfa Aesar. PVC powder (OxyVinyls 240F suspension-grade) was manufactured by Oxy Vinyls, LP. Epoxidized soybean oil (ESO) (Plas-Check 775 ESO) was manufactured by Ferro

Corporation. These particular grades of PVC and ESO and their properties are discussed in literature.[5] Helium and nitrogen were obtained from Airgas.

5.2.2 Synthesis of 9,12,15-Triepoxylinolenic Acid

5.4 mL (0.049 mol) of neat linolenic acid were added to the reaction vessel and placed into an ice bath. 18 mL (0.069 mol) peracetic acid were mixed with 1.1 g (0.069 mol) sodium acetate before being added to the stirring reaction vessel over 1 hour. The reaction was then stirred for an additional 1 hour in the ice bath. Organics were extracted with diethylether (2 washes of 10 mL each) and dried over $MgSO_4$. The resulting solution was placed in a rotary evaporator under vacuum to give 4.6 g (78% yield) of colorless product.

5.2.3 Synthesis of Zinc or Calcium Salt of Triepoxylinolenic Acid

0.5 g (0.132 mol) NaOH in 15 mL water was added to a solution of 4.3 g (0.0132 mol) triepoxylinolenic acid in 10 mL methanol at room temperature. The resulting mixture was stirred for 15 minutes. 1.2 g $Zn(OAc)_2$ (0.007 mol) (or equimolar amount of $Ca(OAc)_2$ for the calcium salt) in 15 mL water were then added to the reaction mixture. A white precipitate was formed. The reaction mixture was then cooled to 0 °C. The precipitate was filtered and washed with water (3 washes of 20 mL each), acetone (2 washes of 10 mL each), and dried under vacuum. The procedure produced 3.5 g (76% yield) of Zn-triepoxylinoleniate (ZnEp). Yield was 51% for Ca-triepoxylinoleniate. To confirm product synthesis, elemental analysis was conducted. The elemental analysis for zinc: calc. 9.13, found 9.33. The elemental analysis for calcium: calc. 5.80, found 6.17.

5.2.4 Fabrication of Blends of PVC, Plasticizers, and Additives

PVC blends were fabricated dry, without the use of solvents. Generally, 3 g of PVC power were mixed with 30 phr (0.9 g) plasticizer (either DIDP or ESO) and 5 phr (0.15 g) additional additives ($ZnSt_2$ and/or $CaSt_2$, or ZnEp and/or CaEp). In the cases when salts of two metal cations were combined, the 5 phr (0.15 g) was divided into 2.5 phr zinc salt and 2.5 phr calcium salt.

The PVC powder was physically combined with half the plasticizer (0.45 g) in a glass vial and heated to 95 °C in an oil bath. The glass transition temperature of unplasticized PVC is reported as 83 °C.[4] Heating above this glass transition (to 95 °C) facilitates the rapid and efficient absorption of additives into the PVC matrix. The mixed PVC and plasticizer were agitated with a glass rod during heating until the mixture appeared dry (e.g., until the plasticizer was absorbed into the PVC).

Separately, the other half of the plasticizer (0.45 g) was mixed with the other additives and heated to 95 °C. This second mixture was then added to the first mixture (of PVC and plasticizer) and both were heated to 95 °C and agitated with a glass rod. The two-pot blending technique was employed to enhance the uptake of the solid metal salts into the PVC.

Plasticizers were necessary for the work reported herein. Neither the zinc epoxide salt nor the calcium epoxide salt are soluble in PVC alone. Plasticizers were therefore employed to incorporate the novel salts into the polymer.

5.2.5 Thermogravimetry of PVC Blends

Thermogravimetric analysis (TGA) was conducted with a TA Instruments TGA Q50. Weight loss studies were conducted isothermally between 150 °C and 180 °C for up to 3 hours under a flow of nitrogen (100 mL / min). For thermal studies, approximately 20 mg of dry blended PVC sample were loaded onto a platinum TGA pan at least twice to verify repeatability. Weight loss reported below is calculated with respect to the amount of PVC in the blend, discounting any additives. The weight losses observed in the blends examined herein are thereby attributed to the loss of HCl through dehydrochlorination.

5.2.6 Epoxide Ring-Opening Studies

HCl (gas phase) was bubbled (3 min) through o-dichlorobenzene (o-DCB, 35 mL) at room temperature. The amount of HCl complexed with the o-DCB was determined by weighing the reaction vessel before and after HCl addition. The epoxides used for this study were cyclohexene oxide, 1,2-epoxyhexane or ESO. Epoxides were reacted in a 1:1 or 20:1 (epoxide:HCl) molar ratio dissolved in o-DCB (2mL) with the HCl solution. The reaction was stirred at room temperature and a sample of the mixture was taken and analyzed for the epoxide conversion and corresponding product formation by ^{1}H NMR spectroscopy.

5.2.7 UV-Visible Spectroscopy of PVC

UV-visible studies of PVC were conducted using an Agilent Cary 100 UV-visible spectrophotometer. Scans were recorded over a range of 200-800 nanometers. PVC

samples of approximately 50 mg were first loaded into the TGA and an accurate mass was recorded. The TGA was used to precisely heat the sample to 180°C for a set reaction time. The heated samples were immediately removed from the TGA upon completion of the heat treatment and quantitatively dissolved in THF (by initial weight) to obtain equal PVC concentrations. UV-visible spectra were obtained in triplicate to ensure repeatability between samples.

5.2.8 Color Examination of Heated PVC Blends

Photographs of the PVC blends were taken post thermal treatment. These photographs were used to qualitatively compare the discoloration of the PVC polymer and to make tentative conclusions regarding stabilization.

5.3 Reactions of ESO with Hydrogen Chloride

Epoxide functionalities are ring systems which are highly reactive with both electrophilic and nucleophilic reagents. As such, a PVC plasticizer such as epoxidized soy bean oil (ESO) is highly susceptible to reaction with HCl liberated during the thermal degradation of PVC. An example of such a reaction is shown below in Figure 5.6.

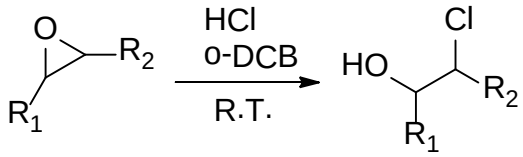

Figure 5.6. Example of a ring-opening reaction caused by attack of HCl.

The chlorohydrin products of such a reaction severely reduce the compatibility of ESO in PVC, reducing its effectiveness as a plasticizer. To measure the vulnerability of ESO, a model system was used to investigate the reaction of ESO with HCl. ESO, dissolved in 1,2-dichlorobenzene, was reacted with dry HCl at room temperature. It should be noted that the ESO structure illustrated in Figure 5.1 is an idealized picture of the molecule. The fatty acid components of the glycerides could be saturated (containing no epoxy groups) or mono unsaturated containing only one epoxide, depending upon the extent of reaction during the manufacturing process. The ^{1}H NMR spectrum of the ESO used in this study is shown in Figure 5.7.

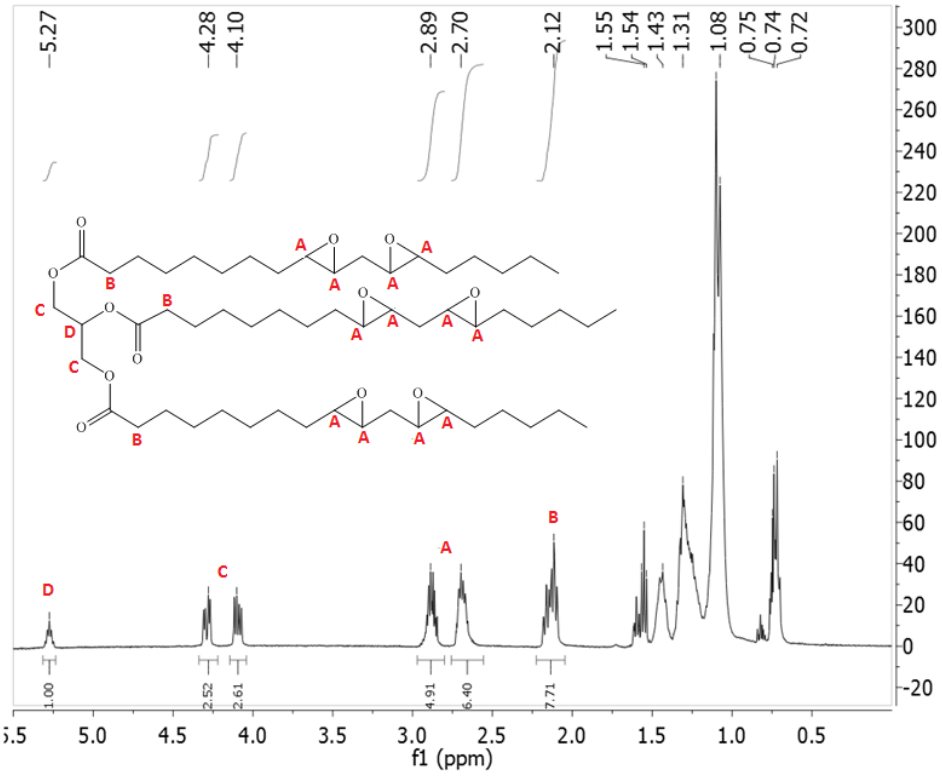

Figure 5.7. Proton NMR spectrum of ESO used in this study.

The signals corresponding to the C-H protons bonded directly to the epoxide ring have chemical shifts of 2.70 and 2.89 ppm; these peaks are labeled A. The peaks at 2.12, 4.10

and 4.28, and 5.27 ppm are assigned to the hydrogens labeled B, C, and D in the figure. Based upon the relative peak integrations, each hydrogen accounts for 1.28 area units. By simple peak comparison, it can be estimated that there are 4.5 epoxide groups per ESO molecule, fewer than the idealized number of six. Nonetheless, the disappearance of the epoxide peaks should still be readily trackable.

ESO was first reacted with HCl at a 1:1 molar ratio. The NMR spectrum taken after reaction is shown below in Figure 5.8.

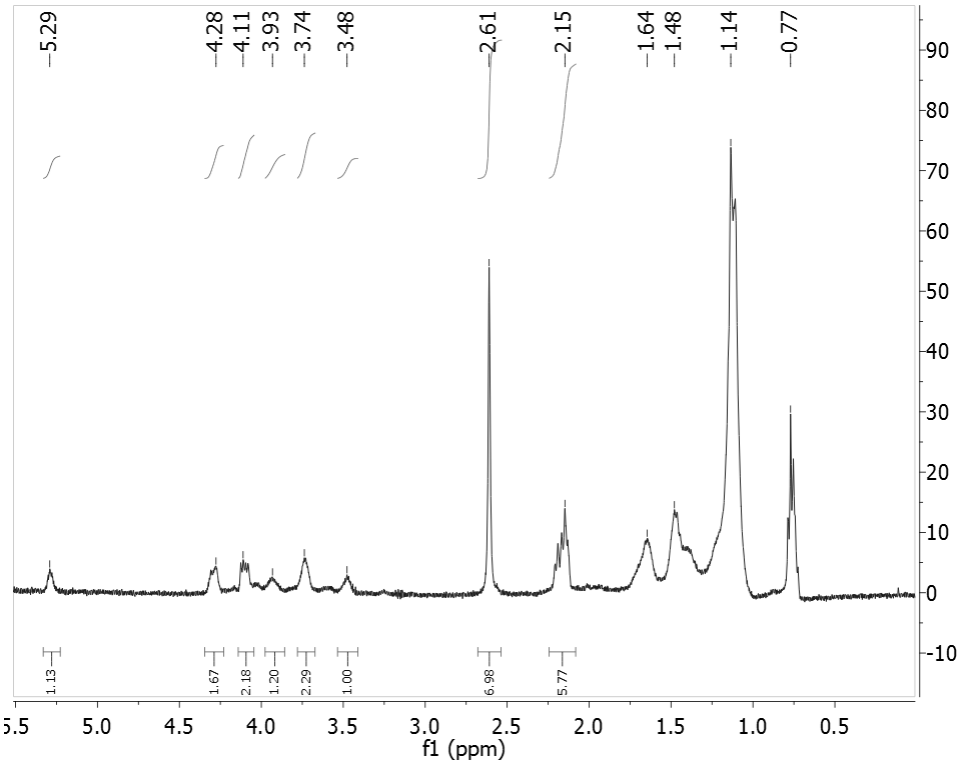

Figure 5.8. Proton NMR spectrum of the products of the reaction of ESO wth HCl at a 1:1 molar ratio.

At a molar ratio of 1:1 ESO:HCl, the epoxides completely reacted within five minutes at room temperature as shown in Figure 5.8. The proton NMR spectrum of the system after reaction shows the disappearance of the peaks at 2.70 ppm and 2.89 ppm (labeled A in

Figure 5.7) and the appearance of peaks between 3.5 ppm and 4.0 ppm. These peaks are attributed to the ring-opened chlorohydrin products and correspond to the protons adjacent to hydroxyl and chloride groups formed after HCl reacts with oxirane rings.

When a ratio of 20:1 ESO:HCl was used, the ^{1}NMR spectrum of the reaction products showed a similar phenomenon. The development of peaks between 3.5 ppm and 4.5 ppm was observed. It is concluded that even at this lower concentration of HCl, epoxy ring-opened products are formed. The ^{1}H NMR spectrum of the reaction products is shown in Figure 5.9 below.

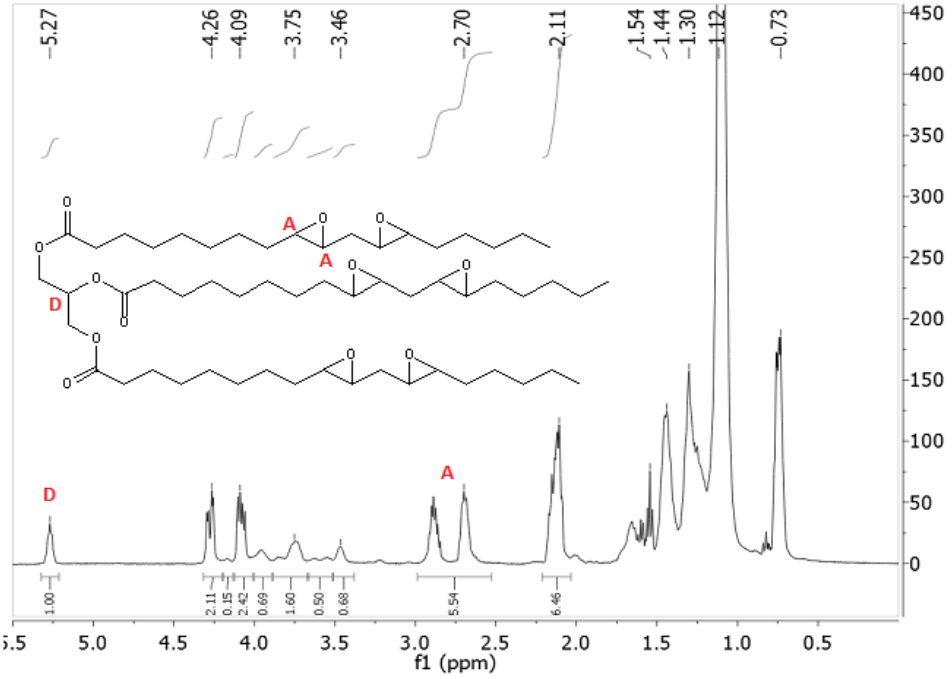

Figure 5.9. Proton NMR spectrum of the products of the reaction of ESO with HCl at a 20:1 molar ratio.

The reactions of ESO with HCl provide strong evidence that ESO is highly susceptible to attack by HCl, even at room temperature. This highlights the need for a stabilizer additive that can protect the epoxide functionality of ESO from attack and preserve its function as a plasticizer.

5.4 TGA of Untreated PVC and Plasticized PVC

Figure 5.10 shows the thermogravimetric profiles of untreated PVC and PVC plasticized with either DIDP or ESO at 170 °C. The temperature of 170 °C was chosen for these studies because it is well within the temperature range for typical industrial processing and it also affords adequate differentiation of performance between the different PVC blends. Untreated PVC, used as a reference for evaluating the plasticized blends, loses less than 1 percent of its starting weight over a period of 2 hours at 170 °C. Since untreated PVC is too rigid and brittle for most applications, plasticizers such as DIDP and ESO are incorporated into the polymer matrix in order to increase flexibility and workability even though they may alter thermal behavior.

From Figure 5.10 it is immediately obvious that DIDP plasticized PVC loses significant weight during the 2 hour time period. In order to estimate how much of the weight loss is due to the volatilization/decomposition of DIDP, a thermogravimetric analysis of neat DIDP (and other additives) was conducted at 180 °C for a period of 2 hours as shown in Figure 5.11. From these data it was determined that the maximum loss of DIDP could only accounts for, as an absolute maximum, 19.7% of the overall weight loss of the DIDP plasticized PVC. Even accounting for this maximal amount of volatilized DIDP, the blend of PVC and DIDP would still lose 7.2% of its initial mass. This is substantially more than either of the other compositions in Figure 5.10. It was hypothesized, therefore, that this increased weight loss of PVC plus DIDP compared to untreated PVC was due to the increased flexibility of the polymer chains as a

consequence of the plasticization of the polymer system. This flexibility allowed motility of HCl molecules leaving the polymer chains, which would thereby lower the activation energy for both the first-order and HCl-catalyzed elimination of HCl.

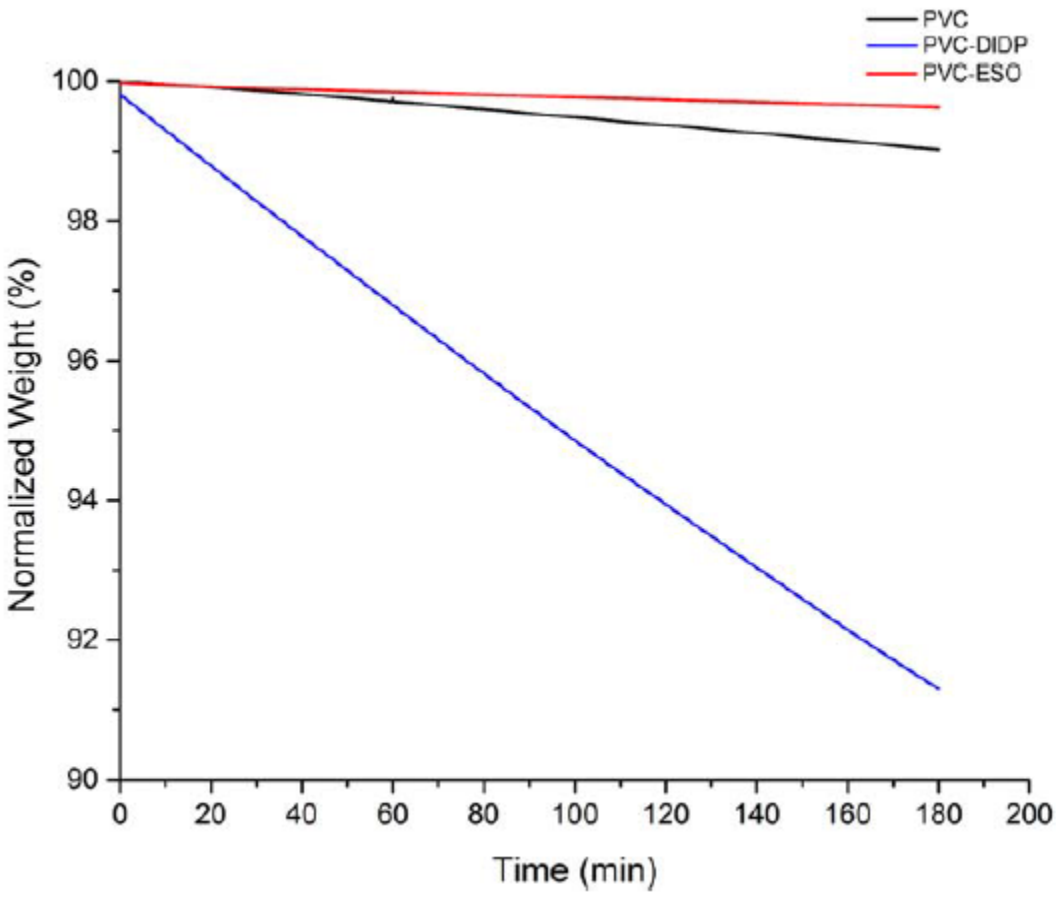

Figure 5.10. Weight profiles as a function of time for PVC and PVC plasticizer blends at 170 °C. The weight is normalized against the mass of PVC (without additives) in the blend.

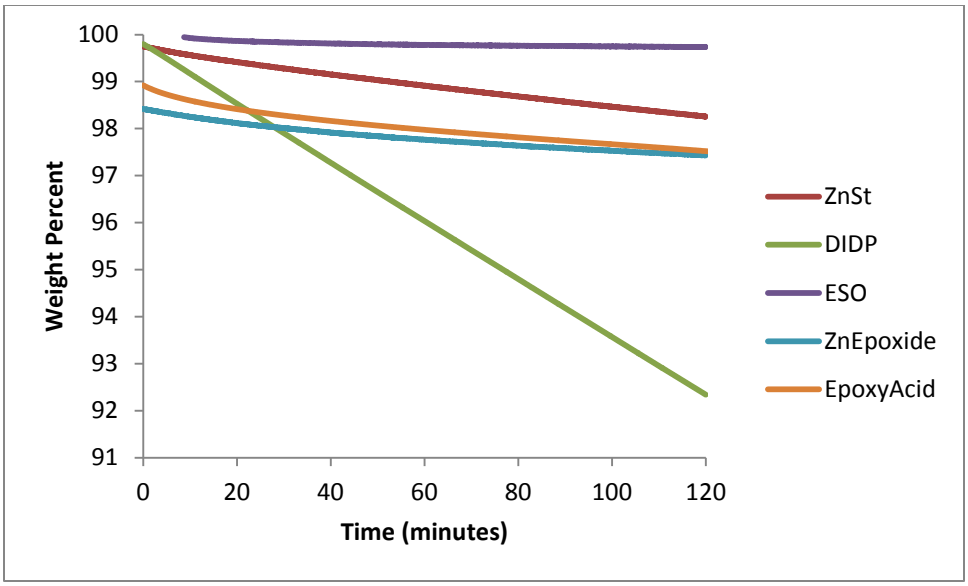

Figure 5.11. Isothermal weight loss of PVC additives as a function of time at 180 °C.

In contrast to DIDP, the ESO plasticized PVC sample loses less weight after 2 hours compared to untreated PVC; the ESO appears to exhibit a stabilization effect. This is attributed to the epoxide functionalities present in the structure. Based upon the previously discussed experiments it is clear that the oxirane rings scavenge the thermally generated HCl at a rate substantially greater than the rate of HCl volatilization from the PVC sample as shown in Figure 5.2. The point at which volatilization of HCl dominates over ring-opening reactions is not evident during the 2 hour period. It is important to note that, in the absence of another heat stabilizer, the structure and plasticizer properties of ESO change as the HCl is scavenged leading to deleterious polymer blend performance. Hence, even though ESO appears to be a good stabilizer on its own, maintaining the integrity of the ESO as a plasticizer is of primary importance.

In addition to the above quantitative thermal weight loss profiles, the visual color change of the bulk polymer supplemented the investigation. Figure 5.12 illustrates that PVC, with or without plasticizer, exhibits poor color stability after 2 hours at 170 °C.

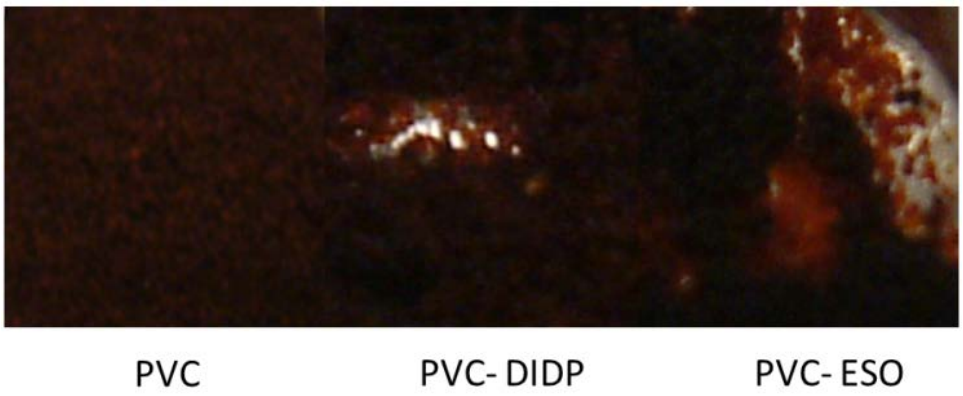

Figure 5.12. Color formation in PVC and PVC blends heated at 170 °C for 2 hours.

The discoloration of PVC plasticized with DIDP is quite similar to that of untreated PVC. Indeed, the differences in the discoloration of untreated PVC and the plasticized PVC blends were minor. Even the blend with ESO, which displayed excellent weight retention, showed poor color retention. This behavior demonstrates the absorption of HCl by ESO. The color change indicates formation of conjugated polyenes (which necessarily requires liberation of HCl). The low extent of weight loss must indicate that the liberated HCl is sequestered in the blend by ESO. Again, this highlights the importance of other thermal stabilizers in protecting ESO. Figure 5.12 will provide a reference point for subsequent color retention observations of PVC systems containing a variety of stabilizing additives.

5.5 Measurement of Activation Energies for Dehydrochlorination of PVC Blends

Activation energies for the PVC degradation process were determined by thermogravimetric analysis (TGA) for PVC, PVC plus DIDP, and PVC plus ESO. In all cases the PVC weight percent was calculated with respect to the amount of PVC in the blend excluding the additives. The weight of any ESO in the blend was assumed constant due to negligible weight losses (approximately 0.25%) of neat ESO at 180°C over a period of 2hrs as shown below in Figure 5.13.

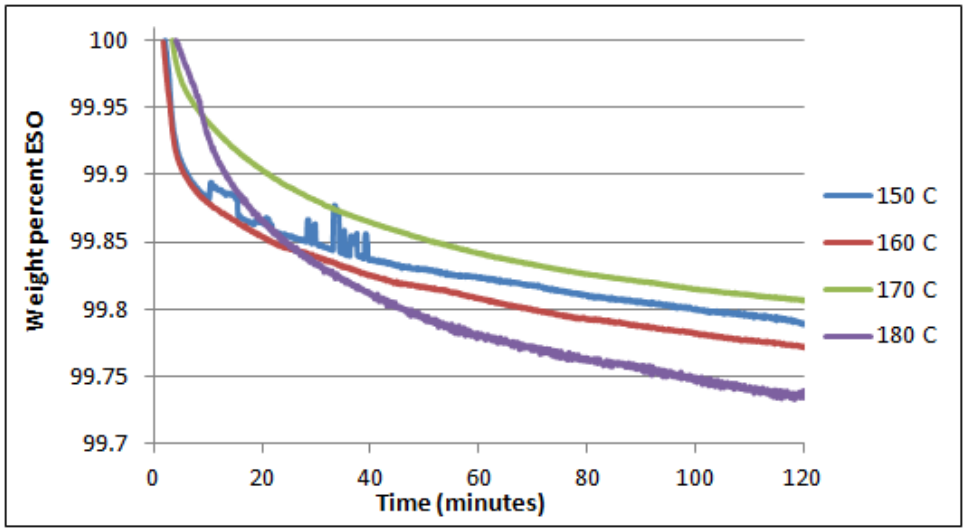

Figure 5.13. Isothermal TGA weight profiles for isothermal treatments of ESO.

The Arrhenius equation was used to calculate the activation energies

$$k = Ae^{\frac{E_a}{RT}}$$

where k is the rate of degradation at a particular temperature, A is the frequency factor, E_a is the activation energy for the degradation process, R is the gas constant, and T is the absolute temperature.

The isothermal weight loss data of untreated PVC, DIDP-plasticized PVC, and ESO-plasticized PVC at various temperatures are shown in Figure 5.14, Figure 5.15, and Figure 5.16, respectively.

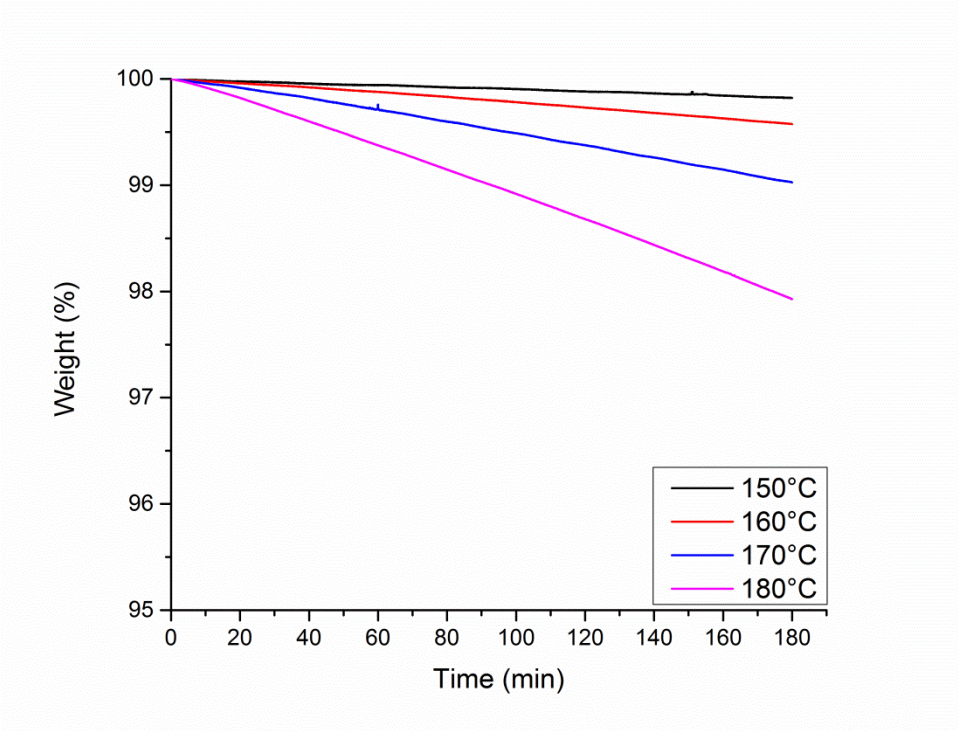

Figure 5.14. Isothermal weight loss profiles of untreated PVC over the course of 3 hours.

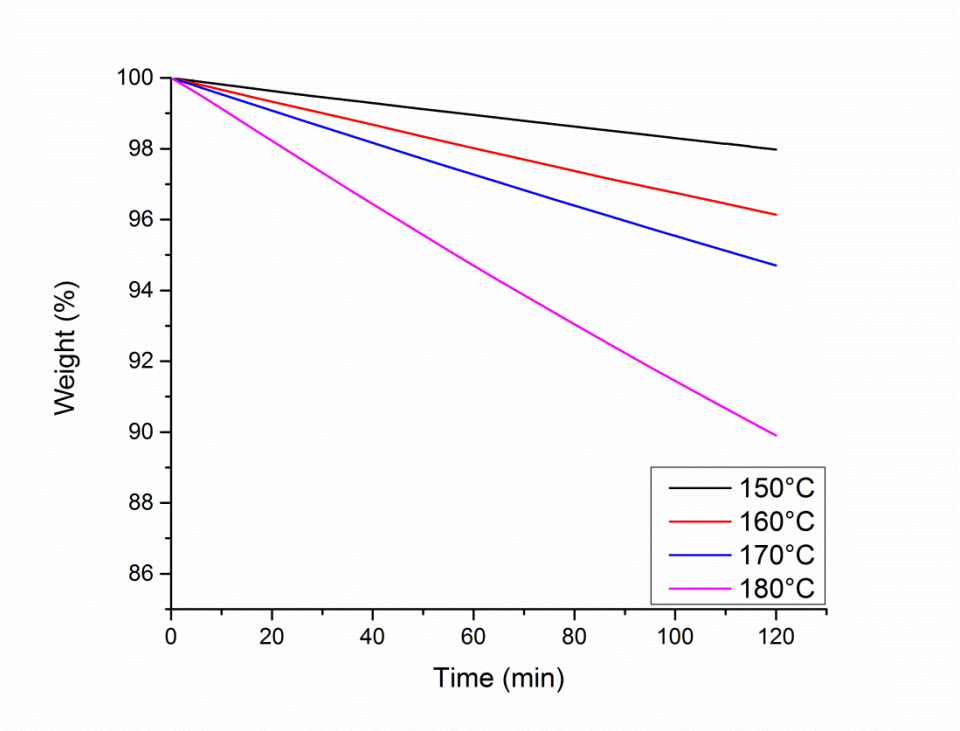

Figure 5.15. Isothermal weight loss profiles of PVC plasticized with DIDP over the course of 2 hours.

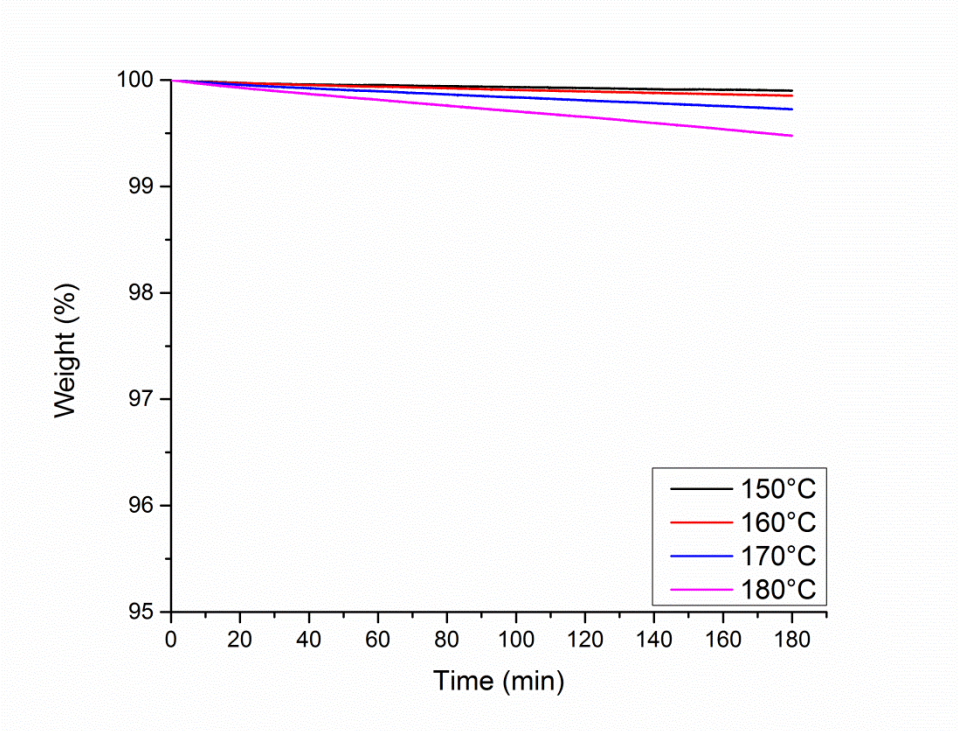

Figure 5.16. Isothermal weight loss profiles of PVC plasticized with ESO over the course of 2 hours.

The weight loss during the first 30 minutes of each set of isothermal treatments was used to determine the initial rate of degradation assuming first order kinetics at each temperature. The slope (average over the first 30 minutes of each isotherm) was taken as the rate constant for each experiment. The Arrhenius plots for each of the samples are shown in Figure 5.17.

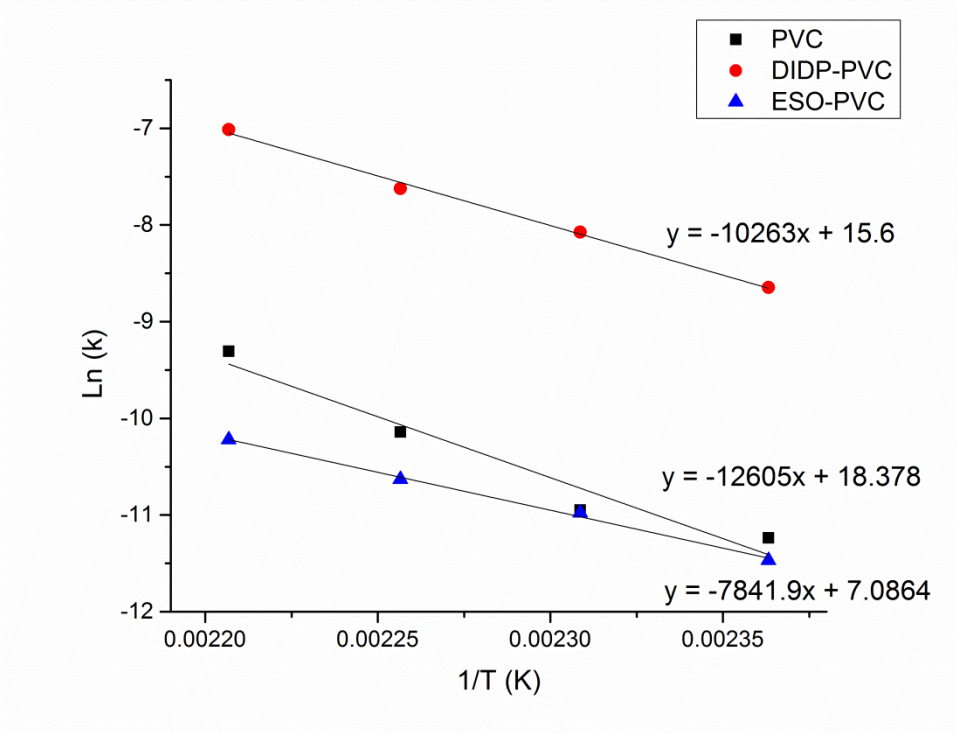

Figure 5.17. Arrhenius plots for the isothermal dehydrochlorination of PVC unplasticized, plasticized with DIDP, and plasticized with ESO.

Using the slopes of the Arrhenius plot, the activation energy for the initial degradation for PVC is 106 ± 14 kJ·mol^{-1} while that for PVC with 30 phr of ESO is 65 ± 7.8 kJ·mol^{-1} and that for PVC with 30 phr of DIDP is 85 ± 3.5 kJ·mol^{-1}.

Employing the ASTM E698 method[25] for determining activation energies through the use of constant heating rate weight loss studies was also used for this study. This method resulted in activation energies for untreated PVC and PVC with 30 phr ESO of 147 $kJ \cdot mol^{-1}$ and 102 $kJ \cdot mol^{-1}$, respectively. In both the ASTM method and the thermogravimetric weight loss method discussed above, the activation energy for the untreated PVC was higher than that of the PVC with 30 phr ESO. However, the overall weight loss is less when PVC is mixed with 30 phr ESO than the weight loss of PVC alone. These observations suggest that when PVC is plasticized with ESO the release of HCl occurs more readily, but the ability of ESO to scavenge the HCl reduces the overall thermal weight loss. As indicated above, this is undesirable since the fundamental structure of the plasticizer is changed. Its hydrophilicity increases and its compatibility with the polymer matrix decreases. As a consequence, the ring-opened product has an increased tendency to migrate from the polymer matrix. To address these issues, it was conjectured that the new ZnEp and CaEp additive package could act as a multifunctional additive by (1) promoting displacement reactions at labile chlorine sites, or undergo ion exchange to form stearic acid and $CaCl_2$ (like the stearate additives) and (2) reacting with thermally generated HCl in a sacrificial capacity thus protecting the plasticizer.

5.6 Effects of ZnEp and CaEp as Stabilizers in Blends of PVC Plasticized with DIDP

As with the blends of PVC and plasticizer, blends of PVC with thermal additives were examined via isothermal treatment and TGA. Figure 5.18 summarizes the thermal behavior DIDP-plasticized PVC blends incorporating the ZnEp and CaEp as well as the

reference blends with Zn and Ca stearate (abbreviated ZnSt2 and CaSt2) additives. The weight loss and color retention are shown below.

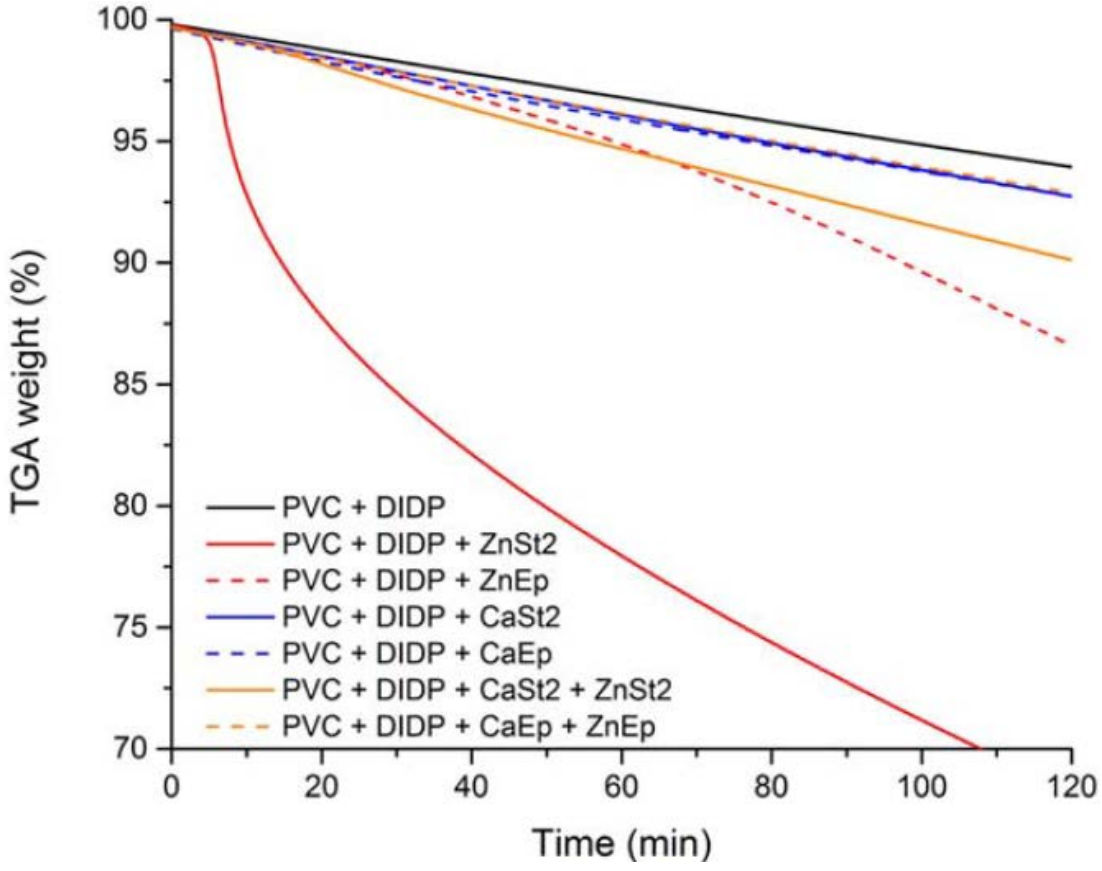

Figure 5.18. Weight loss profiles of DIDP-plasticized PVC blends incorporating novel epoxide salt stabilizers and stearate salts for comparison. Heat treatment was isothermal at 170 °C. Weight is normalized against the mass of PVC in each blend.

All blends containing ZnEp and CaEp exhibit similar or improved weight retention and color retention (shown in Figure 5.20) compared to the reference blends containing the stearate stabilizers. As discussed in Chapter 4, DIDP-plasticized PVC blended with $ZnSt_2$ showed negligible weight loss during the first 7 minutes at 170^{o}C. A dramatic 30% weight loss occurred rapidly thereafter. This is attributed to the production of $ZnCl_2$, a strong Lewis acid, formed from the exchange of zinc stearate with a chloride

on the PVC backbone and/or from the reaction of the zinc stearate with the thermally generated HCl (both possibilities were discussed in Chapter 4). The substitution process proposed in literature (but unconfirmed in Chapter 4) "stabilizes" the polymer toward further unzipping to form polyconjugated structures and the acid-base reaction of stearate with HCl reduces the autocatalytic pathway for HCl loss.

Regardless of which interaction with zinc stearate is dominating, zinc chloride can be formed. A further experiment blended plasticized PVC with $ZnCl_2$ (added at the same molar quantity as the $ZnSt_2$ in other blends), producing a rapid weight loss of 51.5% as shown in Figure 5.19. In the time to heat the sample to 170 °C, an approximate 15% weight loss was observed. Interestingly, the weight loss profiles after approximately 10 minutes for DIDP plasticized PVC with ZnSt and $ZnCl_2$ show very similar slopes, thus providing further evidence for the detrimental role of $ZnCl_2$. However, when $ZnSt_2$ was blended in combination with $CaSt_2$ the rate of weight loss was dramatically reduced and color development was delayed by 90 minutes; no catastrophic weight loss was observed. The results support the following: (1) the Lewis acidity of the zinc center in $ZnSt_2$ facilitates interaction with chloride on the PVC backbone, and (2) the zinc chloride formed as a consequence of these interactions catalyzes the catastrophic weight loss, but (3) $CaSt_2$ present reacts with the $ZnCl_2$ to produce the desirable $ZnSt_2$ and innocuous $CaCl_2$ thus preventing the catastrophic weight loss.[7]

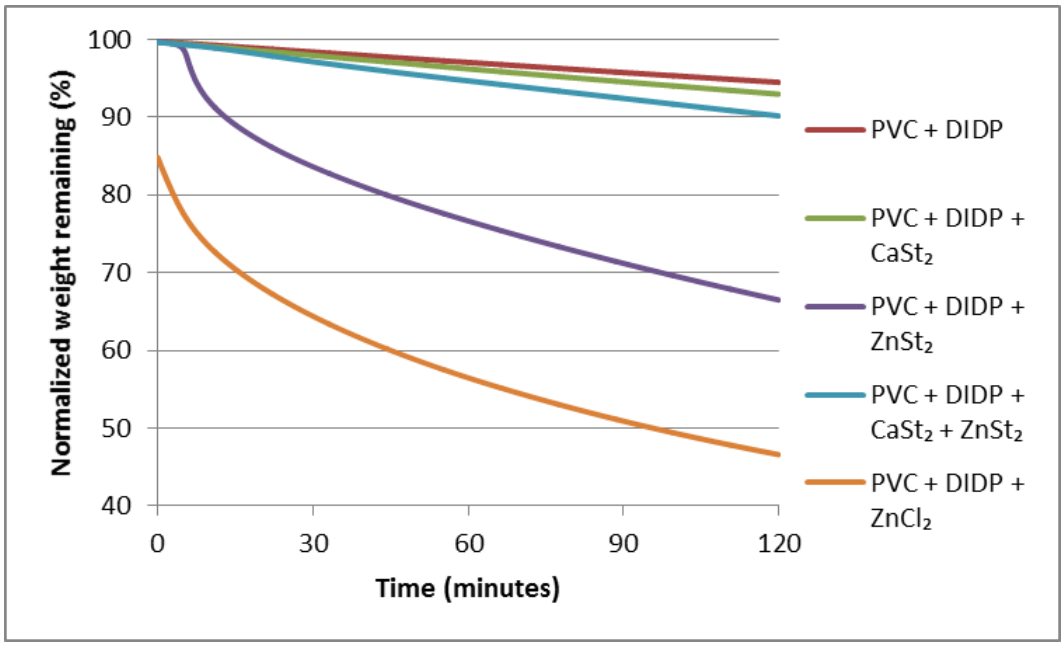

Figure 5.19. Weight loss profiles for blends of DIDP-plasticized PVC with stearate stabilizers and zinc chloride at 170 °C.

In comparison to the blends with stearate additives discussed above, the rate of PVC degradation is significantly reduced when ZnEp is substituted for $ZnSt_2$. A weight loss of less than 15% was observed over a period of 2 hours at 170 °C. A likely explanation is that the epoxy groups in ZnEp scavenge any free HCl. This could both prevent autocatalytic PVC degradation and prevent the formation of $ZnCl_2$, which in turn is capable of catalyzing degradation. CaEp alone did not show any improvement when compared to $CaSt_2$ (which lost 6% of its original mass); the weight profiles for each salt are almost overlapped. From this, we can make a critical extrapolation.

If the mitigated weight loss shown by the blend with ZnEp were cause *only* by the retention of HCl (thereby making the sample appear to lose less weight), then the blend of CaEp would also lose significantly less weight than the blend of $CaSt_2$. Since this is not the case (the CaEp blend and $CaSt_2$ blend perform almost identically), it must be

concluded that some other process is responsible for the superior performance of ZnEp as compared with $ZnSt_2$. The likely explanation is that the formation of $ZnCl_2$ is prevented by the sequestration of a minuscule amount of HCl by the epoxide rings of the epoxide salts. In other words, the amount of HCl scavenged by ZnEp and CaEp is not enough to show a large difference in weight loss; however, it *is* enough to block significant formation of $ZnCl_2$.

The synergistic blend of both epoxide salts lost ~3 percentage points less weight compared to the analogous blend with Zn and Ca stearates, which had a 9.9% loss of weight. As was the case with the ZnEp salt, this may be due to the scavenging of HCl preventing the formation of $ZnCl_2$.

A detailed discussion of the color change exhibited by blends containing the epoxide salts is found below.

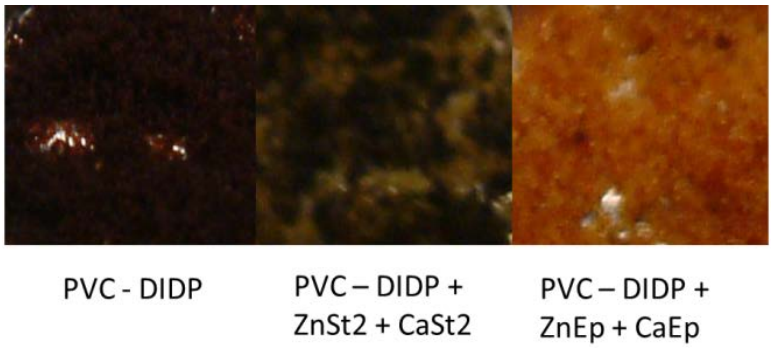

Figure 5.20. Color retention photographs of DIDP-plasticized PVC blends incorporating novel epoxide salt stabilizers compared directly with stearates. Heat treatment was isothermal at 170 °C for 2 hours.

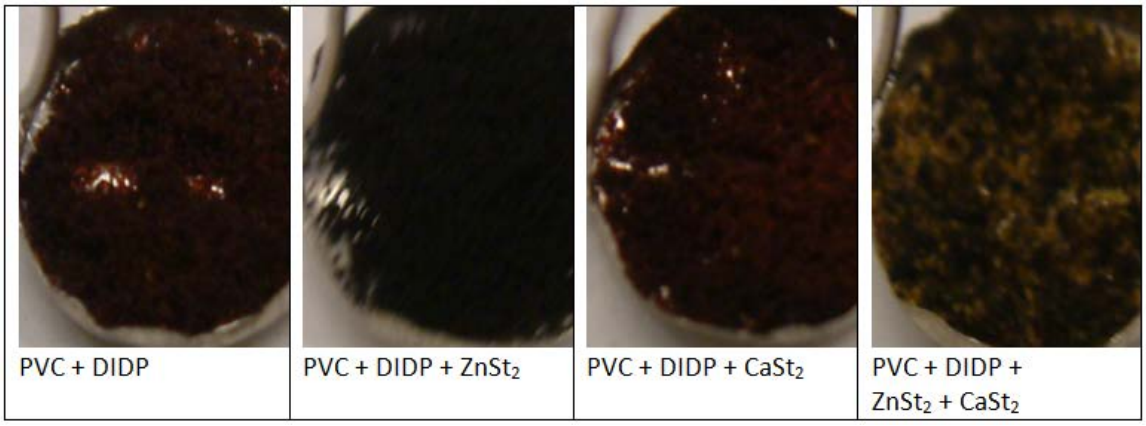

Figure 5.21. Color retention photographs of blends of PVC, DIDP, and stearates after heating at 170 °C for 2 hours.

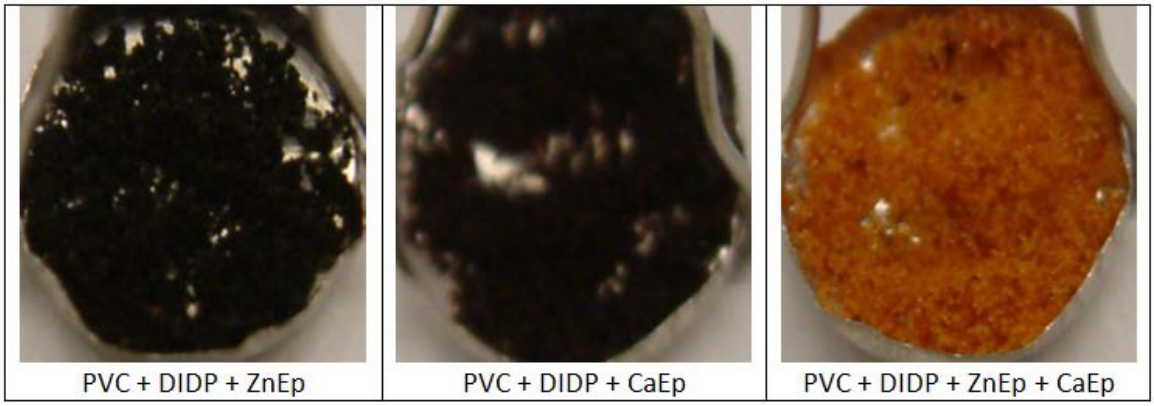

Figure 5.22. Color retention photographs of blends of PVC, DIDP, and novel epoxide salts after 2 hours at 170 °C.

Interestingly, the synergistic blend of ZnEp and CaEp additives was the only DIDP plasticized PVC to show reasonable color retention; all other blends changed from a white powder to a dark brown or black powder as shown in Figure 5.20, Figure 5.21, and Figure 5.22. Each figure allows for a different, but useful, direct comparison to other blends. The mixture of $ZnSt_2$ and $CaSt_2$ afforded a heterogeneous mix of yellow and black powder while the ZnEp plus CaEp blend was a much lighter yellow-orange shade. These results show how effective the Zn and Ca epoxide salts are on the color stability of

the DIDP-PVC system compared to the more traditional stearates. Fascinatingly, the weight loss profile of the blend of PVC, DIDP, and both epoxide salts exactly overlays that of the blend of PVC, DIDP, and calcium stearate. However, a comparison of Figure 5.21 with Figure 5.22 shows an extreme contrast in color retention. This highlights the importance of using multiple criteria to test blend stability.

5.7 Effects of ZnEp and CaEp as Stabilizers in Blends of PVC Plasticized with ESO

The weight loss of ESO-plasticized PVC blends with stearate and epoxy salt additives is shown in Figure 5.23.

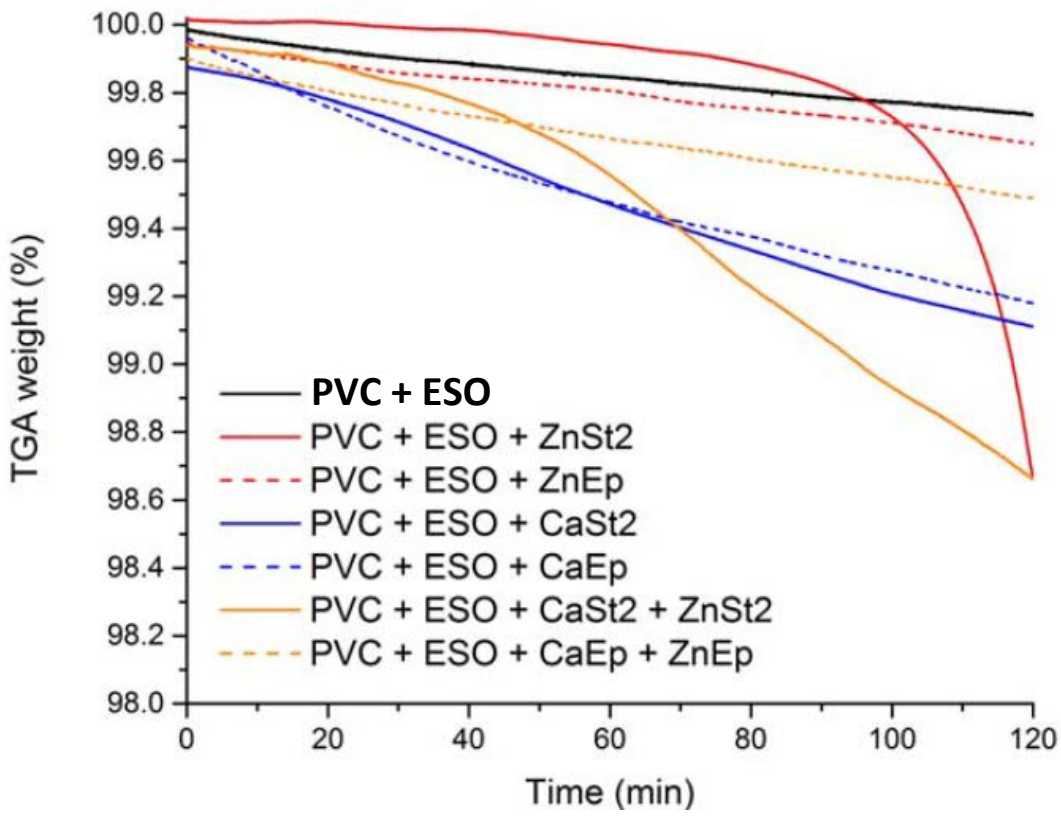

Figure 5.23. Weight loss profiles of ESO-plasticized PVC blends incorporating novel epoxide salt stabilizers and stearate salts for comparison. Heat treatment was isothermal at 170 °C. Weight is normalized against the mass of PVC in each blend.

Upon first inspection, it is obvious that the overall weight loss of ESO-plasticized PVC is much less (less than 2% for all blends presented here) than that of DIDP-plasticized counterparts. However, there are some major differences in the general trends between the two plasticizers when stabilizing salts are added. A drastic drop in weight is still seen for the ESO-plasticized PVC with $ZnSt_2$, similar to that seen with DIDP and $ZnSt_2$. However, in this case, the catastrophic weight loss does not occur until near the end of the 2 hour heat treatment. It is likely that the sequestration of HCl via epoxy ring opening mechanisms delays the onset of weight loss as seen in Figure 5.23.

However, this drastic weight loss with $ZnSt_2$ is not observed in the ESO-plasticized PVC blend with ZnEp within this same time frame. This result supports the hypothesis that the multifunctional additive package presented here can protect ESO by simply adding additional epoxide moieties to the blend. Through the addition of these sacrificial oxirane rings, the novel epoxide salts can protest ESO and its plasticization properties and thus prolong its effectiveness.

In contrast with the DIDP-plasticized PVC (where the blend of both epoxides showed the least weight loss), the ZnEp showed the best performance of all the blends, even including the synergistic blends of both metal salts (ZnEp and CaEp). Likewise, the Ca additives showed the slightly less stability with ESO compared to DIDP: in this case, the blends with calcium salts lost more weight than the blend of ZnEp or the blend of both epoxide salts. Based on the data in Figure 5.18, this was unexpected.

The discoloration of the ESO-plasticized PVC blends with the novel epoxide stabilizers after thermal treatment is shown in Figure 5.24 and discoloration with stearate

salts is Figure 5.25. The ESO-plasticized blend with no additive closely resembles that of PVC, as does the blend with $CaSt_2$: both form dark brown color after heating. When $ZnSt_2$ and a combination of the stearates ($ZnSt_2$ + $CaSt_2$) are used, excellent color stability was observed. However, the weight loss after 2 hours when employing $ZnSt_2$ is a critical limiting factor compared to the multifunctional ZnEp. Interestingly, the ZnEp showed the greatest color retention while the combinations of the two epoxide salts yielded a red tint on the polymer. This is the only case where the combination of zinc and calcium salts yielded worse color performance than either individual metal cation. It seems that the novel epoxide salts do not significantly improve color retention when ESO is used as a plasticizer under these heating conditions. ESO acts as a sufficient sink for HCl to prevent discoloration with stearates to provide good color retention. Weight loss studies still show the benefits of the epoxide salts with ESO.

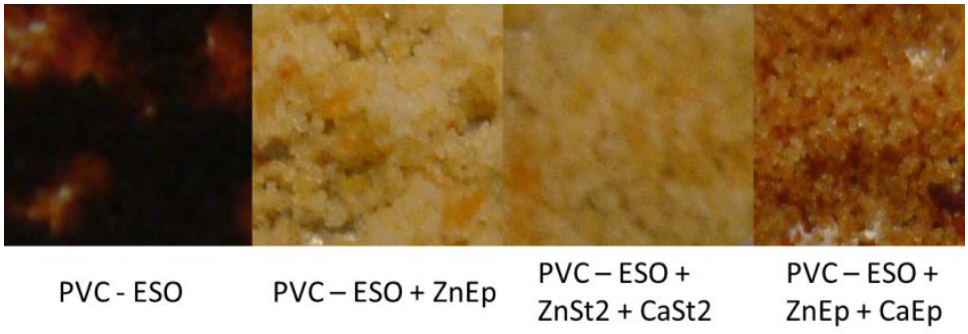

Figure 5.24. Color retention photographs of ESO-plasticized PVC blends incorporating novel epoxide salt stabilizers. Heat treatment was isothermal at 170 °C for 2 hours.

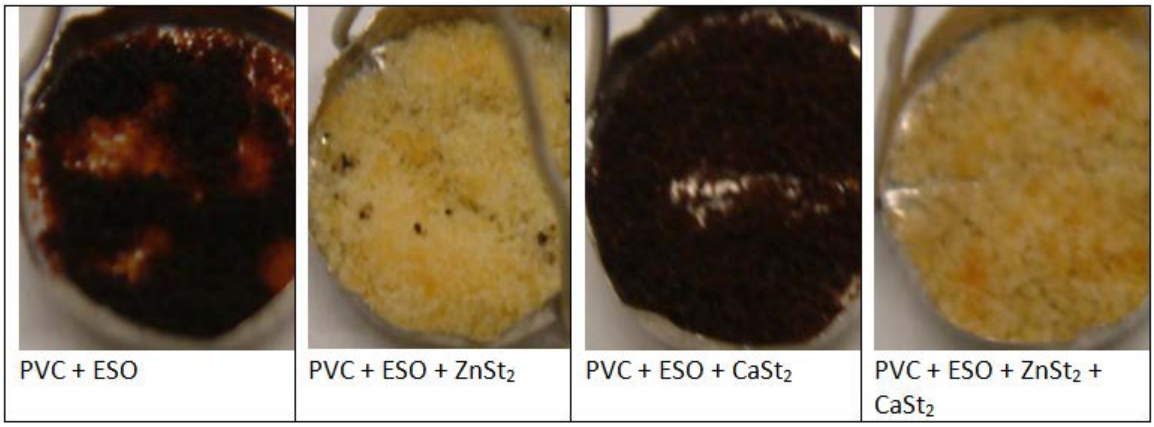

Figure 5.25. Color retention photographs of blends of PVC, ESO, and stearates after 2 hours at 170 °C.

5.8 Studies of Epoxide Ring-Opening

It is clear from weight loss and color studies that epoxide-containing additives such as ZnEp and CaEp have beneficial effects on the stabilization of both DIDP- and ESO-plasticized PVC. The structures of both ZnEp and CaEp have internal epoxide functionalities. To develop a more fundamental understanding of the HCl scavenging efficiency of epoxides and potentially develop new and better additives, a series of simple experiments were conducted to determine the relative reactivities of two epoxide structures. A linear terminal epoxide (1,2-epoxyhexane, EH) and a cyclic epoxide (1,2-cyclohexene oxide, CHO) were both examined. Each epoxide was reacted with HCl individually and the reaction products analyzed. Additionally, a competitive reaction of both epoxides with HCl was conducted and analyzed. In all cases, epoxides were reacted with dry HCl dissolved in 1,2-dichlorobenzene at room temperature. The reactions were analyzed by means of ^{1}H and ^{13}C NMR.

The proton and carbon NMR spectra of 1,2-epoxyhexane are shown below in Figure 5.26 and Figure 5.27, respectively.

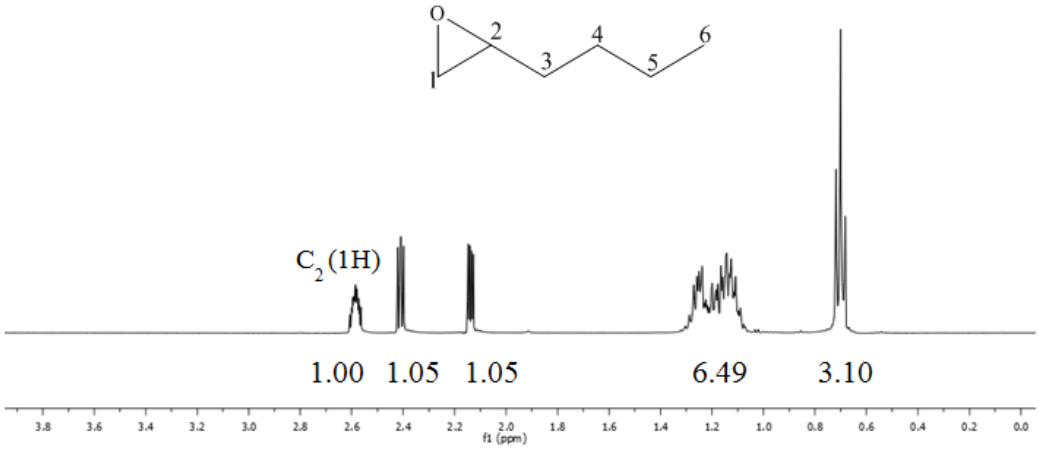

Figure 5.26. Proton NMR spectrum of 1,2-epoxyhexane.

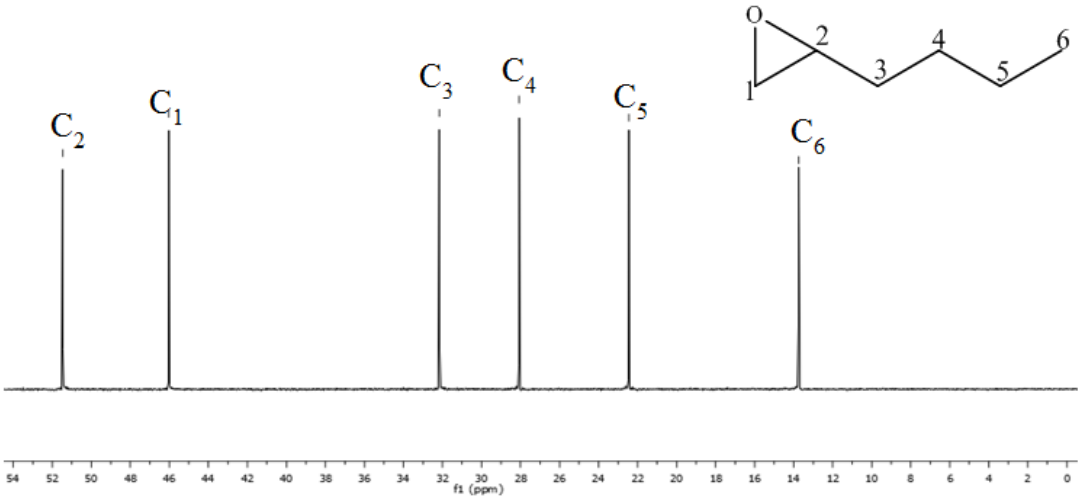

Figure 5.27. Carbon NMR spectrum of 1,2-epoxyhexane.

A simple scheme of the reaction of 1,2-epoxyhexane with dry HCl is shown in Figure 5.28.

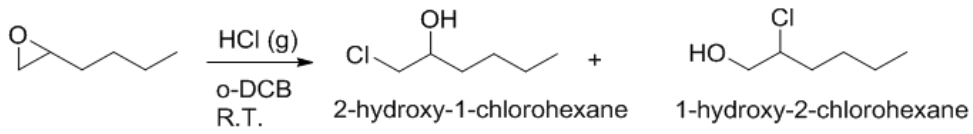

Figure 5.28. Mechanism of epoxide ring opening of 1,2-epoxyhexane by dry HCl in the gas phase.

The reaction of 1,2-epoxyhexane resulted in two products. The major product is 2-hydroxy-1-chlorohexane; the minor product is 1-hydroxy-2-chlorohexane. From the ^{1}H NMR spectrum, shown in Figure 5.29, the ratio of the major and minor products to the starting material was easily determined by the unique chemical shifts of the products. The peak areas of the protons used to determine yields of each product are labeled A (EH), B (major product) and C (minor product). The overall conversion of the EH was 52.2% with yields of 35.9% and 16.3% of 1-hydroxy-2-chlorohexane and 2-hydroxy-1-chlorohexane, respectively, after 90 minutes at room temperature. The products of the reaction are confirmed in the carbon NMR of the reaction, shown in Figure 5.30.

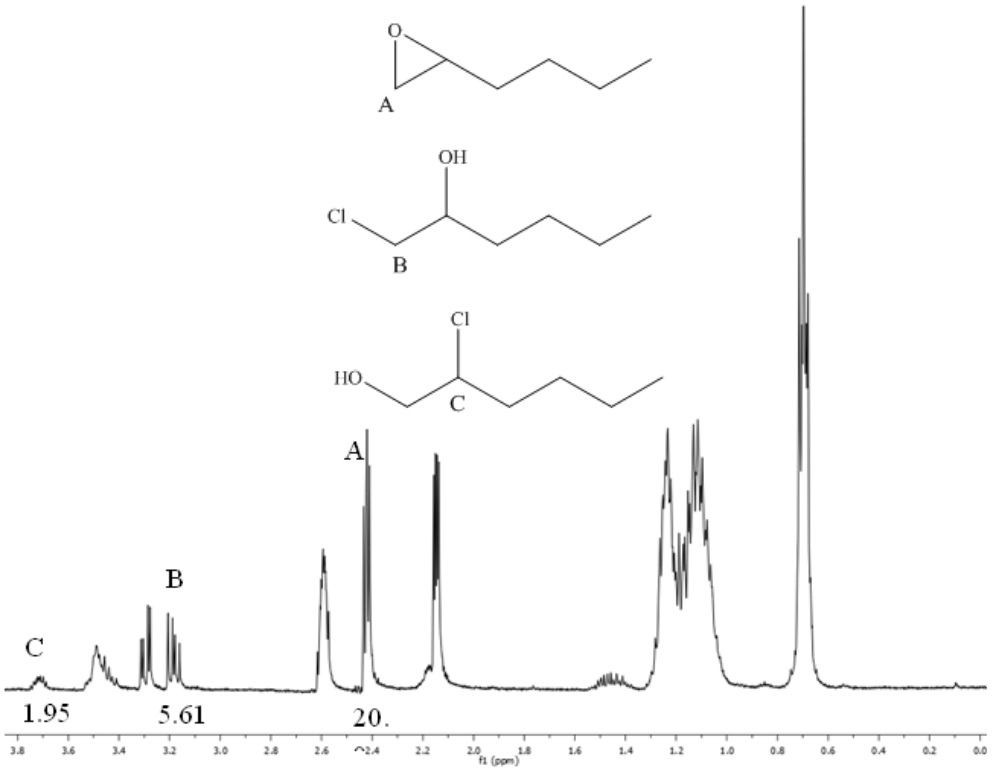

Figure 5.29. Proton NMR spectrum of the reaction of 1,2-epoxyhexane with HCl at a 1:1 molar ratio at room temperature for 90 minutes.

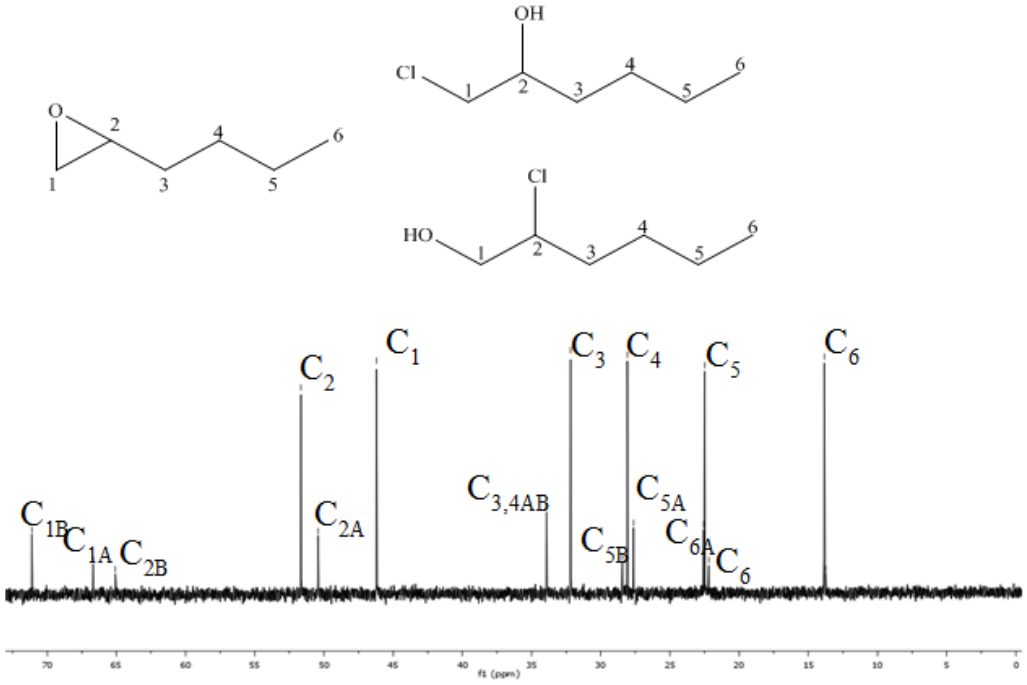

Figure 5.30. Carbon NMR spectrum of the reaction of 1,2-epoxyhexane with HCl at a 1:1 molar ratio at room temperature for 90 minutes.

The epoxide ring opening reaction of the linear epoxide 1,2-epoxyhexane was compared with the cyclic epoxide cyclohexene oxide (CHO). The proton and carbon NMR spectra of CHO are shown below in Figure 5.31 and Figure 5.32, respectively. A simple scheme of the reaction of CHO with HCl is shown in Figure 5.33.

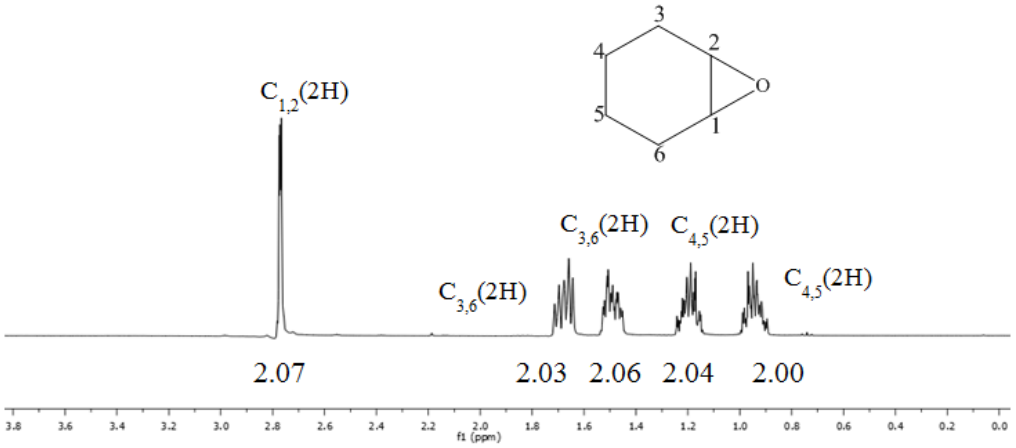

Figure 5.31. Proton NMR spectrum of cyclohexene oxide.

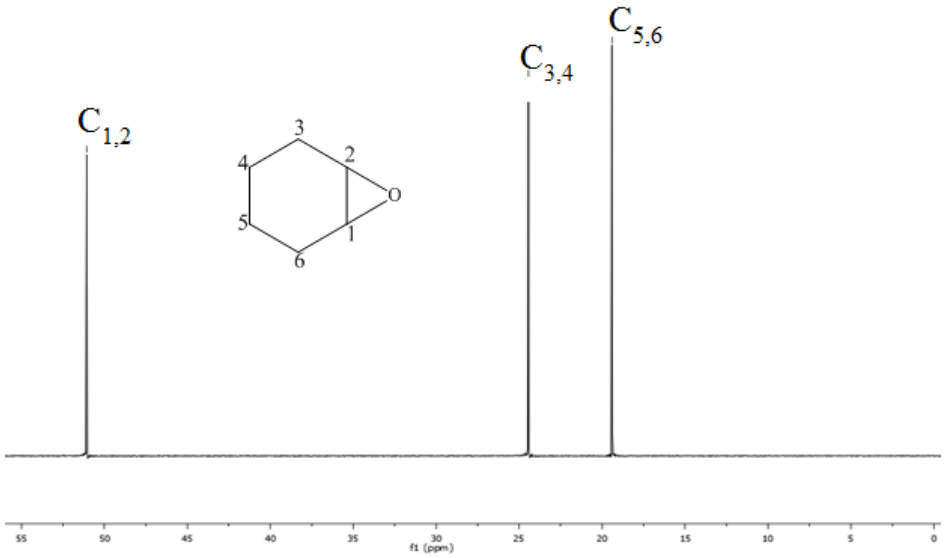

Figure 5.32. Carbon NMR spectrum of cyclohexene oxide.

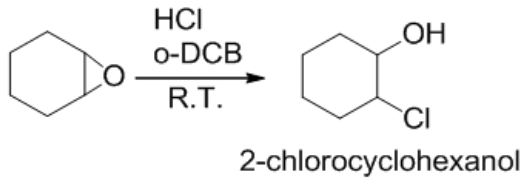

Figure 5.33. Mechanism of the epoxide ring opening reaction of cyclohexene oxide with HCl in the gas phase.

The proton NMR and carbon NMR of the reaction of CHO with HCl (molar ratio of 1:1 CHO:HCl) are shown in Figure 5.34 and Figure 5.35, respectively. As shown in Figure 5.34, the primary product of the reaction was 2-chlorocyclohexanol. The molar ratio of CHO to 2-chlorocyclohexanol was determined by the ratio of the distinct peaks at 2.74 ppm (signal A) and 2.58 ppm (signal B) in the ^{1}H NMR spectrum. From this spectrum and the peak ratios the conversion of CHO was calculated to be 45% after 90 minutes. These results indicate that cyclic epoxides (45% conversion after 90 minutes) react at a similar rate to linear epoxides (52% conversion after 90 minutes) when reacted separately with HCl. The formation of a single primary product is confirmed in the carbon NMR of the reaction shown in Figure 5.35.

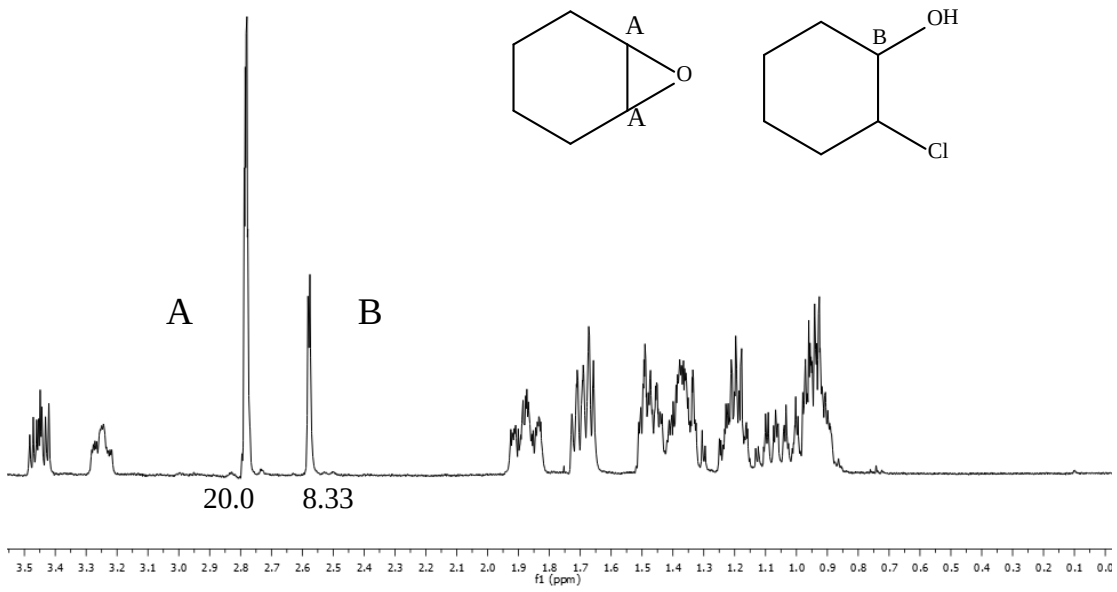

Figure 5.34. Proton NMR spectrum of the reaction of cyclohexene oxide with HCl at a 1:1 molar ratio at room temperature for 90 minutes.

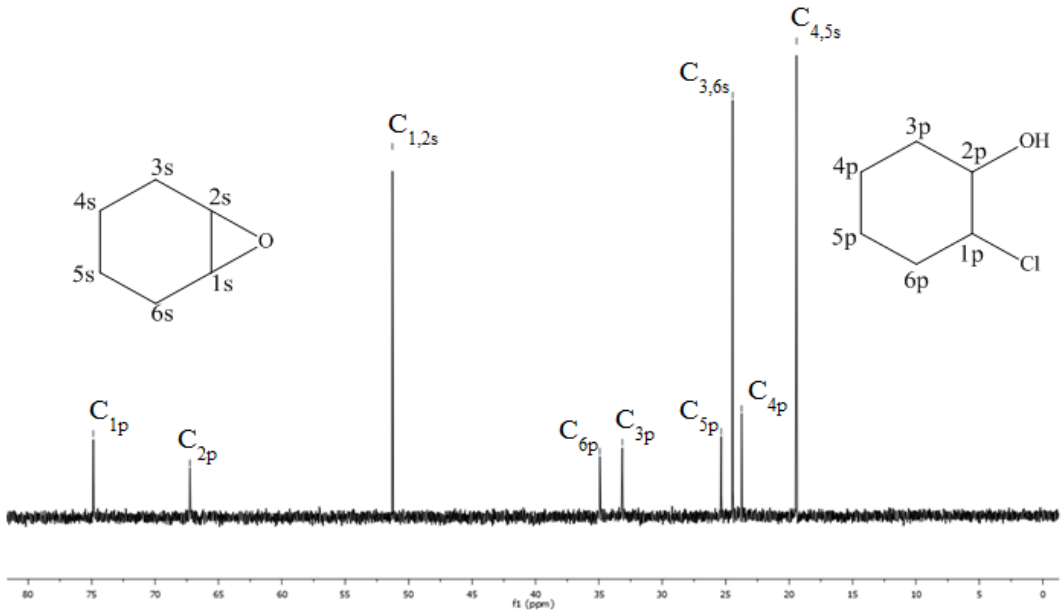

Figure 5.35. Carbon NMR spectrum of the reaction of cyclohexene oxide with HCl at a 1:1 molar ratio at room temperature for 90 minutes.

In a competitive study performed with 0.5 equivalents each of EH and CHO and 1 equivalent of HCl (shown below in Figure 5.36), the CHO was consumed slightly faster

than EH. The same characteristic proton peaks as shown in Figure 5.29 and in Figure 5.34 were used to determine conversions. After 90 minutes, 58.2% of the 1,2-epoxyhexane was converted to 2-hydroxy-1-chlorohexane and 1-hydroxy-2-chlorohexane while 78.4% of cyclohexene oxide was converted to 2-chlorohexanol. This supports our conclusion that epoxides, independent of structure and because of the associated ring strain, react with anhydrous HCL at rapid and similar rates even at room temperature. This conclusion validates the use of the linear epoxides found in the novel epoxide salt stabilizers.

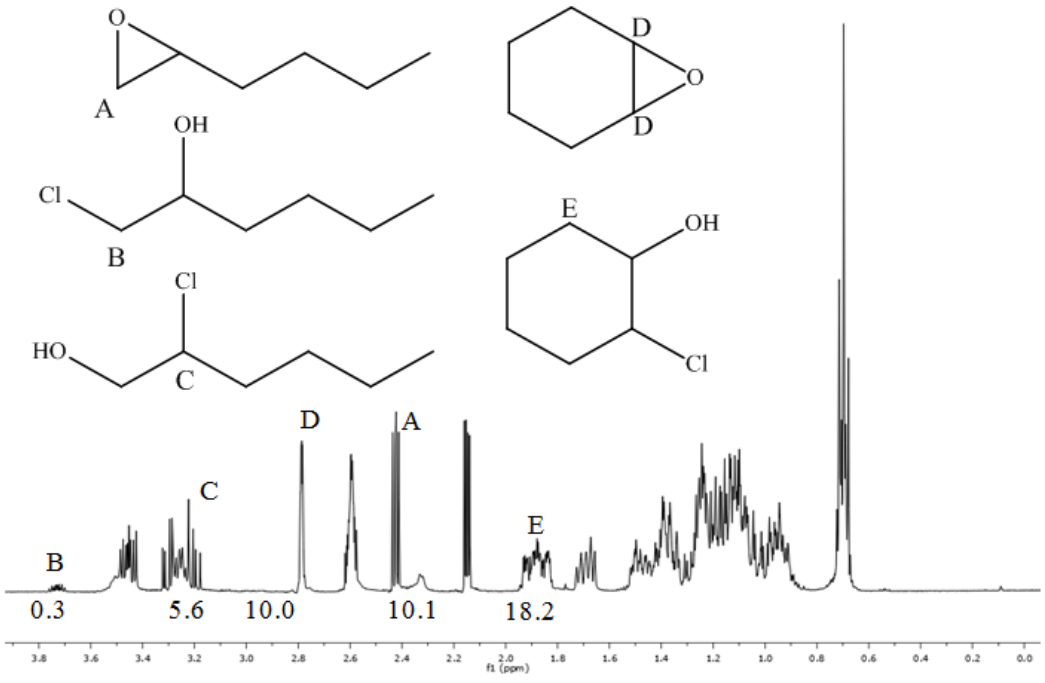

Figure 5.36. Proton NMR spectrum of the competitive reaction of 0.5 equivalents 1,2-epoxyhexane and 0.5 equivalents cyclohexene oxide with 1 equivalent of HCl at room temperature for 90 minutes.

5.9 Conclusions

Novel ZnEp and CaEp additives were created to have multiple functions in the thermal stabilization of plasticized PVC. These properties include promoting (1) substitution reactions via the carboxylate nucleophile at "weak links" on the PVC backbone in order to retard degradation, (2) acid-base reactions between the basic carboxylate anion and the thermally generated HCl to decrease the autocatalytic pathways for dehydrochlorination, and (3) sacrificial ring-opening reactions with HCl to scavenge this catalyst and to protect ESO from consumption. Thermogravimetric analyses, activation energies, and visual color development for untreated PVC and PVC plasticized with DIDP or ESO are reported. Using these data as a reference, $ZnSt_2$, $CaSt_2$, ZnEp, and CaEp additives were blended into DIDP- and ESO-plasticized PVC and compared with respect to rates of weight loss and accompanying visual color development. Compared to the stearate additives, ZnEp and CaEp showed superior weight loss performance and color stability in DIDP-plasticized blends. In ESO-plasticized PVC these novel additives not only reduced the rate of weight loss of the PVC blend but, more importantly, *generally* dramatically decreased discoloration of the polymer.

Probing studied were conducted wherein simple epoxide molecules (1,2-epoxyhexane and cyclohexene oxide) were reacted with gaseous HCl at room temperature. Rates of reaction and products were analyzed using proton and carbon NMR. The results demonstrated that epoxides readily react with HCl regardless of whether they are linear or cyclic. This result validates the choice of epoxidized linolenic acid as a sacrificial epoxide for PVC stabilization.

5.10 References

(1) Zweifel, H.; Amos, S. E.; Maier, R. D.; Schiller, M. *Plastics Additives Handbook*; Hanser, 2009.

(2) Bouchareb, B.; Benaniba, M. T. Effects of epoxidized sunflower oil on the mechanical and dynamical analysis of the plasticized poly(vinyl chloride). *Journal of applied polymer science* **2008**, *107*, 3442.

(3) Huang, H. H.; Yorkgitis, E. M.; Wilkes, G. L. A MORPHOLOGICAL-STUDY ON THE PLASTICIZATION OF POLY(VINYL CHLORIDE) BY DIETHYLHEXYL SUCCINATE AND DIBUTYL PHTHALATE. *Journal of Macromolecular Science-Physics* **1993**, *B32*, 163.

(4) Chaudhary, B. I.; Nguyen, B.-D.; Smith, P.; Sunday, N.; Luong, M.; Zamanskiy, A. Bis(2-ethylhexyl) succinate in mixtures with epoxidized soybean oil as bio-based plasticizers for poly(vinylchloride). *Polymer Engineering & Science* **2014**, n/a.

(5) Sun, B.; Chaudhary, B. I.; Shen, C.-Y.; Mao, D.; Yuan, D.-M.; Dai, G.-C.; Li, B.; Cogen, J. M. Thermal stability of epoxidized soybean oil and its absorption and migration in poly(vinylchloride). *Polymer Engineering & Science* **2013**, *53*, 1645.

(6) Karmalm, P.; Hjertberg, T.; Jansson, A.; Dahl, R. Thermal stability of poly(vinyl chloride) with epoxidised soybean oil as primary plasticizer. *Polymer degradation and stability* **2009**, *94*, 2275.

(7) Campanella, A.; Baltanas, M. A. Degradation of the oxirane ring of epoxidized vegetable oils in liquid-liquid systems: II. Reactivity with solvated acetic and peracetic acids. *Latin American Applied Research* **2005**, *35*, 211.

(8) Wang, Q.; Nagy, S. Improving gamma-radiation stability of PVC--a review. *Journal of Vinyl & Additive Technology* **1999**, *5*, 4.

(9) González-Ortiz, L. J.; Arellano, M.; Sánchez-Peña, M. J.; Mendizábal, E.; Jasso-Gastinel, C. F. Effect of stearate preheating on the thermal stability of plasticized PVC compounds. *Polymer degradation and stability* **2006**, *91*, 2715.

(10) Wypych, G.; PVC Degradation & Stabilization; ChemTec Publishing.

(11) Wypych, J. PVC thermal degradation. III. On the mechanism of action of metal carboxylates. *Journal of Polymer Science: Polymer Letters Edition* **1984**, *22*, 425.

(12) Iida, T.; Nakanishi, M.; Goto, K. STABILIZATION OF POLYVINYL-CHLORIDE) .2. STABILIZATION MECHANISM THROUGH METAL SOAPS BY COMPLEMENTARY COLOR ACTION. *Journal of applied polymer science* **1975**, *19*, 243.

(13) Iida, T.; Kawato, J.; Tanie, S.; Goto, K. STABILIZATION OF POLYVINYL-CHLORIDE) .10. SYNERGISMS BETWEEN EPOXIDIZED POLYBUTADIENES AND METAL SOAPS ON THE STABILIZATION OF POLYVINYL-CHLORIDE). *Journal of applied polymer science* **1989**, *37*, 1685.

(14) Arkis, E.; Balkose, D. Thermal stabilisation of poly(vinyl chloride) by organotin compounds. *Polymer degradation and stability* **2005**, *88*, 46.

(15) Okieimen, F. E. Studies in the utilisation of epoxidised vegetable oils as thermal stabiliser for polyvinyl chloride. *Industrial Crops and Products* **2002**, *15*, 71.

(16) Joseph, R.; Madhusoodhanan, K. N.; Alex, R.; Varghese, S.; George, K. E.; Kuriakose, B. Studies on epoxidised rubber seed oil as secondary plasticiser/stabiliser for polyvinyl chloride. *Plastics Rubber and Composites* **2004**, *33*, 217.

(17) Benaniba, M. T.; Belhaneche-Bensemra, N.; Gelbard, G. Stabilization of PVC by epoxidized sunflower oil in the presence of zinc and calcium stearates. *Polymer degradation and stability* **2003**, *82*, 245.

(18) Frye, A. H.; Horst, R. W. The Mechanism of Poly(Vinyl Chloride) Stabilization by Barium, Cadmium, and Zinc Carboxylates .1. Infrared Studies. *Journal of Polymer Science* **1959**, *40*, 419.

(19) Frye, A. H.; Horst, R. W. The mechanism of polyvinyl chloride stabilization by barium, cadmium, and zinc carboxylates. II. Radioactive tracer studies. *Journal of Polymer Science* **1960**, *45*, 1.

(20) Frye, A. H.; Horst, R. W.; Paliobagis, M. A. The chemistry of poly (vinyl chloride) stabilization. III. Organotin stabilizers having radioactively tagged alkyl groups. *Journal of Polymer Science Part A: General Papers* **1964**, *2*, 1765.

(21) Bueno-Ferrer, C.; Garrigós, M. C.; Jiménez, A. Characterization and thermal stability of poly(vinyl chloride) plasticized with epoxidized soybean oil for food packaging. *Polymer degradation and stability* **2010**, *95*, 2207.

(22) Karmalm, P.; Hjertberg, T.; Jansson, A.; Dahl, R.; Ankner, K. Network formation by epoxidised soybean oil in plastisol poly (vinyl chloride). *Polymer degradation and stability* **2009**, *94*, 1986.

(23) Odilora, C. A. ON THE THERMAL-DEGRADATION OF POLYVINYL-CHLORIDE) - SYNERGISTIC EFFECT OF MIXTURES OF LEAD AND ZINC CARBOXYLATES. *Acta Polymerica* **1989**, *40*, 541.

(24) Worschech, K.; Stoll, G.; Brand, E.-U.; Wedl, P.; Stabilizers containing ketofatty acid glycerides for Ca/Zn-stabilized PVC molding compounds; Google Patents: 1994.

(25) ASTM Standard E698, “Standard Test Method for Arrhenius Kinetic Constants for Thermally Unstable Materials Using Differential Scanning Calorimetry and the Flynn/Wall/Ozawa Method"; ASTM International: West Conshohocken, PA, 2011.

CHAPTER 6 – USE OF ZINC AND CALCIUM SALTS OF 11-MALEIMIDOUNDECANOIC ACID AS THERMAL STABILIZERS FOR PVC

6.1 Introduction

The conjugated polyenes that arise from the chain-unzipping of PVC (discussed in Chapter 4) change the mechanical properties of the polymer (degrading the performance of end products) and can undergo a variety of intra- and intermolecular reactions to further change the polymer matrix. In addition, conjugated polyene sequences result in the development of discoloration, potentially making a PVC product unusable. Both the loss of mechanical properties and the discoloration pose limitations for industrial and consumer applications.

Common stabilization practice uses metal carboxylate additives, such as Ca and Zn stearates (discussed in Chapter 4), to synergistically retard (but not eliminate) the unzipping process. While reports suggest that these metal soaps have some success in preventing degradation, they are ineffective at reducing the number of polyenes in the polymer once they are formed.

If the extended conjugation of polyenes in PVC during or after thermal degradation could be effectively reduced, the associated loss of mechanical performance and discoloration could be controlled. A potential means of reducing conjugation is to employ an additive that can react with conjugated polyenes which, when reacted, creates saturated carbon centers that effectively breaking up the conjugated network. One such class of additive could be a reactive dieneophile. A reactive dienophile could initiate

pericyclic processes to reduce the degree of conjugation, by extension, the accompanying discoloration. Further, if conjugation can be reduced during the thermal degradation (instead of after), additional chlorine atoms could be stabilized against dehydrochlorination (as longer conjugated chains increase lability of neighboring chlorines). The relevant pericyclic processes include the Diels-Alder reaction and the ene reaction, both shown in Figure 6.1.

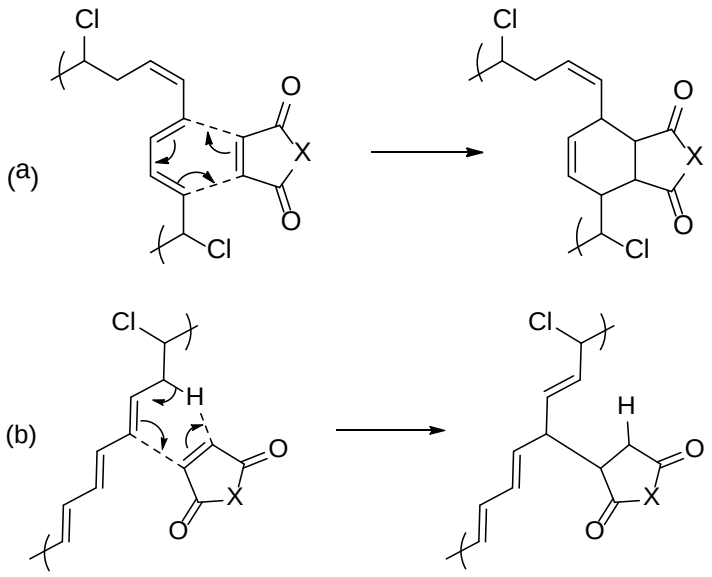

Figure 6.1. The reaction of a conjugated polyene with a dienophile via (a) Diels-Alder Reaction, and (b) the Ene Reaction.

Several studies have appeared in the literature in which maleic anhydride, chloromaleic anhydride, maleate esters, and maleimide derivatives have been employed for the purpose of initiating pericyclic reactions.[1-6] Al-Dossary et. al.[7] reported the synthesis and use of *N*-(*N*'-arylamine)maleimide derivatives in which the aryl group contained highly electron withdrawing substituents, thereby enhancing the acidity of the amino hydrogen. The maleimide derivative was incorporated into PVC with a variety of

basic additives, wherein it was ionized and acted as both: (i) a nucleophilic species which performed substitution reactions of the PVC polymers, and (ii) a dienophile with the developing conjugated polyene. The authors state that the substitution of labile chlorines dominates in the early stages of PVC degradation leaving the maleimide portion of the additive to react in a Diels-Alder capacity at longer degradation times. Tran et. al.[1] reported the Diels-Alder reaction of maleic anhydrides with partially dehydrochlorinated PVC and beta-carotene using infrared spectroscopy, while Yi et. al.[2] have recently employed the zinc and calcium salts of maleic acid which they claim functioned as (i) a dienophile in Diels-Alder reactions, and (ii) a nucleophile in substitution processes of labile chlorines. It should be emphasized that the reports cited above used either rigid PVC or base-treated PVC which produced a partially degraded polymer containing conjugated polyenes. None of the above studies employed plasticized PVC in realistic blends relevant to industrial processing.

Herein, the works reported in various literature regarding maleimides in PVC was expanded. This chapter investigates the effective use of a highly reactive dieneophile in reducing both the weight loss due to dehydrochlorination and the color production of PVC plasticized with either diisododecyl phthalate (DIDP) or epoxidized soy bean oil (ESO). More specifically, the investigated compound is the Zn or Ca salt of a long chain carboxylic acid-11-maleimidoundecanoic acid, shown in Figure 6.2. Although the effects of plasticizers such as di(2-ethylhexyl) phthalate and epoxidized soy bean oil (ESO), and additives such as zinc and calcium stearate, on dehydrochlorination and thermal stability of PVC have been reported in the literature,[3,4] the zinc and calcium salts of 11-maleimidoundecanoic acid have not previously been investigated as PVC stabilizers. To

understand the behavior of Zn11M and Ca11M in relationship to the move conventional stabilizers, the following experiments are be presented: (1) the UV-Visible absorption behavior of untreated PVC heated at 180 °C as a function of time; (2) a comparative visual and TGA analysis of PVC plasticized by DIDP in the presence of a variety of stabilizing additives including Zn11M and Ca11M; (3) the UV-Visible absorption behavior of DIDP-plasticized PVC and DIDP-plasticized PVC in the presence of stabilizing additives including Zn11M and Ca11M heated at 180 °C as a function of time; and (4) a similar comparative visual and TGA analysis of ESO plasticized PVC containing these same stabilizer combinations.

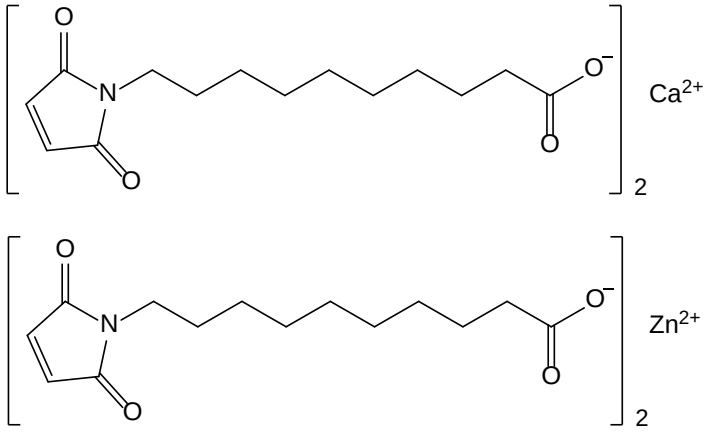

Figure 6.2. Structures of the novel maleimide stabilizers Zn11M and Ca11M.

6.2 Methodology

6.2.1 Materials

Diisodecyl phthalate (DIDP), calcium acetate ($Ca(OAc)_2$), sodium acetate (NaOAc, anhydrous) and zinc stearate ($ZnSt_2$, purum, 10-12% zinc metal basis) were purchased from Sigma-Aldrich. Calcium stearate ($CaSt_2$) was purchased from Alfa Aesar. The PVC powder (OxyVinyls 240F suspension-grade homopolymer) was manufactured by Oxy Vinyls, LP, and Plas-Chek 775 epoxidized soybean oil (ESO) was manufacturd by Ferro Corporation. The properties of these grades of PVC and ESO have been reported in literature.[5] Helium and nitrogen were obtained from Airgas. All materials were >97% purity or ultra-high purity unless otherwise stated and used as received from the manufacturer.

6.2.2 Synthesis of 11-Maleimidoundecanoic acid

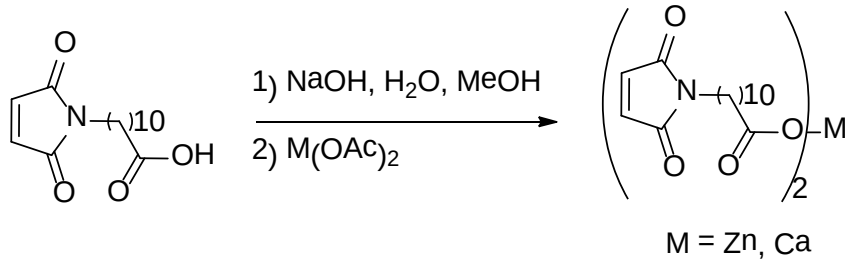

Figure 6.3. Synthesis pathway of the zinc or calcium salt of 11-maleimidoundecanoic acid. "M" represents a metal cation, either Zn or Ca.

0.95 g NaOH (0.024 mol) in 15 mL water was added to 5.0 g 11-maleimido-undecanoic acid (0.024 mol) dissolved in 10 mL methanol. The homogenous solution was stirred for 15 min at room temperature. 2.2 g $Zn(OAc)_2$ (0.012 mol) (or $Ca(OAc)_2$ for preparation of Ca salt) in 15mL water was then added and a white precipitate was observed. The reaction mixture was cooled to 0^{o}C, filtered, and the solid was washed

with water (3 washes of x 20 mL each) and acetone (2 washes of 10 mL each) then dried under vacuum resulting in 1.75 g (32% yield) of Zn11M (or a 51% yield of Ca11M) as white solid.

6.2.3 Preparation of Blends of PVC, Plasticizers, and Novel Additives

PVC blends were fabricated dry, without the use of solvents. Generally, 3 g of PVC power were mixed with 30 phr (0.9 g) plasticizer (either DIDP or ESO) and 5 phr (0.15 g) additional additives ($ZnSt_2$ and/or $CaSt_2$, or Zn11M and/or Ca11M). In the cases when salts of two metal cations were combined, the 5 phr (0.15 g) was divided into 2.5 phr zinc salt and 2.5 phr calcium salt.

The PVC powder was physically combined with half the plasticizer (0.45 g) in a glass vial and heated to 95 °C in an oil bath. The glass transition temperature of unplasticized PVC is reported as 83 °C.[5] Heating above this glass transition (to 95 °C) facilitates the rapid and efficient absorption of additives into the PVC matrix. The mixed PVC and plasticizer were agitated with a glass rod during heating until the mixture appeared dry (e.g., until the plasticizer was absorbed into the PVC).

Separately, the other half of the plasticizer (0.45 g) was mixed with the other additives and heated to 95 °C. This second mixture was then added to the first mixture (of PVC and plasticizer) and both were heated to 95 °C and agitated with a glass rod. The two-pot blending technique was employed to enhance the uptake of the solid metal salts into the PVC.

Plasticizers were necessary for the work reported herein. Neither the zinc maleimide salt nor the calcium maleimide salt is soluble in PVC alone. Plasticizers were therefore employed to incorporate the novel salts into the polymer.

6.2.4 Thermogravimetric Analysis of PVC Blends

Thermogravimetric analysis (TGA) was performed using a TA Instruments TGA Q50. Isothermal weight loss studies were conducted at 170 °C and 180 °C for up to three hours under a flow of nitrogen (100 mL/min) in all cases. Approximately 20 mg of a dry blended sample were used in duplicate runs to confirm repeatability. Weight losses reported are with respect to the PVC, not including the additives. TGA of the additives showed minimal weight loss; DIDP exhibited a ~ 7.8% weight loss while ESO lost less than 1% at a temperature of 180 °C, as shown in Figure 6.4. Other additives had weight losses of less than or equal to 2% after 120 minutes at 170 °C, as shown in Figure 6.5. Assuming low concentrations of the other additives (5phr), the weight losses of the additives were considered negligible compared to the bulk PVC. Therefore, the weight losses observed in the PVC blends are attributed to dehydrochlorination of the PVC backbone. This enables us to better observe and quantify the overall effect of the additives on the plasticisized PVC itself compared to untreated PVC.

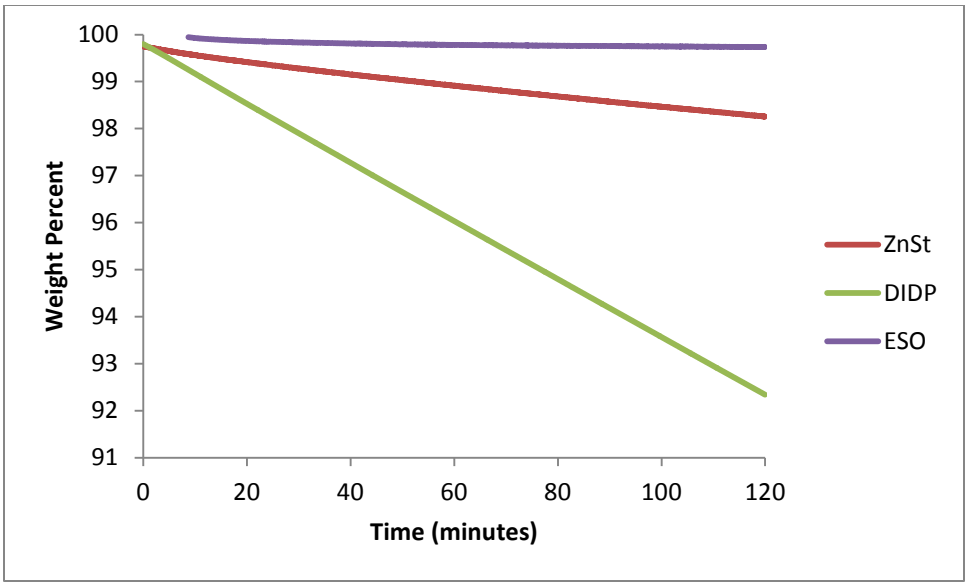

Figure 6.4. Isothermal weight losses of several additives after 2 hours at 180 °C.

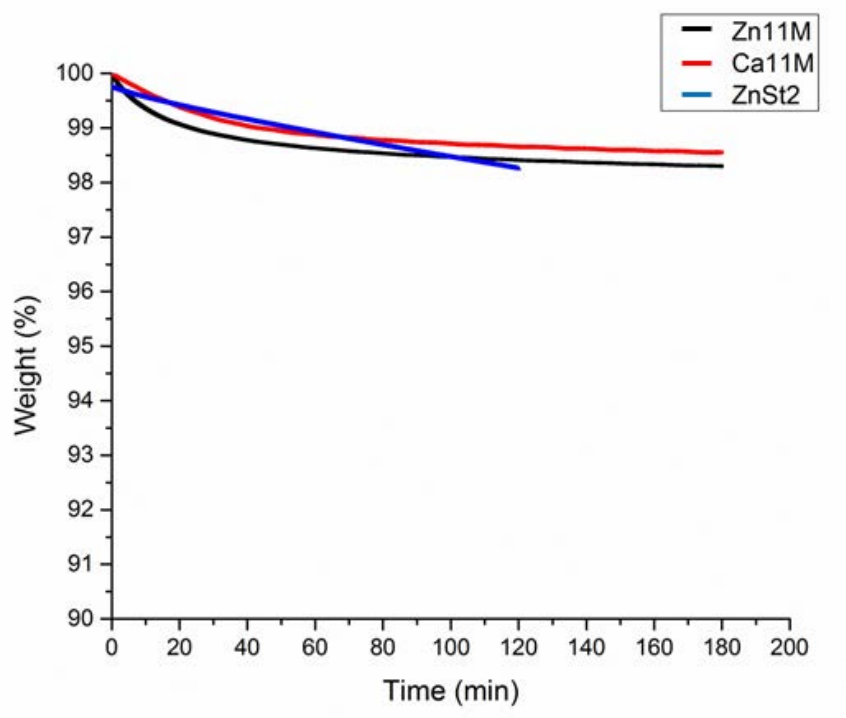

Figure 6.5. Isothermal weight losses of maliemide salts and zinc stearate after treatment at 170 °C.

6.2.5 UV-Visible Spectroscopy of PVC

UV-visible studies of PVC were performed using an Agilent Cary 100 UV-visible spectrophotometer. Scans were recorded over a range of 200-800 nanometers. PVC samples (of approximately 50 mg) were first loaded into the TGA and an accurate mass was recorded. The TGA was used to precisely heat the sample to 180 °C for a specific time. The heated samples were immediately removed from the TGA upon completion of the heat treatment and quantitatively dissolved in THF to obtain equal PVC concentrations (based on pre-heated weights). UV-visible spectra were obtained in triplicate to ensure repeatability between samples.

6.2.6 Color Change Examination of PVC Blends

Photographs of the each PVC blend were taken after thermal treatment. These photographs were used to qualitatively compare the discoloration of the PVC polymer.

6.3 UV-Visible Absorption of PVC (With No Additives) Heated at 180 °C

The thermal instability of PVC arises from dehydrochlorination which leads to polyene chains in the polymer backbone. Dehydrochlorination results in weight loss (as HCl is liberated) and the embrittlement and discoloration of the polymer. The embrittlement is primarily due to cross-linking processes (shown in Figure 6.8) while the discoloration is due to the formation of conjugated polyenes. The latter can be observed using UV-Vis spectroscopy. Figure 6.6 shows the UV-Visible absorption spectra of untreated PVC heated at 180 °C from 0 to 45 minutes. Initially, there is essentially no

absorbance between 250 and 600 nm. As time progresses, however, a broad "absorbance envelope" appears and grows between these same wave lengths. This is indicative of the formation of conjugated polyenes.

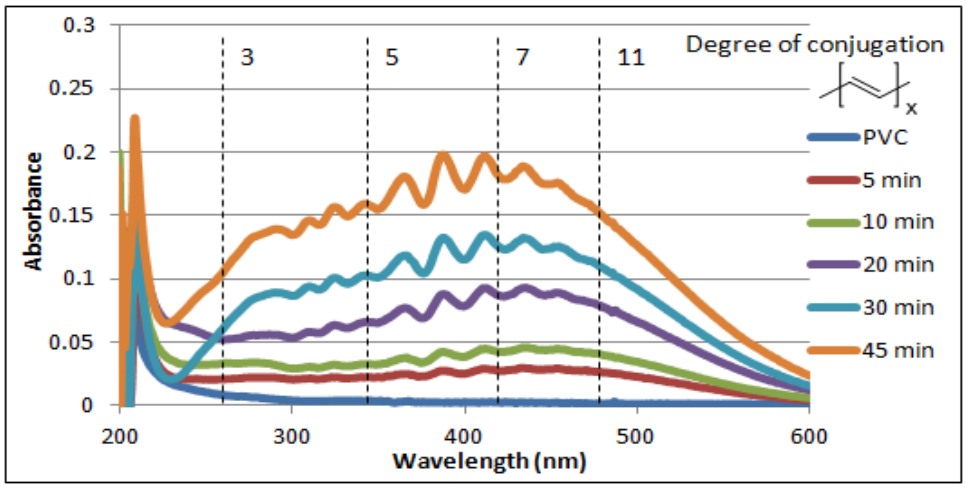

Figure 6.6. UV-Visible absorption spectra of unblended PVC heated at 180 °C for various time increments.

A graph of the integrated areas (in area units [au]) between 250 and 600 nm as a function of time time is displayed in Figure 6.7. A linear increase in absorption area from 1.5 au at 5 minutes up to 18 au at 45 minutes is observed with a slope of 0.418 au/min. Visually, the PVC sample proceeds from initially white to yellow, brown, and eventually black over the 45 minute period. Figure 6.6 also indicates the absorption maxima for conjugated polyene sequences from three to eleven double bonds.[6] It is clear that the degree of conjugation in the degrading PVC approaches a limit of approximately 11 double bonds.

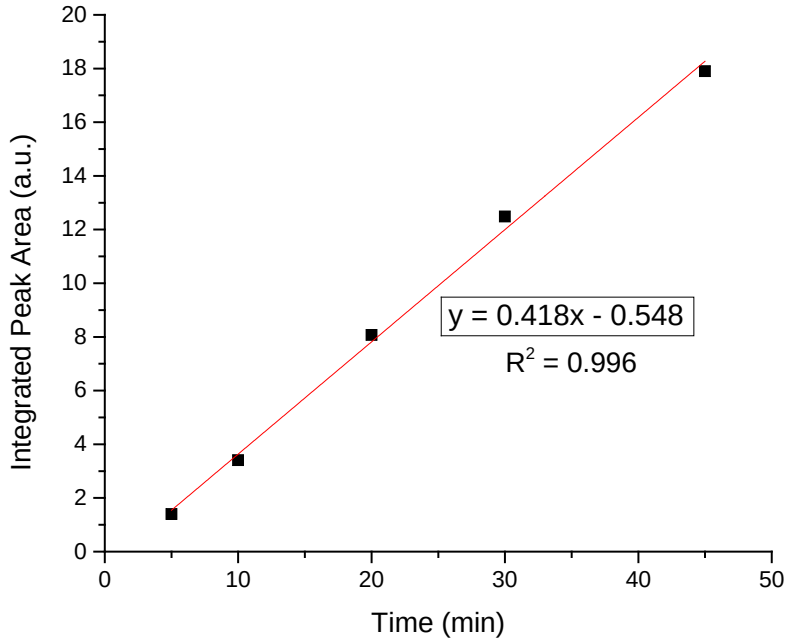

Figure 6.7. Integrated UV-Absorption areas (obtained from Figure 6.6) plotted as a function of time. Absorption of UV-visible wavelengths by polyenes increases as the dehydrochlorination reaction proceeds.

Initially, it was expected that the absorbance of the high wavelengths (representing extended conjugation) would increase over the measured time period. This, however, was not the case; most of the increase in absorption occurred near 400 nm, corresponding to sequences of roughly 6 double bonds. A possible explanation is that as the length of the conjugated sequence increases, intramolecular and intermolecular chemical processes (with relatively low activation energies) take place. These include intramolecular electrocyclic ring formation and intermolecular cycloaddition reactions. As illustrated in Figure 6.8, these processes create saturated carbon centers which interfere with the polyene conjugation. It is conjectured that these processes effectively

limit the degree of conjugation observed, thereby accounting for the low absorption of the higher extents of conjugation in Figure 6.6.

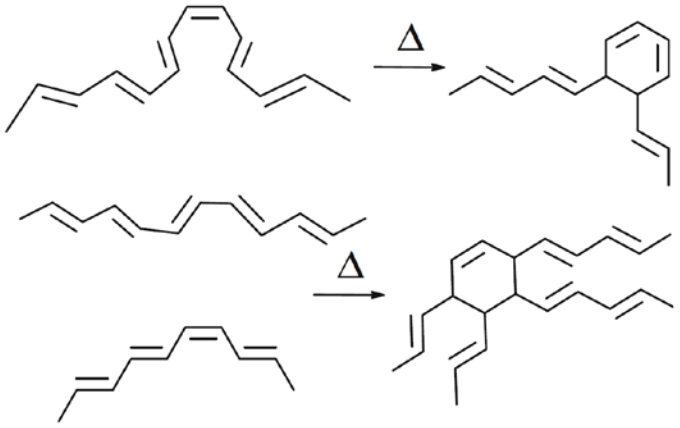

Figure 6.8. Cyclization processes by polyene sequences that can limit conjugation of polyenes.[7]

6.4 Zn11M and Ca11M as Stabilizers in Blends of PVC and DIDP

According to literature hypotheses, PVC heat stabilizers will inhibit the liberation of HCl upon heating (limiting autocatalysis), effectively blocking the formation of conjugated double bond sequences. Therefore, weight loss performance and color change can be used as indications of the performance of Zn11M and Ca11M as thermal stabilizers in PVC. Weight loss is representative of the amount of liberated HCl, while discoloration correlates directly with the amount of conjugation in the sample. Figure 6.9 below shows weight loss profiles of the DIDP plasticized PVC blended with multiple combinations of thermal stabilizing additives at 170 °C over a period of 2 hours.

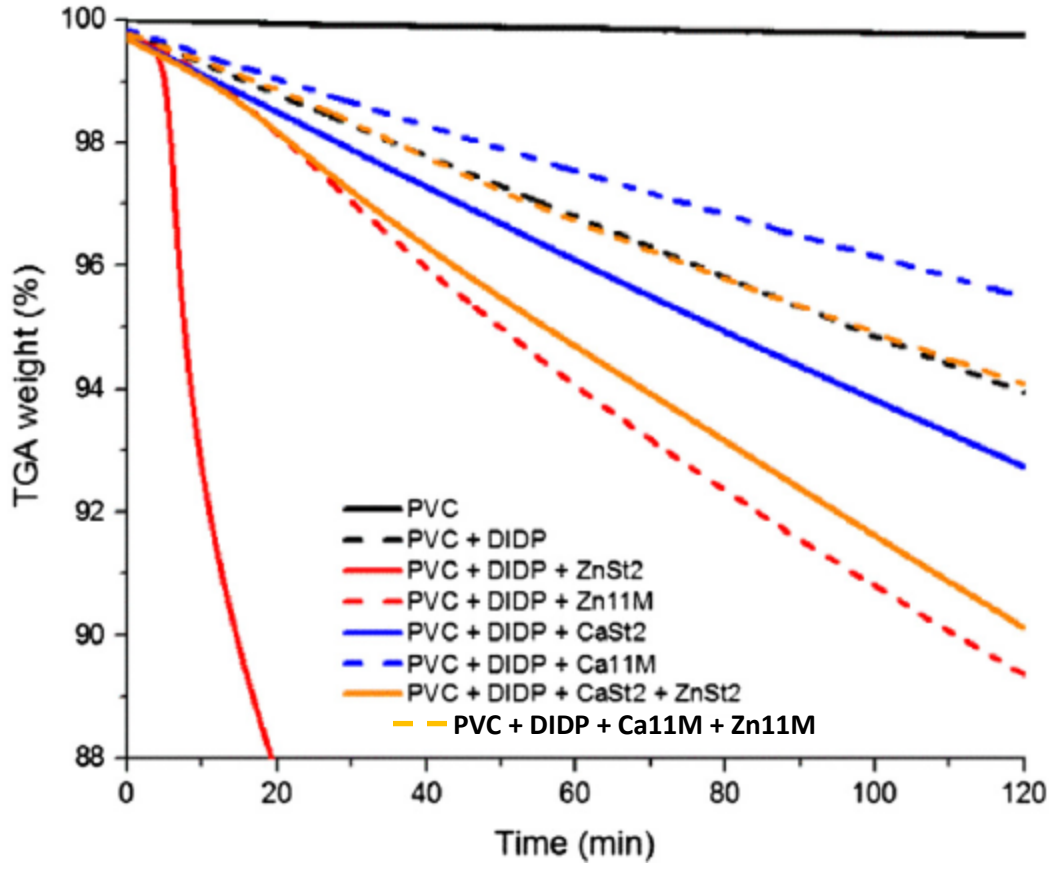

Figure 6.9. Weight loss of PVC plasticized by DIDP with added zinc and calcium stearates and zinc and calcium maleimide salts as thermal stabilizers. Samples were heated at 170 °C. Weight percent is based on the weight of PVC in each blend, neglecting the weight of additives.

The most notable observation from Figure 6.9 is the drastic decline in weight when zinc stearate ($ZnSt_2$) is used as the sole stabilizer. The reason for this observation is discussed at length in Chapter 4. Briefly, it has been generally accepted that the zinc salt can interact with PVC at positions containing reactive chloride to produce stearate ester complexes on the polymer backbone. As a consequence, zinc chloride, a potent Lewis acid which rapidly promotes dehydrochlorination of the polymer, is produced. This is clearly consistent with the catastrophic 31.7% decrease in weight illustrated in Figure 6.9. When calcium stearate ($CaSt_2$) is used in conjunction with its zinc counterpart, a dramatic

improvement in both the weight loss profile and the color retention of the DIDP-PVC (Figure 6.10) is observed. The synergistic ion exchange between calcium and zinc stearates is addressed in Chapter 4.

The Zn11M was conjectured to behave in a similar manner to $ZnSt_2$ in interacting with labile carbon-chlorine bonds in PVC. However, in comparison with the corresponding stearate, the Zn11M did not exhibit the catastrophic loss in weight. Ca11M also displays little weight loss: the DIDP-plasticized PVC blended with Ca11M showed only a 4.5% overall weight loss compared to 7.2% for DIDP-plasticized PVC with $CaSt_2$ alone. From weight loss alone, Ca11M appears to be a highly effective thermal stabilizer. However, its color retention (shown in Figure 6.10) was very poor and not suitable as a stand-alone additive. Zn11M showed a slightly decreased discoloration, most likely indicative of interaction labile chlorine replacement leading to reduced dehydrochlorination. All other blends with a single stabilizer became dark black/brown.

As expected, the synergistic blend with both Zn11M and Ca11M lost less weight than the corresponding $ZnSt_2$ + $CaSt_2$ blend and also showed the best color retention (Figure 6.10) of any blend with DIDP. It is believed that the same ion-exchange reaction is occurring for the Zn11M-Ca11M as was postulated for the $ZnSt_2$-$CaSt_2$ combination; calcium chloride was formed from interaction of $CaSt_2$ with $ZnCl_2$ and the Zn11M was regenerated. In principle, this new additive salt combination would function in a dual capacity by both (i) reducing the rate of dehydrochlorination through interaction with labile chlorides, and (ii) reducing color development in the polymer. Within the framework of this study, the Zn11M-Ca11M combination is the best performer of all the DIDP-PVC blends.

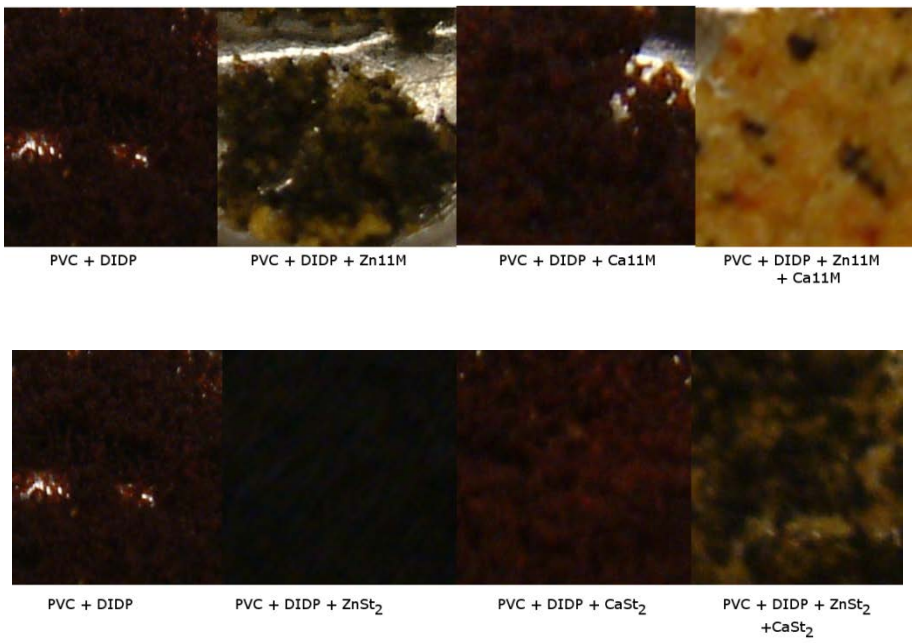

Figure 6.10. Color comparison photographs of blends of PVC plasticized with DIDP with added stearate and maleimide salts for thermal stabilization. Samples were heated at 170 °C for 2 hours.

6.5. UV-Visible Absorption

The increased color retention of the synergistic Zn11M-Ca11M combination in PVC plasticized by DIDP (Figure 6.10) was also tracked via UV-Vis spectroscopy. Figure 6.11 shows the UV-Visible absorption area integrations from 310 nm to 600 nm (normalized to sample mass) for blends of DIDP plasticized PVC without and with Zn11M-Ca11M and $ZnSt_2$-$CaSt_2$ stabilizer systems. The absorption spectra for each sample were examined over 30 minutes of heating at 180 °C.

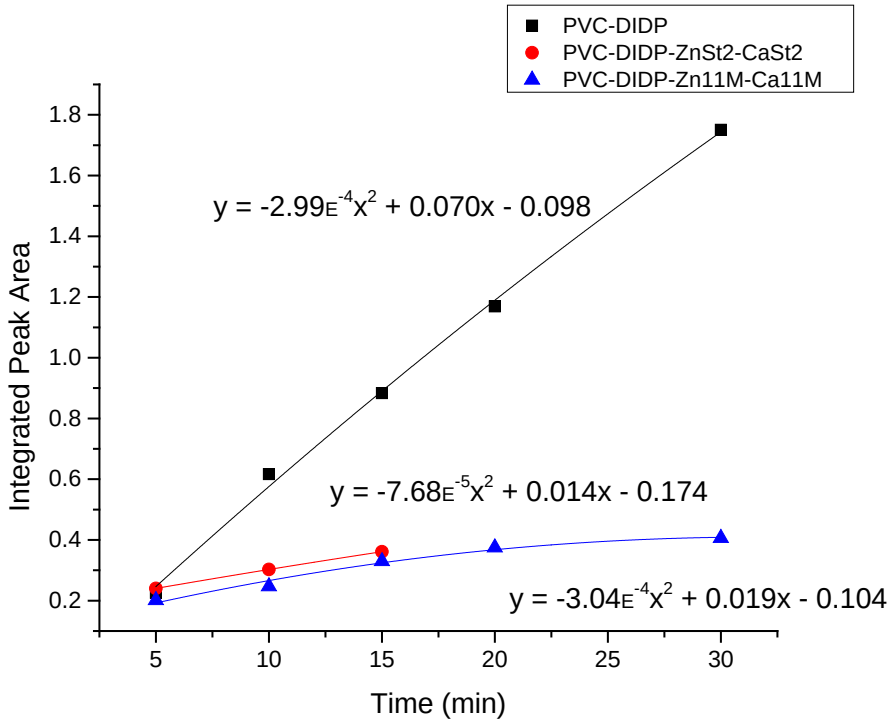

Figure 6.11. Integrated areas of UV-Visible absorption peaks of PVC plasticized with DIDP as a function of time. The presence of zinc/calcium stearates and zinc/calcium maleimides drastically reduce the extent of absorption by polyene sequences.

The effect of both stearates and novel maleimide salts on color retention of DIDP-plasticized PVC blends during the early stages of thermal treatment is clearly illustrated in Figure 6.11. Both salt systems show less UV-Visible absorption (e.g., color change) than the control blend of PVC plasticized by DIDP. Interestingly, the maleimide salt blend shows essentially the same absorption profile (albeit slightly less absorption) as the stearate salt blend. This result may suggest that during the early stages of degradation, the interaction of the metal carboxylate with chlorine on the PVC backbone is the dominant stabilization process for both stearates and maleimides. However, after extended degradation, as the polyene concentrations increase, the maleimide salts can take part in pericyclic processes (Diels-Alder and Ene reactions) and reduce the amount

of conjugated double-bond sequences. This conjecture is supported by the superior weight loss (Figure 6.9) and color retention (Figure 6.11) of the maleimide salt system.

This hypothesis comports well with current understanding of PVC degradation. Diels-Alder and Ene reactions should only readily occur when a significant amount of conjugated polyene sequences are already present on the PVC backbone (e.g., when concentrations are high enough for reaction rates to become relevant). Such conjugated systems only occur later in the degradation process. This conclusion is consistent with the work of Tran et. al.[1] who reported that the grafting of maleic anhydride onto partially dehydrochlorinated PVC would only readily occur in the presence of a strong Lewis acid. A strong Lewis acid (as demonstrated in chapter 4) is effective in catalyzing rapid dehydrochlorination of PVC. Thus, it is concluded that the Zn11M-Ca11M combination operates in two time regimes: (1) during the early thermal treatment stages it facilitates substitution processes on the polymer; (2) during the later stages it promotes pericyclic processes to reduce the extent of polyene formation.

6.6 Zn11M and Ca11M as Stabilizers in Blends of PVC and ESO

Figure 6.12 shows weight loss profiles of the PVC plasticized by ESO blended with multiple combinations of thermal stabilizers at 170 °C over a period of 2 hours.

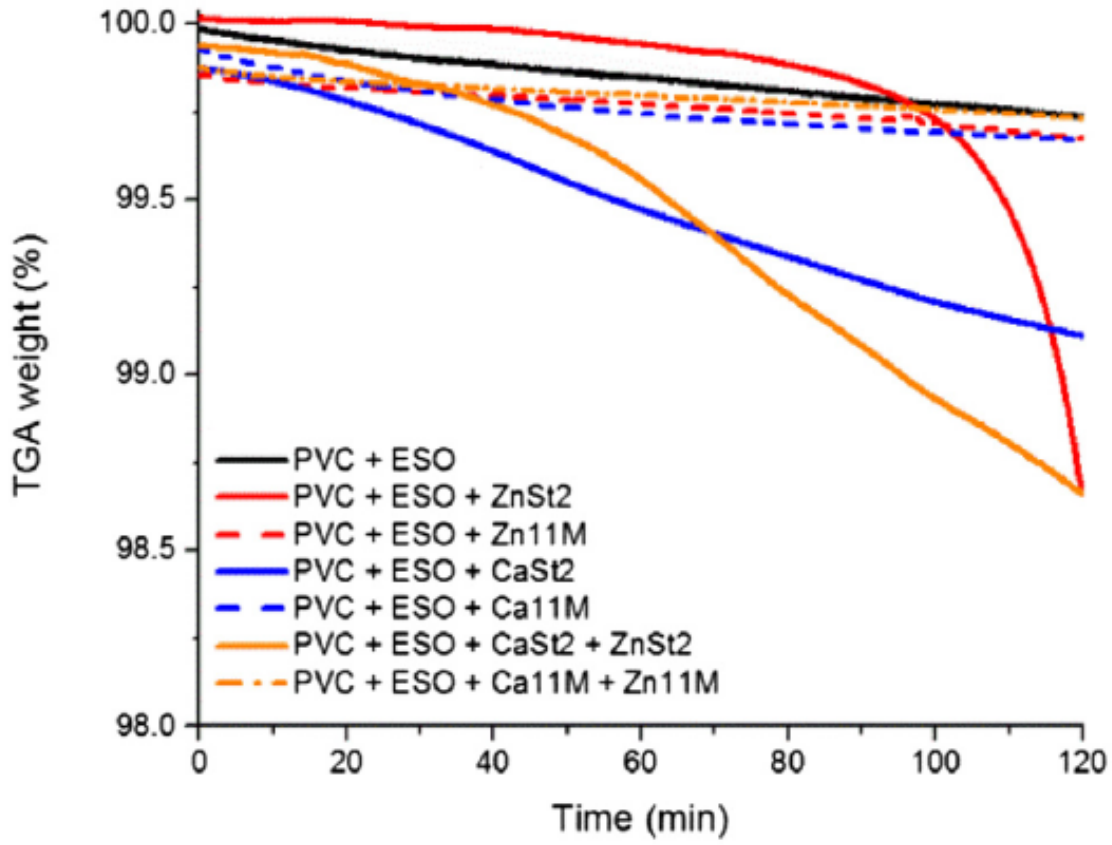

Figure 6.12. Weight loss of PVC plasticized by ESO with added zinc and calcium stearates and zinc and calcium maleimide salts as thermal stabilizers. Samples were heated at 170 °C. Weight percent is based on the weight of PVC in each blend, neglecting the weight of additives.

When compared to the DIDP, maleimide salts blends improved performance for all the blended additives, even for the $ZnSt_2$. It took 100 minutes before the onset of catastrophic degradation in the presence of $ZnSt_2$ alone. The epoxide rings present in ESO are vulnerable to attack and opening by hydrogen chloride (HCl) molecules as shown in Figure 6.13. Hence, it acts as a thermal stabilizer as well as a plasticizer, consistent with previous reports in the literature[3,5,8] and the studies shown in Chapter 5. This dual functionality of the ESO is one of the major reasons for the significant improvement in weight retention compared with the use of DIDP.

Overall, the trends for each additive combination with DIDP-plasticized PVC were also seen with ESO-plasticized PVC. The blend with both Zn11M and Ca11M exhibited the best overall performance out of all additive blends studied. The blend with $ZnSt_2$ did initially retain more weight, but it also suffered the catastrophic weight loss after 100 minutes.

In fact, none of the 11-maleimidoundecanoic salt blends lose more than 0.4 weight percent PVC over the 2hrs at 170 °C, with weight losses of 0.33%, 0.33% and 0.27% for Ca11M, Zn11M and Ca11M+Zn11M, respectively This represents an 80% improvement in stability for the synergistic blend of Zn11M-Ca11M when compared to the analogous stearate blend.

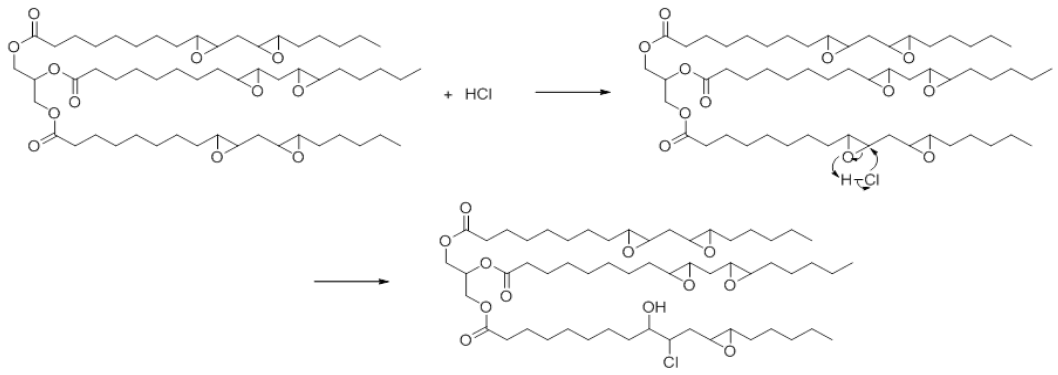

Figure 6.13. Mechanism of the scavenging of HCl by ESO, producing chlorohydrins.

In addition to the improved weight loss profiles, the maleimide stabilizers also exhibit less discoloration than their stearate counterparts. A color comparison is shown in Figure 6.14, below.

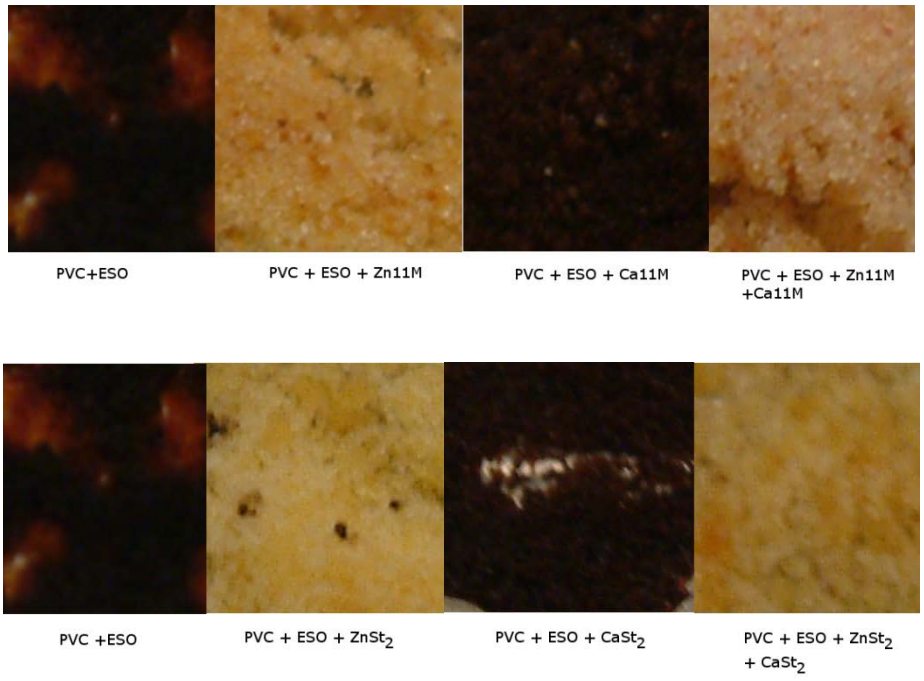

Figure 6.14. Color comparison photographs of blends of PVC plasticized with DIDP with added stearate and maleimide salts for thermal stabilization. Samples were heated at 170 °C for 2 hours.

According to Figure 6.14, the synergistic blend of both maleimides appears more translucent, closer to the appearance of unheated PVC. Regions of discoloration are visible with the other blends, which may indicate local regions of accelerated degradation. It should also be noted that the ESO-plasticized blend containing Zn11M alone also exhibited excellent color stability while the ESO-plasticized PVC blend incorporating only Ca11M discolors to nearly the same extent as the blend containing $CaSt_2$. This observation confirms our initial suspicions that the Ca11M may neither facilitate chloride displacement reactions nor contribute to the polyene crosslinking attributed with the Zn11M. All of the results regarding calcium-substituted carboxylates presented suggest that calcium stabilizers have very limited solubility in the polymer and do not engage in a significant level of reactivity with the polymer itself. However, when

combined with zinc, a significant improvement in color stability is observed that further confirms the ion-exchange stabilization mechanism.

6.7 Preliminary Studies with Beta-Carotene

Qualitative data presented thus far have provided some evidence that the novel maleimide salts are acting as effective stabilizers. Since they contain metal carboxylate functionality, it's likely that they can mimic the function of stearate salts. The color retention displayed in Figure 6.10 and in Figure 6.14 suggests that the maleimide salts are capable of initiating Diels-Alder chemistry. To confirm that Diels-Alder reactions actually occur, the Zn11M salt was reacted with beta-carotene in o-DCB.

Beta-carotene was used as a model for degraded PVC since it is comprised of a long chain of conjugated double bonds. The structure of beta-carotene is shown below in Figure 6.15.

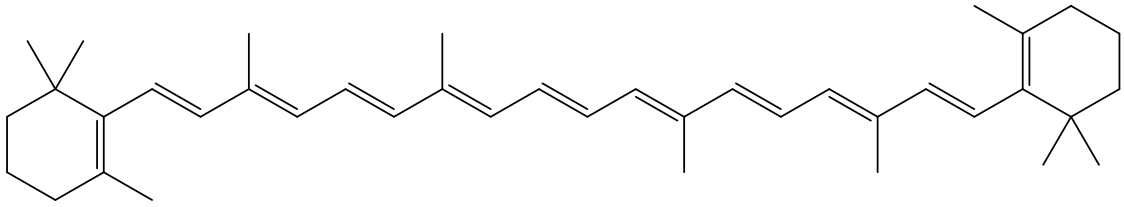

Figure 6.15. Structure of beta-carotene.

Beta-carotene is strongly active in the UV-visible regions (its solutions are a deep red color). As such, UV-Visible spectroscopy was used to monitor its disappearance as a function of time. The UV-Visible absorption spectra of beta-carotene and Zn11M in o-DCB are shown below in Figure 6.16.

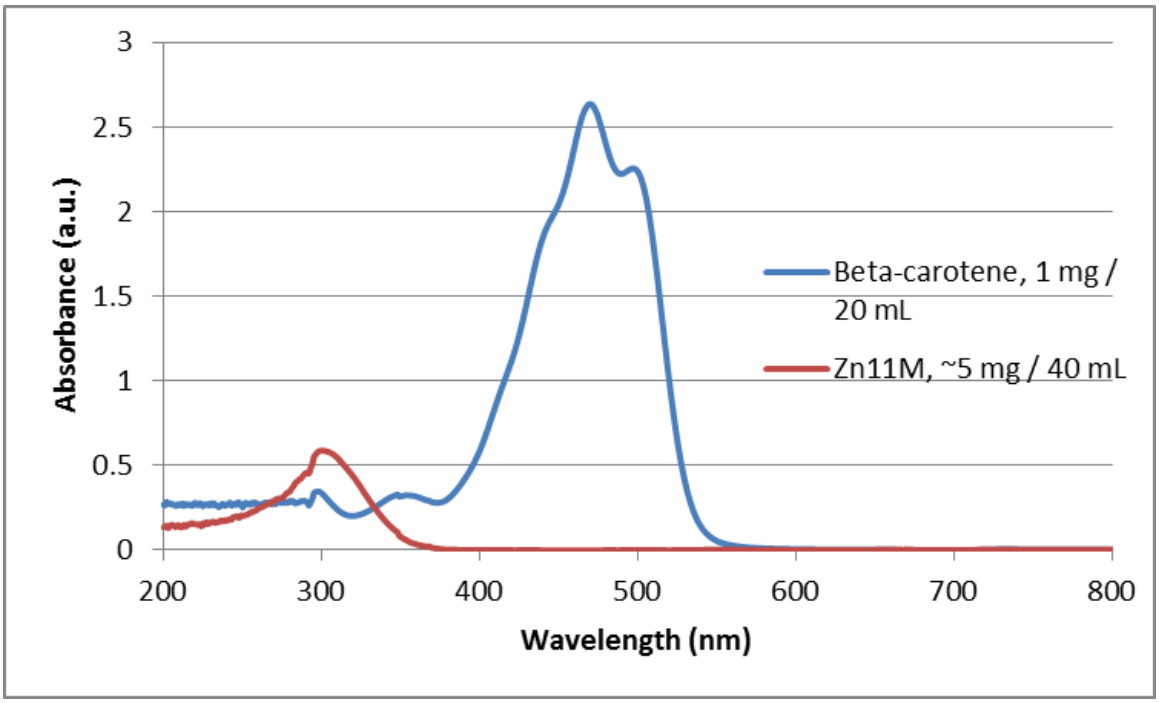

Figure 6.16. UV-Visible absorption spectra of beta-carotene and Zn11M in o-DCB, measured at room temperature.

Beta-carotene displays a very large and distinct UV-Visible peak at approximately 475 nm. The absorption at λ_{max} was measured and taken as indicative of the concentration of beta-carotene in solution.

Zn11M is insoluble in o-DCB below 140 °C. To combat this issue, the reaction was run at 145 °C in a vessel purged with argon. UV-Visible absorption spectra were measured at room temperature (with Zn11M precipitated from solution). At elevated temperatures, beta-carotene may be vulnerable to pericyclic process that can reduce conjugation without the presence of a dienophile (shown in Figure 6.8). As such, two experiments were conducted: (i) beta-carotene at a concentration of 1 mg / 10 mL o-DCB were heated at 145 °C, and (ii) beta-carotene at a concentration of 1 mg / 10 mL o-DCB with equimolar Zn11M were heated at 145 °C. Reactions were conducted for 2 hours.

Samples were taken at 30 minute intervals and analyzed via UV-Visible spectroscopy at room temperature.

The UV-Visible spectra for each study are shown below at 30 minutes and at 120 minutes in Figure 6.17.

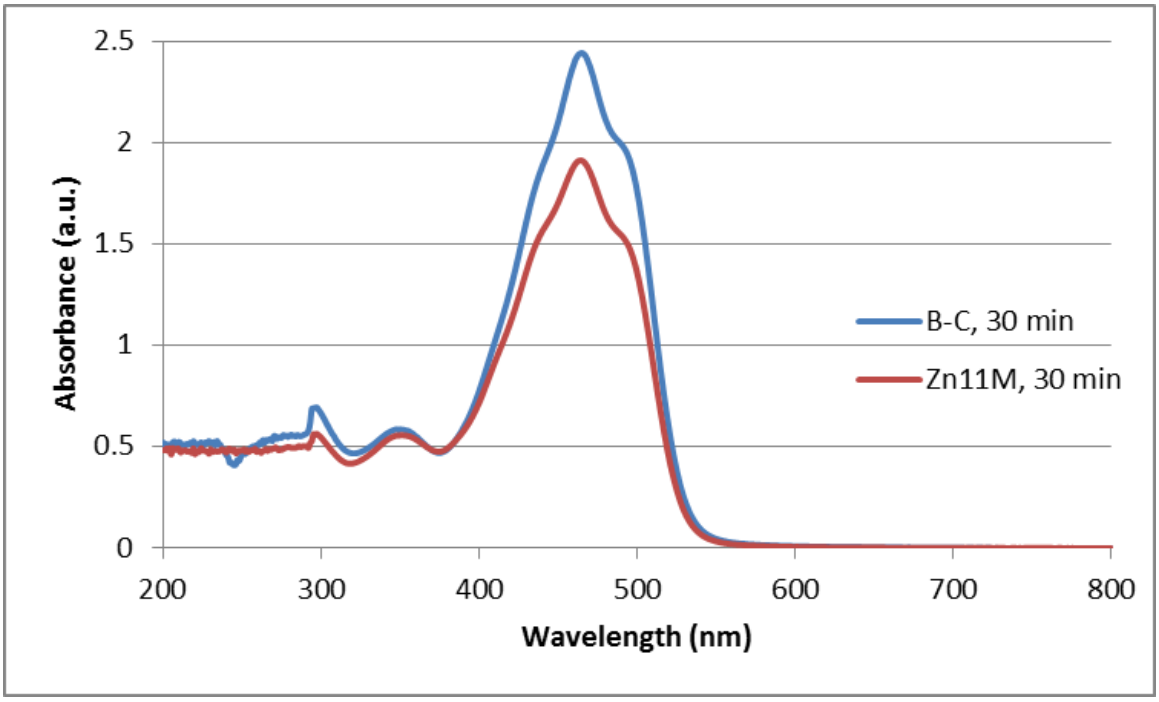

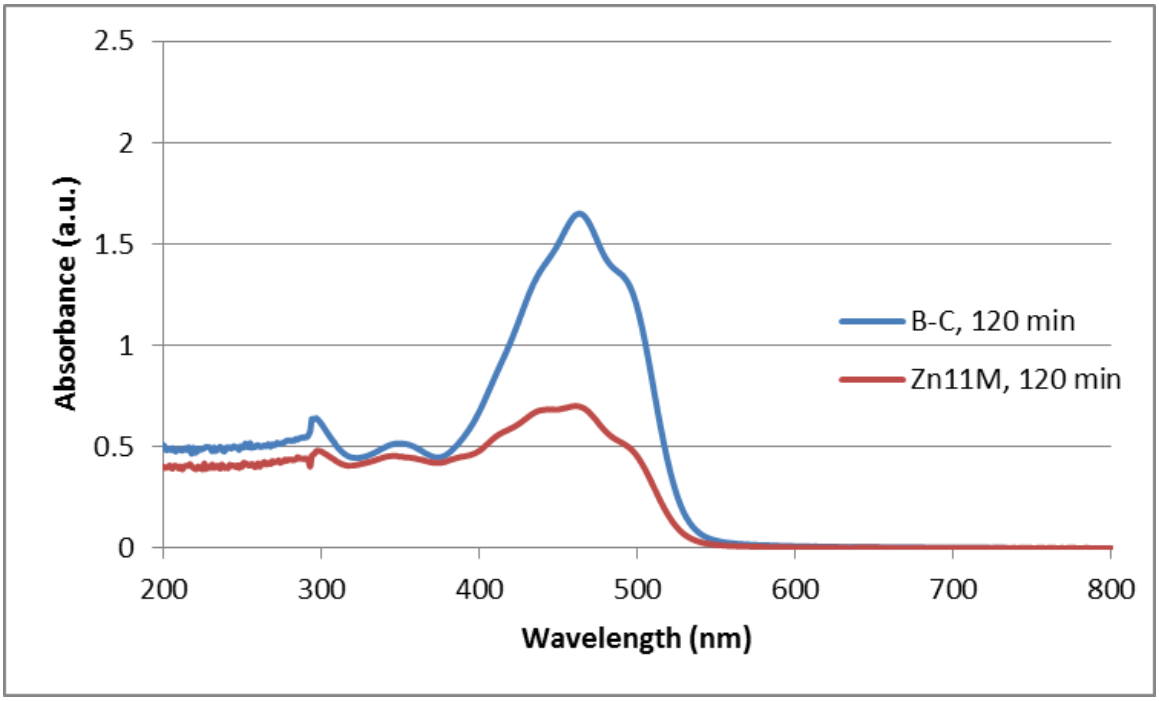

Figure 6.17. UV-Visible spectra for the reactions of (i) beta-carotene in o-DCB at 145 °C (blue lines) and (ii) beta-carotene with equimolar Zn11M in o-DCB at 145 °C (red lines).

It is clear from Figure 6.17 that the reaction with Zn11M present loses beta-carotene at a higher rate than the reaction without. The magnitude of the beta-carotene peak for the red spectra decreases faster than the magnitude of the same peak for the blue spectra. However, it's also clear that beta-carotene is consumed even when Zn11M is absent. The ratio of the magnitude of the peak with Zn11M to the magnitude of the peak without Zn11M is tabulated below in Table 6.1.

Table 6.1. Ratio of the magnitude of the maximum absorptions for the reactions of beta-carotene in o-DCB at 145 °C (Figure 6.17) as a function of time. "Zn11M" = peak for the reaction mixture containing Zn11M. "B-C" = peak for the reaction mixture with ONLY beta-carotene in o-DCB.

Time (min)	Ratio of λ_{max} (Zn11M : B-C)
30	0.78
60	0.65
90	0.54
120	0.42

The data in Table 6.1 make it clear that, even though beta-carotene is consumed with or without added Zn11M, the rate of consumption is measurably higher with added Zn11M. This is evidence that Zn11M is capable of inducing Diels-Alder ring closure reactions in systems of conjugated polyenes. This may account for the color retention displayed in the PVC thermal studies.

6.8 Conclusions

It has been demonstrated through UV-Visible absorption, thermogravimetry, and qualitative color comparison that zinc and calcium salt combinations of 11-

maleimidoundecanoic acid perform a dual function in PVC stabilization. The novel maleimide salts (1) decrease the rate of thermally induced weight loss due to dehydrochlorination processes and (2) effectively reduce color formation of PVC plasticized with didodecyl phthalate (DIDP) or epoxidized soy bean oil (ESO). The maleimide stabilizers effectively fulfill multiple stabilization objectives. It is hypothesized that the Zn11M-Ca11M combination operates in two regimes at different stages of PVC thermal degradation: during the early thermal treatment stages it facilitates substitution processes on the PVC backbone, while during the later stages it promotes pericyclic processes to reduce the extent of conjugation of polyenes.

6.9 References

(1) Garrigues, C.; Guyot, A.; Tran, V. H. THERMAL DEHYDROCHLORINATION AND STABILIZATION OF POLYVINYLCHLORIDE IN SOLUTION .9. DIALKYLTIN MALEATES - DIELS-ALDER REACTION. *Polymer degradation and stability* **1994**, *43*, 307.

(2) Wang, M.; Li, H.; Huang, X.; Yi, L. Zinc maleate and calcium stearate as a complex thermal stabilizer for poly(vinyl chloride). *Journal of Vinyl and Additive Technology* **2014**, *20*, 1.

(3) González-Ortiz, L. J.; Arellano, M.; Sánchez-Peña, M. J.; Mendizábal, E.; Jasso-Gastinel, C. F. Effect of stearate preheating on the thermal stability of plasticized PVC compounds. *Polymer degradation and stability* **2006**, *91*, 2715.

(4) Zheng, X.-G.; Tang, L.-H.; Zhang, N.; Gao, Q.-H.; Zhang, C.-F.; Zhu, Z.-B. Dehydrochlorination of PVC Materials at High Temperature. *Energy & Fuels* **2003**, *17*, 896.

(5) Sun, B.; Chaudhary, B. I.; Shen, C.-Y.; Mao, D.; Yuan, D.-M.; Dai, G.-C.; Li, B.; Cogen, J. M. Thermal stability of epoxidized soybean oil and its absorption and migration in poly(vinylchloride). *Polymer Engineering & Science* **2013**, *53*, 1645.

(6) Nayler, P.; Whiting, M. C. Researches on polyenes. Part III. The synthesis and light absorption of dimethylpolyenes. *Journal of the Chemical Society (Resumed)* **1955**, 3037.

(7) Ivan, B.; Kelen, T.; Tudos, F. THE MAIN ELEMENTARY EVENTS OF DEGRADATION AND STABILIZATION OF PVC. *Makromolekulare Chemie-Macromolecular Symposia* **1989**, *29*, 59.

(8) Chaudhary, B. I.; Nguyen, B.-D.; Smith, P.; Sunday, N.; Luong, M.; Zamanskiy, A. Bis(2-ethylhexyl) succinate in mixtures with epoxidized soybean oil as bio-based plasticizers for poly(vinylchloride). *Polymer Engineering & Science* **2014**.

CHAPTER 7 – CONCLUSIONS

The work presented in the chapters herein (with the exception of Chapter 3) investigates various aspects of the thermal stabilization of polymer processing. Specifically, the protection of polyethylene from premature radical crosslinking and the prevention of thermal degradation of PVC are both addressed. Polyethylene and PVC are two of the most common polymers produced globally. Optimization of processing techniques for these polymers therefore has the potential to make tremendous impact on the economy of the polymer industry by either (i) decreasing required energy expenditures, or (ii) allowing for optimized methods using fewer or lower-cost materials.

The first portion of this work focused on the prevention of premature crosslinking in polyethylene. More specifically, a common crosslink initiator, dicumyl peroxide (DCP) was observed to have a very low level of premature crosslinking when used in blends with distearyl thiodipropionate (DSTDP). However, the exact reason for this beneficial observation was previously unknown. A thorough investigation was conducted to determine the exact mechanistic interactions when DCP is combined with DSTDP in polyethylene. A combination of kinetics and product identification of carefully designed experiments allowed the proposal of a consistent mechanism that accounted for all experimental observations.

Part of the proposed mechanism involved a reaction hitherto unreported in literature. The formation of a hydroperoxide from the acid-catalyzed decomposition of a peroxide was a crucial, yet unproven, aspect of the overall mechanism. A separate

investigation of the acid-catalyzed mechanism allowed for the concrete demonstration and quantification of this proposed phenomenon.

The second overall portion of this thesis focused on the thermal degradation of PVC and the mechanisms of stabilization. First, model compounds of PVC and PVC defect sites were reacted with a metal carboxylate. This study provided a picture of the relative reaction rates and vulnerability to decomposition of the defect sites present in PVC. Additionally, a model for defect-free PVC was reacted with zinc and calcium stearates, both of which are common industrial stabilizers. Thermal gravimetric studies were also conducted of real PVC blended with a common plasticizer and stearate stabilizers. The information gained from that study allowed for the proposal of a revised mechanism of interaction between PVC and metal carboxylate stabilizers.

The insights gained in the kinetic and mechanistic investigations of PVC allowed for the design of novel stabilizer additive systems. The plasticizer epoxidized soybean oil (ESO) was introduced and its vulnerability to reaction with hydrogen chloride was confirmed. Epoxidized salts of linolenic acid were synthesized as dual-function stabilizers to both protect ESO from attack and to perform typical stearate roles in stabilization.

Additionally, the formation of long conjugated double bond sequences during PVC degradation led to the development of a dienophile stabilizer to reduce the extent of conjugation. Salts of maleimidoundecanoic acid were designed to induce Diels-Alder ring closures (reducing conjugation) and to perform typical stearate chemistry to stabilize PVC.

7.1 Mechanism of the Interactions of DCP with DSTDP

Prior research noted that when combined with DCP, the antioxidant DSTDP causes a dramatic reduction in premature crosslinking of polyethylene blends during treatments at extrusion temperatures. Several preliminary observations guided the investigation discussed herein, including:

- DCP and DSTDP must be blended together, in air, to produce the reduction in premature crosslinking.
- DCP, among various peroxides examined, provided the most reduction in crosslinking.

Chapter 2 sought to expand on these observations and uncover their cause. First, the kinetics and products of the thermal homolytic cleavage of DCP were examined in dodecane, a model solvent for polyethylene. Kinetics and products were also identified for reactions of DCP with DSTDP. These reactions were conducted under varying atmospheric conditions to determine the effects of air.

The reactions products and rates for the decomposition of DCP and the reaction of DCP with DSTDP under inert were virtually identical. The consumption of DCP proceeded at the rate of homolytic cleavage in both cases. Under air, the reaction of DCP with DSTDP was greatly accelerated, producing several new species that were not observed in the decomposition of DCP alone. The products formed in the presence of air, and the s-shaped degradation curve of DCP, were combined to propose a complete mechanism.

In brief, the proposed mechanism suggests that the radical decomposition of DCP produces alkyl radicals in the dodecane solution. The alky radicals react with atmospheric oxygen and (via hydrogen abstraction) produce alkyl hydroperoxides. The alkyl hydroperoxides oxidize DSTDP to a sulfoxide, which rapidly undergoes retro-Michael addition to form a sulfenic acid and stearyl acrylate. The sulfenic acid is then oxidized to a sulfinic acid by hydroperoxides. The sulfinic acid is sufficiently reactive to induce the acid-catalyed decomposition of DCP. The acid-catalyzed decomposition produces cumene hydroperoxide as a product, feeding back into earlier steps of the mechanism. Acid-catalyzed decomposition of DCP also produces α-methyl styrene, which is hypothesized to account for the reduction in premature crosslinking observed with this reaction.

7.1.1 Future Work and Recommendations

7.1.1.1 Proof of the Mechanism of Crosslink Reduction

The work presented in Chapter 2 proposed a mechanism consistent with all experimental observations. Some specific steps of the mechanism were concretely proven with some supplemental experiments. However, the hypothesis that α-methyl styrene reduces the extent of crosslinking was never tested.

A straightforward analytical technique to examine the extent of crosslinking in these experiments was not discussed. Proton NMR would not be effective. As shown with the various proton NMR spectra presented in Chapter 2, dodecane produces large

overlapping proton signals in the methyl region. Since multiple proton peaks overlap, quantifiying the changes accompanying crosslinking would be effectively impossible. Carbon NMR would likely allow some measurement of crosslinking. Dodecane ordinarily contains no tertiary carbons; crosslinking would likely produce mostly tertiary carbons (simply based on the high proportion of secondary to primary carbons in dodecane). Tracking the formation of tertiary carbons may be possible via carbon NMR. However, the concentrations of tertiary carbons associated with the reaction systems of interest may be far too low for meaningful quantification with this technique. Perhaps if isotopically labeled dodecane were available, this technique could be used.

A much more feasible option would be to use viscometry. As was discussed in chapter 2, researchers have previously used rheology to examine the extent of crosslinking in polyethylene samples. A similar technique can be applied with this work, using a viscometer in conjunction with model liquid solvents.

Depending on the equipment available, a variety of liquid media could be used to produce reaction solutions of appropriate viscosity. For reference, the viscosities of some aliphatic materials are tabulated below in Table 7.1.

Table 7.1. Viscosities of some polyethylene model solvents.

Material	Viscosity (mPa s)
Dodecane	1.3585[1]
Tetradecane	2.078[1]
Paraffin oil	110 - 230[2]

Different viscometry equipment has different sensitivities and minimum readable viscosity levels. A model solvent can be selected depending on cost and required viscosity.

To verify the effectiveness of radical scavengers at reducing crosslinking, the following experimental design should be used:

1. Determine the viscosity of the model solvent.
2. Determine the viscosity of the model solvent after thermal treatment at a relevant time and temperature (for example, 120 °C for 3 hours). The difference in viscosity between this and the previous step represents the baseline for comparison.
3. Dissolve DCP in the model solvent at an appropriate concentration (for example, 0.0589 M) and decompose it at a relevant time and temperature. The presence of a relatively low concentration of peroxide should not significantly alter viscosity.
4. Measure the viscosity of the sample after peroxide decomposition. The viscosity should measurably increase due to radical-induced crosslinking.
5. Repeat step 3 while adding up to 1 equivalent of α-methyl styrene or stearyl acrylate dropwise into the solution during reaction. The goal is to introduce radical scavengers at low enough concentrations to avoid polymerization, but high enough concentrations to scavenge radicals.
6. Measure the viscosity of solutions after step 5. The change in viscosity from the baseline will confirm or deny the importance of these radical scavengers in preventing crosslinking.

The methodology summarized above should elucidate the effects of the proposed radical scavengers of the crosslinking behavior of DCP. Furthermore, if neither α-methyl styrene nor stearyl acrylate are effective at reducing crosslinking, the same methods could be used to screen any other hypothesis as well.

7.1.2 Improvement of Blend Performance

The mechanistic investigations were initiated with the ultimate goal of utilizing mechanistic knowledge to propose improvements to polyethylene processing techniques. Possible techniques to optimize polyethylene processing and blending are the subject of a research proposal written and submitted to Dow Chemical. The proposal cannot be included due to intellectual property controls. Some of the suggestions are summarized here.

7.1.2.1 New Combinations of Additives

The mechanism proposed in Chapter 2 states that DSTDP is oxidized via hydroperoxides to a sulfoxide. A possible method of improving the process could be to simply use the sulfoxide directly in the peroxide blend. This could drastically reduce the required blending time as several mechanistic steps would be bypassed. Blends using the sulfoxide could be prepared in model solvents (or in polyethylene) and the crosslinking performance could be subsequently examined via viscometry as discussed above.

Alternatively, the proposed mechanism suggests that hydroperoxides are required to oxidize the DSTDP and to oxidize the sulfenic acid formed via retro-Michael addition. A possible optimization could be to include a hydroperoxide in the blend mixture. This would also reduce the required processing time since hydroperoxide formation would no longer be a rate-limiting step in the mechanism.

There are a few other commercially available species that may be useful for this mechanism. Two sulfide structures and their CAS numbers are presented below in Figure 7.1.

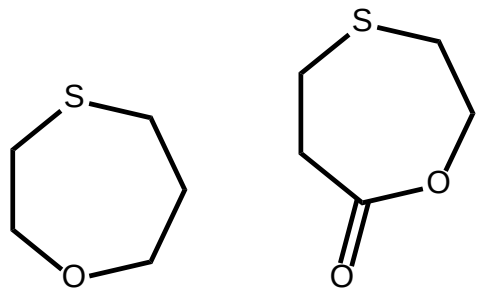

Figure 7.1. Commercially available, potential sulfur additives. CAS numbers from left to right: 23640-00-8, 5512-72-1.

The molecule on the left may have use if properly functionalized. The molecule on the right should be immediately ready for use, as its sulfoxide derivative should undergo a retro-Michael addition to form an acrylate and a sulfenic acid in the same molecule. The cyclic structures would likely exhibit a much faster rate of oxidation from hydroperoxides than DSTDP due to the relative lack of steric hindrance, and may shorten necessary processing times.

The incorporation of existing, commercially available or easily synthesizable is advantageous. These species would not require rigorous reactivity and safety profiling before commercial use as such information is already available.

7.1.2.2 Novel Additives

As an alternative to using new combinations of existing species, novel additives could be synthesized specifically for this reaction system. Some possible options for such molecules are shown below in Figure 7.2.

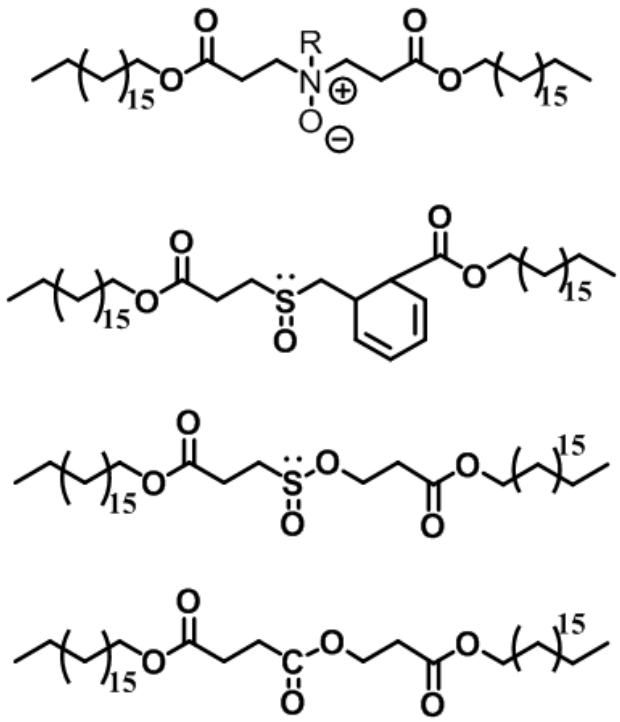

Figure 7.2. Possible novel compounds for use in preventing premature crosslinking of polyethylene by DCP.

The first and second molecules in Figure 7.2 are designed to have exceptionally fast rates of retro-Michael addition. The first utilizes the electronics surrounding the nitrogen atom to facilitate the cleavage. The second utilizes the formation of aromaticity to drive the cleavage. In the case of the second molecule, it's likely that the sulfide form would be a more practical additive. The sulfoxide would likely undergo retro-Michael addition at room temperature. In both cases, the acceleration of the retro-Michael step could reduce processing times.

The third and fourth molecules of Figure 7.2 are designed to form acid species of varying strength after retro-Michael addition. The mechanism in Chapter 2 results in the formation of a sulfenic acid. These two molecules would form a sulfinic acid or a carboxylic acid, both of which would adjust the rate of acid-catalyzed attack of DCP.

The sulfinic acid would also eliminate the need for oxidation of the sulfenic acid by a hydroperoxide.

The goal in the use of these different or novel additives is to tune the rates of different individual steps of the mechanism proposed in Chapter 2. The ultimate purpose of such exploratory studies would be to minimize the premature crosslinking caused by DCP. Tuning the mechanistic rates could allow for maximal generation of radical scavengers (to provide even better performance), or could shorten or simplify necessary processing conditions (to optimize the process).

7.2 Acid-Catalyzed Degradation of DCP to Produce Cumene Hydroperoxide

The mechanism of the interaction of DCP with DSTDP in air (Chapter 2) proposes that upon acid-catalyzed decomposition, DCP produces cumene hydroperoxide (which then oxidizes species in solution). This hypothesis was previously undocumented, so a full investigation was necessary. Prior literature stated that the acid-catalyzed decomposition of DCP forms phenol, acetone, and α-methyl styrene as the exclusive products.

DCP was reacted with a model acid, dodecylbenzenesulfonic acid (DBSA) in the presence of tetrahydrothiophene (THTP). THTP, as a cyclic sulfide, is readily oxidizable to a sulfoxide by cumene hydroperoxide. DCP was previously reacted with THTP to confirm that it could not, on its own, produce a sulfoxide. When the three reactants were combined, formation of sulfoxide was visible. This proved that DBSA decomposed DCP to form cumene hydroperoxide, which subsequently oxidized THTP.

The kinetics of the acid-catalyzed mechanism were then examined. The concentration of DCP as a function of time was tracked for reactions with DBSA at various temperatures. The resulting Arrhenius plot was convex, instead of the ordinary straight line. A hypothesis to explain the convex Arrhenius plot was proposed: in the nonpolar dodecane, instead of a straightforward protonation step, DBSA interacts with DCP by first reversibly forming a hydrogen-bonded complex. The complex can either revert to starting materials, or react in the forward direction to consume DCP. The reversible first step, followed by the irreversible second step, was scrutinized and could account for the convex Arrhenius plot.

From the acid-catalyzed reactions of DCP, phenol was also observed as a product. This suggested that previous literature was not incorrect, merely incomplete. Product analysis of sealed reactions (to prevent volatilization) was conducted to determine exactly how much cumene hydroperoxide forms per mole of acid-catalyzed DCP degradation. A temperature from each regime of the convex Arrhenius plot was selected for study. In each case, a large majority of DCP decomposed through a pathway to form cumene hydroperoxide.

7.2.1 Future Work and Recommendations

As was mentioned, the production of a hydroperoxide from the acid-catalyzed decomposition of DCP was previously unreported. It is unknown, however, whether or not the conclusions from Chapter 3 are only valid in a completely nonpolar medium such as dodecane.

It's possible that in a solvent which facilitates more straightforward protonation steps (thereby generating ion pairs), the formation of cumene hydroperoxide not possible. Perhaps the hydrogen-bonded complex formed in dodecane allows the cleavage of DCP to follow the proper pathway. It would be worthwhile for future work to determine the exact circumstances that allow the formation of cumene hydroperoxide from the acid-catalyzed decomposition of DCP.

This could be accomplished by simply reacting DCP with acid and THTP in a variety of solvents. Multiple reactions would need to be run screening various acids (or acid functionalities) and solvents. It is recommended to examine a suite of solvents ranging from nonpolar (such as dodecane) to as highly polar as possible (while still maintaining reactant solubility).

Additionally, the effect of the acid functionality should be screened. It's possible that only sulfonic or sulfinic acids (with a carbonyl neighboring the acidic proton) allow for the generation of cumene hydroperoxide through the rearrangement shown in Chapter 3. Other acids should be examined to determine their effect, such as sulfinic acid, which has an available carbonyl group but is considerably weaker as an acid. Simple inorganic acids (such as nitric acid) or carboxylic acids (such as acetic acid) could also be examined.

Generally, the observation of cumene hydroperoxide in Chapter 3 is novel and potentially useful. However, the limitations of the observation are worthy of further investigation.

7.3 Degradation and Stabilization of PVC

Chapter 4 presented a comprehensive investigation of PVC thermal degradation and stabilization using neat model compounds and bulk PVC blends. Kinetics studies using models of PVC defects were conducted using an acetate salt in the presence of a phase-transfer catalyst (PTC). With the PTC present, the acetate effectively represented an uncoordinated carboxylate anion with minimal influence from the metal cation. This allowed for a straightforward comparison of relative reaction rates of various model compounds.

It was found that the two functionalities most highly susceptible to reaction with a carboxylate anion were defect-free PVC and allylic chlorides. The models of allylic defects had reaction rates roughly an order of magnitude higher than defect-free PVC. However, the concentration of allylic chlorides in PVC is very low and the interaction of carboxylate with defect-free PVC is therefore highly significant.

The model of defect-free PVC was then reacted with zinc and calcium stearate salts (commonly used for PVC stabilization). Qualitative color analysis showed that zinc stearate induced rapid degradation of the model compound. The presence of calcium stearate mitigated this degradation significantly, supporting the ion-exchange mechanism between the two cations reported in literature. NMR analysis of these reactions revealed stearic acid in the liquid phase. Gas chromatography analysis of the headspace showed evidence of large amounts of elimination products, suggesting that zinc stearate induces elimination in defect-free PVC.

The thermal gravimetric analysis of PVC blends with a plasticizer and stearates supported the results of the model studies. Zinc stearate caused a catastrophic degradation in heated samples; added calcium stearate mitigated this effect. The blend of both calcium and zinc stearates exhibited the best color retention of all blends studied, affirming their synergistic effect.

The evidence gathered from the model and bulk PVC studies allowed for the proposal of a mechanism of interaction between stearate stabilizers and PVC. The proposed mechanism was slightly different from that seen in previous literature and was supported by experimental evidence.

7.3.1 Future Work and Recommendations

The work presented in Chapter 4 was lacking in two key aspects which can be addressed with the recommendations here.

First, as was discussed, stearate salts were only reacted with the model of defect-free PVC. Zinc stearate incontrovertibly induced the degradation of this model compound, inspiring the hypothesized revised mechanism. However, no examination was conducted of the interaction of stearates with models of defect sites. It's possible that while zinc stearate can only cause elimination of defect free PVC, it may substitute rapidly at defect sites along the PVC backbone. This would provide a barrier to dehydrochlorination and stabilize the polymer. The work presented in this thesis allows for no conclusion to be drawn in this respect. Reactions of stearates with defect models,

analyzed by NMR for evidence of substitution products, would complete the picture of the stabilization effects of stearates.

Second, PVC polymer should be analyzed by solid-state NMR. The thermal gravimetry and color studies are largely qualitative and limited in their ability to reveal mechanistic processes. On its own, weight loss data does not reveal exactly what processes are causing loss in weight. The problem is further compounded by the fact that weight loss data did not correlate with color change. Some blends with almost identical weight loss profiles exhibited vastly different color change after heating. Solid state NMR has been used in literature for the examination of PVC and might allow for the quantification of dehydrochlorination after heat treatments.[3]

7.4 Epoxidized Salts of Linolenic Acid as Dual-Function PVC Stabilizers

PVC products are largely dependent on plasticizers to provide desired mechanical properties. One plasticizer of interest in industry is epoxidized soybean oil (ESO). ESO is derived from natural plant sources (soybeans) and is therefore less toxic and less environmentally damaging than traditional, petroleum-derived plasticizers. However, ESO is vulnerable to the HCl liberated during PVC degradation.

The work in Chapter 5 investigated the use of a novel class of PVC stabilizer: epoxidized salts of linolenic acid. First, ESO was reacted with HCl to confirm its high vulnerability to attack. It was therefore hypothesized that stabilizers with sacrificial epoxide functionalities would protect ESO from attack by HCl. The goal was to combine

epoxide functionalities with the industrially common stearate functionalities. The epoxidized salts of linolenic acid contain both epoxides and metal carboxylate sites.

The novel salts were synthesized and their effectiveness tested using thermal gravimetric analysis and color change studies. As compared with control-group blends of stearate salts, the epoxidized linolenic acids provided improve weight retention and color retention of heated PVC blends.

7.4.1 Future Work and Recommendations

The results of the weight loss and color studies indicate that the epoxide salts are highly effective as stabilizers. However, more thorough insight into the performance of this stabilizer system would be beneficial.

Specifically, the epoxide salts should be dissolved in solution with ESO. The solution of both species should be reacted with gaseous HCl as described in Chapter 5. The amount of epoxide rings opened by HCl in each species can be tracked to verify that the epoxide salts are an effective sacrificial species. The reaction would likely need to be monitored by carbon NMR, as there would be minimal difference in chemical shifts for the protons near the epoxides in either species.

Beyond this suggestion, the epoxide salts are demonstrated to be an effective PVC stabilizer.

7.5 Salts of Maleimidoundecanoic Acid as PVC Stabilizers

The work in Chapter 6 examined the use of carboxate salts of a dienophile as novel stabilizers for PVC. Just as in Chapter 5, the aim was to produce a dual-function stabilizer system. The maleimide salts can potentially undergo the reactions of stearate stabilization since they possess metal carboxylate functionality. Additionally, they can potentially induce Diels-Alder ring closures of segments of conjugated double bonds in degraded PVC.

Maleimide salts were synthesized and examined as PVC stabilizers. UV-Visible spectroscopy studies of PVC blends containing these salts showed less absorption (e.g., less color change and therefore fewer conjugated double-bond systems) than those containing stearate salts.

Weight loss studies and color retention studies both affirmed that the maleimide salts are highly effective as thermal stabilizers (as compared with stearates). The blends with maleimide salts exhibited superior weight retention and (usually) superior color retention. It is hypothesized that the Diels-Alder ring closures induced by the dienophile limit the extent of conjugation of double-bond sequences in PVC. This lowers the lability of neighboring chlorides and also reduces color formation.

7.5.1 Future Work and Recommendations

It would be useful to gain a more rigorous understanding of how effectively the novel maleimide salts can induce Diels-Alder ring closures in PVC. The best method for

examining this system in a mechanistic sense would be through the use of model compounds.

The maleimide salts were already reacted with a model for degraded PVC (beta-carotene). The results indicate that the dienophile can indeed facilitate ring closures. However, it would be interesting to examine the reaction of the salts with a large model of undegraded PVC. A good starting point could be pentachloroundecane. The products from either substitutions or eliminations of this model would be readily trackable by proton NMR. An experimental technique would involve first reacting the model with zinc and calcium stearates and, for comparison, reacting it with the zinc and calcium maleimide salts. The expectation is that both stearate and maleimide salts would induce elimination of the model compound. NMR should be used in both cases to determine the amount of vinyl protons. In the stearate case, the eliminated products will remain as conjugated polyenes. In the maleimide case, the end reaction solution should have a lower concentration of vinyl protons on the model due to induced Diels-Alder ring closures.

In general, reactions of the maleimide salts with model compounds (possibly containing defects to accelerate decomposition) would provide further understanding of the role of these salts in stabilization.

7.6 References

(1) Dymond, J. Viscosity of selected liquid n-alkanes. *Journal of Physical and Chemical Reference Data* **1994**, *23*, 41.

(2) Paraffin oil; Sigma-Aldrich: 2015; Vol. 2015.

(3) Tavares, M. I. B. Carbon-13 high resolution solid state NMR study of poly (vinyl chloride). *Polymer testing* **1997**, *16*, 271.

VITA

Mark Conley was born in May 1986 in Lansing, Michigan. After his family moved to Frederick, Maryland in 1996, he attended Tuscarora High School and participated in Mock Trial and political volunteering. After graduating from high school in 2007, Mark attended the University of Maryland to study chemical engineering. While at the University, he was a part of the GEMSTONE program and conducted research over the course of 3 years under the purview of Dr. Joseph Sullivan. Mark completed internships at Fugro Earth Data, Inc., and Bechtel Corporation. After graduating with his bachelor's degree in 2011, he began studying for his doctoral degree in chemical engineering at the Georgia Institute of Technology. He conducted research there as a member of the Eckert-Liotta research group.